University of Genova

DISTAV

Department of Earth, Environment and Life Sciences

Doctoral Research of Science and Technology

for Environment and Territory

Research Topic:

"Advances in the Exploration of Geothermal Resources of the East Africa Rift System (EARS)"

Curriculum: ***Earth Science***

PhD student: ***Dr. Claudio Pasqua***

XXIX Cycle

Tutor: ***Prof. Massimo Verdoya***
(University of Genova, DISTAV)

Coordinator: ***Prof. Marco Firpo***
(University of Genova, DISTAV)

Table of Contents

ABSTRACT 1
ACRONYMS 3
1. INTRODUCTION 5
2. GOALS AND PHASES OF GEOTHERMAL EXPLORATION 6
2.1. FOREWORD 6
2.2. GEOTHERMAL ENERGY 6
2.3. GEOTHERMAL PLAYS 7
2.3.1. Greenfield survey 9
2.3.2. Geoscientific exploration 10
2.3.3. Drilling and testing 10
2.3.4. Feasibility study 10
2.3.5. Field development 13
2.3.6. Power plant construction 13
2.3.7. Power plant operation 13
2.4. RISKS AND INVESTMENT PROFILE IN GEOTHERMAL EXPLORATION AND EXPLOITATION 13
2.5. STANDARDS AND PROTOCOL FOR ESTIMATING AND REPORTING GEOTHERMAL POTENTIAL 14
3. INVESTIGATION METHODS AND DATA COLLECTION 16
3.1. REMOTE SENSING 16
3.2. GEOLOGICAL SURVEYS 18
3.3. GEOCHEMICAL SURVEYS 19
3.4. CO_2 FLUX AND GROUND SURFACE TEMPERATURE 20
3.6. GRAVITY SURVEYS 21
3.7. TRANSIENT ELECTROMAGNETIC (TEM) AND MAGNETOTELLURIC (MT) SURVEYS 22
3.9. EXPLORATION DRILLING 26
3.9.1. Foreword 26
3.9.2. Monitoring of drilling data 27
3.9.3. Basics of well testing 27
3.9.4. Well testing description 28
3.9.5. Wellbore storage 28
3.9.6. Skin effect and turbulence 29
3.9.7. Types of well tests 29
4. THE EAST AFRICAN RIFT SYSTEM 32
4.1. REGIONAL TECTONIC SETTING 32
4.2. THE KENYA RIFT (EASTERN BRANCH) 34
4.3. WESTERN BRANCH 35
4.4. REGIONAL GEOPHYSICAL FEATURES 36
4.4.1. Gravity studies 36
4.4.2. Seismicity 38
4.4.3. Teleseismic studies 40

4.4.4. Seismic refraction and wide-angle reflection surveys 41
4.4.5. Combined seismic and gravity models 44
4.4.6. Heat flow studies 45
4.4.7. Electrical conductivity 46
5. EARS GEOTHERMAL RESOURCES 48
5.1. GEOTHERMAL POTENTIAL 48
5.2. COUNTRY UPDATES 48
5.2.1. Djibouti 48
5.2.2. Eritrea 48
5.2.3. Ethiopia 48
5.2.4. Kenya 49
5.2.5. Tanzania 49
5.2.6. Rwanda 49
5.2.7. Democratic Republic of Congo 49
5.2.8. Uganda 49
5.2.9. Zambia 50
5.2.10. Malawi 50
5.2.11. Mozambique 50
5.3. RECENT ADVANCES IN THE GEOTHERMAL STUDIES OF EARS 50
5.3.1. Alalobeda - Ethiopia 51
5.3.2. Aluto-Langano field - Ethiopia 52
5.3.3. Menengai field - Kenya 54
5.3.4. Kiejo-Mbaka and Luhoi fields - Tanzania 55
5.3.5. Chiweta and Kasitu fields - Malawi 56
5.4. CASE STUDIES 57
5.4.1. The Alalobeda geothermal field 58
5.4.2. The Menengai geothermal field 75
5.4.3. The Kiejo-Mbaka geothermal field 97
6. CONCLUSIONS 118
REFERENCES 124

In memory of my Mother

and of Antonio,
who lost his life in Alalobeda

ABSTRACT

This work focuses on the geological, geophysical and geochemical exploration of the geothermal reservoirs located in the East Africa Rift System (EARS), with particular reference to the characterisation of some geothermal fields located in Ethiopia, Kenya, Tanzania and Malawi. Moreover, this study provides an updated overview of the procedures for the exploration of geothermal resources and can serve therefore as a best-practice guide for future endeavours. Field activities included geological surveys, geophysical investigations (gravity, electromagnetic and seismic measurements) and geochemical survey/analyses. Moreover, stratigraphic data and P&T logs were available at some explored geothermal prospects. An overview of the main investigated geothermal fields was given and three case studies were described in detail as representative examples of geothermal play types of EARS: (i) the *Alalobeda field (Ethiopia)*, located in correspondence of the triple junction Read Sea-Aden Gulf-Main Ethiopian Rift and (ii) the *Kiejo-Mbaka field (Tanzania)*, belonging to EARS' western branch, both falling in the extensional domain play type, fault controlled or fault-leakage controlled; (iii) the *Menengai field (Kenya)*, the second most important geothermal field in EARS, where a huge quantity of direct data from more than twenty drilled wells is available. The latter can be classified as convection-dominated magmatic play type.

Compared to geothermal fields of South-East Asia and Central America, the geothermal of EARS presents some peculiar characters and differences. The plutonic play-type (convection dominated), occurring in fore- or back-arc regions of fold-thrust belts along subduction zones, denotes a well-developed thick and continuous cap rock mainly formed by clay minerals. In the plutonic play of Menengai, the typical impermeable cap rock is practically missing. *A "zonation" of the play types occurring in EARS can be recognized*. The Western Branch is characterised by the presence of fault/fault-leakage controlled play types. In the Eastern Branch, geothermal plays are associated to active or quite recent volcanoes.

Due to the foregoing characters, a different approach should be followed in order to characterize properly the geothermal fields present in EARS. In a subduction context, geophysical results from electromagnetic investigations play a fundamental role in the exploration of potential geothermal reservoirs, as in such an environment they are often succesfully used to detect the occurrence of an impermeable cap rock overlying the reservoir (target zone). Therefore, if the resistivity structures inferred in EARS geothermal plays are simply associated with "standard" resistivity models of cap rock-reservoir formations, the inferred geophysical conceptual model may be grossly incorrect. Wherefore, an accurate and integrated interpretation of all the geoscientific data is essential. In this regard, a *detailed structural survey is of primary importance especially in the fault-controlled plays, whereas its importance is often under-estimated in subduction realms*. A high-resolution structural survey allows to define a detailed configuration of fractures and faults that may control the fluid upflow from the reservoir.

Concerning the application of geochemical methods, in EARS, typical approaches and models developed in the subduction geothermal systems should be re-evaluated. The high-temperature geothermal reservoirs of the Eastern branch (e.g., Olkaria and Menengai in Kenya, and Aluto-Langano in Ethiopia) host not only mature chloride waters, as the geothermal systems situated along subduction zones, but also mature bicarbonate-chloride and mature bicarbonate waters. In volcanic-magmatic regions, deep geothermal liquids are assumed to be produced through neutralization of initially acidic meteoric-magmatic aqueous solutions. The few available data for volcanic gases indicate that subduction zones volcanic gases are enriched in Cl relative to hot-spot and divergent-plate volcanic gases. Therefore, the comparatively small supply of Cl-bearing magmatic gas species (chiefly HCl) in the root of the Eastern EARS geothermal systems might be responsible for the comparatively low Cl contents of related geothermal liquids. The situation might be even more complicated in the western EARS, due to the absence of magmatic systems. Therefore, a more comprehensive approach to water classification is needed to distinguish mature waters from immature ones.
In view of the differences with the geothermal systems hosted in subduction zone environments, the future exploration and development of geothermal resources of EARS should thus consider that geothermal

resources are rarely due to the presence of a hot magmatic source, but rather to the crustal thinning, which determines thermal anomalies of moderate intensity. Moreover, favorable thermal conditions are not always accompanied by an adequate hydrogeological setting, expecially when they occur in low permeability basalts. In these cases, it is essential to pay attention to the structural setting, in order to design the wells with the highest likelihood of intersecting permeable tectonic structures. Unlike in most Indonesian fields, where permeability tends to be widespread throughout the rock, in the EARS permeability appears in many cases limited to major faults. The planned program of drilling in several prospects of Ethiopia and Tanzania will make available further information improving the overall understanding of the geothermal characteristics of EARS.

ACRONYMS

B/C	Benefit/Cost ratio
Bara	Bar absolute
BTD	Brittle-ductile transition
CSG	Production casing
EARS	East Africa Rift System
ECE	Economic Commission for Europe
EEP	Ethiopian Electric Power
EIRR	Economic Internal Rate of Return
EOS	Equation of state
ESIA	Environmental Social Impact Assessment
ETM+	Enhanced Thematic Mapper Plus
FCRS	Fluid Collection and Re-injection System
φCth	Storativity
GDC	Geothermal Development Company - Kenya
GDEM	Global Digital Elevation Model
GPP	Geothermal Power Plant
GSE	Geological Service of Ethiopia
ICEIDA	Icelandic International Development Agency
IFDM	Integral Finite Difference Model
IGA	International Geothermal Association
II	Injectivity index
ISOR	Iceland GeoSurvey
kh	Reservoir transmissivity
MER	Main Ethiopian Rift
MFA	Ministry for Foreign Affairs in Iceland
MoNREM	Ministry of Natural Resources, Energy and Mining
MT	Magnetotelluric
MWD	Measured while drilling
η	Hydraulic diffusivity of formations
NCG	Non-Condensable Gases
NDF	Nordic Development Fund
NPV	Net Present Value
OH	Open hole
ORC	Organic Rankine Cycle
P&T	Pressure and Temperature
PPA	power purchase agreement
RVP	Rungwe Volcanic Province
SH	Superheated steam

SS	Saturated steam
STA/LTA	Short Time Average over Long Time Average
TDEM	Time-domain electromagnetic
TEM	Transient Electromagnetic
TGH	Thermal gradient hole
TOUGH	Transport Of Unsaturated Groundwater and Heath
TRM	Tanganyika-Rukwa-Malawi
TVA	Tectono-Volcanic Axes
UNECE	United Nations Economic Commission for Europe Energy Industry
UNEP	United Nation Environment Program
VNIR	Visible and Near InfraRed
WB	World Bank
WHP	Well head pressure
XRD	X-Ray Diffraction
3G	Geology, Geochemistry and Geophysics

1. INTRODUCTION

Geothermal energy is obtained by exploiting the subsurface heat, which may accumulate in correspondence of peculiar geodynamic environments such as continental rifts, convergent plate margins, hot spots and deep magmatic structures. Commonly, the term "geothermal resource" indicates the part of the Earth's heat that can, or could, be commercially recovered and exploited, becoming a significant source of renewable and sustainable energy, for both direct uses and electric power generation.

Temperature or enthalpy alone cannot describe a geothermal resource, because at least two thermodynamic properties are required to characterise a geothermal reservoir, which should be better defined in terms of steam dominated or liquid dominated system. Therefore, talking about high-enthalpy or high-temperature systems is not properly correct. Geothermal resources can be classified into *High Energy Resources* by their capacity to generate electricity directly, and into *Low Energy Resources*, which are good for direct uses only.

In the last four years, I had the opportunity to study in detail several geothermal fields in the East Africa Rift System (EARS). Therefore, this PhD thesis is focused on the geological, geochemical and geophysical exploration of the geothermal reservoirs located in the EARS. The study is aimed at characterising some geothermal fields of Ethiopia, Kenya, Tanzania and Malawi, and thus giving a picture of the recent advances in the exploration of geothermal resources in the EARS. Moreover, this study can provide an updated overview of the procedures for the exploration of geothermal resources and can serve therefore as a best-practice guide for future endeavours.

This study is based on the data obtained thanks to my direct participation in seven international projects, four of which (Ethiopia, Kenya, Tanzania) co-financed by the Ministry for Foreign Affairs in Iceland (MFA)-Directorate for International Development Cooperation (ICEIDA) and by the Nordic Development Fund (NDF) and the two (Malawi) financed by the World Bank. The seventh project was commissioned directly to my employer (ELC Electroconsult) by the Geothermal Development Company (GDC, Kenya). My contribution to these projects implied field activities, collection, processing and interpretation of geological, geochemical and geophysical data as well as the integrated interpretation of the results deriving from the different geoscientific investigations.

The thesis addresses the following issues:

- *Exploration and exploitation of the geothermal resources*. Overview on the i) different geothermal plays; ii) phases and goals during the geothermal development; iii) risks in geothermal exploration and exploitation; iv) standards and protocols for estimating and reporting geothermal potential.
- *Investigation methods and data collection*. Description of the most used techniques for geothermal investigations.
- *Case-studies*. Definition of the rationale to select the case-studies and describe the geoscientific investigation results, as well as to report direct information derived from the drilled wells.
- *Assessment of the geothermal resource*. Integrated interpretations of the geological, geochemical and geophysical models, and definition of conceptual models for the selected geothermal fields.
- *Comparison of the case studies.* General guidelines for the optimum procedures in the exploration of the geothermal resource are finally addressed.

2. GOALS AND PHASES OF GEOTHERMAL EXPLORATION

2.1. Foreword

In the following paragraphs the meaning of geothermal energy, the main targets of geothermal exploration, as well as the development phases of a geothermal field are defined. The study of a geothermal prospects starts from the definition/characterization of the resource up to its possible exploitation.

2.2. Geothermal energy

The New Mexico Geothermal Resources Conservation Act (1978) defines the Geothermal Resource/Energy as the natural heat of the Earth, in whatever form, which may be extracted from natural heated fluids found below the Earth surface.

There is no standard international nomenclature in use throughout the geothermal community, which is unfortunate, as this would facilitate mutual comprehension (International Geothermal Association - IGA website). The following are some of the most common definitions and classifications in this discipline (Armstrong, 2016):

- AUSTRALIA (Queensland): *Geothermal Energy* - the heat energy derived from Earth's natural (sub-surface) heat. *Geothermal Resources* - the geological strata and associated material in which elevated levels of geothermal energy exist.
- EUROPEAN UNION: *Geothermal Energy* - the energy stored in the form of heat beneath the surface of the solid Earth.
- ICELAND: *Geothermal Energy* - reserves of energy in the bedrock; a constant flow of heat from the depths of the Earth, which does not constitute ground water.
- KENYA: *Geothermal Resources* - any product derived from and produced within the Earth by natural heat; and includes steam, water, and a mixture of any of them that has been heated by natural heat whether as a direct product or resulting from other material introduced artificially into an underground formation and heated by natural heat.
- PHILIPPINES: *Geothermal Resources* - mineral resources, classified as renewable energy resources, in the form of: (i) all products of geothermal processes, embracing endogenous steam, hot water, and hot brines; (ii) steam and other gases, hot water, and hot brines resulting from water, gas, or other fluids artificially introduced into geothermal formations; (iii) heat or associated energy found in geothermal formations; and (iv) any by-product derived from them.
- UNITED STATES OF AMERICA: *Geothermal Resources* (Geothermal steam and associated resources) - (i) all products of geothermal processes, embracing endogenous steam, hot water, and hot brines; (ii) steam and other gases, hot water, and hot brines resulting from water, gas, or other fluids artificially introduced into geothermal formations; (iii) heat or other associated energy found in geothermal formations; and (iv) any by-products derived from them.

2.3. Geothermal plays

A "*Play Type*" might be defined by the type of heat source, the geological controls on the heat migration pathway, the heat/fluid storage capacity and the potential for economic recovery of the heat, allowing worldwide analogy comparison. Ultimately, the geological framework does not only control the play type but also the decision for applied heat recovery technology (Moeck, 2014).

The identification of the geothermal resource type of the prospect under exploration is of paramount importance, since such identification affects the interpretation of the assumed geometric configuration and characteristics of the system and consequently the strategy to be adopted in the course of the deep exploration stage.

Cataloguing of geothermal systems by geothermal play type has been discussed in several papers by Moeck (2014) and Moeck et al. (2014). A play type describes the generic geological environment that might host an economic accumulation of the commodity.

Making specific reference to the geothermal resource, geothermal plays can be broadly separated into two types related to the mechanism by which heat is transported into the reservoir, inasmuch as the heat transport is dominated by either convection or conduction.

Convection-dominated geothermal plays host medium to high enthalpy resources (> 150-200 °C) and occur at plate tectonic margins or settings of active tectonism or volcanism (see Figure 2-1). Convection of thermal fluids induced by a heat source or by an anomalous thermal gradient transports heat from deeper (shallower than 3,000 m) levels towards surface.

Structural elements have a major influence on the fluid flow pathways and high permeability is necessary to allow significant convection. The magmatic, plutonic and extensional domains are the common convection-dominated geothermal plays; they are therefore characterized by a high thermal gradient, natural fluids flow and fluids dynamics.

Conduction-dominated geothermal plays, on the other side, host low to medium enthalpy resources (< 150-200 °C) and are predominantly located in tectonic plates, where no significant recent tectonism or volcanism has occurred (see Figure 2-1).

The thermal gradient is average, wherefore the reservoir is located at greater depth than in the case of convection-dominated plays (deeper than 3000 m). Faults can play an important role as fluids conduit or barrier during production and may induce compartmentalization of the system into separate fault blocks. Intracratonic basins, orogenic belts and foreland basin, crystalline rock/basement are the common conduction-dominated geothermal plays.

Each play type lies within a geological/tectonic environment, and it is possible for specific geothermal systems to have geological characteristics of more than one play type (Moeck, 2014). Figure 2-2 shows all 187 producing geothermal fields included in Figure 2-1, separated into three regional triangles for the Americas, Europe/Atlantic/Africa and Asia/Pacific.

Analysing plots of Figure 2-2, it is evident that most of the developed geothermal systems in the world represent convection-dominated magmatic play types (including volcanic and plutonic plays). Developed extensional domain plays are mainly located in the Basin-and-Range in the U.S.A. and in western Turkey.

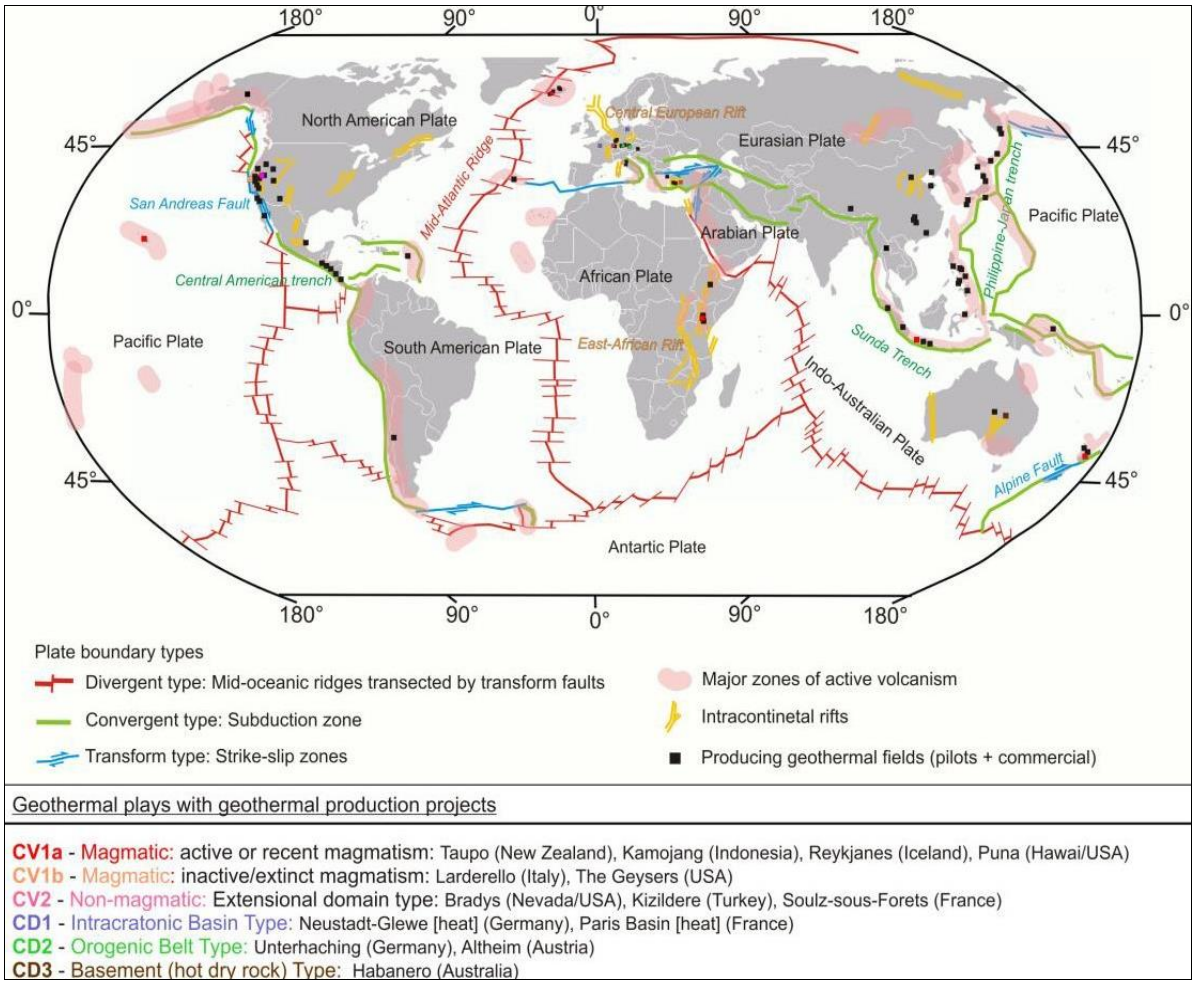

Figure 2-1 Worldwide producing geothermal fields related to the plate tectonic setting. Example fields a selected as play types. Modified from Moeck (2014), installed geothermal fields compiled from http://geothermal-powerplant.blogspot.com; www.thinkgeoenergy.com

The development of conduction-dominated geothermal plays has predominantly been restricted to Europe (precisely Germany) where the regulatory framework has supported their development. Differently, not a single conduction-dominated play has been developed in the Americas, and only two in the Asia/Pacific region (precisely Australia). Conduction-dominated geothermal plays usually host 'tight' reservoirs that require specific technologies to achieve an economical productivity.

The developed conduction-dominated geothermal plays in Germany are mainly located in the Bavarian Molasse Basin, where the fail-safe German feed-in tariffs for geothermal power guarantees the dynamically evolving geothermal technology improvement. The lessons learned from the Bavarian geothermal fields show that geothermal developments are more cost-effective to date compared to 10 years ago, when geothermal field development began with exploration and drilling stimulated by Germany's 'Renewable Energy Act' (Lentsch and Schubert, 2013; Lentsch et al., 2012). The producing reservoir within the Bavarian Molasse Basin is an example of a previously non-economic play type with high recovery uncertainty that has evolved into a play type with greater probability of exploitation efficiency.

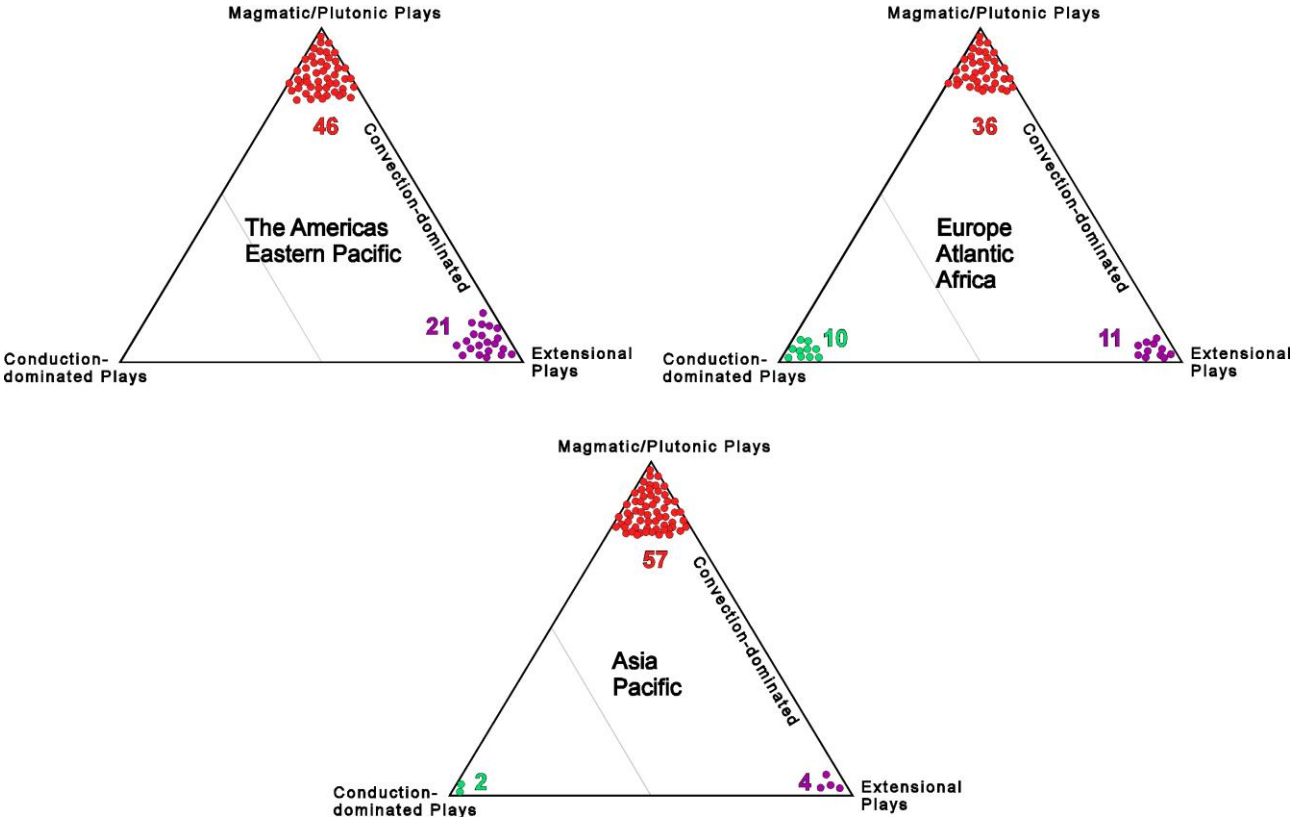

Figure 2-2 Worldwide developed geothermal systems, grouped into play types and into three regions. Geothermal systems are taken from the map in Figure 2-1. Notice the cluster on conduction dominated plays in the regional triangle of Europe/Atlantic/Africa representing the German developed systems in the Bavarian Molasse Basin (after Moeck, 2014)

2.3.1. Greenfield survey

In a geothermal context, *a greenfield survey* means the early stage exploration of a geothermal prospect that have a total lack of geoscientific information or only very limited data sets.

The first "greenfield investigation stage" is to perform a Preliminary Reconnaissance Survey, which includes but it is not limited to the following phases:

i) analyse all the available technical documentation regarding the identified greenfield;

ii) visit the prospects in order to get a general assessment of their geological setting and to collect a few water samples, which may provide some indications on the origin of the fluids and on the underground temperatures;

iii) at conclusion of the previous activities, it is possible to rank these geothermal features according to the probability that the manifestations are the surface expression of a geothermal system. Ranking is essentially based on technical grounds, but also takes into account non-technical factors, such as morphology, accessibility, land use, environmental and social framework, distance from the national grid, etc.

In accordance with the established ranking, some prospects will be selected to be covered by more detailed investigations (geoscientific exploration), which will include remote sensing study, geological mapping, geochemical sampling of thermal fluids (waters and gases) and geophysical surveys (magnetometry, gravity, electromagnetic methods and microseismicity records).

2.3.2. *Geoscientific exploration*

This stage aims at collecting and providing enough information for a proper technical analysis, due to allow a sound decision on the opportunity to pursue the development of the selected site. The foreseen investigations include a refinement and integration of the previously conducted geological and geochemical surveys, but are mainly focused on the implementation of geophysical survey. The choice of geophysical methods to be adopted is left to the experts, depending on the characteristics of the prospect, but in principle, electromagnetic and gravimetric investigations are mostly applied.

At the conclusion of this phase, a detailed geo-scientific report is developed covering the explored area, including a preliminary conceptual model of the geothermal prospect (Monroy Parada, 2016). The report should present recommendations on the strategy to be pursued for extending the exploration of the geothermal resource, as well as preliminary development strategies for the area.

2.3.3. *Drilling and testing*

The continuation of the exploratory phase has the main goal to prove the existence and potential of the geothermal resource (Monroy Parada, 2016) through the definition of the boreholes geology, thermodynamic properties and geometry (boundaries) of the reservoir. A drilling program is designed and a set of a few slim holes or full size geothermal wells, ranging from 1000 to 3000 m depth, are drilled based on the preliminary conceptual model defined during the geoscientific exploration phase. It is worth mentioning that the drilling program has to be evaluated/updated continuously during the drilling activity as a function of the geological and well testing results progressively acquired. Location of wellpads will not only be depending on geoscientific information but also on social-environmental considerations in the area.

The first well is the most critical one, as it is meant to maximize downhole information. If the first well does not encounter hot fluids, downhole data must be evaluated in conjunction with the initial geological, geochemical and geophysical studies before deciding on the next well target. If the first exploration well is a success, a step-out well is drilled. Step-out wells should not be too distant from the exploration well (~1-2 km) and should normally target high fractured rocks and other geological structures (e.g. faults). Well logging and discharge tests follow the completion of drilling. Results of the well surveys and tests may confirm the resource and, together with the earlier investigation results, a refined conceptual model can be developed.

Wells often do not readily discharge after drilling even if there are sufficient indications of permeability and high temperature. In such cases, well discharge is stimulated by using compressors and boosters of suitable pressure and volume either for pressurizing the well or for coil tubing operation. Prior to implementation of the drilling operations, an Environmental Social Impact Assessment (ESIA) needs to be prepared, in order to obtain permits from the appropriate entities.

2.3.4. *Feasibility study*

The results of the exploratory drilling activities are utilized to develop a technical and economic feasibility study, which will provide the owner of the geothermal concession with all information and data necessary to take an informed decision on the convenience to proceed with the implementation of the geothermal development of the prospect.

➢ *Resource feasibility*

The modern analysis and evaluation methodology of geothermal resources (reservoirs) is based on the use of mathematical simulation models. These models describe the physical processes of heat and mass transport within the reservoir through numerical solution of the appropriate mass and energy balance equations, allowing to study the dynamic reservoir behaviour, in both its natural state and under exploitation conditions.

The numerical model represents an idealization of the real reservoir in its present state, formulated taking into account the main system characteristics summarized in the conceptual model. It always implies a simplification of the natural system, which is characterized by an extreme complexity and only partially is directly known. In spite of this, the use of an appropriate mathematical model can give very valuable answers to the basic questions on the field capacity and exploitability, greatly contributing to the formulation of safe development plans and reducing the risk of oversizing of the power plant. The first step is the development of a 3-D natural state numerical model of the geothermal system. The input data of the simulation model shall include:

- model geometry, involving the definition of model extension and 3-D gridding;
- assigning of boundary conditions (pressure and temperature/heat flow, fluid recharge and outflow);
- assigning of initial conditions (pressure, temperature, saturation, composition);
- rock petro-physical properties distribution (density, specific heat, thermal conductivity, compressibility, permeability, relative permeability curves, capillary pressure curves).

The natural state model needs to be calibrated in order to reproduce inferred thermodynamic conditions, measured well pressure and temperature profiles. It is used to run sensitivity studies on key parameters whose incertitude may considerably affect the natural state of the geothermal system. The natural state model is built using numerical reservoir simulation.

➢ *Field development plan*

The objective of the field development plan is to ensure the presence of suitable geothermal fluids for the full life of a power plant. Such target is achieved through the definition of: i) the optimal production conditions; ii) the reinjection strategy; iii) the required number and location of production, reinjection and make-up wells.

The natural state model is the basis for constructing the 3-D exploitation model of the geothermal system, which will inherit from the former the initial and boundary conditions and the petrophysical properties distribution. As far as the representation of wells within the numerical model is concerned, two approaches can be followed: a well-by-well approach, in which each well is explicitly represented within the discretization grid; a lumped well field approach, in which groups of wells are producing from the same grid elements. The first approach has the advantage to allow the calibration of single wells productivity against production test results and to supply a more reliable estimate of wells deliverability evolution during reservoir exploitation.

The 3-D exploitation model is used to:

- determine the full and sustainable electric power production potential of the geothermal reservoir for planned field development;
- predict the reservoir response to the above-mentioned exploitation, assessing in particular the impact of possible additional expansions;

- establish future requirements of replacement (make-up) wells, due to reservoir pressure decline, and of re-injection wells;
- evaluate the long-term trend of wells deliverability features (enthalpy and composition) and reservoir conditions (pressure, temperature, saturations and thermodynamic conditions).

The field development strategy has to be elaborated in conjunction with the conceptual design of the fluid collection and re-injection system (FCRS).

➢ *Engineering feasibility*

This step involves the definition of the essential characteristics of the power plant/transmission system in terms of thermal cycle, power station basic design, location and interconnection to the power grid. The configuration of the thermal cycle of the geothermal power plant (GPP) has the main purpose of optimizing the plant output capacity. The cycle and the scheme of resources exploitation, outlined at a preliminary level during this phase, will be examined in detail during the field development stage, in order to optimize the most significant parameters and the criteria of conceptual design.

Design of the FCRS should ensure a reliable and economic operation of the GPP. The optimization of the FCRS includes the general architecture, layout, well-pads arrangement, steam-brine separation strategy, piping sizing, fluid-dynamic simulations in static and dynamic conditions, piping stress analysis.

➢ *Financial and economic feasibility*

The feasibility study shows also project cost estimates, development timelines and the economic and financial analyses under probable power demand scenarios. The cost estimate is carried out for each component and structure, on the basis of the engineering options defined during the feasibility study. The cost estimate shows the direct construction cost, labour and equipment, split into local and foreign currency and subdivided into the following sections: i) geothermal field, that is wells, fluids separation and conveyance system, taking into account estimated depth and productivity of the wells, accessibility, morphology, geological and geotechnical conditions, etc.; ii) power plant, through an itemized list of the systems and sub-systems; iii) transmission line; iv) costs related to the introduction of mitigation measures as a result of the Environmental and Social Impact Analysis.

The Economic Analysis shall evaluate the economic costs and benefits of the project, utilizing the cost estimate as described above and assuming as benefit the "avoided cost", that is the energy cost which would be incurred in the absence of the studied geothermal exploitation or feed-in tariff. This analysis, based on economic prices with and without social prices shall compute the usual parameters, which indicate the project's viability: i) economic internal rate of return (EIRR); ii) net benefit (B-C) or net present value (NPV); iii) benefit/cost ratio (B/C); iv) payback period; v). In the economic analysis, also costs and benefits related to the environment will be taken into account.

The financial viability of the project will be evaluated by elaborating projections of the investments for the construction and the costs-benefits of the operation, as well as the origin and application of funds and a general balance, considering first separately and then as a whole power producers.

➢ *Environmental-social feasibility*

At this stage, in accordance with national environmental laws and regulations, an Environmental Social Impact Assessment (ESIA) need to be prepared in the framework of the full geothermal field development. During this phase, some consultations with local communities and authorities are performed, to assess and evaluate the perception of the project by local communities and to collect

environmental information on the project area. Once completed these activities the ESIA identifies the potential environmental and socio-economic impacts of: i) drilling activities; ii) FCRS construction; iii) the power plant construction; iv) the power plant operation, v) the alternative transmission line options for connecting the plant(s) to the National grid.

2.3.5. Field development

The words "field development" refer to the realization (drilling) and testing of the production/reinjection wells, as well as to the FCRS construction. Several steps lead up to the drilling/construction activities, namely: i) preparation of technical specifications; ii) preparation of the bidding documents; iii) evaluation of offers; iv) contract negotiation and award. Only after the completion of both wells and fluid collection/reinjection system the geothermal resource is available to be fully exploited.

2.3.6. Power plant construction

Power plant construction phase begins once the resource is defined and proven. The general configuration of the thermal cycle of the GPP, as defined in the feasibility study, needs to be updated and a detail design is prepared. As in the field development phase, the following steps are preparatory to the GPP construction activities, namely: i) preparation of technical specifications; ii) preparation of the bidding documents; iii) evaluation of offers; iv) contract negotiation and award.

The plant erection phase is associated with factory and field tests of the mechanical/electromechanical equipment. Finally, the last action in a geothermal project is the commissioning and start-up of the GPP.

2.3.7. Power plant operation

Even in the presence of a good resource, it is essential to manage it properly through a power plant operation optimization. Moreover, also an adequate maintenance planning is necessary to guarantee a plant long-life. From the economic point of view spare parts & consumable material procurement plan, as well as periodic operating cost controls, are to be envisaged.

2.4. Risks and investment profile in geothermal exploration and exploitation

A full-size geothermal project typically takes more than 7-8 years to be completed (Gehringer et al., 2012). During the project development, a number of risks are faced, either associated with any investment in the power sector, or specifically connected to the peculiarities of the geothermal energy; specifically:

- *Risks common to other types of power projects*: delay, off-take, price/tariff, operational, regulatory risk, financing (high upfront costs)
- *Risks specific to geothermal energy* (see Figure 2-3):

i) Exploration Phase, up to Test Drilling: surface studies are not able to significantly reduce project risks. However, they imply low investment costs; the following exploratory drilling phase is more capital intensive, but not yet able to minimize risks related to the exploitability of the resource, at least till the test completion. Wherefore, significant investments are not completely repaid by a proportional risk reduction; in fact, geothermal resource characteristics remain largely unknown (i.e. enthalpy, permeability, chemical composition, etc.);

ii) Resource Risk During Project Implementation: As any other mining business, this risk depends on the nature of the resource that remains largely unknown till when commercial wells are drilled and tested, i.e. at the end of the project development, when investors and lenders are highly exposed.

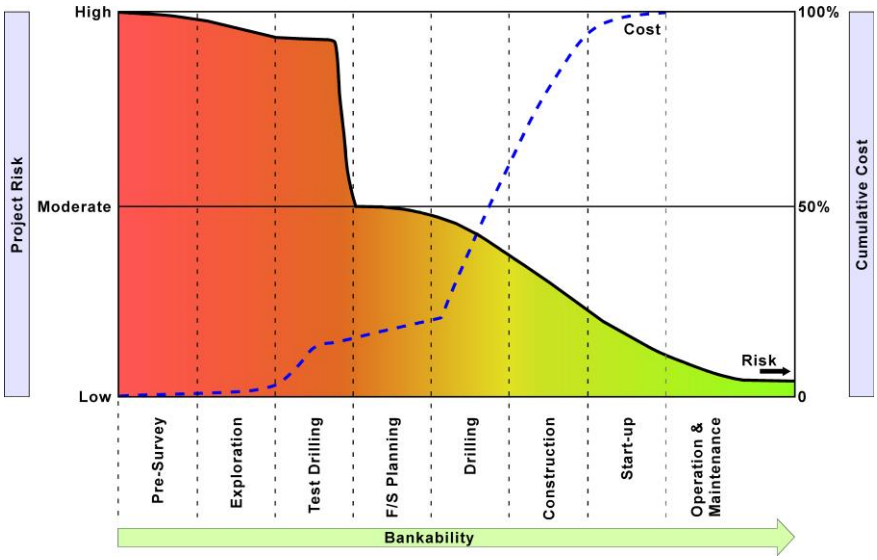

Figure 2-3 Typical Costs and Risk Profile of Geothermal Development. Modified from Gehringer, M. and Loksha, V. (2012)

2.5. Standards and protocol for estimating and reporting geothermal potential

Originally, the resource assessment process of geothermal prospects was based on stored heat (also known as volumetric) methods, while in the last decades it has been based on numerical reservoir modelling (Grant, 2011). Several attempts to codify such assessment process have been tempted. The proposed reporting codes are represented by the following guidelines:

- Australian Geothermal Reporting Code (AGEA, AGEG, 2010a,b);
- Canadian Geothermal Code for Public Reporting, the Geothermal Energy Association (Deibert et al., 2010);
- New Geothermal Terms and Definitions - a Guide to Reporting Resource Development Progress and Results to the Geothermal Energy Association (GEA, 2011);
- Application of United Nation Framework Classification for Fossil Energy and Mineral Reserves and Resources 2009 to Geothermal Energy Resources - ECE 2010 (UNECE-IGA, 2016).

The United Nation (UN) approach has to be pointed out as the evaluation of geothermal resource potential integrated with the evaluation of the resource feasibility and economic viability.

It should be mentioned that some of the above listed codes/classifications based on the heat stored method have been harshly disapproved by world-renowned experts (e.g. Grant, 2011), as shown for instance by the review of the Australian Code. As a matter of fact, the comparison between the actual and the originally estimated performance for a significant number of examined geothermal resources proved that the method proposed by the Australian Code based on the heat stored method is highly unreliable, and usually strongly biased. In particular, the tendency to overestimate has led to the reduced credibility of the method, inasmuch as the main problem lies in the assumed "recovery factor" (Grant, 2011).

At the end, the preferred methodology to classify and report geothermal resources is the recently published UNECE - IGA specifications for the application of United Nations framework, "Classification for Fossil Energy and Mineral Reserves and Resources", which is likely to become a standard for the geothermal industry. It is a generic principle-based system (using a numerical and language independent coding scheme) in which input data from different assessments are classified on the basis of: i) fundamental criteria of economic and social viability (E); ii) field project status and feasibility (F); iii) geological knowledge (G). The method combines these criteria to create a three-dimensional system (Figure 2-4). This means that what is customarily called geothermal resources assessment is only part of the overall description, to be completed with other information.

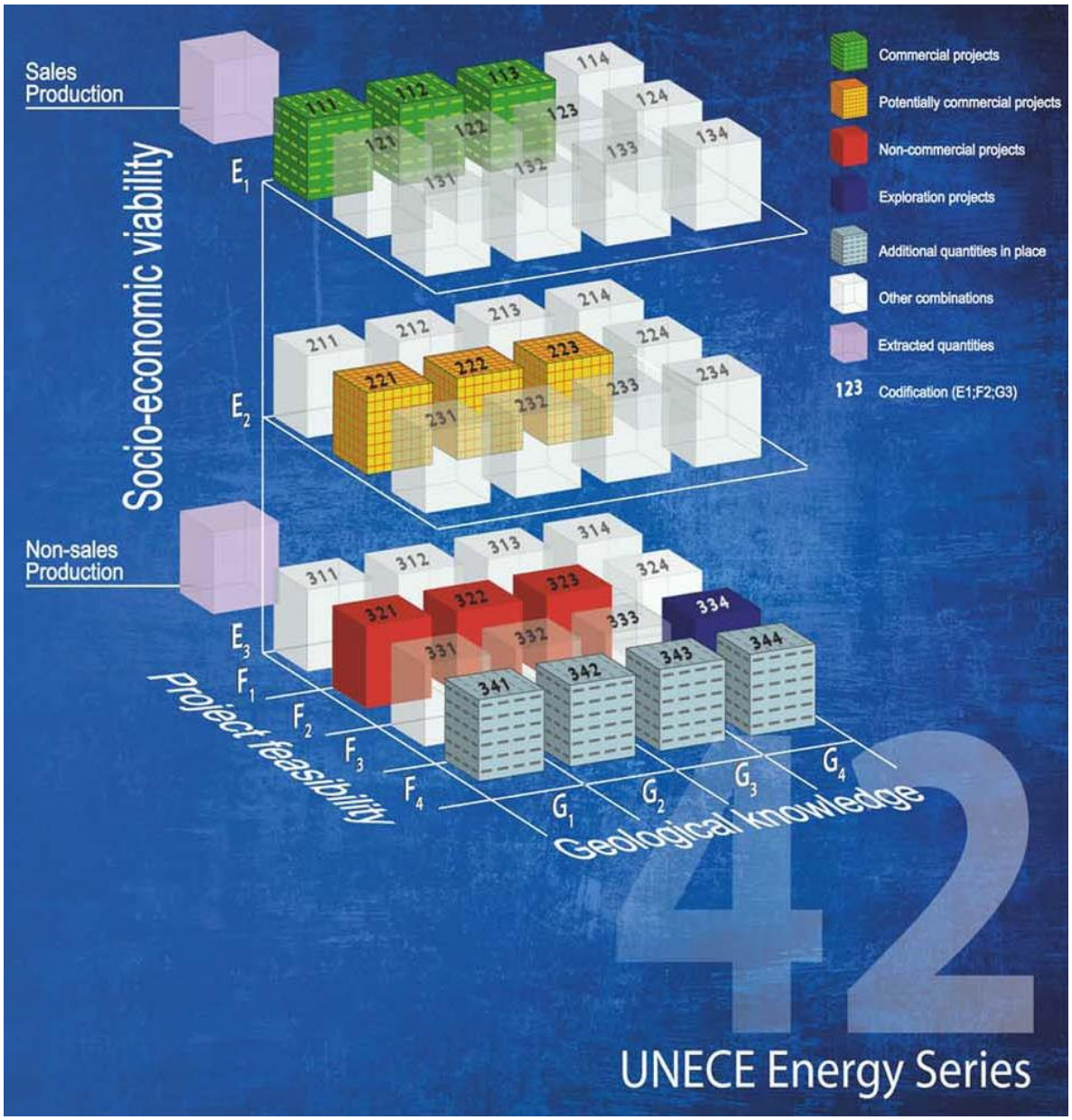

Figure 2-4 UN 2009 3D-classification system

3. INVESTIGATION METHODS AND DATA COLLECTION

Several indirect and direct approaches are commonly used to explore and identify the occurrence of geothermal resources. Indirect studies are developed during the preliminary phase of geoscientific exploration, whereas direct investigations are carried out in the subsequent exploratory phase. Among the numerous indirect methods, the worldwide standard generally includes investigations of remote sensing, geology, geochemistry (including soil gas), and geophysics. On the other hand, the data obtained during the direct investigation phase provide the only direct information on the hydraulic-thermodynamic-chemical characteristics of the geothermal reservoir. The overall objectives of the geothermal exploration are aimed at:

- identifying the heat source of the potential geothermal system;
- estimating the position, depth and boundary of the reservoir;
- identifying possible hazards in the geothermal area, such as volcanism, seismicity, etc.;
- assessing the reservoir characteristics (enthalpy, hydrodynamic status, scaling and corrosion potential, content of non-condensable gases, etc.);
- estimating the electric power capacity of the resources;
- providing recommendations on location, depth and target of exploratory wells;

If the results of the geoscientific investigations are consistent, a preliminary conceptual model of the geothermal system can be formulated and suitable sites for exploratory drilling can be pointed out. Geological samples (drill cuttings and occasionally cores) are obtained from the wells to determine the lithology and alteration of the rocks. The wells make it possible to introduce various measuring tools right into the heart of the geothermal reservoir and to carry out measurements for estimating reservoir parameters, the most important of which are reservoir temperature and pressure (Steingrimsson, 2006).

In this Chapter, I will briefly present the main geological and geophysical approaches that were applied to the geothermal plays of the East African Rift System during the present PhD thesis work.

3.1. Remote sensing

Recent significant improvements in the wavelength coverage, spectral resolution and quality of remote sensing imagery have led to the extensive application of this investigation approach in exploration and site characterization. Traditional techniques in spectral and spatial analysis of imagery, coupled with new, high signal-to-noise data, allow their direct application to problems in geothermal energy exploration and development (Calvin et al., 2005). The remote sensing study is planned to support the geo-structural interpretation of a geothermal area, focused to the exploration and exploitation of the geothermal resources. Different types of remotely sensed images were utilized in the framework of this work to the EARS geothermal systems; this multiple choice was dictated by the fact that different sensors offer distinct types of information, increasing the possibilities of interpretation. The most common analysed images were, as follows:

- ✓ *Landsat ETM+ 7*: these scenes can be acquired, already ortho-rectified, from the Global Land Cover Facility imagery archive (*http://glcf.umiacs.umd.edu/*). For the purposes of the interpretation, the scenes needed to be processed by means of: i) a pan-sharpening process; ii) preparation of a series of colour composites to be directly interpreted on the computer screen, in order to verify the different appearance of morphologic and structural features.

- ✓ *Terra Aster VNIR*: The Aster Volcano Archive (*ava.jpl.nasa.gov/*) provides a number of free Aster images concerning all the volcanic areas of the world. The images are colour composites of the three VNIR (Visible and Near InfraRed) bands 3, 2, 1.
- ✓ *Aster GDEM*: Among the products provided by the Terra Aster sensor, there is the Global Digital Elevation Model generated by the processing of stereo pair images. The Aster GDEM has a ground resolution of 30 m and average vertical accuracy of 20 m (see *http://asterweb.jpl.nasa.gov/gdem.asp*).
- ✓ *Orthophoto*: A true colour orthophoto, generated by the mosaic of aerial photos acquired specifically for the geothermal prospect, is utilized. The orthophoto has a ground resolution of 0.4 m (40 cm) and no coordinate conversion is required.

The simplest results deriving from the remote sensing study is geomorphological information, in terms of drainage pattern and landforms. However, in geothermal exploration, the most important issue is the *fracture analysis*. Linear features are therefore considered as the surface expression of fractures affecting the bedrock, even where blanketed by thick soil or vegetation. Another assumption is that the observed linear features are the surface expression of structural deformations affecting a considerable thickness of rocks at depth. During the interpretation, linear features may be classified according to their length and photographic expression, unless they are directly recognized as faults or dykes. Thus, the linear features of the study area can be classified, as follows: i) *regional lineaments*; ii) *faults*; iii) *major Fractures*; iv) *lineations*.

The information offered by the total field of linear features is generally so rich that an attempt of analysis without proper logical tools may lead to an almost infinite number of possible combinations and interpretations. For this reason, a statistical analysis is generally applied. This refers mainly to two series of data: i) orientation and relative importance of recognizable fracture trends; ii) distribution of the intensity of fracturing, i.e. fracture density.

For the first purpose, the strike and length of each feature is measured and the results are elaborated to obtain azimuth distribution diagrams. The analysis of the azimuth distribution frequencies and their variability leads to the definition of azimuth sectors, for which it is assumed that the linear features there included are the expression of a discrete structural dynamics. Such structural directions are referred to as *trends*. The relative importance of the trends, their relationships with the geological or structural units and their distribution in a studied region, allow drawing hypotheses about the dynamics and the succession of the structural deformations that affected a region.

The second type of elaboration of the total field takes into consideration the areal density distribution of the linear features, irrespective of their azimuths, to produce a density map of the total field. This map can be considered to represent effects of various origins, mainly the mechanical properties and age of the outcropping formations and the amount and type of structural deformation. In the case of the application of fracture analysis to hydrogeology and to geothermal exploration, it becomes of interest to analyse the distribution and density of the crossing points of two or more linear features (*nodal points*, or *nodes*). In fact, this type of analysis helps to evaluate the secondary permeability.

Besides the density of nodes, for a correct analysis of the fracturing intensity, a weight is attributed to the linear features according to a series of parameters reflecting their classification as well as the tectonic and morphological conditions of the area. The weight is inferred by combining the different parameters through a *multicriterial analysis*, which assigns to each parameter a specific value and calculates a final weight through the application of an appropriate algorithm. In

geothermal exploration, the final aim is to assign to each linear feature a numeric value representing its potential to allow groundwater or, more generally, fluids circulation.

3.2. Geological surveys

Geological surveys are aimed at defining the characteristics of the geothermal prospects in relation with the potential presence and geometrical configuration of the geothermal system. The survey is accordingly focused on the reconstruction of the stratigraphic and structural setting, identification of possible heat sources and analysis of the thermal manifestations considered as surface expression of the geothermal system. In order to reach the above objectives, in the investigated geothermal fields the geological study was conducted at two distinct levels of detail, namely:

- At semi-regional scale, where emphasis was given on structural aspects, as derived from the analysis of the existing documentation and on the results of the remote sensing study.
- At local scale, where the geological study was based, besides the existing documentation and remote sensing study, on the findings of a field mapping program and of the associated laboratory analyses.

In general, geological surveys include the following phases:

- ✓ *Analysis of existing documentation*: The available geological literature, in the form of published and confidential reports, aerial photos interpretation, papers and maps, is thoroughly analysed, in order to finalize the program of geological investigations, identifying those aspects, which deserve specific attention in both field and laboratory activities.
- ✓ *Geological mapping*: A detailed geological mapping of the prospect needs to be carried out utilizing large-scale topographic maps (1:10000 or 1:25000). Mapping is also based on the data from the remote sensing study. Lithological formations are mapped and geological structures are traced to provide comprehensive information on the extent of faults and other lineaments, as well as of their age. Primary and secondary permeability of geological formations is also assessed and potential geological hazards identified. Moreover, careful examination of thermal manifestations and hydrothermal alteration zones may reveal relations between fracture-controlled permeability and fluid flow.
- ✓ *Laboratory analyses*: Representative rock samples of the different formations are collected in the course of the mapping and studied in laboratory through petrographic and chemical analysis, in order to define composition, texture and alteration of the various lithological units. Moreover, *ad-hoc* selected samples of deposition or alteration minerals are collected from hydrothermal manifestation zones for XRD analyses, to provide information on the thermal conditions occurring during the deposition/alteration phases.
- ✓ *Data interpretation*: The information derived from the available literature, the remote sensing study, the geological mapping and the laboratory analyses is interpreted jointly to come up with a reconstruction of the stratigraphic, structural and hydrogeological setting of the geothermal prospect and the identification of the relationship between geological and hydrothermal features and the possible presence of a geothermal system.

The final stage of the geological survey consists of a *report* in which the available documentation is critically reviewed, and the regional geology, the litho-stratigraphic setting, the structural pattern, the volcanological features (if the prospect is located in a volcanic area) are described.

Moreover, the report is particularly focussed on the identification of potential heat sources and phreatic structures, the drainage system and the precipitation regime, the type and degree of permeability of the geological formations, geological hazards (seismic, volcanic, slopes stability, flooding, etc.), the natural recharge and the potential role of the geological formations in the geothermal system. A synthesis of the geological features and a preliminary evaluation of the "priority zones", i.e. the zones of the geothermal area in which geothermal resources are more likely to occur, are finally included in georeferenced geological maps at adequate scale in a GIS environment, as well as of geological profiles. These maps also describe the hydrothermal manifestations and the respective temperature, flow rate, pH and electrical conductivity, as well as secondary mineral deposits and alteration.

3.3. Geochemical surveys

The geochemical surveys aim at defining the characteristics of the geothermal fluids, in terms of composition and temperature, as inferred from the chemistry of the thermal manifestations, to reconstruct the deep circulation of the geothermal system (recharge, upflow and outflow) and to identify possible drawbacks such as scaling/sealing and corrosion. A geochemical survey is generally focussed in the same area of the local-scale geological mapping, but may be extended, if necessary, to the peripheral part of the prospect. The scheme of geochemical investigations (Giggenbach, 1984) carried out in this study includes:

- ✓ *Fluids sampling (waters and gases)*: water samples were collected from thermal springs, cold springs/shallow wells discharging local groundwater and surface water bodies. Moreover, gas samples were collected from gas-bubbling hot springs, cold gas vents and fumaroles. Each sampling spot was documented by photos and sampling cards, indicating: GPS coordinates and elevation, geological/structural setting, rock alteration and mineral deposition, dimension of surface manifestation or sampling point area, approximate water flow rate, ambient temperature and results of field determinations (Giggenbach, 1991a,b). Temperature, pH (and temperature of pH measurement), electrical conductivity (and temperature of conductivity measurement), total alkalinity and total sulfide concentration were measured in the field by means of portable instruments. Field pH and total alkalinity, together with other chemical data obtained in the laboratory, were used to compute total dissolved inorganic carbon.

  With reference to gas sampling from fumarolic areas or bubbling pools, two different gas samples were collected: (i) a gas sample (including water vapour) in the Giggenbach bottle; (ii) a dry gas sample (without water vapour) in a glass bottle previously evacuated.

- ✓ *Laboratory analyses*: Chemical and isotopic analyses of all collected samples of water and gas were carried out in laboratories (Craig, 1961). In the water samples, the following chemical components were commonly analyzed: i) anions (Cl, HCO_3, SO_4, F, NO_3); ii) major cations (Na, K, Mg, Ca) and some minor components (B, Li, Fe, As); iii) SiO_2; iv) δ^2H and $\delta^{18}O$. pH, electrical conductivity and alkalinity were again determined in the laboratory with the same approach of field determinations. In the gas samples, O_2, N_2, Ar, CO_2, CH_4, H_2, and He were commonly analyzed. In addition, H_2S and CO were also measured, being fundamental for the characterization and geothermometric determination of the gas mixtures (Chiodini and Marini, 1998). The stable isotope ratio of carbon in CO_2 ($\delta^{13}C$-CO_2) was also determined (Giggenbach, 1991). Carbon monoxide and $\delta^{13}C$-CO_2 values were measured in dry gas bottles, whereas all the other gas species were determined in the Giggenbach's bottles. Carbon dioxide was measured on the alkaline solution by titration against HCl using an automatic titrator. Hydrogen sulfide determination is performed by ion-chromatography upon complete conversion

of H_2S to SO_4. All the other gas species were determined by gas chromatography; the $\delta^{13}C$-CO_2 value was measured using a Delta S (Finnigan) mass spectrometer, after standard extraction and purification procedures of the dry gas mixtures.

- ✓ *Data Interpretation*: The main outcomes of the processing and interpretation of the geochemical data were: (i) the water chemical classification on the basis of ternary diagrams of major anions and major cations; (ii) chloride plots to investigate mixing processes and boiling processes (if any); (iii) the origin of water and the estimation of the elevation of the meteoric recharge of the geothermal system by means of stable isotopes of oxygen and hydrogen; calculation of reservoir temperatures (Fournier, 1979) based on solute geothermometers (Na-K, silica/quartz and K-Mg) and use of suitable geothermometric plots (Guidi et al., 1990), namely ternary plot of Na-K-$Mg^{0.5}$, plot of log(Na/K) vs. log(SiO_2) and plot of log(K^2/Mg) vs. log(SiO_2); (iv) evaluation of mixing with surface/ground waters and estimation of chemical composition and temperature of reservoir water by means of the iso-chemical geothermometric approach (if needed); (v) correlation plots of gas ratios (e.g. CO_2/H_2 and H_2/Ar) for the estimation of reservoir temperature and steam/(water + steam) mass ratio; (vi) characterization of the origin of the CO_2 gas based on carbon isotopes (Bertrami et al., 1985); (vii) characterization of the origin of He based on the He isotope ratio (Ballentine and Burnard, 2002); (viii) evaluation of scaling and corrosion potential of the geothermal fluids.

All the results of the geochemical survey formed the basis for the formulation of the final geochemical model of the geothermal prospect.

3.4. CO_2 flux and ground surface temperature

This survey was aimed at detecting CO_2 flux and temperature anomalies, which may be caused by circulation and upwelling of hydrothermal fluids in correspondence of permeable structures associated with active faults or fractures (Chiodini et al., 1998). Measurements have to be taken along profiles, at spots approximately spaced 20-30 m. If flux or temperature anomalies are detected, additional profiles should be investigated, and spacing among stations decreased to 10 m the spacing among stations. Under this measurement scheme, the choice of the priority sector/s becomes very critical and should be taken after a close examination of the structural, hydrothermal and hydrogeological conditions. The surveys of CO_2 emission and temperature consisted of the following phases:

- ✓ *Field Work*: CO_2 flux and temperature at a depth of 0.5 m was measured simultaneously. Location of the measurement stations was determined with GPS units. To avoid potential problems caused by water saturation of soil porosity, the soil gas survey needs to be performed as much as possible during the dry season, in principle some days after the last rainy day (Battaglini et al., 2013). Determination of CO_2 flux was carried out through the accumulation chamber method by means of the CO_2 flux meter, which was equipped with an infrared gas analyser, a "type-B" accumulation chamber and palmtop device. The chamber was pressed firmly against the ground and loose soil was packed around the chamber, to avoid gas exchanges with the atmosphere. Temperature at 0.5 m bgl was determined by using a thermocouple after the insertion of a titanium pipe in the ground to the programmed depth.
- ✓ *Data Interpretation*: The collected soil gas and temperature data were interpreted by means of probability plots, utilizing the partitioning procedure of Sinclair (1991), to identify individual populations and their statistical parameters, as well as thresholds to be adopted both in the classed

post maps and in the contour maps. Contour maps were drawn by means of geostatistical approaches, such as Kriging (e.g. Clark, 1979). The distribution of gas flux and temperature in the soil was interpreted in terms of possible correlations between anomalies and structural and hydrothermal features (Chiodini et al., 2008).

3.5. Ground magnetic surveys

Subsurface geology can be investigated on the basis of anomalies of the Earth's magnetic field resulting from the lateral variations of magnetic properties of the underlying rocks (see e.g. Telford et al., 1990; Kelly and Mareŝ, 1993). In general, the magnetic behaviour (susceptibility) of rocks is extremely variable depending on the lithotypes and its alteration degree. In a geothermal environment, due to high temperatures, magnetic susceptibility tends to decrease compared to normal geological conditions. High-resolution ground magnetic data can provide maps and models the magnetic anomalies and additional constraints for the structural modelling of the geothermal area. The main results, in terms of magnetic linear trends, can be compared and integrated with the magnetotelluric, gravimetric and geological data. The scheme I usually applied in the magnetic survey field work included the following phases:

- ✓ *Field Work*: The ground magnetic survey was carried out along lines perpendicular to the main geological structures and spaced 50 to 100 m, an optimal spacing between measurement spots is 5 m. During the field campaigns, two proton procession magnetometers were commonly used for the survey. One magnetometer recorded the magnetic field at a fixed base station to monitor the diurnal variation. Three readings were taken at each station and nearby sources of potential interference were annotated in the field book.
- ✓ *Data Correction and Interpretation*: Raw data were corrected for diurnal variation and then displayed as individual profiles and contour maps. An interpretation of the results was finally performed. Digital enhanced maps (vertical and horizontal derivatives, filtering, continuations, terracing, Werner deconvolution) and 2D/3D modelling helped detection of faults and geological contacts, as well as of possible buried volcanic bodies and dykes.

3.6. Gravity surveys

Hidden geological structures and associated faults and fractures, can be revealed by the analysis of the gravity anomalies, in particular in correspondence of positive/negative anomalies or in presence of sharp lateral gradients (see e.g. Parasnis, 1986). Information on subsurface structures can be of help to understand groundwater flow path and, consequently, the geothermal pattern of the investigated area. Positive anomalies could be related to deep magmatic bodies, i.e. potential heat sources, or to layers affected by high-temperature alteration (e.g. propylitization).

Concerning the integration of the different geophysical information, gravity surveys offer significant benefits to the interpretation of magnetotelluric (MT) data (see e.g. Tulinius et al., 2008 and Yu et al., 2009). It is well known that the density models obtained from gravity data are intrinsically non-unique and that the resolution of these models is generally low. Gravity information can be successfully utilized in conjunction with conventional MT data interpretation by performing joint and/or integrated analyses. The resultant models are then reciprocally consistent, because they represent the simultaneous solution of a joint process honouring observed MT and gravity data at the same time and location.

The common scheme of gravity stations distribution used in this study consists of:

- a regular grid with 600-700 m spacing;
- about 15-20 stations at distances of 10 to 20 km away from the focal area for a more realistic definition of the residual Bouguer anomaly map.

Additional stations were sometimes located where abrupt lateral gravimetric variations were recorded, with the objective to clarify these anomalous situations.

The gravity surveys usually included two phases:

- ✓ *Field Work*: Five readings at one minute interval were taken at every station, taking care to avoid actual shifts in the reading point caused by severe vibrations from wind or nearby human activity. Moreover, a reference station was established at a convenient spot and readings were taken at this site every day before starting and at the end of the survey operations, in order to determine the gravimeter drift. All surveys were conducted with a Lacoste-Romberg gravimeter (model G) with a sensitivity of 0.001 mGal, coupled with a high-precision geodetic GPS (vertical accuracy ±10 cm).
- ✓ *Data Interpretation*: Each raw observation from the gravity meter was processed to get the Free Air and Bouguer Anomaly value. The following standard corrections were applied to the acquired gravimetric data: instrument scale factor correction, tide correction, drift correction, gravity computation, normal gravity, free air anomaly, Simple Bouguer anomaly, terrain correction, complete and residual Bouguer anomaly. The Bouguer and terrain corrections both assume a uniform normal reference density to be estimated. Whenever it was possible, rock samples of the different formations were collected form the survey areas, in order to characterize the lithological sequence and use the density values determined in the collected samples for the gravimetric modelling.

  The gravity surveys results were represented in a set of maps (Free air, Bouguer and residual Anomaly maps) and 2D and 3D gravity model, in both the form of cross-sections and slices.

3.7. Transient electromagnetic (TEM) and magnetotelluric (MT) surveys

In modern geothermal exploration, the reconstruction of the underground structure of the geothermal prospects is performed mainly through transient electromagnetic (TEM) and magnetotelluric (MT) techniques. The TEM method employs a transmitter that drives an alternating current into a square loop of insulated electrical cable laid on the ground. The time-variant nature of the primary electromagnetic field creates a secondary electromagnetic field in the ground beneath the loop. Measurements of the secondary currents are made only during the time-off period by a receiver located in the center of the transmitter loop. The intensity of the eddy currents at specific times and depths is determined by the bulk conductivity of subsurface rock units and their contained fluids (see e.g. McNeill, 1994).

The MT (low frequency-deep investigations) methods allow the mapping of the electrical resistivity distribution downward the earth from measurements of natural variations of the surface electric and magnetic fields over a high frequency range. Operations were preceded by one day simultaneous record of the local electromagnetic field via three different stations to verify the plane wave assumption and identify the less disturbed hours (from electromagnetic noise) of the day in which operate (Egbert, 1997; Siripunvaraporn and Egbert, 2000). The application of the remote reference method was evaluated on the base of the preliminary results recorded during the calibration tests. The

simultaneous use of three stations allowed cross-correlation and coherence checks for external electromagnetic noise.

The combination of TEM and MT methods usually gives information of the underground structure to 4-5 km depth. The MT method (low frequency, deep investigations) allows mapping of the electrical resistivity distribution downwards through measurements of natural variations of the surface electric and magnetic fields over a high-frequency range. In particular, the MT method was successfully used to measure subsurface electrical resistivity in complex geothermal systems, detecting variations related to high and low-temperature fluid flows and to distribution of hydrothermal minerals (e.g., Revil et al., 1998; Ólafur, 2005).

The electromagnetic methods allow detection of resistivity anomalies at various depths, which could be associated with geothermal reservoirs (low-resistivity values in the order of 30-50 Ω m), faults and the presence of a cap rock (low-resistivity values in the order of 1-10 Ω m). Geothermal water has high concentrations of dissolved salts, which result in conducting electrolytes within a rock matrix. The electrolytes and the rock matrix (to a lesser extent) are temperature-dependent in such a way that there is large reduction in the bulk resistivity due to increasing temperature. The resulting resistivity is also related to the mineralogical nature of the formations: for example, the presence of clay minerals determines a sharp decrease of resistivity. Therefore, the correlation between low resistivity and fluid concentration/temperature could be not so straightforward (Ussher et al., 2000).

In all the investigated geothermal areas of EARS, the stations distribution followed a common scheme:

- at first, stations were set within the focal area with a regular spacing of about 750 m.
- about 15 more stations were set at the periphery of the focal area with a spacing of 1.5 km.
- finally, additional stations were located where abrupt lateral electro-stratigraphic variations were recorded, with the objective to clarify such anomalous situations.

TEM and MT surveys were developed in this way:

✓ *Field Work*: TEM stations were located through GPS measurements and set in the same spots of the MT stations. They were carried out to furnish detailed shallow conductivity imaging and correct for static shift effect the MT measurements. TEM measurements were usually carried out with external loop of 200x200 m, injecting current of at least 20 A, recording transients from 90 μs to 70 ms with at least 10 data per cycle.

The MT surveys were usually carried out utilizing three MT units, one of which serving as reference station, to be placed at a distance of 20 to 100 km from the geothermal prospect at an electro-magnetically quiet place and to operate throughout the whole duration of the surveys. The other two roving units were operated contemporaneously, recording frequencies between 300 Hz and 0.001 Hz for a period of at least 20 hours. The five electric field sensors (porous pots) for each MT unit were non-polarizable electrodes, to avoid electrochemical effects, and an electrical dipole length of about 100 m was adopted. To avoid potential drift due to bentonite drying, wet bentonite (clay) in electrode holes was sometimes used depending on the recording duration and climatic conditions. The magnetic sensors (one vertical and two horizontal) were broad band induction coils to minimize noise and maximize sensitivity. They were installed in holes, to protect them by temperature variations. The data-acquisition system was based on a 24-bit analogue-to-digital (A/D) converter. In all stations, the vertical component of the magnetic field was measured in addition to the horizontal components of the electric and magnetic fields.

- ✓ *Quality Control*: Quality control and pre-processing was carried out on MT data in the field. It consisted of direct visual inspection of the records, cross-correlation/coherence between channels and three different stations operating simultaneously in the geothermal prospect, computation and analysis of the complex impedance tensor and geomagnetic transfer functions (tipper), determination of 1D apparent resistivities, impedance phases and resistivity pseudosections plots. Both TEM and MT measurements were controlled and pre-processed on a daily basis to verify consistency of the data.

Data Interpretation: The MT and TEM data were finally interpreted with dedicated software, mostly developed in-house. 1D electrical conductivity models up to 400-500 m depth were obtained from of the TEM soundings. MT data were corrected for the static shift error by joint inversion with TEM data and the impedance tensor and tipper were computed by robust MT data processing. MT 1D and 3D inversion and modeling were carried out by *ad-hoc* magnetotelluric inversion codes (e.g. Tulinius et al., 2010). Results were presented as contour maps of resistivity at different elevations; 3D electrical conductivity models, with iso-resistivity maps and resistivity cross sections up to 5 km depth, Moreover Strike analysis with maps showing the Tipper strike were also drawn.

3.8. Microseismicity surveys

This technique is applied to monitor the occurrence of local earthquakes within the neighbourhood of a geothermal play. This yields earthquakes location and their characterization and seismic velocity models (P and S waves) of the geothermal play types. Usually, the area to be studied with micro-seismic monitoring corresponds approximately to the most promising sector of the prospect, which could cover a surface of some tens square kilometers up to more than one hundred square kilometers.

Before analysing the results concerning the earthquake distribution and its interpretation in the key of the geothermal characterization, the conceptual model of seismicity in the geothermal play should be introduced. High-temperature hydrothermal systems are rheologically zoned with depth. A schematic model for active magmatic-hydrothermal systems, involving the seismicity component and derived from several studies of geothermal fields, was proposed by Nielson (1996).

Above the heat source, usually a magmatic zone, intruded by igneous bodies, which may also contribute variable amounts of magmatic fluid to the system, there is a zone that due to the high temperature, has a ductile response to stress. Between the cap rock and the ductile zone, a horizon responding to stress in a brittle way is present, wherein water is able to circulate through fractures. This horizon corresponds to the geothermal reservoir - generally termed hydrothermal circulation zone - and is also characterized by formation of hydrothermal breccia, normally along fault zones. The base of the hydrothermal circulation zone is marked by an increase in the number of earthquakes resulting from an increase in shear resistance. Below this, a discontinuity or a transition zone separates brittle from ductile behaviour. In continental realms, the brittle-ductile transition (BTD) is recognized to occur at temperatures as high as 370-450 °C (e.g. Pasquale et al., 2010 and references therein). By analogy with the oceanic crust, Foulger (1995) claimed that the temperature at which seismic failure likely ceases at Hengill geothermal area (southern Iceland) is about 650±50 °C.

Below the BTD, the temperature gradient increases due to restricted fluid circulation resulting from closure of microcracks related to increase in pressure and sealing by hydrothermal phases. This results in a sharp decrease of seismicity with depth (hypocentral cut-off). According to this conceptual model, one can conclude that the main contribution of a microseismicity survey is the characterization

of the hydrothermal circulation zone (the number of earthquake in this zone can be a proxy of the fracturation degree and permeability) and the identification of brittle-ductile transition zone which can be regarded as a proxy of the 450±100 °C isotherm.

- ✓ *Field Work*: Micro-seismic survey was performed in some of the investigated geothermal plays of EARS (i.e. Alalobeda and Aluto-Langano fields) by using a network of digital mobile seismic stations (e.g. broadband seismic recorder Reftek, model 130S-01/3) equipped with short period 1 Hz seismometers (Lennartz, mod. LE-3Dlite MKII). Stations were synchronized and localized with GPS and equipped with GPRS communication protocol for remote control and data download. Each station was commonly supplied with a 12V battery, re-charged with solar panel. Data were recorded in continuous mode. The seismic networks were planned in order to locate the local earthquakes with a nominal network mesh-grid not exceeding 5 km. As refers to network installation and operation, the following actions were taken:
  - In the course of the installation period, a short acquisition test is needed therefore a survey should last at least 9 months (better 1 year).
  - On site, instrumental control was made performing a cluster test of all stations. This consists of placing all stations with seismometers in a small area (maximum 10 m^2) and in recording the background noise and an active seismic source (mass drop or hammer). Data of cluster test were analysed with component/component and H/V spectral ratio techniques.
  - For each planned site, a preliminary site characterization was made and micro-tremors measurements were performed in order to assess the seismic noise background and to obtain a semi-quantitative indication on the presence of local amplification seismic effects and/or on the stratigraphy of the site. Data were acquired and analyzed using SESAME European Project protocol (Broekstra et al., 2002).
  - After 4-5 months of micro-seismicity monitoring and data processing, if the collected data allowed it, a reconfiguration of the seismic network geometry was possible, in order to optimize the earthquake locations.
- ✓ *Data Interpretation*: The following processing steps were the standard adopted for the recorded data:
  - Events coincidence analysis, consisting of: i) internal coincidence of the seismic network: from the continuous recording of all stations, triggered events were detected by a Short Time Average over Long Time Average (LTA/STA) procedure using different filter parameters; ii) external coincidence with regional events and international earthquakes list; iii) internal and external event coincidences were merged and allowed to extract the final recordings data set of the seismic network.
  - Events spectral characterization, in order to recover the signature and magnitude of the local earthquakes.
  - P and S travel time reading. This operation was performed using the manual P and S picking aided with spectral and particle motion analysis. A check of pickings was performed with a consistence and error analysis.
  - 1D P and S velocity model assessment with travel-time analysis and minimum apparent velocity analysis.
  - Earthquakes location with 1D P-S velocity model using standard location programs (i.e. HYPO type, NLLOC (Klein, 2014). Focal mechanism calculation.
  - Earthquake location and 2D/3D velocity inversion (Thurber, 1992; Lomax et al., 2000).

3.9. Exploration drilling

3.9.1. Foreword

The results of the above described geoscientific investigations should converge in a preliminary conceptual model of the geothermal system and point out suitable sites for exploratory drilling. Once surface exploration of a geothermal system has been carried out, further exploration and evaluation of the geothermal system is mainly based on information gained from wells drilled into the reservoir. Geological samples (drill cuttings and occasionally cores) are obtained from the wells to determine the lithology and alteration of the rocks. The wells make it possible to introduce various measuring instruments right into the heart of the geothermal reservoir and to carry out measurements for estimating reservoir parameters, of which the most important ones for geothermal purposes are reservoir temperature and pressure (Steingrimsson et al., 2006).

Geothermal specialists are stationed at the well site for longer or shorter periods of time throughout the drilling of the well, which typically takes 40-50 days from start to completion of a 2 km deep well. The specialists group consists of well site geologists, logging engineers, and reservoir and drilling engineers. Their duty is to monitor the progress of drilling, analyse drilling parameters and drill cuttings and carry out well logging operations and well tests. They make the preliminary interpretation of the collected data, write daily and preliminary reports. An important part of their work is consultancy at the drill site to the Client and the drilling Contractor and participation in meetings regarding the work. Such consultancy demands a solid general knowledge of geothermal drilling and experience in analysing well data (Gudmundsson, 2005).

In a couple of the case studies (Menengai and Aluto-Langano), object of this thesis, a detailed processing and interpretation of the available wells data were performed and then, the achieved results were utilized as essential input for both feasibility study and numerical simulation of the geothermal reservoirs.

The reconstruction of the temperature and pressure distribution in the reservoir is one of the essential aspects of the geothermal reservoir assessment and is going to be based on the static temperature and pressure profiles of the wells taken after sufficient thermal stabilization. Pressure and Temperature (P&T) distribution gives information on the reservoir extension and on the fluid flow path, with possible location of recharge and outflow zones (Stefanson and Steingrímsson, 1980). P&T conditions, together with the composition of reservoir fluids in terms of Non-Condensable Gases (NCG) and salt content, allow to infer the distribution of thermodynamic conditions distinguishing liquid dominated or vapour dominated zones (if any) and single or two-phase conditions. State-of-the-art models for H_2O-NaCl-CO_2 ternary mixtures are employed to check thermodynamic conditions and evaluate phase properties as function of pressure, temperature and composition (Battistelli et al., 2002).

Well production characteristics need to be analysed, as follows: i) wells deliverability curve, describing how wellhead pressure and production enthalpy change with flow rate; ii) downhole P&T surveys recorded under flowing conditions. A detailed study of the production characteristics of the individual wells is of paramount importance for defining lay-out and design of the conveyance system, as well as to optimize the design parameters of the power plant. The analysis shall also include the reinjection wells, to verify their water absorption capacity (Battistelli et al., 2012).

Dynamic P&T surveys are reviewed to supplement the interpretation of P&T surveys recorded under shut-in conditions, and to evaluate: flash depth and conditions, if any; production temperature of deeper feed zones; pressure drawdown at the bottom as function of production rate. These data are also

used for the calibration of wellbore flow models necessary for the subsequent study of the convenience of using large-diameter instead of conventional diameter wells in order to increase the productivity of the individual well and reduce accordingly the number of required wells.

3.9.2. Monitoring of drilling data

- *Analysis of drill cuttings*

The basic method of geological monitoring during the drilling activities is to analyse the drill cuttings and prepare lithological and alteration logs. Drill cuttings are commonly collected at 5 m intervals. The instrument used for analysis of cuttings at the drill site is a binocular microscope, but if required, XRD-analyses can be performed (within 24 hours). For a better definition of the primary and secondary characteristics of the collected samples, thin sections can be prepared out of the cuttings and studied by means of petrographic microscope. In addition to lithological analyses of the cuttings, other analyses pertinent at the drill site are carried out, such as identification of a possible collapse in a well, metal fragment contamination in the cuttings to trace malfunction in the drill string, and structure of the fragments to assess the conditions of the bit. However, the main purpose is to analyse the geological formations being penetrated and to identify the secondary minerals. During drilling in high-temperature areas it is important to evaluate simultaneously the formation temperature by identifying main index minerals (e.g. actinolite min. temp. of formation: 280 °C (see Franzson, 1998; Kristmannsdóttir, 1979).

Mapping the subsurface stratigraphy is a direct continuation of surface geological mapping. The first exploration well shows the main formations penetrated to some depth and extends the first conceptual model into the geothermal reservoir, including porosity, permeable zones, and chemical composition of the rock. The first wells are located to confirm the geological and geochemical interpretation derived from the surface exploration. Furthermore, drill cuttings together with geophysical logs allow extrapolation with more confidence of tectonic features to some depth.

- *Monitoring of drilling data*

Monitoring of the performance of the drilling operation is conducted through various electronic sensors, the data being computerized and displayed continuously on computer screens. The main parameters monitored are: well depth, penetration rate, weight on bit, rotation of bit, pump pressure, pump rate of the circulating fluid, fluid returns, circulation loss/gain, temperature of circulating fluid and fluid return (Bourdet et al., 1983). Besides, there are some other technical parameters for the rig. The geothermal data collection has been divided into four main categories: i) Measuring the gain or loss of the circulation fluid; ii) Measuring the temperature of the circulation fluid up and down; iii) Measuring the amount of the circulation fluid pumped down and the pressure of the pumps; iv) Measuring the temperature close to the bit while drilling (MWD).

3.9.3. Basics of well testing

One of the early stages of reservoir engineering is to estimate the relevant reservoir and wellbore parameters by a P&T test (Rutagarama, 2012). This information is needed to confirm whether a well is satisfactorily drilled and decide how to exploit the reservoir. The main reservoir and wellbore parameters to be determined are permeability, formation storage (or the storativity), skin factor and wellbore storage. The type of reservoir (porous or fractured) and the type and location of the reservoir boundaries are also important. Several kinds of tests may be designed to determine the above-mentioned parameters and reservoir properties.

3.9.4. *Well testing description*

A well test can be defined as a fluid flow test conducted in wells to obtain data and information on the properties of the reservoir and of the well. Well tests are conducted before exploiting the reservoir, as well as after a period of production, to see whether and how much the reservoir properties have changed/evolved. During a well test, the temperature and the pressure response of the reservoir to changing production (or injection) conditions is monitored. The pressure can be measured within the well itself where the flow rate has been changed or in neighbouring wells (Horne, 1995), performing an interference test. Since the pressure response depends on the properties of the reservoir, it is possible to deduce various reservoir properties from the pressure response.

In practice, well testing (or pressure transient tests) essentially consists of changing the well's flow rate in terms of either fluid production from it or injection into it and measuring the well's response as a function of time. The shape of the reservoir response can then be matched against an archive of type curves to identify a suitable reservoir model/type. Finally, the model is fitted to the data and the reservoir and well parameters deduced from the model. To do so a mathematical model is built to describe the fluid flow in the reservoir/well system (Horne, 1995; Bourdarot, 1998). The procedure is illustrated in Figure 3-1.

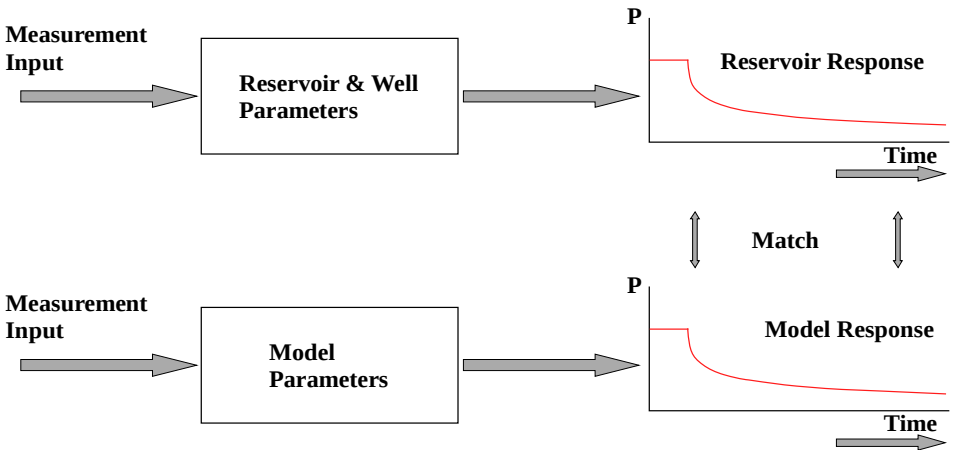

Figure 3-1 Well testing procedure (modified from Horne, 1995)

3.9.5. *Wellbore storage*

Well testing measurements are commonly carried out at two specific locations, namely: downhole and at the wellhead. In the latter case, an additional parameter, the wellbore storage, has to be considered when evaluating the reservoir system. When the well is opened to flow, the fluid at surface is initially dominated by the expansion of the fluid stored in the wellbore and the reservoir contribution is negligible. Similarly, when a well is shut-in, the flow rate will be zero at the top of the well, but will not drop to zero instantaneously at the bottom of the well, due to the compressibility of the fluid in the wellbore. In this case, the wellbore storage effect is called "after-flow" (Bourdet, 2002).

It has to be emphasised that the wellbore storage cannot be interpreted literally to give a wellbore volume. It should be considered as a nuisance effect that affects the form of the pressure transient curves. The wellbore storage is quantified in terms of a coefficient, C, which represents the volume of fluid that the wellbore itself will produce due to a unit drop of pressure (Grant & Bixley, 2011).

3.9.6. *Skin effect and turbulence*

Drilling of a well and well treatment operations cause changes of the reservoir characteristics in the vicinity of the well as compared to those further away in the reservoir. This effect is known as the *skin effect*. Mathematically, in a reservoir model, skin is represented as a region of increased or decreased permeability surrounding the wellbore (Figure 3-2). The skin factor, *s*, can be positive or negative.

Positive skin (damaged well) means an increase in pressure drop and negative skin (stimulated well) means a decrease in pressure drop at the interface between the reservoir and the wellbore (Agarwal et al., 1970; Ramey, 1970). Productive geothermal wells usually display a negative skin factor. According to Horne (1995), the skin effect can be described in terms of an effective wellbore radius, corresponding to the apparent well radius due to the reduction or increase in flow caused by the skin effect.

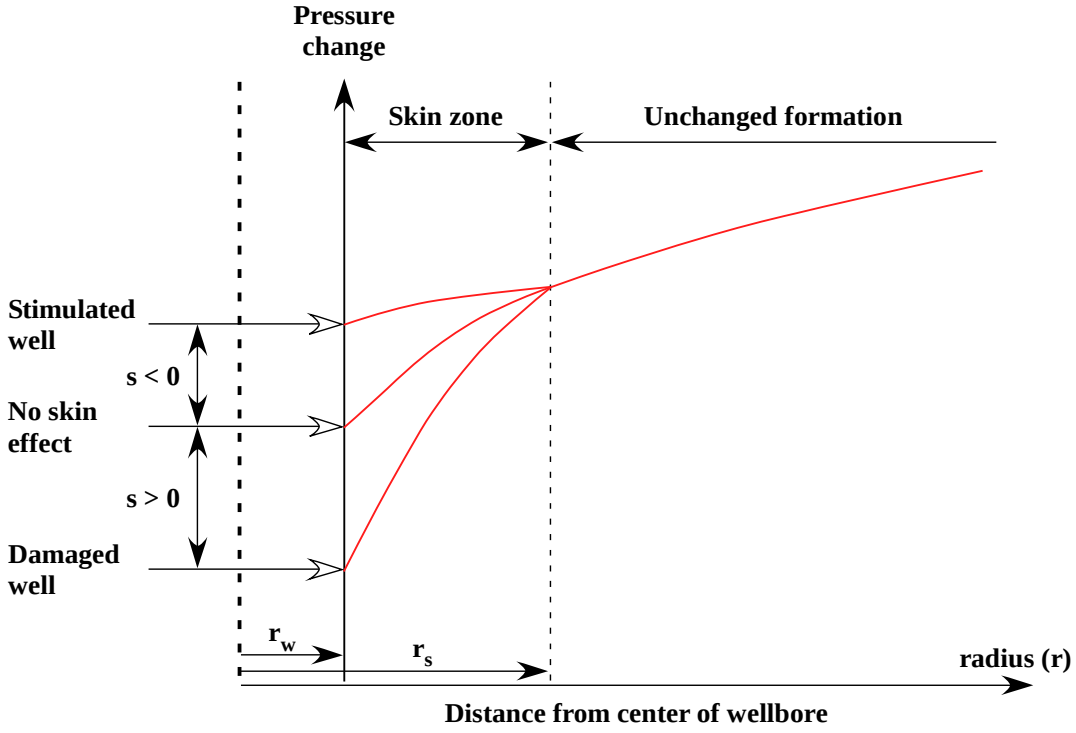

Figure 3-2 Pressure changes around a wellbore due to the skin effect (modified from Horne, 1995). Where: r_w is the wellbore radius; r_s is the altered zone radius; *s* is the skin factor

At high flow rates, or in fractured reservoirs, fluid flow tends to be turbulent, and Darcy's law is no longer applicable. Skin due to turbulent flow or non-Darcy flow is the additional pressure drop caused by high fluid velocity near the wellbore. Depending on the rate this effect can be significant and must be accounted for. It has to be noted that skin due to turbulence is always positive and is a part of the total skin. Thus, a production test on a stimulated well can still yield a positive total skin, s, value due to the turbulent component, even if no skin damage is present.

3.9.7. *Types of well tests*

During conventional well tests, fluid is extracted to the surface or injected into the well at controlled rates. A program of flow and shut in periods is used to establish deliverability and completion efficiency of the well. Tests can involve a single well or many wells. Depending on test objectives and

operational considerations, a range of well tests can be carried out. The tests usually fall into the following categories (Horne, 1995; Bourdet, 2002):

- *Build-up test*: This test is conducted in a well that has been producing for some time at a constant rate and is then shut-in. The build-up downhole pressure, measured in correspondence of the main feed zone or in case of doubts in front of the deepest one, is then recorded for a given time.
- *Drawdown test*: This test is conducted with a well flowed at a constant rate. The downhole pressure and the production rate are measured as functions of time and analysed to estimate the reservoir properties. The major difficulty of this test is the difficulty of maintaining a constant flow rate.
- *Injection test*: This test is identical to a drawdown test, except for the fact that flow takes place into the well rather than outside of it. Fluid is injected into the well at a constant rate and the injection rate and the downhole pressure are measured as functions of time.
- *Fall-off test*: This test is analogous to a build-up test and measures the pressure decline as a function of time subsequent to the interruption of injection. Measurements are taken in correspondence of the main feed zone or, in case of doubts, in front of the deepest one.

The combined response can be interpreted in a number of ways to estimate the permeability-thickness and the skin factor. Figure 3-3 illustrates the types of well tests defined here.

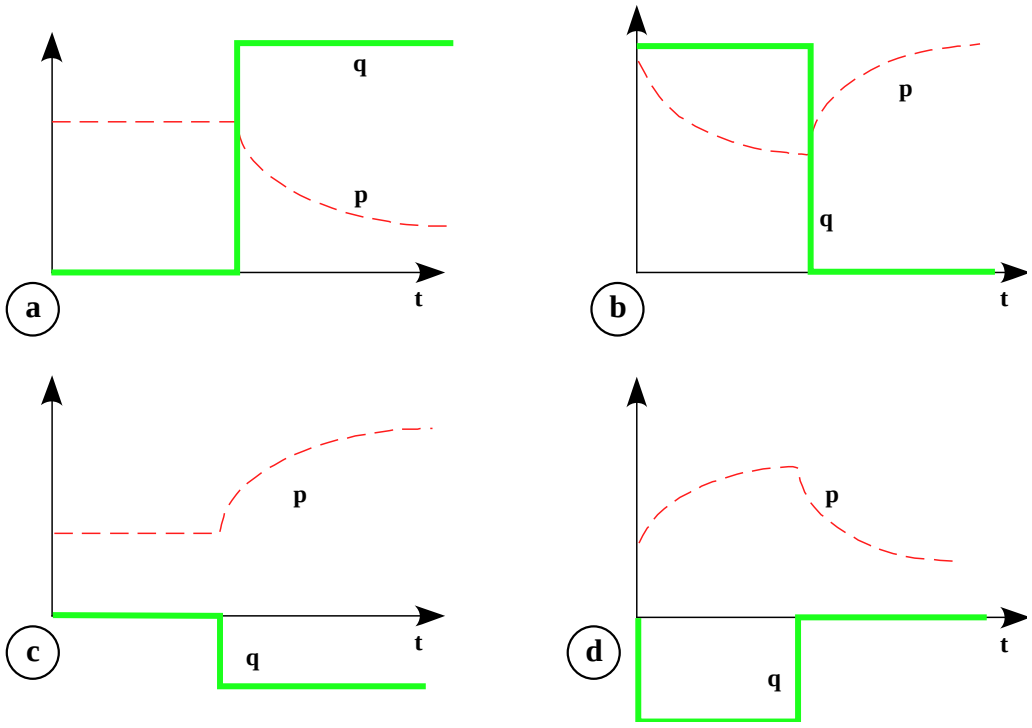

Figure 3-3 Types of well tests: a) Drawdown test, b) Build-up test, c) Injection test and d) Falloff test (Horne, 1995) (modified from Horne, 1995). Where: *t* is time; *p* is pressure; *q* is flow

One of the most important tests to be performed once a few wells have been drilled in different wellpads is the *Interference Test*. In this test, one well is under production and pressure is monitored in a different well (or wells). An interference test monitors pressure changes out in the reservoir, at a distance from the original producing well. The advantage of interference testing is that a much greater area of the reservoir is tested, providing estimates of reservoir properties between wells.

In addition, the interference response is little affected by the complicating factors of wellbore storage and skin effect that make single well test interpretation more difficult. Furthermore, the nature of the response over distance makes it possible to estimate not only the *reservoir transmissivity* (*kh*), but also *storativity* (φCth). The disadvantage is that pressure drops can be very small over distance, and are affected by other operational variations in the field at large. However, modern electronic gauges are quite capable of registering such small pressure drops (often less than 1 psi over days or even weeks), and thus interference testing is a powerful method of proving up new discoveries. In "new" reservoirs, an interference test is not affected by other production in the field (since there is none) and serves to prove the existence of productive reservoir between the wells (Horne, 1995).

To process interference test data the type-curve matching technique is commonly used with semi-log method and computerized fitting (Earlougher, 1977; Horne, 1995). There are some other innovative methods described by either Eppelbaum and Kutasov (2008), who introduced the hydraulic diffusivity of formations (η) or Néstor and Fernando (2001), who analysed the pressure interference test through the use of the pressure derivative.

4. THE EAST AFRICAN RIFT SYSTEM

4.1. Regional tectonic setting

The East African Rift System (EARS) is the most extensive, currently active zone of continental rifting in the world and it is often considered as a model for the break-up of continents and the onset of ocean basin formation (Brown and Girdler, 1980; Chorowicz, 2005). The Precambrian basement of East Africa consists of the Archean Tanzanian craton, which is in the center of the East African Plateau, and of a number of Proterozoic mobile surrounding belts (Figure 4-1). The EARS consists of several segments cutting through the continent from the Afar region in Eritrea and Ethiopia down to South Africa. The well-expressed eastern branch traverses Ethiopia (Main Ethiopian Rift) and Kenya (Gregory Rift). At its termination in northeast Tanzania, it intersects the margin of the craton, and the graben structures found to the north give way to a much wider zone of block faulting (Ebinger et al., 1998; Foster et al., 1997).

The western rift, on its side, comprises numerous en-echelon fault bounded basins (Ebinger et al., 1989), many of which contain deep lakes. The Tanzania Craton is surrounded on its southern and eastern sides by the Paleozoic Usugara Belt (Mruma, 1995; Fritz et al., 2005); the northeastern extension is poorly defined, as it was reworked into the Pan-Africa Mozambique Belts (Pinna et al., 2004).

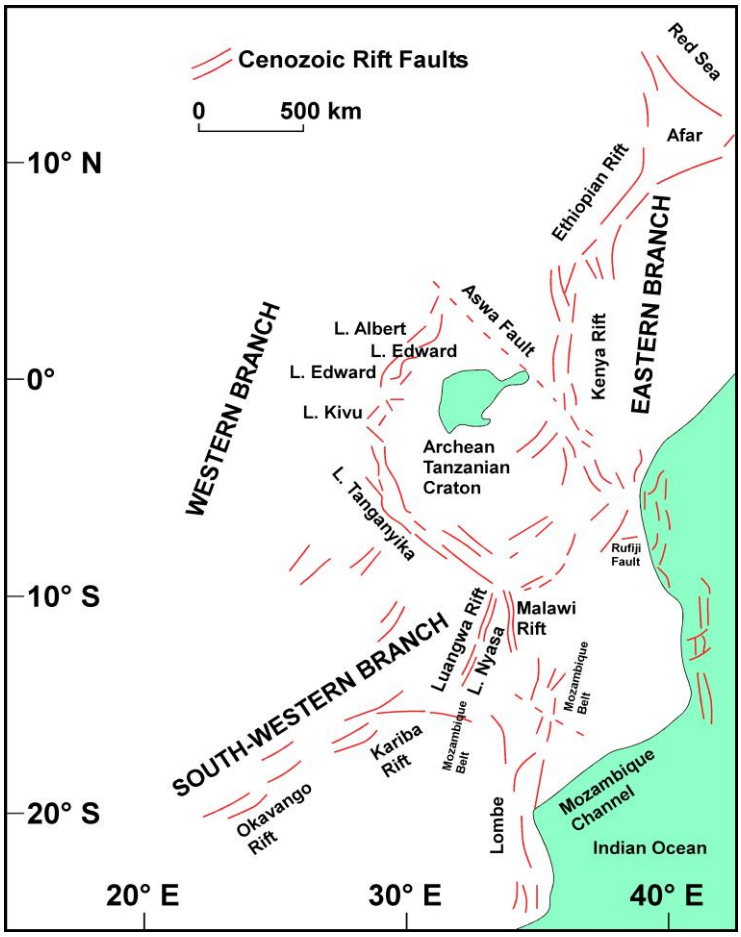

Figure 4-1 Structural scheme showing the African Rift System (Modified from Atekwana et al., 2004)

In the southeastern side of Tanzania, the coastal basin splits in two branches. One branch runs along the margin of the Precambrian basement of the Mozambique Belt, having a NNE-SSW direction. This branch of the basin corresponds to a Karoo rift (Selous rift system) developed since Permo-Triassic. Karoo sediments, in fact, crop out to the west, along the Uluguru basement massif from which they are separated by the Rufiji Fault. The second branch develops in NNW-SSE direction along the coast, separated from the first one by a spur of basement, still belonging to the Proterozoic Mozambique Belt. This portion of the coastal basin contains a sedimentary sequence spanning in time from Permo-Carboniferous to Cretaceous and is affected by faults trending NNW-SSE (Lindi trend system), having a downthrow to the east, representing the western side of the major rift extending into the Mozambique Channel.

In the rift axis of the eastern branch, numerous volcanoes of Quaternary age occur whose products overlie Miocene and Pliocene volcanic products (Omenda, 2010). The shield volcanoes are largely formed by intermediate lavas and the associated pyroclastics, thus indicating the presence of shallow hot bodies (magma chambers). In the Western Branch, there is paucity of volcanism along the entire length of the rift with the main volcanic areas being Virunga and Rungwe. The geothermal activity in the EARS consists of hot springs, fumaroles, hot and hydrothermally altered grounds and is closely associated with shallow hot magma bodies under the Quaternary volcanoes, which act as heat sources. In the Afar rift, where the crust is as thin as 5 km, extensive manifestations and high heat flux are due to a combination of mantle heat and magma bodies occurring at shallow depths. In the less magmatic western branch of the rift, heat sources could be combination of buried plutons and high heat flux associated with thinned crust.

Using today's technologies, Eastern Africa has the potential to generate over 5,000 MW of energy from geothermal power. Despite this potential, so far only Kenya and Ethiopia have a geothermal generation of 270 MW and 7.2 MW, respectively. Different projects of geothermal exploration and research have been undertaken in Djibouti, Eritrea, Uganda, Tanzania, Zambia and Malawi (Zemedkun, 2018).

The Main Ethiopian Rift (MER) and Afar Rift represent the northernmost part of the East African Rift (Figure 4-1). Volcanic activity in Djibouti, Eritrea and Ethiopia started at about 30 Ma with uplift followed by eruption of large volumes of basalts (Mohr and Zanettin, 1988). However, activity reduced since the Miocene times with eruptions of bimodal suite (basalts and more alkaline silicic lavas) concentrated within the rift zone. More recent activity in the axis of the rift consisted of rhyolite volcanoes and domes as well as ignimbrites and nonconsolidated pyroclastics. Studies by Mohr (1992) indicate that over 90 % of the eruptive are of silicic composition.

In the axis of the rift occurs the Wonji fault belt (central part of Ethiopia), which is a region of Quaternary crustal extension. The fault zone is offset in several locations along its length and some of the large volcanoes, including Aluto-Langano (one of the case studies) are located at the fault intersections (Omenda, 2010).

The Afar rift is the most active segment of the entire EARS, with the Erta Ale's lava lake (Ethiopia) being presently active. The Afar rift floor is dotted with a large number of rhyolitic volcanoes in the south and more basaltic centres in the north. The surface geology in the south is similar to that of the MER, where ignimbrites are abundant whereas in the north basalt sheets of Quaternary age dominate. The volcanics overlie older sedimentary rocks in the Afar rift zone.

Geothermal manifestations occur as fumaroles, hydrothermally altered grounds, steaming grounds and hot springs in many locations, most of which are associated with young volcanic fields in

the rift valley. Hot springs also occur on the flanks of the rift where they are associated with Tertiary faulting episodes. The manifestations are more pronounced and vigorous within the axis of the rifts than on the flanks due to the favourable hydrology and relatively shallow heat sources. The heat sources for the geothermal systems are related to (1) shallow magma chambers associated with the young rhyolite volcanoes that are common in the southern Afar and MER and (2) upper mantle intrusion/upwelling associated with the thin crust in the area that averages between 5 and 20 km.

4.2. The Kenya Rift (Eastern Branch)

The Kenya rift (Gregory Rift) is the segment of EARS that extends from Lake Turkana to northern Tanzania (see Figure 4-2). The formation of the Kenya rift started about early Miocene in the north around Lake Turkana and migrated southwards, being active from about middle to late Miocene in the central segment. The development of the rift largely occurred within the Late Proterozoic basement of Mozambique belt and close to the eastern margin of the Tanzania craton.

In terms of geodynamic processes the formation of the rift begun by up-doming and volcanism on the crest of uplift and followed by faulting to form a half graben. The formation of a full graben occurred during the early Pleistocene, on the floor lava flows of basaltic and trachytic composition were erupted, and intercalated with tuffs. Subsequently, sheet trachytes were grid faulted with dominant north-south closely spaced faults. In Quaternary times, many large shield volcanoes of silicic composition in the axis of the rift developed (Dunkley et al., 1993).

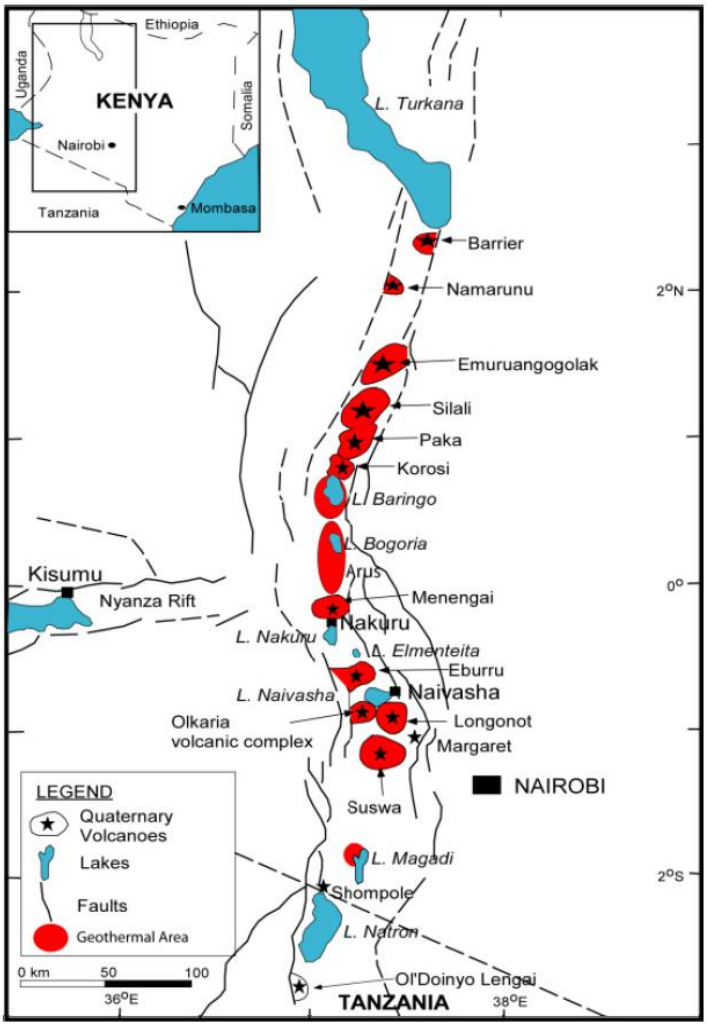

Figure 4-2 Map of the Kenya rift showing the locations of geothermal areas (modified from Omenda, 2010)

Activity in the southern extreme of Kenya and northern Tanzania segment of the Kenya rift is dominated by alkaline and carbonatitic volcanism of which Ol'Doinyo Lengai is well known. Prevalence of the carbonatites in the region is attributed to deep source of the lavas occasioned by the thick cratonic crust in the region (Van Straaten, 1989). Alkaline lavas are predominant in the areas around Kilimanjaro where micro-rift grabens occur near Arusha and further south.

The entire length of the Kenya rift from Lake Turkana in the north (northern Tanzania) has young volcanoes dominantly of silicic composition in its axis. The youthfulness of the volcanoes attests to active magmatism under the rift. Similarly, geothermal manifestations are more abundant and stronger within the rift and in many cases, they are associated with the Quaternary volcanoes.

Geothermal manifestations in the Kenya rift include fumaroles, hot springs, spouting springs, hot and hydrothermally altered grounds and solfatara (sulphur deposits). Fumaroles commonly occur on the mountains whreas hot springs and geysers are common on the lowlands.

Olkaria and Menengai (one the case studies analyzed) geothermal prospects were developed for electricity generation while a pilot plant is planned for Eburru. The Olkaria, Menengai and Eburru geothermal systems are volcano hosted resources and thus, the heat driving the systems are associated with hot intrusive bodies under the volcanic complexes.

4.3. Western Branch

The western branch of the rift runs along the western side of Lake Victoria and along the edge of the East African plateau (Figure 4-3). It typically exhibits half grabens characterized by high-angle normal rift faults. The western branch of the rift is characterized by paucity of volcanism with respect to the Kenyan and Ethiopian rifts. Whereas the volcanism and tectonic activity in eastern branch commenced about 30 Ma ago in the eastern branch of the rift, volcanic activity in the western branch started about 12 Ma in the north, near Lake Albert and about 7 Ma in the Tanganyika rift (Ebinger et al., 1989).

The northern zones of the rift comprise several basins that define the Albertine Graben near Lake Albert. The Lake Albert rift started early Miocene and is dominated by thick sequence of sediments and is largely non-magmatic, except for the southern basins wherein volcanic products occur. The Albertine basin is also thought to have petroleum potential. The western branch is characterized by the abundance of potassic alkaline rocks that consists of carbonatites, ultrapotassic mafic rocks and potassic mafic-felsic lava. Volcanic activity is more intense in the Virunga volcanic field where Nyiragongo and Nyamuragira in the DR Congo are active with generally silica-undersatured basaltic eruptives.

The Tanganyika-Rukwa-Malawi (TRM) segment of the western branch follows the fabric of the basement structures inherited from the Proterozoic period (Bennett, 2008). The rift is characterized by normal boundary faults, which define half grabens, horsts and step faults with riftward tiled blocks and monoclinal structures (ELC-MoNREM, 2018). The Malawi segment extends south to the Urema and Lebombo grabens in southern Mozambique. Within the rifts occur lakes Tanganyika and Malawi, which are deep sedimentary basins. The rift segment was largely non-magmatic during the Quaternary times since volcanic fields only occur at Rungwe between lakes Tanganyika and Rukwa. Late Cenozoic volcanism started about 9-7 Ma ago in the Rungwe volcanic province where the rift follows the NE-SW trend in line with the Kenya rift. The volcanic products include Quaternary mafic and felsic rocks (Laó-Dávila et al., 2015).

There is scarcity of recent volcanism in this segment of the rift (Scholz, 2006). The manifestations in the TRM Rift include mainly hot springs at temperatures of up to 86 °C, which occur at Mbeya within the Quaternary Rungwe Volcanic Province (RVP), but they seem controlled by fault leakage (ELC-TGDC, 2018). The area is also characterized by high seismicity signifying that the area is still tectonically and magmatically active (Kiejo eruption occurred in the last 17th Century). Other hot springs occurring in Malawi, Zambia and Mozambique are fault-controlled and are associated with the border faults (ELC-TGDC, 2018). The hot springs are probably due to deep circulation of groundwater through the rift structures.

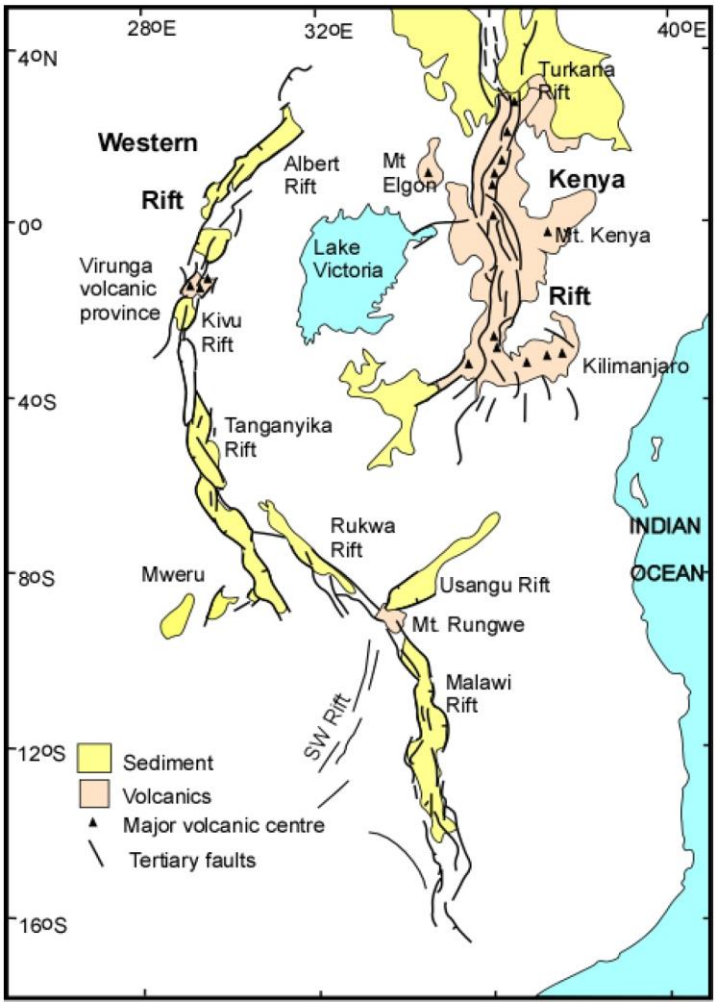

Figure 4-3 Map showing the structural relationship between the Eastern (Kenya) and Western branches of the EA Rift system (modified from Omenda, 2010)

4.4. Regional geophysical features

The East African Rift System is generally considered as an example of continental breakup at its early stages. In this section, such breakup is examined trough results of investigations, obtained from various geophysical techniques, of the deep structure below the EARS, focussed the Kenyan Rift, wherein several important geothermal systems occur.

4.4.1. Gravity studies

From a general understanding of rifts, it is expected that gravity anomalies could result from a number of causes. The infilling on the rift floor by low-density lavas and sediments should produce a

negative anomaly. However, the shallowing in depth to the Moho resulting from crustal thinning, which brings the denser mantle closer to the surface, will produce a positive anomaly (e.g. Arab, 1972). However, this positive anomaly is likely to be reduced by the mantle beneath the rift being hotter and so having a lower density than normal mantle to either side. The crust shows lateral variations of density due to the association with rocks of different density. Resolving all these causes is not possible by gravity alone, but because of the effort and cost of obtaining seismic and other geophysical data on a regional scale, many of the early concepts about the deep structure of the rift were based on gravity data, and some of the early models are described hereinafter.

The first study was carried out in the early 1930s (using pendulum measurements rather than modern gravimeters). It was a large-scale survey and established that the uplifted plateau on the east side of the rift was isostatically compensated but over the rift gravity is negative (Birt et al., 1997). Later, more detailed surveys exhibited that gravity in the rift is much more complicated than the simple broad negative anomaly found in the early studies (see Figure 4-4).

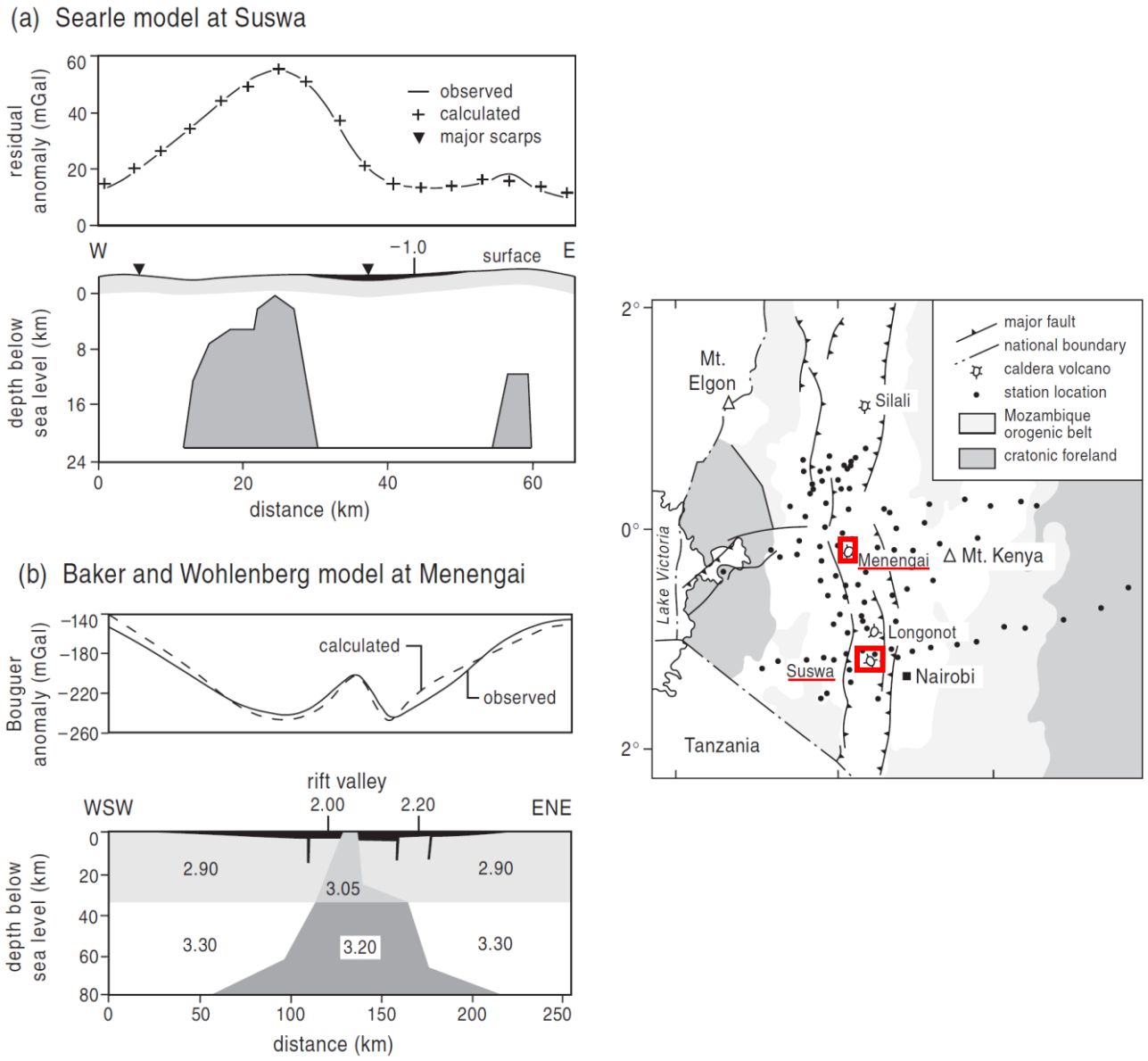

Figure 4-4 Gravity profile models across the Kenya Rift (densities in Mg/m^3) in (a) Suswa and (b) Menengai geothermal prospects (modified from Musset et al., 2000)

For example, a gravity profile across the rift in the vicinity of the volcano Suswa showed a positive anomaly within the broad negative (Figure 4-4a). This was interpreted by Searle (1970) in terms of a dense mantle-derived intrusion 20 km wide extending from a depth of 20 km to within 2 or 3 km of the rift floor. Independently, Baker and Wohlenberg (1971) interpreted the positive anomaly observed along the Menengai profile (further north) as also being due to high-density material intruded into the crust. In addition, they attributed the broad negative anomaly to anomalous mantle material with lower than average density due to higher temperature beneath the rift (Searle, 1970). Menengai geothermal prospect is one of the case studies analyzed in the present thesis and the above-described interpretation was validated by new gravimetric survey/data processing carried out in the present study.

These two models stimulated a lot of interest in the rift because they implied, by their wide intrusions along the axis of the rift, that crustal separation had already taken place by ten or more kilometres (i.e., that the continent had already split). Clearly, the gravity models proposed are speculative, largely due to the no uniqueness of the method, as they lack independent information on densities or depths of the postulated bodies. This could be provided from boreholes data (as from the geothermal deep wells drilled in the Menengai prospect in 2011-2014) or seismic surveys. Furthermore, a more refined model has been defined by combining seismic and gravity data (see section 4.4.5. Combined seismic and gravity models).

4.4.2. Seismicity

The continuous belt of earthquakes extending from the Carlsberg Ridge into the Gulf of Aden, (Red Sea) and the East African Rift System is well known and clearly delineates the plate boundaries (Figure 4-5). Though seismicity is clearly associated with the Rift (Birt et al., 1997), fewer earthquakes with high magnitude were being recorded in the Ethiopian-Kenya Rift system than the Western Rift even though the greater volcanism in the Eastern Rift suggests there would be greater activity there. However, there is the probability that additional "weak" earthquakes might be occurring in the Eastern Rift but were too small to be recorded by the global network, which had only a single station in Kenya. To verify this hypothesis, temporary local networks with up to a few tens of stations were set up in the Kenya Rift in the 1990's (Birt et al., 1997). The new seismicity records showed that tens of small earthquakes did occur every day, with magnitudes down to $M \leq 3$ (Figure 4-6).

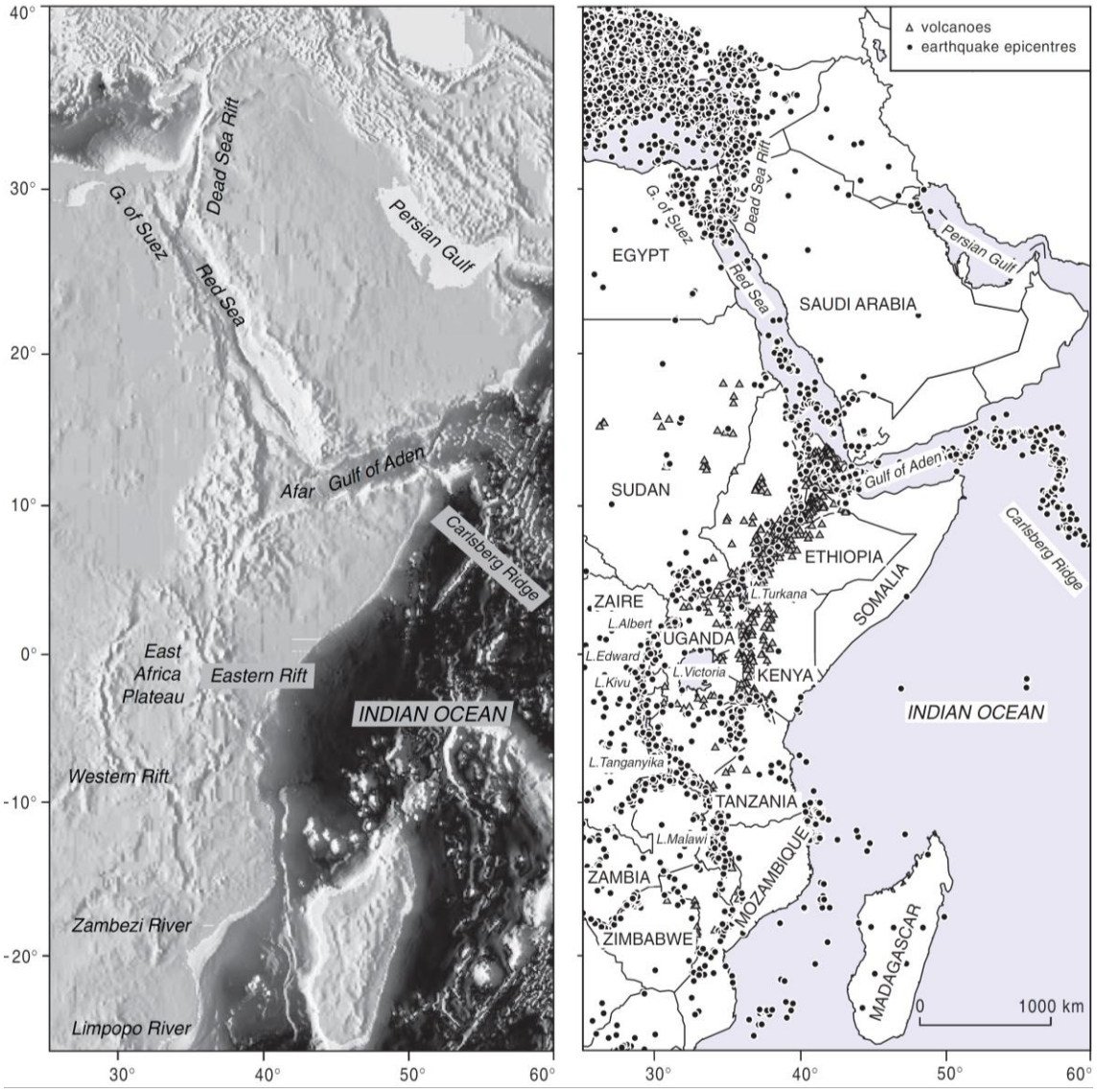

Figure 4-5 Left: digital elevation model. Right: earthquakes location, and volcanoes of the Afro-Arabian Rift System. Earthquakes epicentres were derived from events recorded by World Wide Standard Seismograph Network (WWSSN). (modified from Musset et al., 2000)

Most of the seismic activity occurs as swarms within the rift, at depths ranging from 5 to 10 km; surprisingly few occur on the main rift faults. Some of this activity was attributed to movement of geothermal fluids (as directly verified in the Menengai case study) or the propagation of dykes in the upper crust. In addition to the location of earthquakes, seismic recordings can reveal their fault planes and sense of motion, or the tensional and compressional axes associated with them. Wherefore, data recorded by the WWSSN and by the temporary local networks in Kenya show that the stress directions are those expected for crustal extension across the rifts.

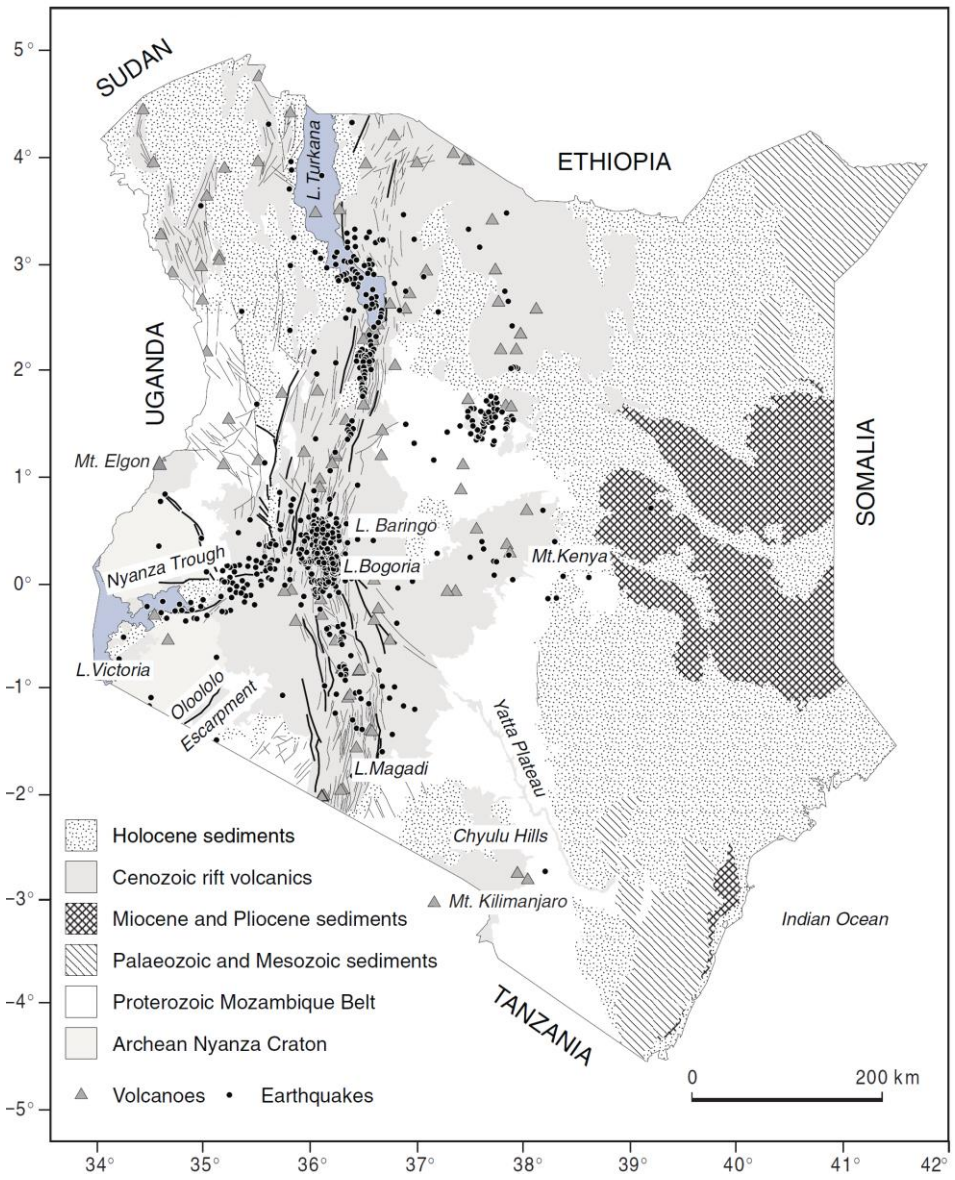

Figure 4-6 Simplified geologic map of Kenya with earthquake epicentres and volcanoes (modified from Musset et al., 2000)

4.4.3. Teleseismic studies

Besides composition, the seismic velocities of rocks depend on temperature, especially towards the melting points. This can be used for comparing temperatures in the upper mantle beneath different parts of a region, because at this depth the composition is likely to be laterally uniform. Velocities can be found using refraction surveys, but these imply large costs. A less expensive, though less accurate, alternative is to utilise distant earthquakes as seismic sources (Khan et al., 1998). For Teleseismic sources, which are at least 2000 km (18° epicentral angle) distant, the rays travel up to the surface at a fairly steep angle and so spend minimal time in the variable crustal rocks. In case of some portions of the subsurface are hotter, the seismic velocity will be lowered and so rays that pass through them will be delayed relative to those travelling through cooler rocks. By recording arrivals from earthquakes in different directions, the hotter region can be located and its form roughly estimated tomographically. In Kenya, the WWSSN station near Nairobi, which is very close to the Rift, recorded arrivals about 2 sec late relative to Bulawayo (Zimbabwe), which is undoubtedly on normal continental crust, therefore indicating that the rocks at depth near the Rift are hotter.

4.4.4. Seismic refraction and wide-angle reflection surveys

Teleseismic studies, for their resolution (lack of details) is limited by station spacing, and uncertainties in the origin time, location, and source characteristics of the earthquakes recorded. For higher resolution, controlled sources and closely spaced stations are needed, though the depth of investigation is limited to about 50 km for practical reasons (e.g. Brabham and McDonald, 1992).

In the Kenya Rift International Seismic Project (KRISP, 1989-1990), a series of experiments, were conducted applying controlled sources (Prodehla et al., 1997). Five profiles were shot (see Figure 4-7). For the required resolution, an average station spacing of less than 2 km was needed and over 200 portable recorders were used. One profile was along the Rift axis (A to C), two across the Rift (D and G), and two outside the Rift (E and F). Figure 4-8 shows a sample of the data, with each trace (reduced plot) showing the vertical component of a seismic recorder.

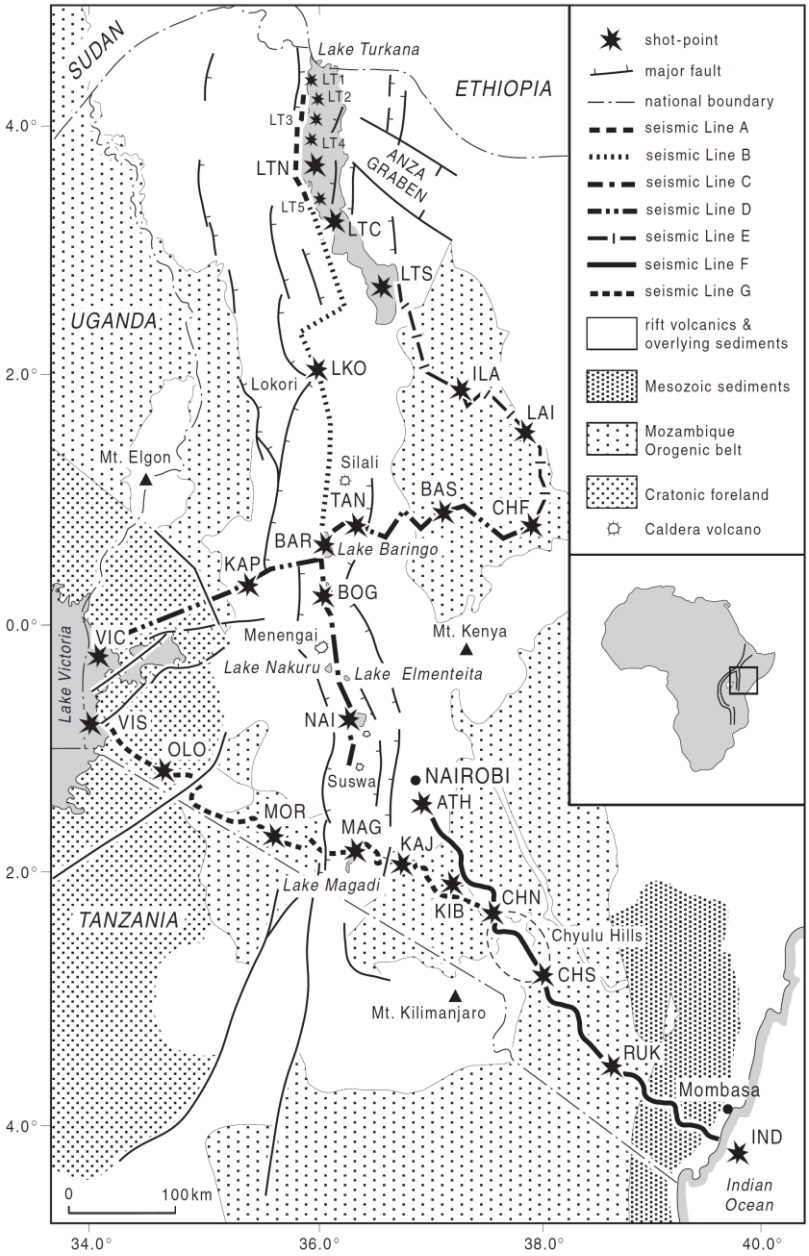

Figure 4-7 Locations of seismic refraction lines performed during the KRISP experiments (modified from Prodehla et al., 1997)

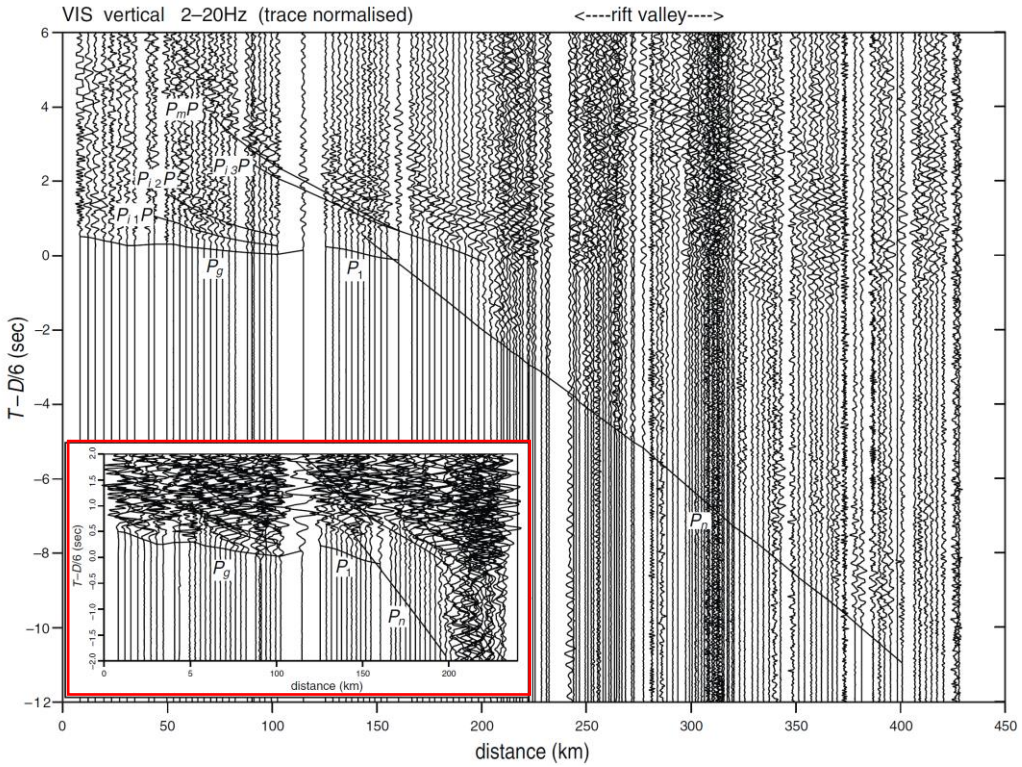

Figure 4-8 Reduced record section for Line G (modified from Prodehl et al., 1997)

Together with the refracted phases Pg, P1 and Pn, there are some later phases, Pi1P, Pi2P, Pi3P, and PmP, which are due to wide angle reflections from the tops of intracrustal boundaries and the Moho (Prodehla et al., 1997). In the inset (red rectangle in Figure 4-8), the amplitudes were increased to show the mantle arrivals more clearly. Figure 4-9 shows the model inferred to account for the arrival times of the phases, obtained from a preliminary simple model, built from the slope and intercept times, refined by adjusting the velocities until the travel times calculated for the rays shown on the model (Figure 4-9a) matched the ones recorded. Figure 4-9b shows the travel-times calculated from the model and those shown on Figure 4-8, Figure 4-9c is the final model, taking into account all the arrivals from all shots into the line (Slack and Davis, 1994). Other profiles were treated in the same way.

There are some clear differences in the crustal structure below the Rift compared to outside it. Far from the Rift, the crust is "stratified", with thickness varying between 33 and 44 km, and overlies mantle with the typical velocity of 8.0 to 8.2 km s^{-1}; underneath the rift, the mantle velocity is anomalously low, being between 7.5 and 7.7 km s^{-1} (Prodehla et al., 1997).

The crustal thickness also changes, being thicker (about 35 km) north of Nairobi and close to the summit of the Kenya dome, where the Rift is about 60 km wide up to only 20 km in Turkana, where the rifted zone is about 180 km wide, indicating that extension has been much greater in the latter area. A thinned crust is expected from the combination of elevation and high Bouguer anomaly in the region. Observing in detail at the E-W section of Line D (Figure 4-7), it crosses the Rift near the top of the Kenya dome, the uppermost layer is referred to a basin filled with sediments and volcanics, which have low seismic velocities (Khan et al., 1998). The basin is asymmetric, being about 8.7 km thick against the bounding fault to the west but thinning eastwards. Velocity increases from 3.8 km s^{-1} at the top of the infill to about 5.8 km s^{-1} at its base. Below the sedimentary basin, in the upper crust, velocity is from 6.1 to 6.4 km s^{-1}, the highest values being in the Archaean rocks at the western side. Velocity also increases downwards through the middle and lower crust to 7.1 km s^{-1}. The section also shows that crustal thinning of about 5 km, overlying anomalous mantle, is confined to the Rift zone itself. Across the

southern flank of the dome uplift, the structure beneath Line G (see Figure 4-9) shows similar features, but more subdued compared to the above-described Line D.

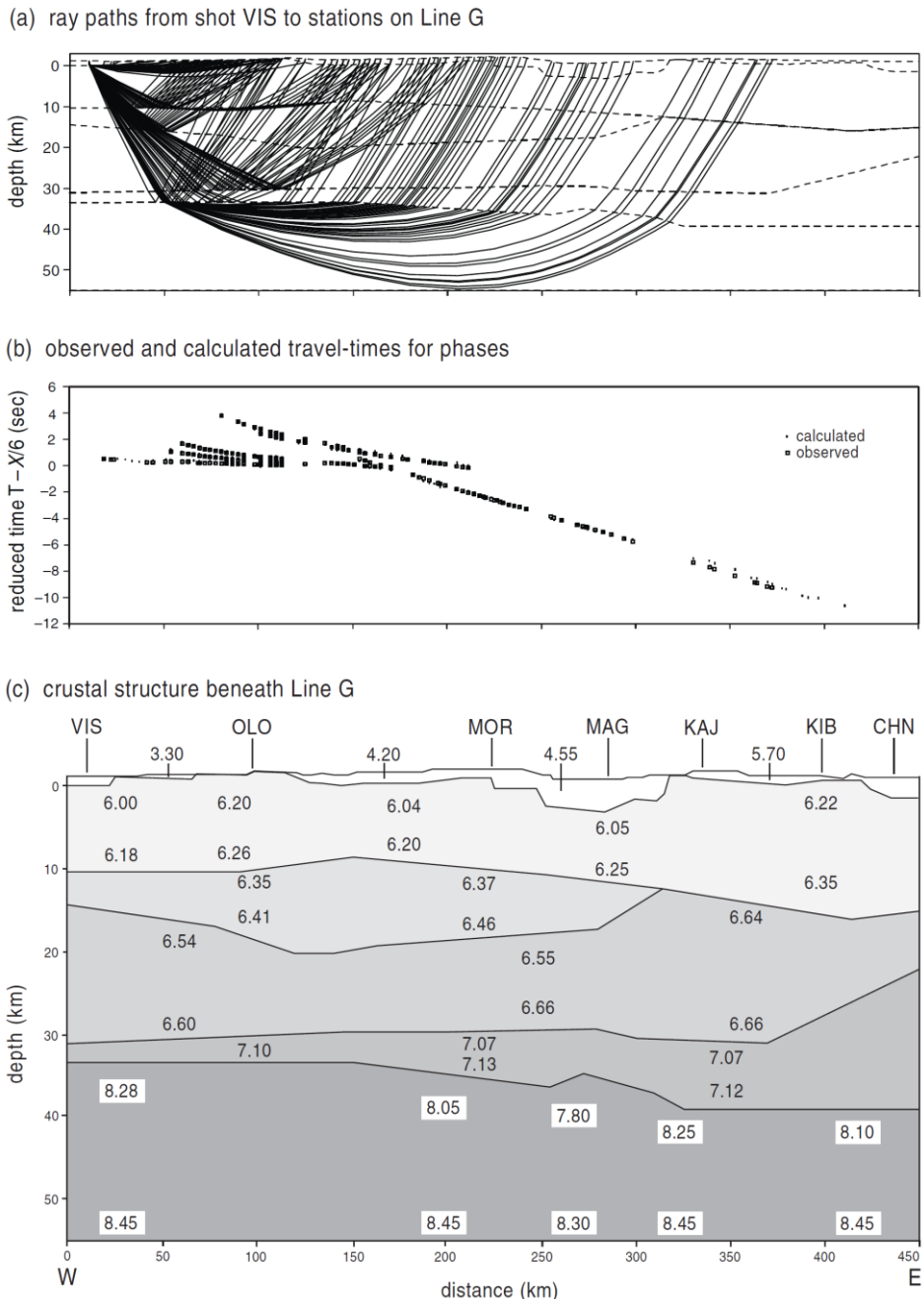

Figure 4-9 Seismic model for Line G (see also Figure 4-7 for location; modified from Prodehla et al., 1997)

The differences between the properties of the crust east and west of the Rift support the idea that the rifting is developing along the old suture zone between the Archaean Nyanza craton to the west and the Proterozoic Mozambique Belt to the east, as illustrated in the schematic cross-section of Figure 4-10.

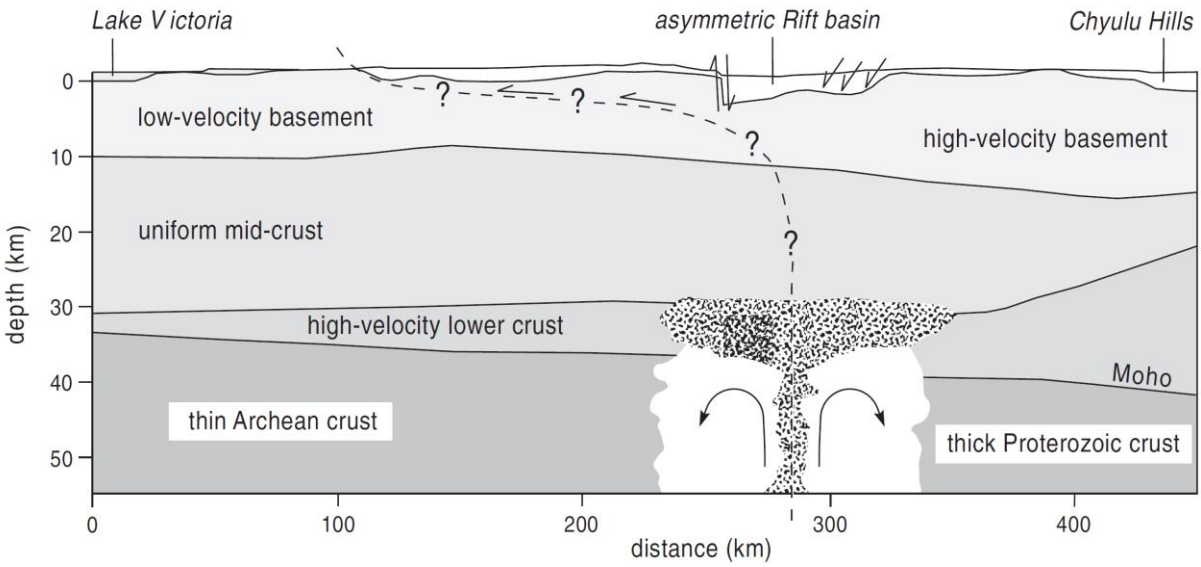

Figure 4-10 Schematic section across the Rift along Line G (modified from Prodehla et al., 1997). Details as in Figure 4-9

4.4.5. Combined seismic and gravity models

Integrated interpretation of the seismic and gravity data provides better models than either separately, not just because they depend on different physical variables - seismic velocities and density - but also because these are related to each other, allowing a seismic model to be tested against the gravity results as well as the seismic ones.

During the gravity surveys (Section 4.4.1), many density laboratory measurements were made, thus values are available for the near-surface rocks. For the deeper layers, densities were estimated from the seismic velocities using the empirical Nafe-Drake curve. The density model corresponding to the seismic model of Figure 4-9c is shown in Figure 4-11d, while Figure 4-11a compares the calculated and observed Bouguer anomalies (Birt et al., 1997). The main features of the observed profile are reproduced in the calculated one except for the general rise from west to east shown in Figure 4-11b. After removing this regional effect, the model of Figure 4-11c, was obtained, which agrees well with the observed values.

The regional increase in gravity from west to east is to be expected from the observation, noted in Section 4.4.1., that the elevated topography is isostatically compensated. The compensation mechanism must have its origin below 60 km depth, i.e. the base of the model. A model of the lithosphere extending to over 100 km, that accounts for this compensation, shows a low-density region beneath the plateau, which could be due to the higher temperatures, producing velocity perturbations.

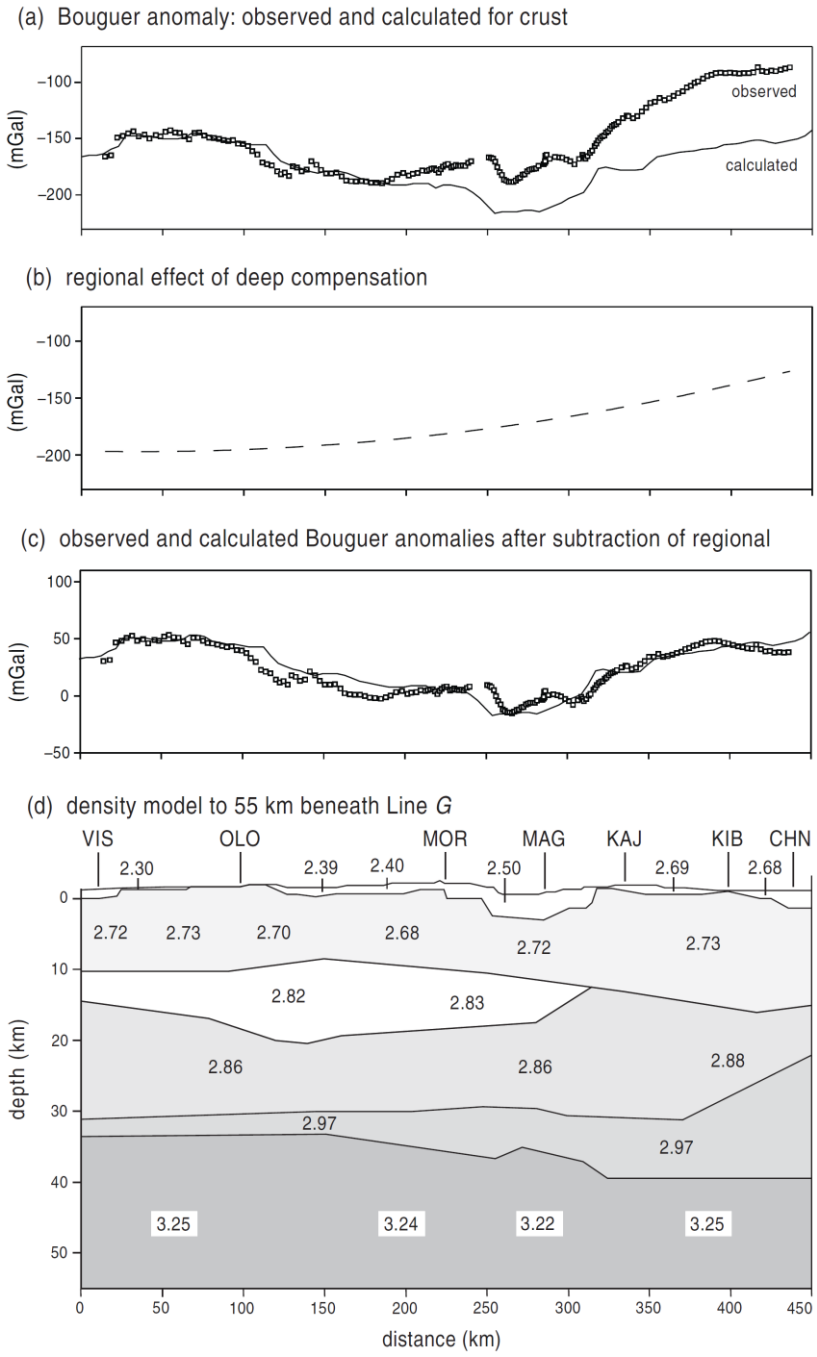

Figure 4-11 Gravity model for seismic Line G (densities in Mg/m^3) (modified from Prodehla et al., 1997)

4.4.6. Heat flow studies

High heat-flow values in the rift is expected, not only because the widespread occurrences of active volcanism involve shallow heat sources, but also because continental rifting would be accompanied by upwelling of hot mantle. Upwelling may not simply be a consequence of the splitting but actually initiate it, by the force of buoyancy, particularly if it occurs as a plume. Measuring heat flow offers a way to understand more about thermal processes at depth (e.g. Lachenbruch, 1970; Pasqua et al., 2016; Chiozzi and Verdoya 2018).

The results of heat flow measurements in Kenya, recorded in several shallow holes drilled for water and in others drilled for oil exploration purpose (Wheildon et al., 1994) are presented in Figure 4-12. The values are slightly scattered, but in general are higher within the Rift than outside it, as

expected. Unfortunately, the measured heat flow depends not only upon the temperature at depth in the crust and mantle, but also from the type of the near surface rocks and shallow hydrothermal processes. Therefore, it can be affected by the variability in thermal conductivity and by groundwater flow, which in turn depends upon permeability (pores and fractures of the rocks).

The high heat flow in the Kenya Rift could be due in part to an anomalously hot mantle, but it is more likely related to magmatic activity and hydrothermal circulation. Simple thermal calculations (see e.g. Pasquale et al., 2017) indeed indicate that there has not been sufficient time for heat to conduct up from the Moho, about 30 km deep.

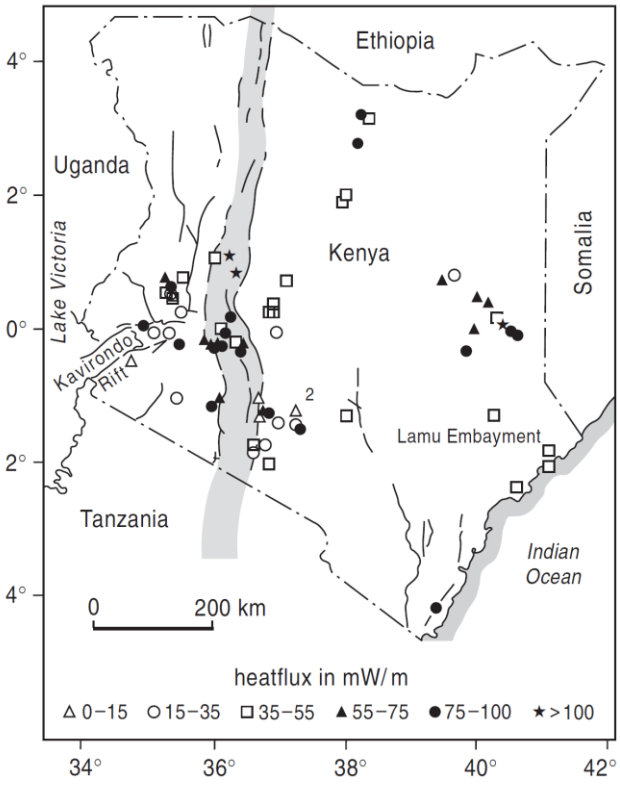

Figure 4-12 Heat flux data recorded in Kenya (after Wheildon et al., 1994)

Heat flow studies are also important to locate places where geothermal resources might be exploited. Shallow magma chambers that have fed the volcanics of the rift can be sources of heat. However, for a productive geothermal field, water is also essential to create and recharge the geothermal reservoir (porous rocks filled mainly by water/steam). Hydrothermal alteration of the volcanic rocks near the surface may lead to the formation of an impermeable layer (clay cap), which has a confining role, providing a seal for containing the superheated water until it is penetrated by drilling and gives rise to high-pressure fluids/steam, which is used to drive turbines. Kenya already produces a significant amount of electricity (about 650 MW) in this way. In addition, there may be geothermal fields associated with dyke injection that has no surface expression but could be inferred from seismicity.

4.4.7. Electrical conductivity

As explained in paragraph 3.7, the reconstruction of deep structure of the geothermal prospects is largely based on electrical conductivity studies (TEM and MT). Conductivity often depends on the amount of water the rock contains and the amount of dissolved salts in the water. However, high conductivities (or low resistivities) are often found in the middle and lower crust associated with high temperatures due to the presence of magma or fluids released from them. Such depths are usually too

deep for investigation using resistivity methods because these would need extremely large arrays with many tens of kilometres of cables. However, to define conductivities at great depth (study of the crust and upper mantle) it is possible apply the magnetotelluric (MT) method. A limitation of the method is that it cannot define electromagnetic sequence with enough detail; it only indicates large volumes of higher or lower conductivity.

MT surveys have been largely applied in Kenya to investigate the conductivities of the deep crust and uppermost mantle. They indicated a region of high conductivity about 20 km beneath the Rift axis, which was already associated with positive gravity anomalies and several very prominent volcanoes and probably due to the presence of magma. Another high-conductivity zone 50 km was recognized deep near Mount Kenya, which could be related to the presence of magma. This greater depth is consistent with the petrologic evidence that volcanics outside the Rift originated at greater depth than those inside.

Birt et al. (1997) measured conductivity below seismic lines F and G of Figure 4-7, and the results are schematically shown in Figure 4-13. As expected, there is higher conductivity in the crust and mantle below the Rift. The Rift infill is particularly conducting, probably due to the porous volcanics and sediments containing saline water. The infill has higher conductivity to the west than that to the east, consistent with the seismic section described in Figure 4-11, which shows the infill to be much thicker to the west. There is a sharper contrast between the Rift and western flank than for the eastern one. Beneath the western flank, the upper mantle shows low conductivity but is underlain by conductive mantle. Away from the Rift to the east are the Chyulu Hills, a young volcanic field, and there are highly conducting zones within 1 km of the surface. The high conductivities in the lower crust and upper mantle support the models, derived from the gravity and seismic data, which are consistent with partially molten zones.

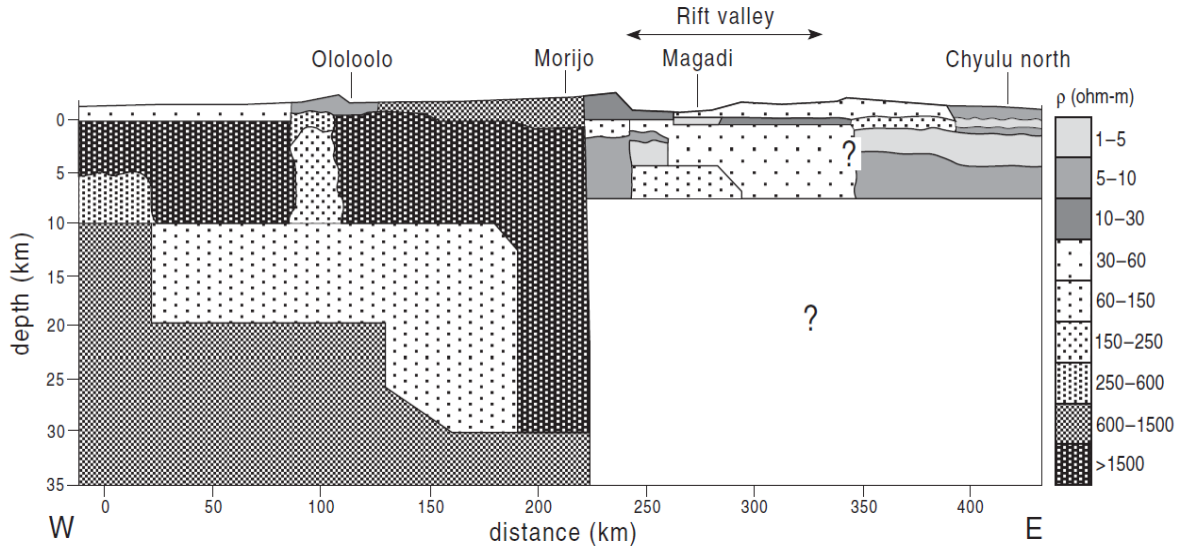

Figure 4-13 Conducting regions beneath the Kenya Rift and its flanks

5. EARS GEOTHERMAL RESOURCES

5.1. Geothermal Potential

Several African Countries located along the EARS, have important geothermal resources for both power generation and direct use application, namely Djibouti, Democratic Republic of Congo, Eritrea, Ethiopia, Kenya, Malawi, Mozambique, Rwanda, Tanzania, Uganda and Zambia. The geothermal exploration in Burundi is only at reconnaissance stage.

The United Nation Environment Program (UNEP) is the main key player, leading the development of geothermal energy in Africa. UN Environment supports countries to improve energy efficiency and increase the use of renewable energy as part of their effort to achieve low-carbon and climate resilient development. In November 2018, UNEP took a picture of the Geothermal Resource Potential in East Africa. In summary, (i) Africa's geothermal potential in the Eastern Africa Rift is estimated larger than 20000 MWe; (ii) at present, only Kenya and Ethiopia have operational geothermal power stations; (iii) there are plans to increase geothermal installation in Eastern Africa by over 3000 MWe over the next 10 years.

In the following, a summary of the main geothermal resources in the several countries is presented, then a brief outline some of the most important geothermal fields of EARS is described with particular reference to those areas that were investigated during this PhD word. Finally, specific details some of them, i.e. those characterised by high-quality data and peculiar geological, geochemical and geophysical characteristics, are reported. The presented case-studies can provide guidelines for the optimum procedures of geothermal resource exploration in the EARS region.

5.2. Country Updates

5.2.1. Djibouti

The geothermal potential of Djibouti was estimated to be about 1,000 MWe (Zemedkun, 2018). The exploration wells are preparation in Fiale and other parts of Lake Assal. Moreover, geoscientific studies are on-going in Hanle Gagade, Arta, Obok and Gubbet prospects.

5.2.2. Eritrea

An active crustal spreading center, characterized with numerous NW trending fissures, faults, felsic volcanoes and thinned crust, occurs in Eritrea. The Alid area was identified as the most promising high enthalpy prospect for geothermal utilization. Detailed geoscientific studies in Alid started in 2015 and supported by UN Environment and ICEIDA. Detailed surface studies of the other prospects (e.g. Nabro-Dubbi) are planned.

5.2.3. Ethiopia

Ethiopia is being explored for its geothermal resources since 1969, over twenty-three high-temperature possible geothermal areas were identified, but only three geothermal prospects are subject to drilling, namely Alalobeda, Tendaho-Dubti and Aluto-Langano. Zemedkun (2018) estimated a geothermal potential >10000 MWe. Furthermore, a larger number of areas have potential for medium-low temperature resources throughout the Ethiopian Rift System. To date, only the Aluto-Langano field

is generating electricity, the installed capacity of the Geothermal Combined Cycle Unit built in 1998 is 7.2 MWe. Preparation for additional drilling is underway to allow for expansion of the field of 70 MWe.

In the Tendaho-Dubti field, a total of 3 deep and 3 shallow exploration wells were drilled between 1993-1998, confirming the presence of high-temperature geothermal resources. Tendaho-Alalobeda field is being evaluated for development of a 12 MWe pilot plant (ELC, 2016). An expansion to 100 MWe in subsequent phases is planned. Moreover, the Corbetti geothermal prospect is managed by Corbetti Geothermal Ltd. (private investor), a power purchase agreement (PPA) for 500 MWe was signed and the exploratory drilling started in 2018.

5.2.4. Kenya

Zemedkun (2018) estimated a geothermal potential of >10000 MWe in over twenty-three sites. However, to date only Menengai, Olkaria and Eburru are under production. The potential of the Menengai Block is 1600 MWe, the drilling still on-going and a 105 MWe (ELC, 2014) tender was awarded to private developers. The potential of the Olkaria Block is 1200 MWe of which 636 MWe installed and the remaining 560 MW are under development. In the Eburru geothermal field, six exploratory wells were drilled, with an estimated potential amount of 60 MW. KenGen installed in 2012 a 2.5 MW well-head power plant.

5.2.5. Tanzania

Geothermal systems in Tanzania are mainly associated with both the eastern and western rift branches and five prospects are prioritized, namely: Ngozi, Songwe, Kiejo-Mbaka, Luhoi and Lake Natron. To date, geoscientific investigations were done in all the above-mentioned prospect. On the other hand, slim wells were planned in Ngozi (2019) and Kiejo-Mbaka (2020), while detailed surface studies and thermal gradient holes (TGH) are planned for Songwe. TGDC (2018) estimated a geothermal potential of the country >500 MWe.

5.2.6. Rwanda

Geothermal prospects in Rwanda, Gisenyi and Mashyuza, are associated with the Virunga volcanic complex: All the resources in Rwanda are classified as medium to lower temperature. Deep exploration drilling in Karisimbi did not intersect a geothermal system. Gisenyi and other areas are being evaluated for only direct use applications.

5.2.7. Democratic Republic of Congo

In 1950s, shallow wells were drilled at Kiabukwa hot springs. The discovered geothermal resource has a temperature of 91 °C and a flow rate of 40 l/s. In order to support the mining operations in such area a 0.2 MWe binary plant was installed in 1952. Others geothermal areas are at reconnaissance stage.

5.2.8. Uganda

Most of the geothermal potential areas are associated with the western branch of the EARS. The four major geothermal prospects are Katwe-Kikorongo, Buranga, Kibiro and Panyimur and geothermal systems are considered to be fault controlled (Zemedkun, 2018). The two prospects in which the geoscientific studies were concentrated are Kibiro and Buranga. For Kibiro, geothermometryic estimations indicated reservoir temperatures >150 °C and drilling of thermal gradient hole (TGH) is planned. The Buranga prospect has the largest geothermal manifestation in Uganda, i.e. hot springs,

mud pools, fumaroles, etc. The prospect is located at the foot of the Ruwenzori Mt, and it is associated to a fracture-controlled system.

5.2.9. Zambia

Since 1980s, the government of Zambia and Italy have been carrying out exploration studies in Kapsiya and Chinyunyu prospect areas. In 1986, a pilot plant in Kapisya was installed by the Italians. This power plant has two Organic Rankine Cycle (ORC) turbo-generators of 200 kW, but it never operated.

5.2.10. Malawi

Over twenty geothermal areas are discharging hot water at T=40-80 °C. Detailed surface studies are ongoing in some prospects, and only low to medium temperature resources were so far discovered. Two prospects, Kasitu and Chiweta, were selected for a pre-feasibility study.

5.2.11. Mozambique

The Renewable Energy Atlas of Mozambique - Resources and Projects for Power Generation (Gesto-Energia, 2014) describes thermal springs that reach temperatures exceeding 60 °C. Even a temperature of 95 °C was historically recorded. The provinces with geothermal occurrences are Tete, Manica, Sofala, Zambézia, Nampula and Niassa.

A geochemistry campaign was conducted in 2012, in which twenty-two water samples were collected from hot springs, mineral springs, water pumps, rivers and sea, in 6 provinces: Manica, Tete, Nampula, Niassa, Zambézia and Sofala. At four sites, geothermometers indicate enough temperature for electricity production: Boroma (164 °C), Morrumbala (153 °C), Maganja da Costa and Namacurra (155 °C). An additional geophysical campaign was performed in 2013 in the six selected locations, distributed by the provinces of Tete, Zambézia and Niassa, with the acquisition of approximately 250 magnetotelluric and gravity stations. The analysis of geophysical data indicated areas with low resistivities that may correspond to potential geothermal reservoirs at depths ranging between 1500 and 2500 m.

5.3. Recent advances in the geothermal studies of EARS

During this PhD work, several geothermal fields in the East Africa Rift System (EARS) were studied in detail. In particular two geothermal prospects located in Ethiopia, one in Kenya two in Malawi and Tanzania. These investigated prospects are well widespread along the Eastern and Western Branches of the EARS, and give representative insights into the different geothermal play types of the Region (Figure 5-1).

This PhD study was based on the data obtained thanks to my direct participation in seven international projects, four of which co-financed by the Ministry for Foreign Affairs in Iceland (MFA)-Directorate for International Development Cooperation (ICEIDA) and by the Nordic Development Fund (NDF) and two by the World Bank (WB). The seventh project was commissioned directly to my employer (ELC Electroconsult) by the Geothermal Development Company (GDC, Kenya).

The contribution reported in this PhD work in the above listed projects implied:

- Field activities (geological, geochemical and geophysical surveys);
- Laboratory analyses (petrographic, XRD and chemical);
- Well data analysis;

- Integrated interpretation of the results deriving from the different geoscientific investigations and from the deep/shallow exploratory drilling (conceptual model);
- Numerical modelling;
- Wells targeting.

First, the investigated geothermal fields are briefly introduced, while in the following a detailed picture of three of them (Alalobeda, Menengai and Kiejio-Mbaka) is reported, as derived from the several geological, geochemical and geophysical campaigns during which I operated.

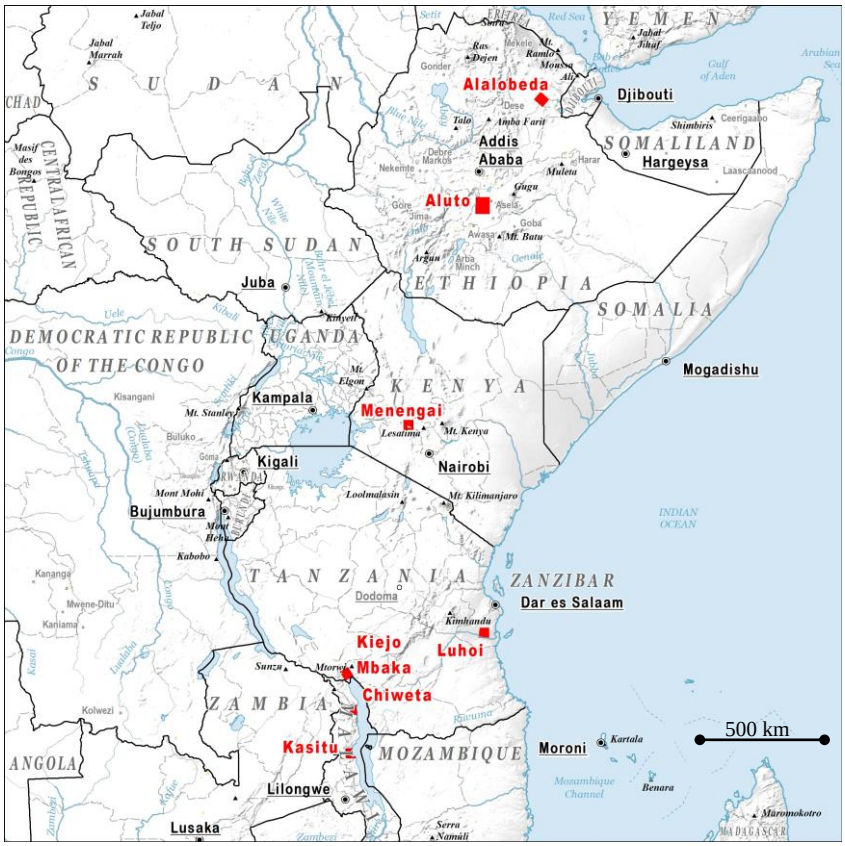

Figure 5-1 Location of the investigated geothermal fields (little red squares) during the present PhD activities

5.3.1. Alalobeda - Ethiopia

The Alalobeda geothermal prospect is located in the western sector of the Tendaho Graben (see Figure 5-2), a major structure extending within the Northern Afar Region, which hosts also the prospects of Dubti and Ayrobera. These two prospects were extensively investigated, as well as deep exploratory wells were drilled. In Dubti, the existence of a shallow reservoir of commercial interest was proved, whereas the deep reservoir, albeit characterized by high temperature, is characterized by a rather low permeability.

In the framework of the full development of the geothermal resources of the country, the Geological Service of Ethiopia (GSE) decided to pursue the exploration of the Alalobeda prospect through the implementation of a series of geoscientific investigations aimed at improving the knowledge of Alalobeda and acquiring factual elements needed for the identification of favorable drilling targets, whose results were combined to elaborate the conceptual model of the field. A surface exploration program, including geological, geochemical and geophysical surveys, as accordingly commissioned to ELC-GSE (2016). In the project organization, I held the position of both Project Manager and Lead Geologist. The results of the geoscientific study are described in detail in Section 5.4.

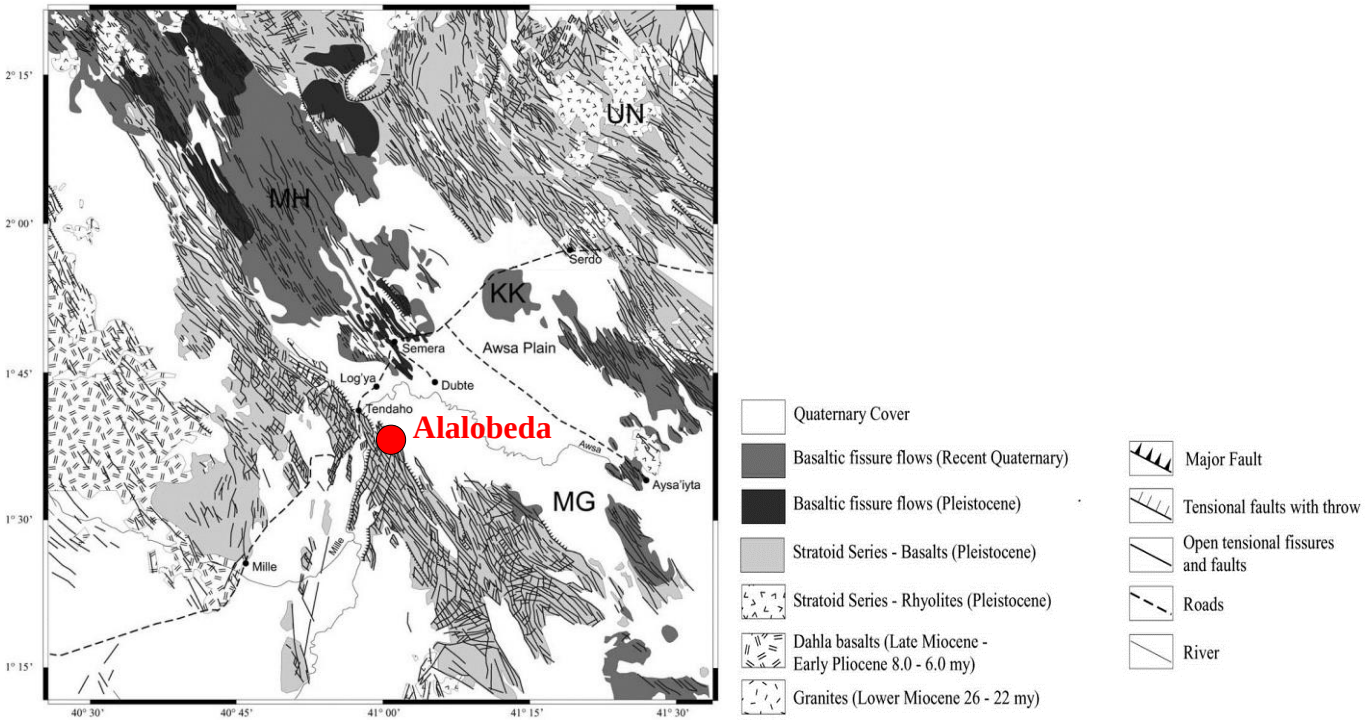

Figure 5-2 Generalized geological map of the Tendaho Graben: MH =Manda Hararo; MG =Manda Gobaad; KK = Kurab Koma; UN = Undurur (from Thurmond et al., 2006). Red dot indicates the Alalobeda prospect location

5.3.2. Aluto-Langano field - Ethiopia

The Aluto-Langano geothermal prospect is located in the floor of the Ethiopian Rift Valley, close to its eastern escarpment, some 200 km south of Addis Ababa (see Figure 5-3). In the framework of the full development of the geothermal resources of the country, the Ethiopian Electric Power (EEP), with the support of the Geological Service of Ethiopia (GSE), decided to pursue the exploration of the Aluto-Langano prospect through the implementation of a series of geoscientific investigations, aimed to advance the state of knowledge of the prospect. This program falls within the Geothermal Exploration Project (GEP), co-financed by the Icelandic International Development Agency (ICEIDA) and the Nordic Development Fund (NDF) and aimed at supporting geothermal exploration and capacity building in East Africa. Iceland GeoSurvey (ISOR) was designated to provide technical support throughout the implementation of the GEP.

Since 1969, the Aluto-Langano prospect has been the object of a number of investigations and during 1980s of a program of deep exploratory drilling, which led to the discovery of a geothermal field of commercial interest and the installation of a small geothermoelectric power plant. Following the execution of additional geoscientific investigations and a review of all documentation by West JEC, the geothermal potential of the Aluto-Langano field was estimated at 35 MWe (Aluto I) and a field development plan for the exploitation of this potential was outlined. The plan foresees the initial drilling of two "appraisal" wells, to be followed by the implementation of a full development drilling campaign. Drilling of the first of the two appraisal wells (LA-9 and LA-10) was completed.

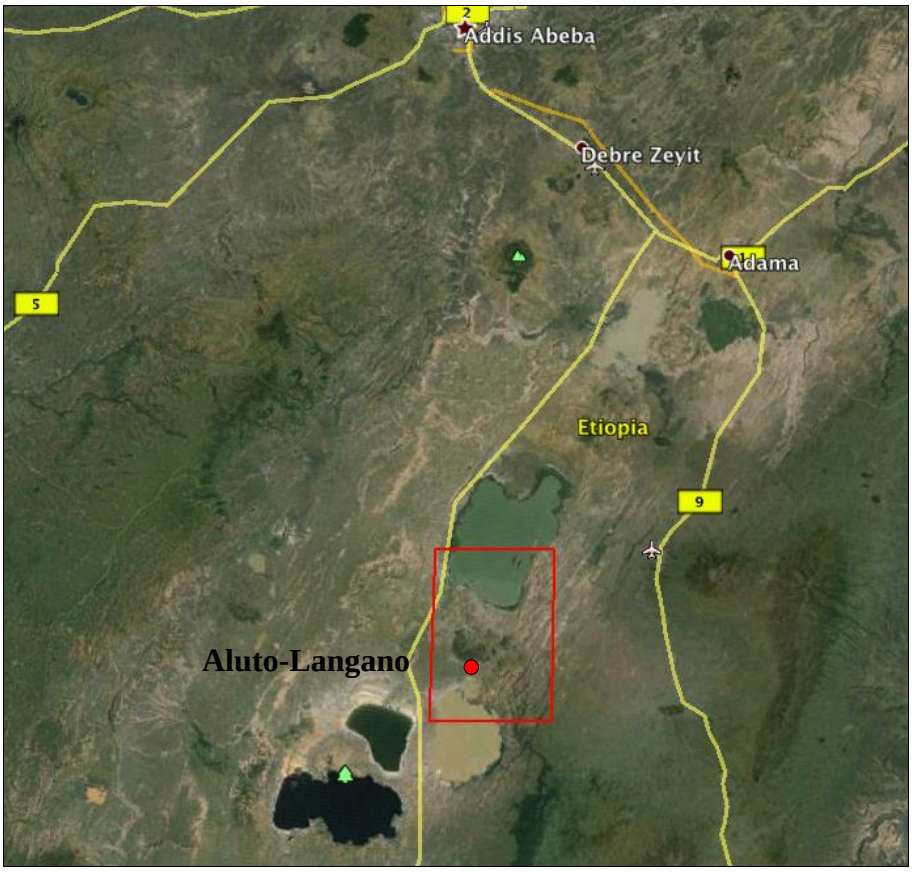

Figure 5-3 Location of the Aluto-Langano study area

To fully develop the Aluto-Langano prospect, it was planned to extend the exploration beyond the sector now under development, with the final object to increase the electric potential to additional 35 and possibly 70 MWe (Aluto II and III). This implied the implementation of geological, geochemical and geophysical surveys over the whole Aluto Volcanic Complex (AVC), which covers an area of about 100 km^2.

Within the framework of this program, a surface exploration survey was commissioned to ELC-GSE (2016). In the project organization, I was both Team Leader and Lead Geologist. The results of the geoscientific study were, as follows:

- A model of the subsurface resistivity within the AVC.
- A Bouguer gravity map of the AVC area.
- A micro-seismic survey over the AVC system, maps and cross sections showing earthquakes distribution, frequency, focal depth and magnitude.
- A map of soil gas chemistry (CO_2 flux, and ^{220}Rn and ^{222}Rn concentrations).
- A detailed structural analysis of the AVC and Wonji Fault Belt that elucidates the connection between the regional tectonics and geothermal activity at the geothermal field.

The foregoing outcomes were integrated with other data provided by GSE (including temperature and production data from previously drilled wells) to obtain a conceptual model of the Aluto geothermal system (supported by 3D modelling software). A proposal for potential drilling targets was formulated, adequate enough to sustain the proposed a second 35 MW unit. In case of positive outcome, this would lead to a further stage of the Aluto development through implementation of a deep exploratory drilling program to exploit the geothermal potential of the field.

5.3.3. Menengai field - Kenya

The Menengai geothermal prospect is located at the outskirts of Nakuru Town, situated about 180 km NW of Nairobi (see Figure 5-4), and covers an area of about 110 km^2. The Government of Kenya through the Ministry of Energy appointed the Geothermal Development Company Limited (GDC) to develop a study of the Menengai field, which is located in a recent caldera.

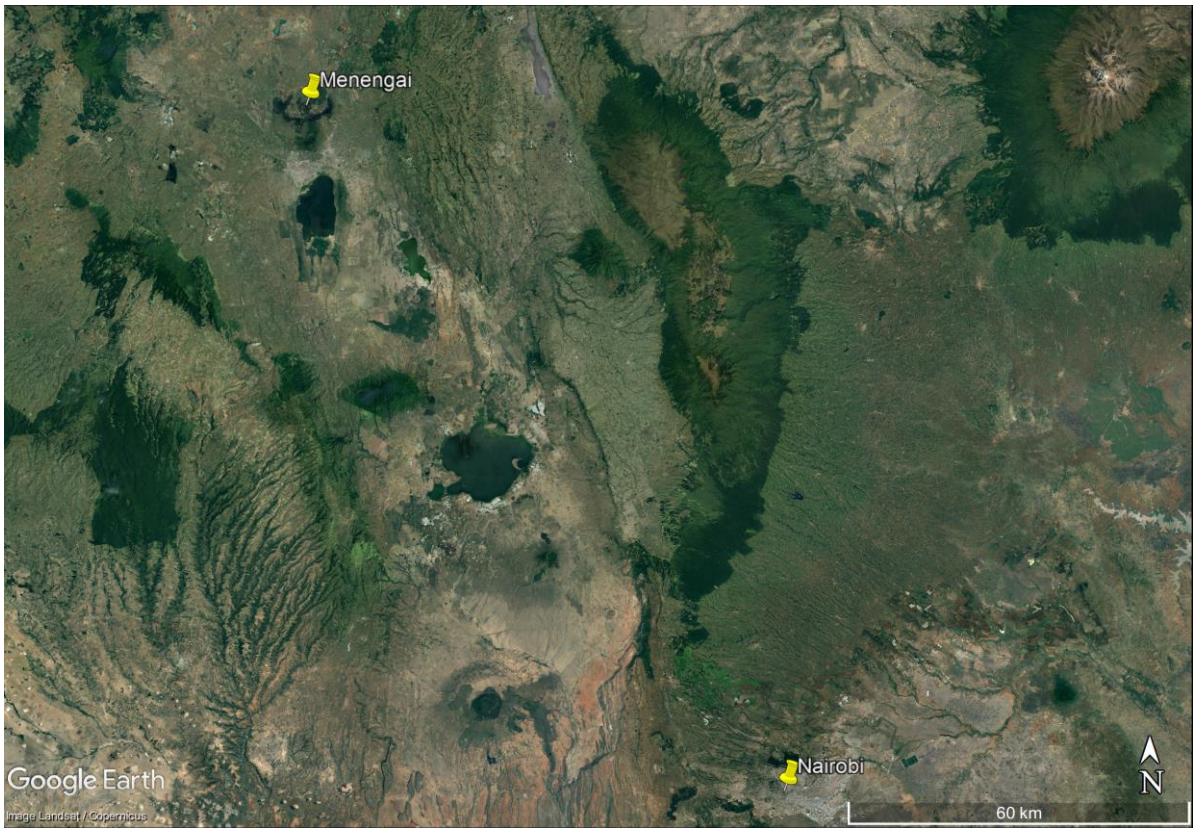

Figure 5-4 Location of the Menengai study area

The Menengai caldera is occurs in correspondence of the "triple junction" of the African rift, i.e. the intersection of the ENE-WSW trending Kavirondo (also called Nyanza) Rift with the Gregory Rift in the point where the latter changes its direction from NNE-SSW to NW-SE. Such a junction is considered to be the surface evidence of a mantle plume (Omenda, 2010) and corresponds to a concentration of large calderas associated with huge explosive eruptions, contrasting with the predominantly lavic and fissural activity of the northern and southern sectors of the rift (Figures 4-2 and 5-4).

Menengai has been the object of geoscientific investigations since 1960s. Integrated results of these studies indicated the existence of a geothermal resource that could be commercially exploited under the Menengai caldera, characterized by high temperature (more than 300 °C) and extending over an area of about 50 km^2. Underground exploration started in February 2011 through an extensive drilling program consisting of deep wells (up to 3 km).

A study was commissioned to ELC-GDC (2011-2015), to evaluate the full potential and the development of the geothermal resources. In the study organization, I held the position of both Project Manager and Hydro-geologist. The results of the study and the characteristics of the Menengai geothermal field are described in detail in section 5.4.

5.3.4. Kiejo-Mbaka and Luhoi fields - Tanzania

Kiejo-Mbaka Prospect (Figure 5-5) is located some 50 km north of the Malawi border, along the NW-SE trending Mbaka Fault, which extends within the Karonga basin in the East African Rift. Several recent volcanoes of the Rungwe Volcanic Province are found within the rift, being aligned along its NW-SE direction. About 10 years ago, the prospect was the object of a reconnaissance study by the Geological Survey of Tanzania and BGR and in 2012 of additional studies by Geothermal Power Tanzania Ltd (GPT).

Luhoi Prospect (Figure 5-6) is located ca. 160 km south of Dar es Salaam in the coastal region, within the Rufiji sedimentary basin, where hot springs are attributed to rifting and magmatic intrusions. The prospect was in the past concessioned to First Energy Company Ltd (Ethiopia) and object of a reconnaissance study.

In view of the national interest in enhancing and accelerating the development of geothermal energy, a project was started aimed at increasing the knowledge of the Luhoi and Kiejo-Mbaka geothermal prospects, acquiring factual elements needed for elaborating the conceptual model of the field and possibly siting deep exploratory wells (ELC-TGDC, 2017 and 2018). In the project organization, I held the position of both Project Manager and Senior Geothermal Geologist. The surface exploration in Kiejo-Mbaka and Luhoi, was co-financed by the Ministry for Foreign Affairs in Iceland - Directorate for International Development Cooperation (ICEIDA) and by the Nordic Development Fund (NDF). It was implemented by the Tanzania Geothermal Development Company Limited (TGDC), a subsidiary company of the Tanzania Electric Supply Company Limited (TANESCO).

In both the prospects, models of the subsurface resistivity, maps of Bouguer gravity anomaly and CO_2 flux were obtained. Moreover, a magnetometric survey was carried out in Luhoi. The geological and geochemical investigations in both the prospects led to disclose the connection between the regional tectonics and geothermal activity, to propose potential drilling targets and to preliminarly assess environmental and social impacts.

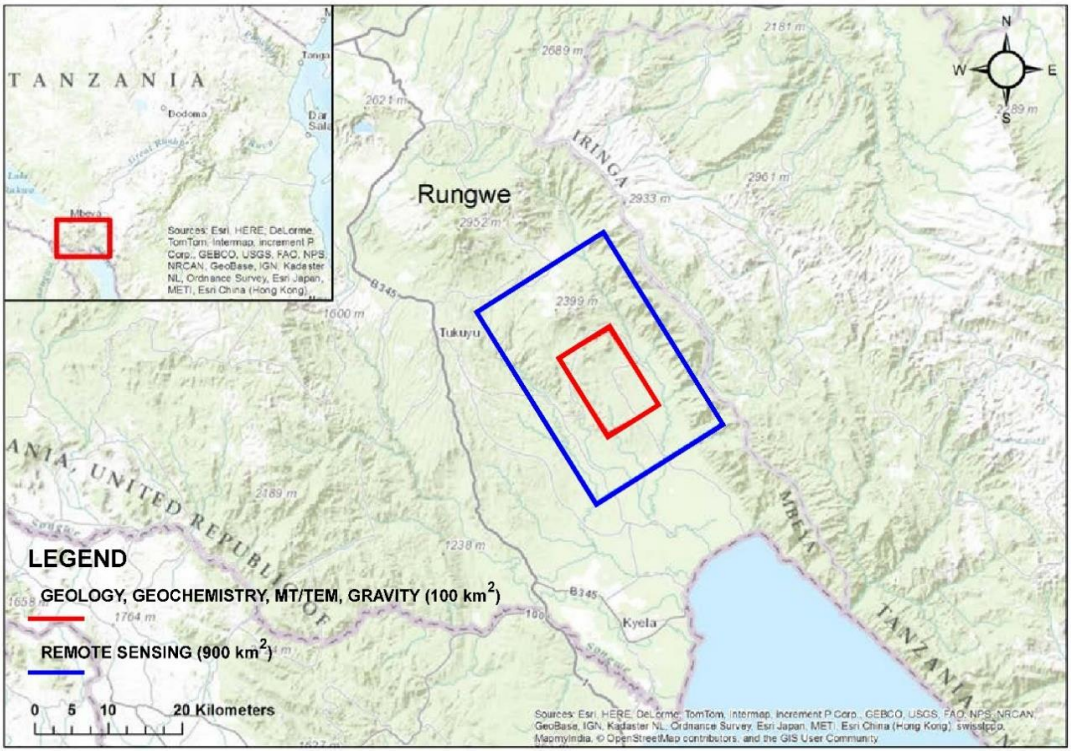

Figure 5-5 Map of the proposed surveys in the Kiejo-Mbaka prospect

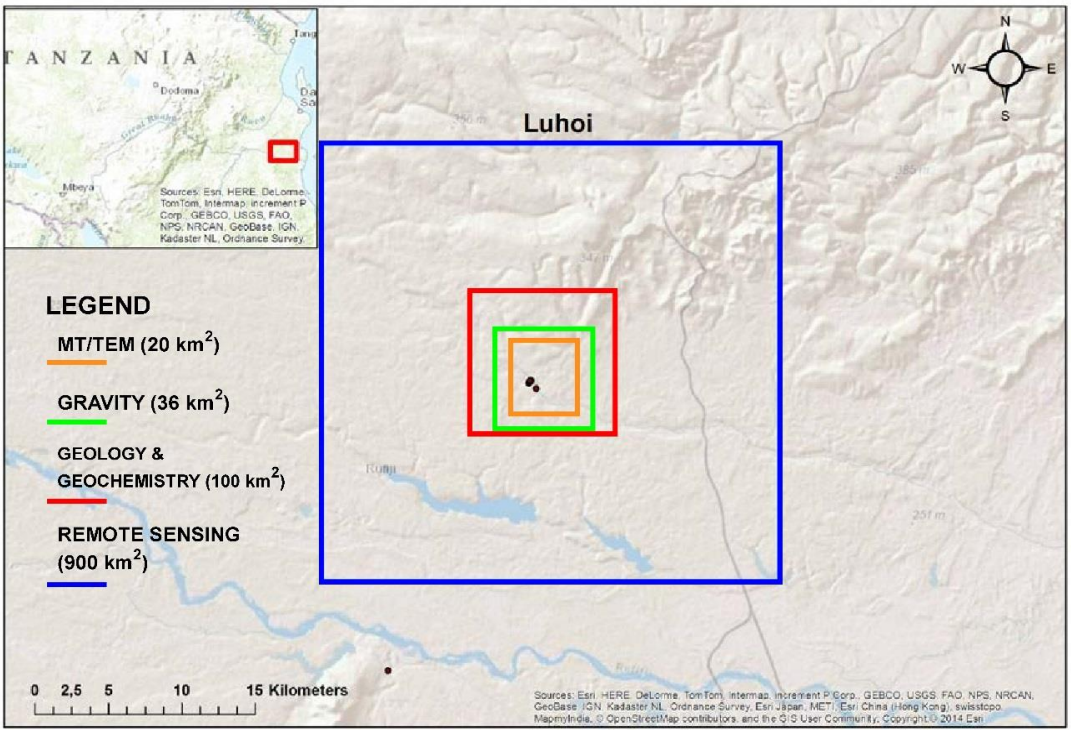

Figure 5-6 Map of the proposed surveys in the Luhoi prospect

5.3.5. Chiweta and Kasitu fields - Malawi

The Ministry of Natural Resources, Energy and Mining (MoNREM) was supporting the implementation of the Malawi Energy Sector Support Project (ESSP). The overall objective of the project was to increase the electricity supply in the major load centers of Malawi, which currently derives almost exclusively from hydroelectrics. The ESSP is expected to build capacity in the electricity generation subsector by bringing about diversification in the use of alternative sources of energy for power generation, including wind, solar, thermal (using coal), biomass (obtained through sugar, tea and timber processing) and geothermal.

With reference to the geothermal sector, in order to stimulate the development in Malawi, a project for the "*Assessment of Geothermal Resources in Malawi: a Reconnaissance and Pre-feasibility Study*" started in 2016 (ELC, 2018). In the project organization, I held the position of Senior Geothermal Geologist. The project was developed in three stages, with increasing level of detail.

- *Stage 1: Reconnaissance Study.* After an analysis of all the available literature information and technical documentation, six prospects, namely *Chiweta*, *Kanunkha*, *Kasanama*, *Kasitu*, *Mawira* and *Chipudzi*, were selected for the preliminary assessment stage (see Figure 5-7).
- *Stage 2: Preliminary Appraisal.* At conclusion of Stage 1, the six selected prospects were subject to more detailed investigations, including remote sensing study, geological mapping and geochemical sampling of waters and gases. Finally, the Chiweta and Kasitu prospects, corresponding to well-known hot springs of the Central region (Dulanya, 2006) resulted with the highest ranking and singled out for additional and more detailed investigations. Chiweta prospect is likely characterised by the hottest springs in the country, where gas emissions and boiling pools are also discharged.
- *Stage 3: Pre-feasibility Study.* The Chiweta and Kasitu prospects were further investigated with detailed remote sensing and geological surveys, as well as geophysical (MT/TEM and gravity)

campaigns. The integrated interpretation of the results led to the elaboration of the "basic" conceptual model of the fields and hence to the estimation of their geoelectrical potential.

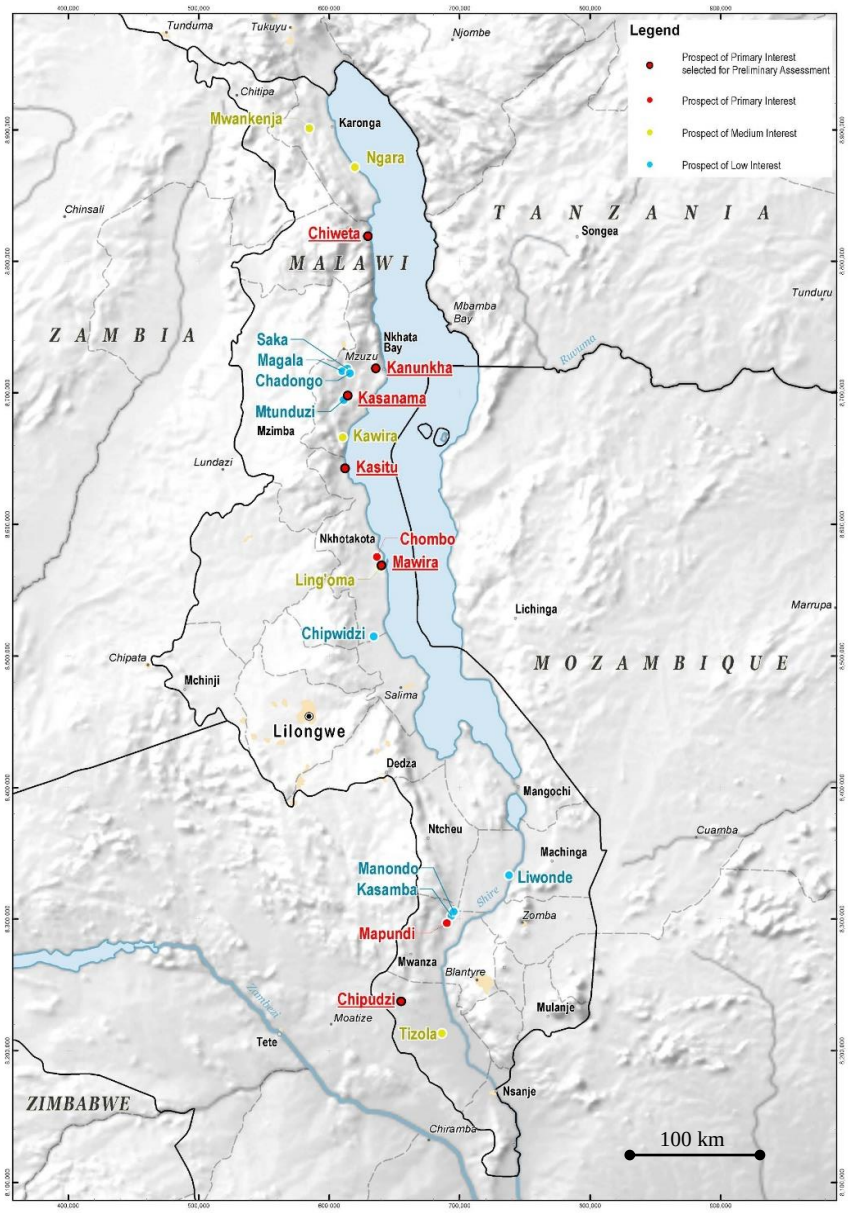

Figure 5-7 Location of the prospects covered by preliminary appraisal

5.4. Case studies

In this section, three case studies are described in detail as they can be considered the most representative examples of geothermal play types present in the EARS:

Alalobeda field: It is located in correspondence of the triple junction *Read Sea-Aden Gulf-Main Ethiopian Rift*. It can be classified as extensional domain play. However, at the present level of knowledge, to discriminate whether Alalobeda system is a fault controlled or fault-leakage controlled is not possible.

Menengai field: It represents the second most important geothermal field in the EARS after Olkaria (Kenya). Moreover, at the current field development stage (feasibility study) a huge quantity of

data, deriving from more than twenty drilled wells is available. Menengai can be classified as convection-dominated magmatic play type.

Kiejo-Mbaka field: It is a typical case of geothermal system present in the EARS's Western Branch. The Kiejo-Mbaka prospect can be classified as extensional domain play fault controlled or fault-leakage controlled.

5.4.1. The Alalobeda geothermal field

The Tendaho Graben, Northern Afar Region (Ethiopia), hosts two well-studied geothermal systems: Dubti and Ayrobera (Aquater, 1979-1996). Previous investigations performed in these prospects proved the existence of an exploitable, shallow geothermal reservoir, whereas a deeper reservoir, albeit characterized by suitable thermal conditions, exhibits rather low permeability. The study of the Alalobeda geothermal field, located in the western sector of the Tendaho Graben, was a further step towards the development of the geothermal resources in the Ethiopia (GSE and BGR, 2012).

5.4.1.1. Geological setting

From the stratigraphic point of view (Figure 5-8), two distinct groups of rocks are outcropping: i) the Plio-Pleistocene age and ridge forming volcanic rocks and their minor intercalated sediments (the Afar Stratoid Series - ASS); ii) the Pleistocene-present, rift floor filling continental sediments intercalated with some lava flows.

For the first time, ASS was subdivided in the present study in three units, namely (from the youngest to the oldest): a. flow laminated trachybasalt; b. plagioclase phyric and perlitic basalt; c. moderately porphyritic basalt. The intercalated sediments are fluvio-lacustrine, sometimes rich in bentonite.

The rift floor filling sediments are highly variable from the viewpoint of grain size, ranging from coarse conglomerate to clay, and are products of river, shallow lake and wind deposition. The several gradient holes and six exploratory wells (deep and shallow) drilled by GSE and Aquater between 1990 and 1998 around the Dubti plantation, that is 10-15 km NE of the Alalobeda prospect, showed that these sediments have a thickness of more than 1200 m (Battistelli, et al., 2002). Moving towards the border of the Tendaho Graben, which is to the Alalobeda prospect, such thickness is expected to decrease progressively.

The poor permeability of the ASS may be due to either hydrothermal self-sealing processes or a limited downwards extension of the normal faults. Under this point of view, primary targets for the future drilling exploration would correspond to zones where neo-tectonic events are expected to be particularly developed, i.e. whenever the two NW-SE and NNE-SSW rift systems are intersecting.

Extrapolation of the drilled wells data (Aquater, 1990-1998) to the south-west located Alalobeda prospect may be useful to select primary targets and predict the lithological sequence. According to this reconstruction (Gebregziabher, 1998), the Upper Extrusive Sequence, in the study area, will be significantly reduced to only few hundred meters, since the Alalobeda zone is very close to the major Logiya fault and the axial basalts may also completely lack. The sediments will probably be on the whole coarse grained, since their source is near, wherefore slope scree and gravel are expected to be the predominating products, intercalated with the finer lacustrine sediments.

From the structural point of view (Figure 5-8), in the study area there are the three rift systems, named Red Sea (NW-SE), Ethiopian Rift (NNE-SSW) and Gulf of Aden (ENE-WSW), that meet around the Dama-ale volcano and Lake Abhe, forming a zone of triple junction. The Red Sea and the Ethiopian Rift trending faults interact in the study area, particularly in the western half, forming NW elongated rhombic blocks. Near the western margin of the Tendaho Graben, where the NW trending faults are younger, they have left laterally displaced the NNE trending faults curving the latter ones to the west.

All hydrothermal manifestations of the study area (hot springs, fumaroles and warm to hot grounds) are confined within the western half of the prospect that is in the sector of interaction between the Red Sea and Ethiopian Rift systems (ELC-GSE, 2016). In particular, along the Logiya fault the fluid manifestations start where the NW system displaces left laterally the NNE one. The fact that these thermal discharges are located exactly in correspondence of the rejuvenated junction of the two fracture systems indicates the presence of a zone of decompression allowing a preferential way for the uprise of thermal fluids, as well, possibly, of magmatic bodies.

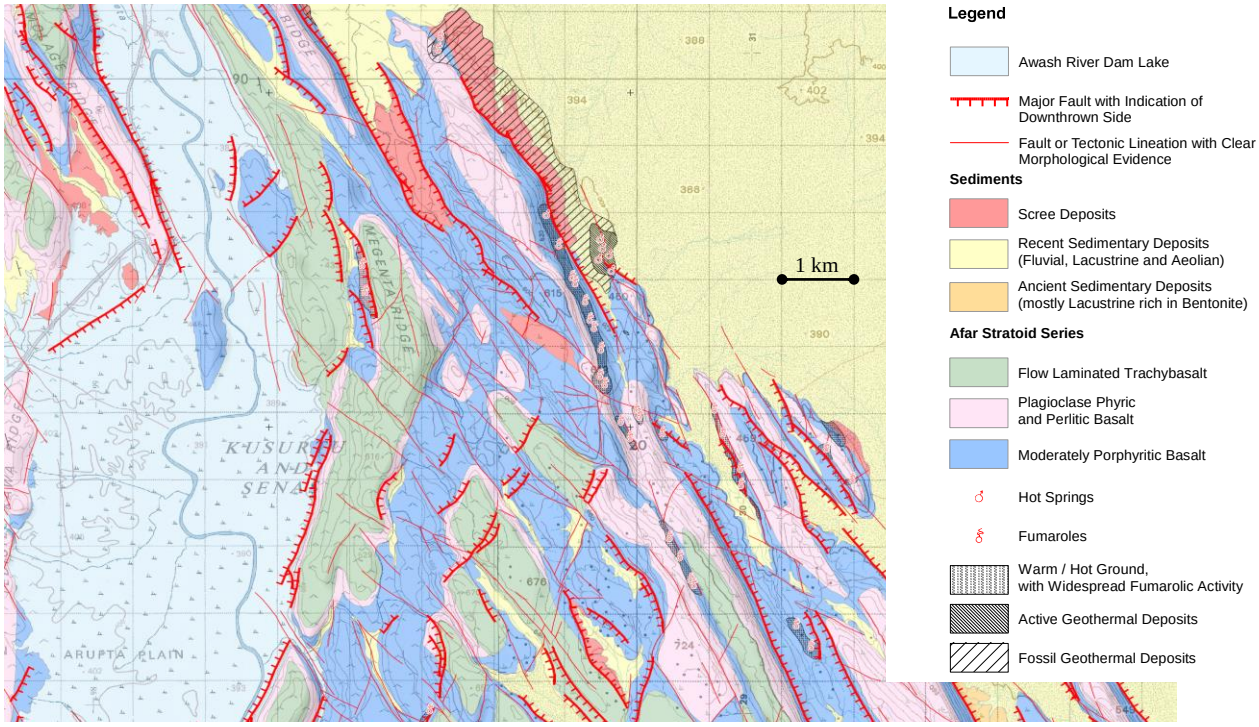

Figure 5-8 Geological-structural map of the Alalobeda geothermal prospect

5.4.1.2. Geophysical data

Gravimetric investigations were carried out in the Alalobeda geothermal prospect. The analysis and interpretation of the gravimetric data (Figure 5-9) indicated that:

i. Graben shoulder is separated from the graben depression by different main fault systems that define different bedrock sectors (ELC-GSE, 2016). The most external main fault is MF0, which is defined by its outstanding topographic escarpment. The correspondent first graben sector D0 has a very thin sedimentary cover (when existing). A second main fault MF1 imaged by gravity (actually a fault system composed by different normal faults) separates the sector D0 from sector D1, where the sedimentary infill is thicker. A third main fault (system) MF2 divides sector D1 from D2 (the deepest).

ii. Both the MF1 and MF2 fault systems are shifted towards NE at the locations indicated by labels SHFT. Shifting may occur along transfer faults that accommodate the evident large-scale NE trending shift of the graben shoulder moving from the survey area to the SE.

iii. The buried ASS bedrock below the sediments in the plain (sector D1) shows a horst-graben structure (white lines in the figure, main local horsts labelled H1, H2, H3), similar to the horsts outcropping from the plain close to the mountains. The graben shoulder (in the survey region) is therefore composed by a set of asymmetrical horst and grabens rather than half-grabens.

iv. The deepest D2 sector of the buried ASS bedrock is located in correspondence of the inferred stripe of dominantly normal-polarity intrusions and/or diking originated in the past 0.78 Ma. The D1 sector on the contrary shows a reversed magnetic polarity due to ASS basalts formed during the reverse Matuyama Chron (>0.78 Ma)

v. A region of enhanced density (density contrast >300 kg/m^3) is located inside the ASS basalts below the graben shoulder at an elevation range modelled approximatively between -500 to -1,500 m asl. The denser region is spatially well correlated with a region of enhanced conductivity (2-3 times larger than the surroundings) detected by the MT survey.

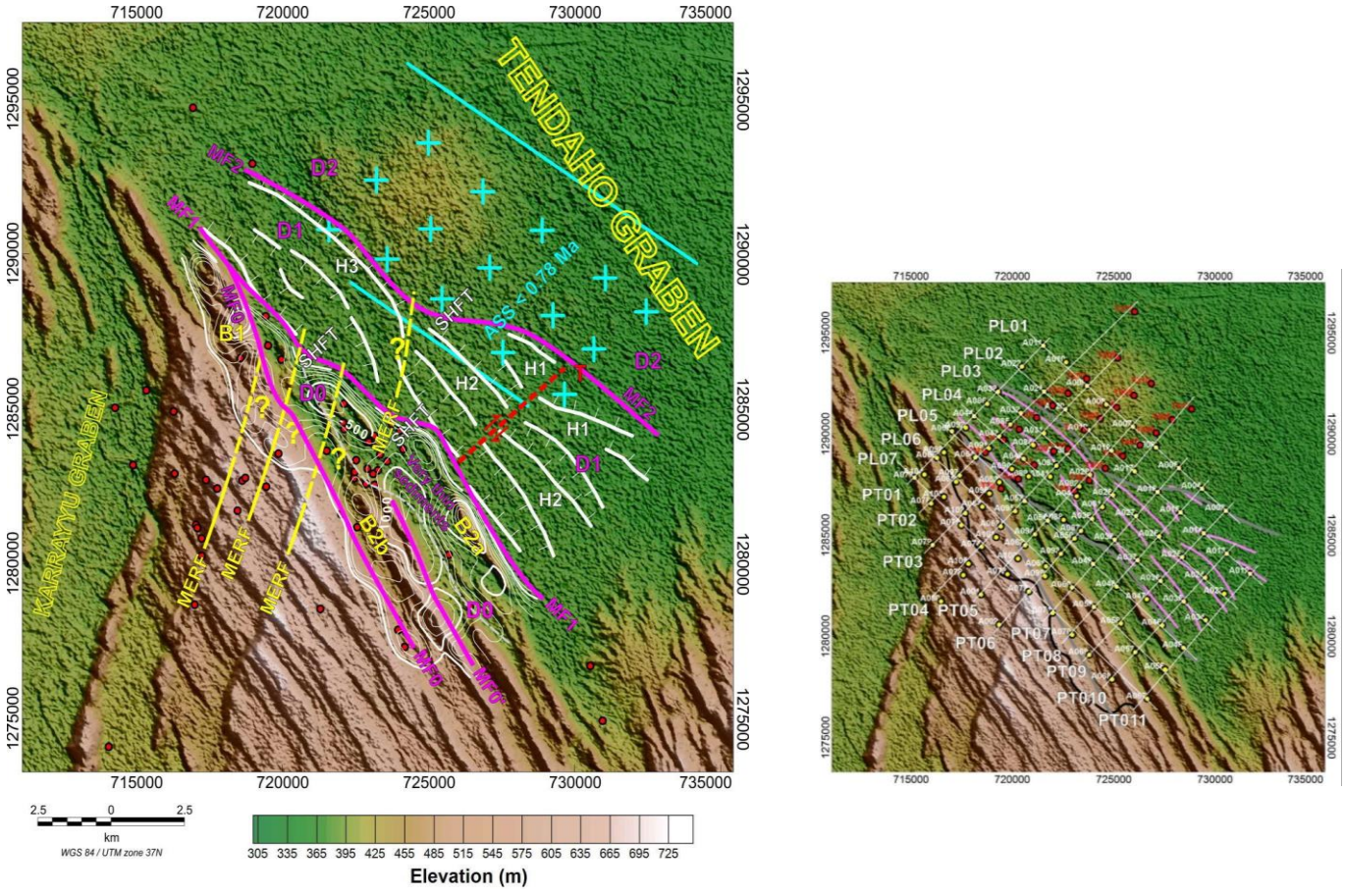

Figure 5-9 LEFT - Structural map derived from the gravimetric interpretation superimposed on the DEM. Epicentres are represented by the small red circles (see text). MF: main fault; H: horst structure. D: structural sector; B: bedrock. RIGHT - Location of resistivity cross sections

From the geomorphological point of view, Alalobeda area can be divided into two domains: (i) Alalobeda Plain, extending along the Tendaho Graben (TG) and (ii) Alalobeda Ridge, overlying basaltic products of the Afar Stratoid Series (ASS). Such lithological differences were also found to be reflected by electromagnetic investigations (MT/TEM).

In the Alalobeda ridge, a 1D inverse modelling example, shown in Figure 5-10, carried out over an outcrop of basalts of the ASS, indicates the following electrostratigraphic sequence:

- A surficial relatively resistive layer (≈20 Ohm m) with a thickness of about 60 m;
- A very conductive layer (≈0.5 Ohm m), denominated ASS-CL1, centered at a depth of about 100 m;
- A moderately resistive layer (≈10 Ohm m) centered at a depth of about 250 m;
- A second very conductive layer (<1 Ohm m), denominated ASS-CL2, centered at a depth of about 500 m;
- A progressive increase of resistivity up to about 50 Ohm m at 2 km;
- The two very conductive layers centered at depths of 100 and 500 m might reflect the existence of important hydrothermal alteration.

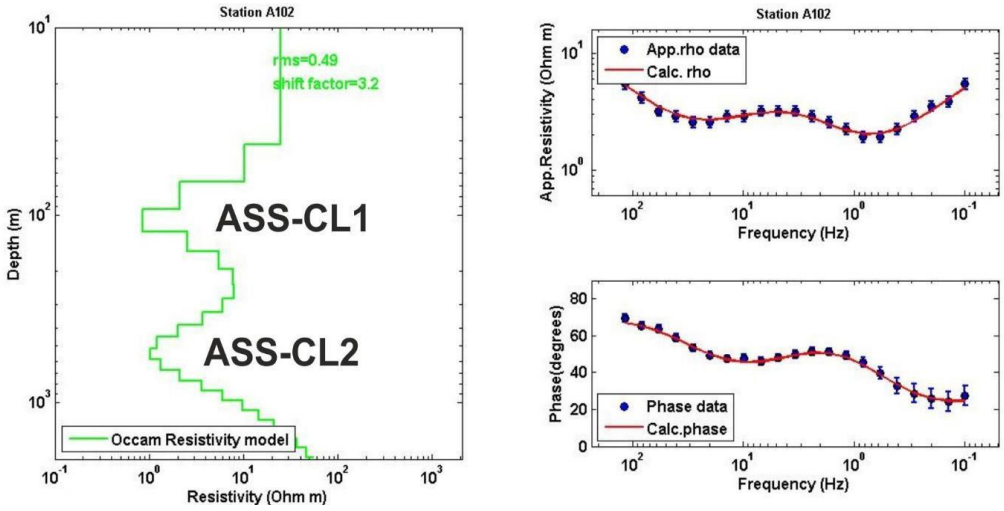

Figure 5-10 Smooth 1D model relevant to A102 station

- An example of 1D inverse modelling for the Alalobeda plain is shown in Figure 5-11. It points out the following electrostratigraphic sequence (the first three layers are denominated S-CL and the fourth one ASS):

- A shallow conductive layer (≈2 Ohm m) with a thickness of about 30 m;
- A very conductive layer (<1 Ohm m) centered at a depth of about 200 m;
- A rise of resistivity up to over 10 Ohm m at 1,000 m depth;
- A further progressive increase of resistivity up to about 40 Ohm m at 2 km.

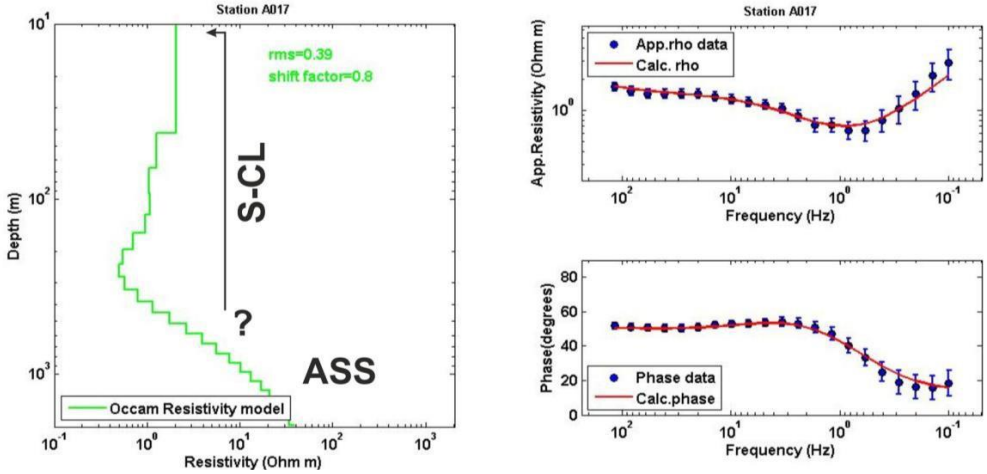

Figure 5-11 Smooth 1D model

The 3D inversion was carried out with different initial models, in order to validate the final model being interpreted. Thus, inversion was performed starting from a 50 Ohm m homogeneous medium, a 10 Ohm m homogeneous medium and a resistivity distribution resulting by the linear interpolation of the smooth 1D models. The data fit obtained from these models is good to excellent.

From the 3D inversion, resistivity cross-sections were prepared. The symbols utilized are the same already described for the 1D model and a selection of these profiles (PT04, see Figure 5-9 right) is represented in Figures 5-12, while Figure 5-13 represents horizontal slice at elevations 0 m asl - 600 m asl.

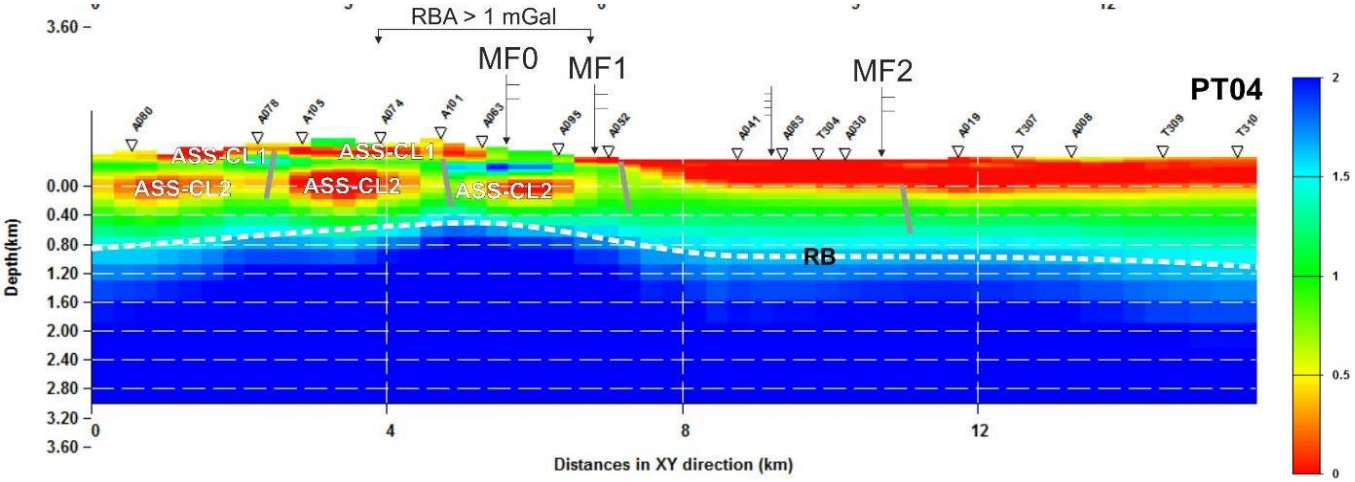

Figure 5-12 PT04 3D longitudinal profile. Scale color in LOG10 [resistivity (ohm.m)]

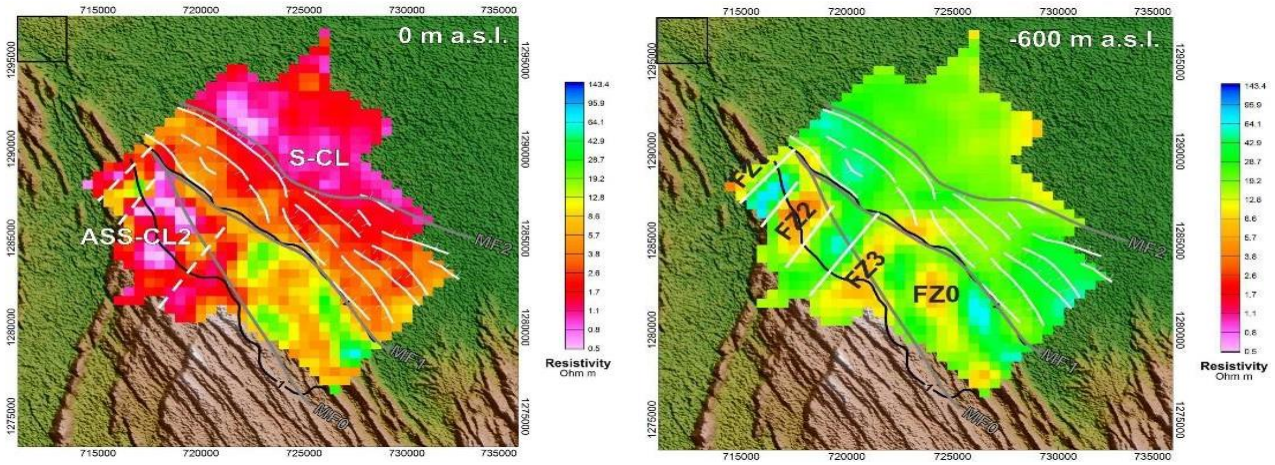

Figure 5-13 PT04 3D longitudinal profile, at 0 m asl (left) and -600 m asl (right)

The overall resistivity distribution is in good agreement with the results from 1D pseudosections. However, greater deviations in the ridge sector led me to a different explanation of the conductivity anomalies.

i. The shallow conductive layer ASS-CL1 (see Figure 5-12) can be identified in the ASS basalts in the ridge sector. It results as a superficial alteration level that extends up to the MF1 fault system. To the NE it is hindered by the sediments and likely forms the base of the S-CL conductive layer in the plain sector.

ii. The deeper conductive anomaly referred to ASS-CL2 (see Figures 5-12 and 5-13) is discontinuous and cannot be identified with a continuous conductive layer. It is made by many different distinct lenticular anomalies at approximatively the same ranging depth. In the figures, we have still labelled every single anomaly as ASS-CL2. Note that it is very hard to identify any fault inside each anomalous body, wherefore faults detection becomes difficult and only undoubted cases have been marked in the sections.

iii. The shallow horizontal slices (from 350 to -200 m asl) show that in the ridge sector the single ASS-CL2 anomalies are elongated along NNE trending lineaments, suggesting a structural control by the NNE trending MER faults. A few longitudinal sections (PL06 and PL07, see Figure 5-9 right) show that below the single ASS-CL2 anomalies, the resistive bedrock RB shows a correspondent deepening. These features were interpreted as generated by enhanced hydrothermal alteration focussed along the permeable narrow fracture zones marked as FZ1-FZ3. High temperature clays cause the deepening of the resistive bedrock at depth, while low temperature clays generate the stronger ASS-CL2 anomalies at shallower depth.

iv. The conductive layer S-CL is well mapped in the plain area and easily used as a proxy to fault detection in the ASS bedrock hindered by sediments. There is a good agreement with the faults inferred by the gravity indicated by black arrows and the faults traced from the 1D pseudosections.

v. The anomaly marked as FZ0 in the longitudinal sections and in slices deeper than -400 m is the most important feature at depth. It may be caused by enhanced hydrothermal alteration focused along a large and deep structural discontinuity trending NS, with no evident relationships with surface structures.

Micro-seismic monitoring has led to identify two elements of primary interest with respect to the possible existence of a geothermal system, namely *depth* and *density of the events*. As refers to *depth*, the Alalobeda area is generally characterized by a relatively shallow seismicity that shows the maximum of event frequency at about 4-5 km of depth (see Figure 5-14). Below this depth, a clear decrease in seismicity is observed, allowing to hypothesise that the seismicity cut-off is located at approximately 5 km depth. This could be interpreted, as the limit of the brittle-ductile zone that may correspond to isotherms characterized by temperature ranging from 350 to 550 °C (Gresta et al., 1997). The seismicity above this zone may be related to the hydrothermal circulation processes, which activate the existent fractures inside that.

As refers to *events density*, five anomalous zones were identified, out of which the most conspicuous one is located in correspondence of the Alalobeda manifestations and exhibits a NNW-SSE trend, sub-parallel to the trend of the Tendaho Graben. Inside this zone, it is possible to recognize two subzones (see Figure 5-9 left), as the northernmost one assumes the highest values of event density with a clear event cluster pattern.

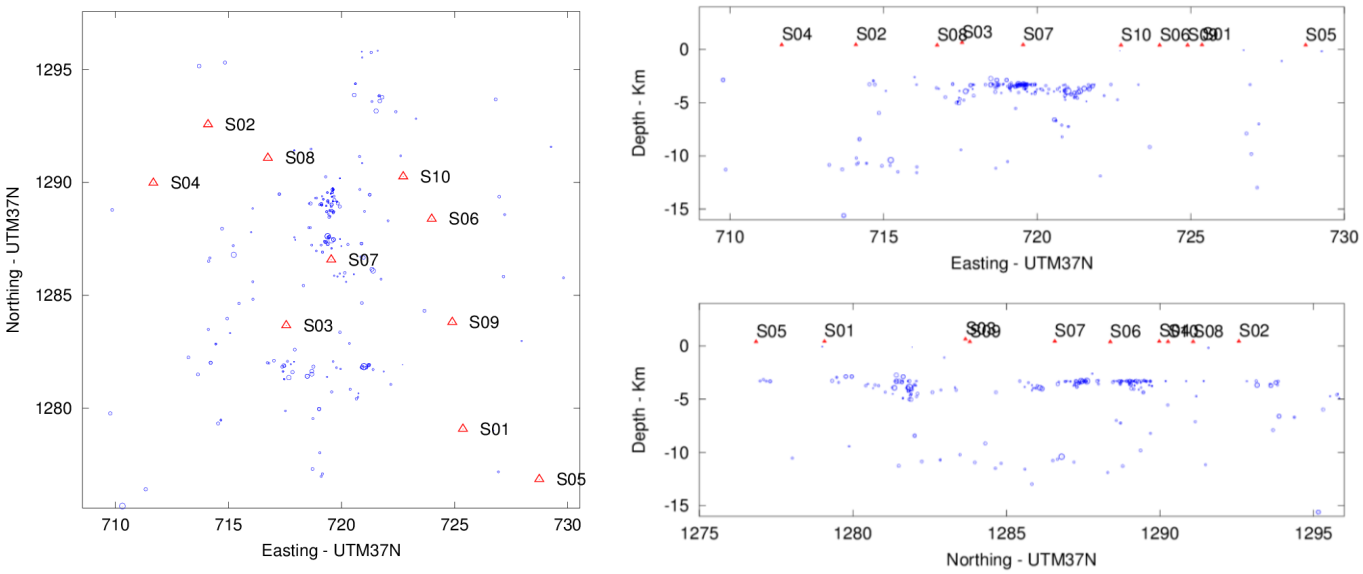

Figure 5-14 LEFT - Map of the earthquake locations in the restricted area of ±10 km, in E and N directions, from station S07. The triangles indicate the stations and the circles the epicentral locations with variable radius depending on their magnitude. The distances are referred to station S07. RIGHT - West-Est and North-South sections of the hypocentral depths in the restricted area. The triangles indicate the stations and the circles the epicentral locations with variable radius depending on their magnitude. The distances are referred to station S07

5.4.1.3. Integrated interpretation of geophysical data

For a better understanding of the overall setting of the Alalobeda prospect, in terms of interrelation between stratigraphy, structure and hydrothermal alteration, the results of the MT survey, were further examined through a detailed analysis of the Blocky 1D inversion of all the soundings. Such analysis was focused on the interpreted depth of the resistive basement and consequent identification of lateral geoelectrical discontinuities. Moreover, the configuration of the shallow and deep conductive units was studied and the presence of a very deep conductive unit was recognized. On the whole, with a few exceptions, a good consistency among adjoining soundings was observed, allowing a reasonable correlation along performed transversal profiles, subject obviously to the inaccuracies which are implicit in geoelectrical interpretation. The investigated area was accordingly subdivided into three distinct sectors (Figure 5-15), and the most interesting findings (see Figure 5-15) of such combined interpretation are mentioned hereafter:

- ✓ The gravimetric survey clearly shows that the structure of the area is mostly controlled by the Red Sea, NW-SE trending system. Transversal elements, either NNE-SSW or WSW-ENE, affect marginally the overall structural pattern.
- ✓ The major structures identified through gravimetry are almost perfectly coincident with the contacts between Sectors A and B and Sectors B and C.
- ✓ Similarly, the positive gravimetric anomaly along the shoulder of the Tendaho Graben follows exactly Sector B in its southern portion. At the height of the WSW-ENE structure causing a shifting of the NE boundary of this sector. The anomaly becomes narrower and tends to be shifted to the SW. It is reminded that the gravimetric anomaly is interpreted as being related to an intermediate depth source, possibly due to hydrothermal alteration (propylitization) of the basalts causing a density increase.
- ✓ The WSW-ENE structures recognized through the geoelectrical and gravimetric surveys may be

interpreted as associated with sinistral strike-slip faults conjugate with the formation of the Tendaho Graben.

- ✓ The micro-seismic survey highlighted two elements, which may have direct correspondence with the existence and configuration of a geothermal system, namely density of the seismic events and depth of the relative hypocenters.
- ✓ As refers to density of the events, a very pronounced anomaly, classified as A3 zone, was identified: this anomaly occurs in the northern portion of Sector B, just south of the WSW-ENE structure which displaces the SW boundary of this sector.
- ✓ As refers to depth of the events, presumably reflecting the boundary between brittle and ductile zones, the above mentioned A3 zone, associated with the maximum density of events in the transitional zone, is also characterized by the shallowest depth of the hypocenters, which does not exceed 5 km

In general, a good consistency of the favorable factors pointing to the potential existence of a geothermal system can be recognized. These factors tend to single out a preferential zone centered around the main hydrothermal manifestations of Alalobeda and are utilized for inferring the extent of the reservoir.

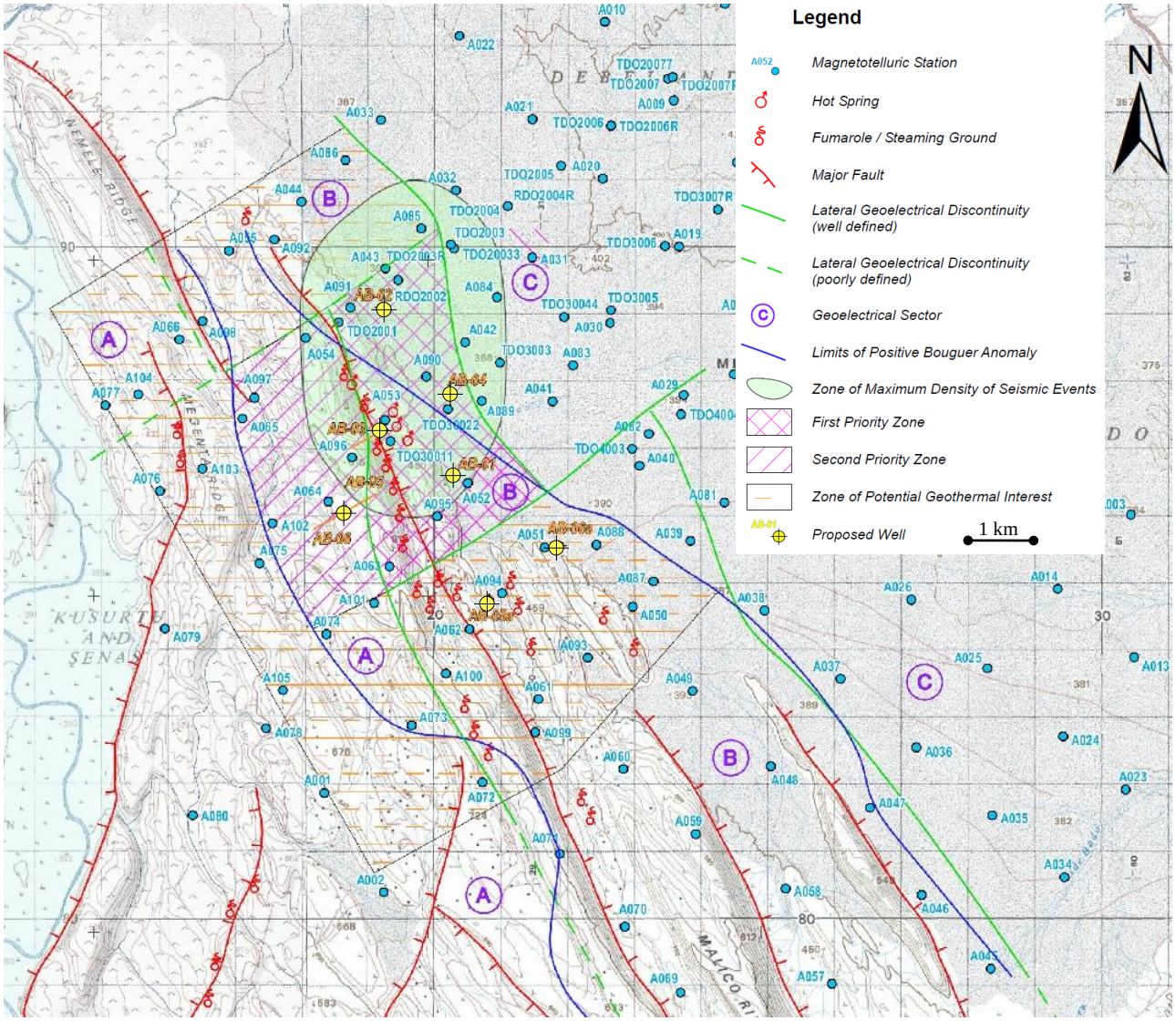

Figure 5-15 Synthesis map of the Alalobeda geothermal prospect

5.4.1.4. Geochemical data

Using concentration of major anions and major cations, three water types were identified (Figure 5-16), namely:

- *Sodium-chloride type*. It is represented by both the thermal manifestations of Alalobeda and the reservoir liquids encountered by the exploratory wells drilled in the Dubti prospect. Limited differences are encountered between the two groups of samples. In spite of these differences, it is reasonable to hypothesize that also the Alalobeda thermal waters are mature aqueous solutions coming from a high enthalpy geothermal reservoir (ELC-TGDC, 2016).
- *Sodium-bicarbonate type*. It is represented by the sample collected from the manifestation situated some 700 m WNW of the main Alalobeda manifestations (ALB-W-10). This sample is a natural steam condensate, possibly affected by mixing with local rainwaters.
- *Sodium (calcium)-bicarbonate (sulfate) type*. It is represented by the sample collected from the Awash River Dam Lake (ALB-W-17). The chloride and sulfate components are presumably related to other natural and/or anthropogenic processes of hard identification.

The concentration of each chemical constituent was examined against the concentration of chloride, chosen as reference component owing to its mobile behaviour. *The main object of this correlation was the identification of the natural causes which may have brought about significant variations in the composition of the water samples collected during the present work and in the previous campaigns*. These variations, and in particular the increase in K and SiO_2 and the decrease in Mg, suggest that (i) the reservoir zones feeding today the Alalobeda hot springs are hotter than those which were delivering hot fluids in the past, and/or (ii) the deep hot waters at present reach the surface more quickly than in the past and, consequently, they are less affected by re-equilibrium upon cooling.

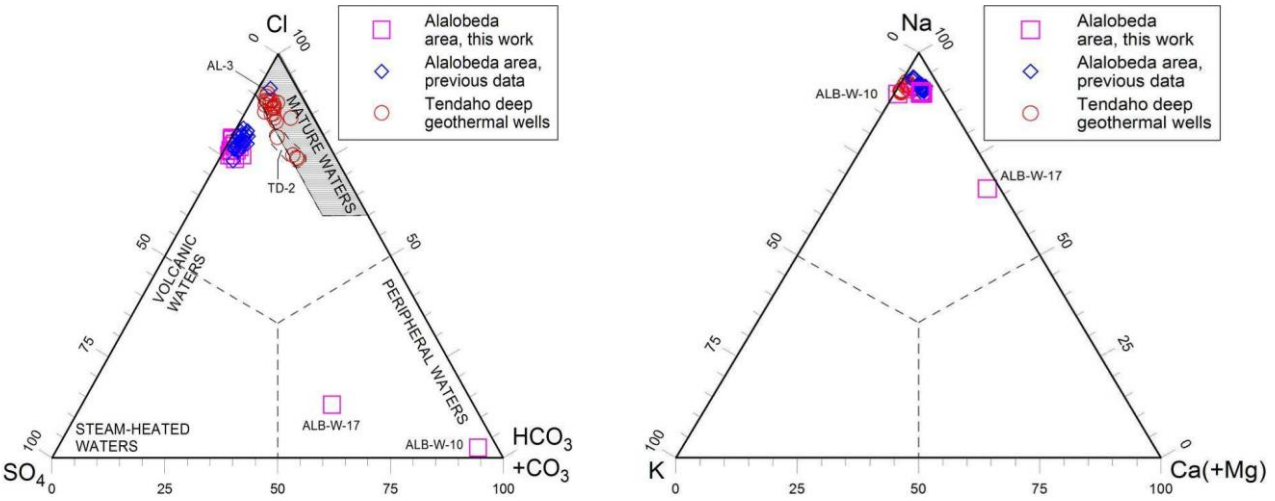

Figure 5-16 LEFT - Triangular diagram of main anions (from Giggenbach, 1988, modified) for the water samples collected in the Alalobeda area during this work. Also shown are the water samples obtained in the Alalobeda area during previous works and the water samples from the Tendaho deep geothermal wells (data computed at reservoir conditions). RIGHT - Triangular diagram of main cations for the water samples collected in the Alalobeda area during this work. Also shown are the water samples obtained in the Alalobeda area during previous works and the water samples from the Tendaho deep geothermal wells (data computed at reservoir conditions)

The observed chemical changes are consistent with the transition from geyser activity to steady hot water discharge, admitting that today the hot uprising water flows through underground conduits

larger than in the past. Moreover, the Cl-B and Cl-Li relationships suggest that chloride is probably contributed almost entirely as magmatic HCl entering the roots of the geothermal system of Alalobeda together with other magmatic gases. These are absorbed into deep circulating groundwaters, whose neutralization generates the deep geothermal liquids.

Based on the Na-K and K-Mg geothermometers of Giggenbach (1988), all the samples from the Alalobeda thermal springs collected during this work indicate that the initial unboiled reservoir liquid is close to equilibrium with albite, K-feldspar, chlorite, illite and a silica mineral at ~220 °C (see Tables 5-1 and 5-2). Assuming maximum steam separation, the silica (quartz) geothermometers by Giggenbach et al. (1994) and Fournier (1973) indicate temperatures close to 200 °C, which are reconciled with Na-K and K-Mg temperatures admitting the occurrence of some silica loss (104-131 mg/kg) through precipitation of amorphous silica upon adiabatic cooling. Considering the increase in K and Ca concentrations due to boiling from 220 °C to 100 °C, an average P_{CO2} of 0.0528 ± 0.0054 bar (1σ) is estimated for the aqueous solutions prior to boiling by using the K-Ca P_{CO2}-indicator.

Alternatively, based on the Na-K geothermometer of Fournier (1979) and the maximum-steam-loss silica (quartz) geothermometers by Giggenbach et al. (1994) and Fournier (1973), the initial unboiled reservoir liquid would be close to equilibrium with albite, K-feldspar, and quartz at ~200 °C. Accepting this interpretation, it must be admitted that the K-Mg temperatures overestimate the reservoir temperature due to secondary processes and/or analytical uncertainties. Considering the increase in K and Ca concentrations due to boiling from 200 °C to 100 °C, an average P_{CO2} of 0.0556 ± 0.0057 bar (1σ) is obtained for the aqueous solutions prior to boiling by means of the K-Ca P_{CO2}-indicator. Samples collected in 1995 from springs AL-1 and AL-2 and samples obtained in 1990 from springs AL-2 and AL-4 substantiate both interpretations, whereas the remaining 25 previous samples are affected by secondary processes and possibly by uncertainties due to analytical problems and improper sample preservation.

Finally, the Na-HCO_3 sample ALB-W-10 (coming from the fumarolic area situated to the NW of the thermal manifestations of Alalobeda, at a distance of ~700 m) could proceed from a relatively shallow peripheral aquifer at 155-160 °C as indicated by chalcedony solubility and the K-Mg geothermometer.

Table 5-1 Temperatures computed through direct application of geothermometric functions for the samples collected from the Alalobeda thermal manifestations during this work

Sample	T_{ch}	T_{qz}	$T_{qz\text{-}msl}$	T_{SiO2}	$T_{SiO2\text{-}msl}$	T_{KMg}	$T_{KMg\text{-}msl}$	$T_{NaK\text{-}F}$	$T_{NaK\text{-}G}$
	°C	°C	°C	°C	°C	°C	°C	°C	°C
ALB-W-01	207	221	201	224	198	202	-195	204	220
ALB-W-02	207	221	201	224	198	218	-210	205	221
ALB-W-03	201	216	197	218	193	195	-189	198	215
ALB-W-04	207	221	201	225	198	-235	226	204	220
ALB-W-05	210	224	203	228	201	-234	225	204	220
ALB-W-06	206	220	200	224	197	-235	226	204	220
ALB-W-07	208	222	202	226	199	205	-198	200	216
ALB-W-08	206	220	200	224	197	217	-209	205	221
ALB-W-09	209	222	202	226	199	209	-202	205	221
ALB-W-11	207	221	201	225	198	216	-208	203	219
ALB-W-12	203	218	198	220	195	212	-205	198	215
ALB-W-13	212	225	204	230	202	-231	222	202	219
ALB-W-14	210	224	203	228	201	-231	222	202	219
ALB-W-15	210	224	203	228	201	-228	220	198	215
Average	***207***	***221***	***201***	***225***	***198***	***209***	***223***	***202***	***219***
Std.dev.	***3***	***2***	***2***	***3***	***2***	***8***	***3***	***3***	***2***
ALB-W-10	157	178	167	169	156	154	151	272	283

Table 5-2 Temperatures computed through direct application of geothermometric functions for the samples collected from the Alalobeda thermal manifestations during previous investigations

Sample	Date	T_{ch}	T_{qz}	$T_{qz\text{-}msl}$	T_{SiO2}	$T_{SiO2\text{-}msl}$	T_{KMg}	$T_{KMg\text{-}msl}$	$T_{NaK\text{-}F}$	$T_{NaK\text{-}G}$
		°C	°C	°C	°C	°C	°C	°C	°C	°C
AL-1	1980	219	231	209	238	208	146	143	190	207
AL-2	1980	204	219	199	221	196	158	155	178	196
AL-3	1980	202	216	197	218	193	150	147	187	205
AL-4	1980	195	211	193	211	188	163	159	193	210
AL-5	1980	209	223	203	227	200	169	165	180	197
AL-6	1980	206	220	200	223	197	150	147	196	213
407	1980	206	220	200	223	197	158	155	187	204
AL-1	11/10/1990	216	229	207	235	206	179	174	202	219
AL-2	11/12/1990	206	220	200	223	197	209	202	194	211
AL-3	11/12/1990	201	216	197	218	193	177	172	195	212
AL-4	11/12/1990	204	219	199	221	196	192	186	194	211
AL-5	13/11/1990	204	219	199	221	196	156	153	192	209
AL-1	05/12/1995	195	211	193	211	188	241	232	186	203
AL-2(8)	05/12/1995	199	214	196	216	192	236	227	195	211
Ala sp-B	02/08/1996	213	226	205	232	203	142	140	177	195
Ala sp-1	02/08/1996	204	219	199	221	196	160	156	181	198
Ala sp-c	02/08/1996	272	274	242	297	-250	163	159	186	204
Ala sp-d	02/08/1996	-125	-151	-144	-135	-129	160	156	181	198
Ala sp-e	02/08/1996	-133	-157	-149	-143	-135	120	119	180	197
Ala sp-g	02/12/1996	197	212	194	213	189	151	148	165	184
Ala sp-f	02/12/1996	201	216	197	217	193	172	167	181	199
AL-1	09/04/2000	207	221	201	224	198	173	168	179	197
AL-1	04/01/2003	201	216	197	217	193	174	169	187	204
73	04/01/2003	201	216	197	217	193	174	169	187	204
AL-2	04/01/2003	199	214	196	216	192	135	132	185	203
AL-3	04/01/2003	193	209	192	209	187	172	167	185	203
AL-1 H.sp	2004	190	206	190	206	184	177	172	192	209
AL-2 H.sp	2004	190	206	190	206	184	176	171	192	209
UN-73 H.sp	2004	185	202	186	200	180	162	158	184	201
Average		***204***	***219***	***199***	***222***	***194***	***169***	***164***	***187***	***204***
Std.dev.		***16***	***13***	***10***	***17***	***7***	***26***	***24***	***8***	***7***

In conclusion, the geochemical analyses of water samples collected from the Alalobeda hot springs indicated reservoir temperatures of 200-220 °C. Such temperatures are substantially consistent with those (on average 185-225 °C) inferred from fumaroles gases.

All the fumarolic gases collected during this work (see Table 5-3) in the Alalobeda and Ayrobera areas have N_2/Ar molar ratio varying from 38.7 to 44.8 around an average value of 41.3 ± 1.5, which is very close to the ASW value, 39.4. This correspondence suggests that both N_2 and Ar are supplied *in toto* as dissolved gases into the meteoric recharge. The only exception is represented by sample G20, whose N_2/Ar ratio is somewhat higher, 53.9, due to addition of atmospheric air.

The gas samples obtained in this work have somewhat different He/Ar and He/N_2 ratios evidently due to variable addition of He deriving from the mantle source to the gases supplied from the meteoric source. In fact, they are situated along the tie line connecting these two endmembers. Quite similarly, most previous data plot along the lines joining the He-rich compositions typical of gases from either the mantle or the crust and the two He-poor atmospheric endmembers (ASW and air), although previous data are more scattered than present-day data.

The He enrichments of both datasets are attributable to involvement of mantle gases rather than crustal gases, considering the high $^3He/^4He$ isotope ratios measured in the Tendaho wells TD-2 and TD-4 and in two manifestations of the Dubti area, which are close to 13 R/R_A (values corrected for air contamination; Aquater, 1995).

These very high He isotope ratios are typical of the so-called Ethiopian mantle plume, whose high-^{3}He signature was established by Craig and Lupton (1977) based on the volcanic gases of the Ethiopian Rift Valley from 6°N (region of Lake Abaya) to 12° (Tendaho Graben). The $^3He/^4He$ isotope ratios in these gases range up to 15.1 R/R_A at 7.3°N in the Corbetti Caldera volcanoes, showing that a Primitive Mantle plume is present in the Ethiopian Flood Basalt province, as passive upwelling of the asthenosphere cannot produce basalts with ratios greater than the characteristic MORB value, 8 R/R_A.

These early findings were later confirmed by Scarsi and Craig (1996) who measured the helium isotope ratios in olivine and pyroxene phenocrysts from basalts of the Ethiopian Rift Valley and Afar Depression. High $^3He/^4He$ isotope ratios were found all along the Ethiopian Rift and into the Afar Depression, with a maximum value of 17.0 R/R_A at 8°N in the Rift Axis and a high value of 14.2 R/R_A, in the central Tat'Ali sector of the Afar Depression. Recently, $^3He/^4He$ isotope ratios of 10.9 to 11.9 R/R_A were reported for a series of hot springs located near Dallol volcano within the Danakil Depression by Darrah et al. (2013).

Table 5-3 Results of the chemical analyses of the samples of total fumarolic fluids (i.e., steam plus gases) collected during this study in Giggenbach's bottles. All the gas samples come from the Alalobeda area, apart from sample G24 which proceeds from Ayrobera. H is altitude, T is outlet temperature, ppmv is the acronym of parts per million by volume, which is numerically equivalent to parts per million by mol or μmol/mol

Sample	Date	T	H_2O	CO_2	H_2S	N_2	CH_4	Ar	O_2	H_2	He
Code		°C	ppmv	ppmv	ppmv	ppmv	ppmv	ppmv	ppmv	ppmv	ppmv
G5	26/09/2014	97.8	994166	5806	-	24	1.7	0.6	1.9	0.0046	0.0263
G5	26/09/2014	97.8	994110	5855	-	30	2	0.7	2.3	0.0033	0.023
G6	26/09/2014	97.9	995632	4344	-	19	3.3	0.48	1.1	0.0061	0.0199
G6	26/09/2014	97.9	995709	4276	-	13	1.2	0.33	0.66	0.003	0.0138
G10	26/09/2014	97.9	995893	3993	-	96	0.0035	2.3	16	0.0032	0.101
G10	26/09/2014	97.9	994483	5456	14	43	1.1	1	1.8	0.033	0.0308
G18	26/09/2014	97.8	994324	5627	-	42	0.0027	1	6	0.0025	0.0425
G18	26/09/2014	97.8	994811	5104	-	71	9.6	1.8	2.8	0.0199	0.0642
G19	27/09/2014	97.9	993903	5985	-	75	33	1.9	1	1.2	0.0863
G20	27/09/2014	98	964315	34782	-	822	2.8	15.3	66	0.046	0.442
G21	27/09/2014	98.2	995978	4007	-	13	1	0.33	0.52	0.011	0.00831
G22	28/09/2014	97.3	994224	5728	9.4	29	8.5	0.67	1.2	0.015	0.0238
G23	28/09/2014	96.7	994322	5599	-	70	3.6	1.7	3.6	0.025	0.0484
G24	28/09/2014	97.2	994336	5578	9.2	65	8.8	1.5	0.039	2.1	0.0697
G24	28/09/2014	97.2	994192	5690	-	101	0.0053	2.3	15	0.0053	0.0614

The tritium content of a groundwater can be used to estimate its residence time in the subterranean circuit, by referring to the two theoretical models of: (i) piston flow and (ii) perfectly mixed reservoir (Pearson and Truesdell, 1978). The first model assumes the absence of mixing along the entire water circuit, from the infiltration point of to the discharge point at the surface. The second model is based on the hypothesis that the water entering the reservoir mixes perfectly with that already contained into it and that the water leaving the reservoir is representative of such a mixture. These theoretical models do not apply if the water of the considered circuit mixes with one or more different waters. The tritium content of many springs is actually due to mixing of virtually tritium-free deep water with tritium-rich shallow water.

Both theoretical models are based on the knowledge of the time changes of the tritium content of local rainwater. The tritium content of the rainwater of the GNIP-IAEA-WMO station of Addis Ababa was determined quite regularly from 1964 to 1974, again from 1984 to 1987, and finally from 1990 to 1997. A time series consisting of 151 tritium data is available for this location in the GNIP-IAEA-WMO

database (IAEA/WMO, 2013). The tritium content of Addis Ababa rainwaters is displayed in Figure 5-17, showing its gradual decrease from 1964 to 1997.

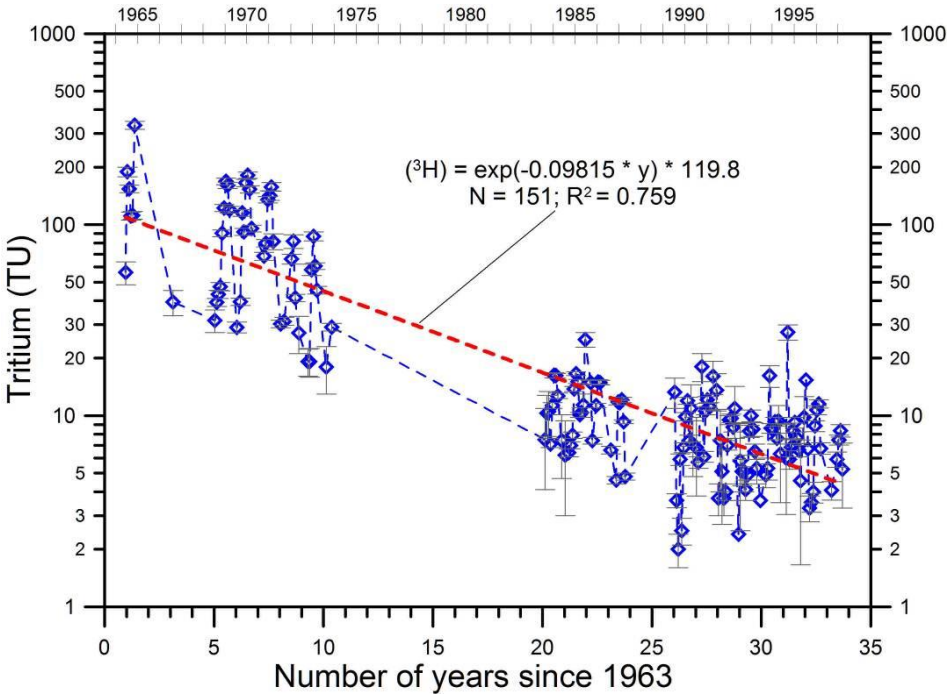

Figure 5-17 Chronogram of tritium content in the rainwaters collected at the GNIP-IAEA-WMO station of Addis Ababa (data from IAEA/WMO, 2013)

The high tritium contents in the 1960s were due to the introduction of large quantities of tritium in the atmosphere through the above-ground testing of nuclear weapons in the mid-1950s and early 1960s. The amount of tritium in the atmosphere from weapons testing peaked in 1963 worldwide and has been decreasing ever since due to the cessation of these activities. This tritium decrease is essentially controlled by its decay through beta emission to stable ^{3}He with a half-life of 12.26 years, corresponding to a radioactive decay constant λ (0.05576 y^{-1}) (Faure, 1986). The tritium data of Addis Ababa rainwaters are conveniently explained by the following regression equation (N= 151; $R^2 = 0.759$):

$$(^{3}H) = \exp(-0.09815 \cdot y) \cdot 119.8$$

where y indicates the number of years since 1964. Tritium data of Addis Ababa rainwaters also exhibit a very pronounced short-period variability, but it is likely that such a variability is significantly attenuated by the mixing processes occurring in the subterranean aquifers.

The above equation was used to obtain the relations between the residence time of water in the subterranean circuit and tritium content for each one of the two reference models. The well-mixed reservoir model is more suitable to the characteristics of both the waters discharged from the Alalobeda hot springs (whose available tritium are summarized in Table 5-4) and the hydrogeological circuit they come from. Nevertheless, Figure 5-18 shows the graphical relationships between residence time and tritium content for both theoretical models for completeness. To be noted that these graphical relations are valid for 1996.

Among the seven samples collected at Alalobeda in that year, four are tritium free whereas the other three have tritium content of 0.1, 0.3, and 0.7 TU (Kalberkamp et al., 2012). Moreover, a tritium content of 0.7 ± 0.51 TU was measured for a sample collected from spring AL-1 on 05/12/1995. To be noted that the absence of correlation between tritium and chloride (R^2 = 0.069) suggests that the

occurrence of mixing (dilution) is very unlikely. Therefore, tritium can be used to estimate the residence time of the Alalobeda thermal waters.

Table 5-4 Tritium data available for the Alalobeda hot springs

Sample	Date	Tritium	Reference	Sample	Date	Tritium	Reference
	dd/mm/y	TU			dd/mm/y	TU	
AL-1	11/10/1990	0.00 ± 0.6	Aquater (1995)	Ala sp-B	02/08/1996	0	Kalberkamp et al. (2012)
AL-2	11/12/1990	0.00 ± 0.6	Aquater (1995)	Ala sp-d	02/08/1996	0	Kalberkamp et al. (2012)
AL-3	11/12/1990	0.00 ± 0.6	Aquater (1995)	Ala sp-e	02/08/1996	0	Kalberkamp et al. (2012)
AL-4	11/12/1990	0.00 ± 0.6	Aquater (1995)	Ala sp-g	02/12/1996	0	Kalberkamp et al. (2012)
AL-5	13/11/1990	0.00 ± 0.7	Aquater (1995)	Ala sp-f	02/12/1996	0.1	Kalberkamp et al. (2012)
				Ala sp-1	02/08/1996	0.3	Kalberkamp et al. (2012)
AL-1	05/12/1995	0.7 ± 0.51	Aquater (1995)	Ala sp-c	02/08/1996	0.7	Kalberkamp et al. (2012)

Based on the theoretical model of the well-mixed reservoir (Figure 5-18, right), the tritium contents of 0.7 and 0.1 TU measured for the Alalobeda thermal springs indicate residence times of 500 and 3000 years, respectively. These values should be considered as minimum estimates as the virtual absence of tritium in many samples points to higher residence times.

However, both the present-day precipitations regime and isotopic data argue that the Alalobeda geothermal reservoir hosts paleo-water seeped in early times. Groundwater is expected to flow mostly in the Afar Stratoid Series, reaching a depth of 1,500-2,500 m.

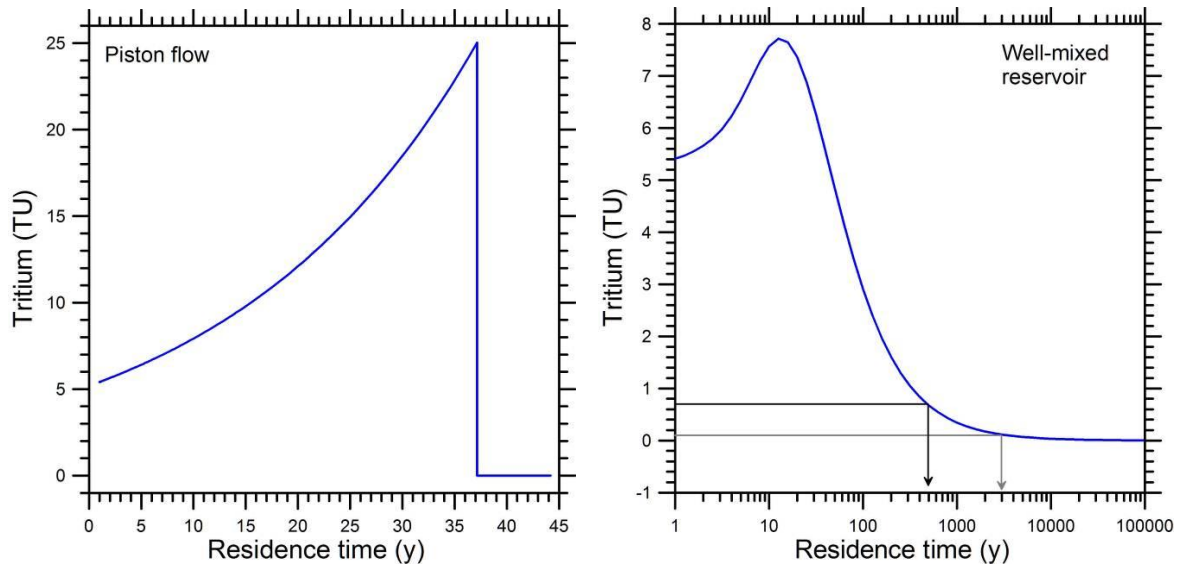

Figure 5-18 Graphical relations between residence time of water in the subterranean circuit and its tritium content in 1996. These graphical relations are based on the theoretical model of (left) piston flow and (right) well-mixed reservoir. The well-mixed reservoir model is used to interpret the tritium data of 0.1 and 0.7 TU for some samples collected in 1996 from the Alalobeda hot springs

5.4.1.5. Conceptual model

The essential features of the Alalobeda geothermal field can be summarized, as follows:

a. *Heat Source*. The magmatic conditions in the Alalobeda prospect can be classified on the whole as *fair* in terms of possibility of occurrence of a suitable heat source. A further confirmation about the likelihood of the existence of an active chamber is provided by the

observation that chloride contained in the reservoir fluids is probably contributed almost entirely by magmatic HCl entering the roots of the system with other magmatic gases (i.e., CO_2 and He, as indicated by $\delta^{13}C$ values of CO_2 and $^{3}He/^{4}He$ ratios; see Table 5-3). The exact geometric configuration of the chamber(s) cannot be inferred just from surface evidences, but, based on structural and resistivity considerations, an extension between the main thermal manifestation and the Debel and Halebayre "dome" may be assumed, at a depth presumably in the order of 10 km.

b. *Geological Setting.* In the peculiar geological setting of the Alalobeda prospect, the basalts of the Afar Stratoid Series are expected to play both roles of cap-rock and reservoir formation, while the underlying Dahla formation would play exclusively the role of reservoir. In fact, the sedimentary sequence, with a thickness nowhere exceeding a few hundred meters, is not adequate by itself to restrict the escape of the geothermal fluids. Obviously, the different roles to be played by the basalt assume the development of well distinct histories which modified the original conditions of the basalt:

- ✓ The basalt associated with the cap-rock formation underwent intense phenomena of argillification at temperatures lower than 200 °C, which determined conditions of imperviousness. Resistivity of the cap-rock formation is expected not to exceed 5 Ohm m.
- ✓ The basalt associated with the reservoir formation underwent phenomena of high temperature hydrothermal alteration (propylitization), which enhanced the brittle nature of the rock: such brittle nature on its side allowed, in presence of neo-tectonic activity, the formation of widespread fracturing and hence the increase of permeability. Resistivity of the reservoir formation is expected, by analogy with other geothermal fields in the world, to be in the order of 20-50 Ohm m.

c. *Reservoir Geometry.* The definition of the geometry of the cap-rock and reservoir formations, in terms of lateral extension and depth, was essentially based on the findings of the MT survey, combined with the indications derived from the geological, gravimetric and micro-seismic surveys. The geographical distribution of fumaroles was not considered because owing to the low vapor/liquid separation temperatures (close to 100 °C), fumaroles might be related to liquids that have experienced substantial lateral migration. The integrated interpretation of these investigations leads to the following main conclusions:

- ✓ Two different causes may be called for to explain the low resistivity units registered through the MT survey. In fact, such low resistivity can derive from the primary lithology of the rocks or from intense argillification phenomena. Making reference to the subdivision into three sectors of the area (see Figure 5-15), it is assumed that the conductive units of Sector C correspond to fine grained sediments, while those of Sectors A and B consist of strongly altered basalts.
- ✓ In Sector A, disregarding the very shallow and narrow conductive unit, of hard interpretation and of negligible bearing over the potential geothermal system, the conductive unit is quite constant in terms of both thickness and resistivity, covering a surface of at least 30 km^2 and being still open in all directions.
- ✓ In Sector B, the very thick horizon of low-medium conductivity can be at least partly attributed to the cap-rock formation. The average value of 5 Ohm m of this horizon rises to 8-10 Ohm m proceeding southwards between transversal profiles and this boundary can be conventionally assumed as the southern limit of the cap-rock.

- ✓ The whole resistive basement of Sectors A and B can in principle play the role of reservoir formation, although the interpreted values of resistivity (often in excess of 100 Ohm m) are somewhat higher than the ones normally recorded in other geothermal fields.
- ✓ From the point of view of structural setting, the priority sector can be referred to the intersection between the shoulder of the Tendaho Graben and the major faults which belong to the Main Ethiopian Rift system, trending NNE-SSW and well developed in the south-western portion of the prospect. The Alalobeda main manifestations are situated in correspondence of such intersection.
- ✓ It should be stressed that the lateral geoelectrical discontinuities between Sectors A, B and C should not be viewed as faults in a strict sense. Actually, they are deemed to delimit structural blocks which underwent distinct tectonic events affecting the permeability of the formations and hence the geothermal fluids circulation pattern and the distribution of secondary mineralogy.

The combined analysis of these observations can be used to carry out a zonation of the prospect based on the probability of existence of a geothermal system and to infer the geometric configuration of the reservoir.

Two clear boundaries were recognized (see Figure 5-15), namely: (1) to the NE the contact between Sectors B and C; (2) to the SE the zone where a marked resistivity increase of the potential cap-rock unit was observed. In the remaining area investigated by the geoelectrical survey encompassing both Sectors A and B, a continuous horizon of low resistivity, possibly associable with the cap-rock of the system, could be recognized. *This area can be classified as zone of potential geothermal interest*.

Such zone extends over a surface of some 60 km^2, out of which about 80 % fall over the basaltic ridge, that is in an environment characterized by very hard accessibility. The bottom of the conductive unit, which may indicate the *top of the reservoir*, occurs at a depth of 800-1,000 m bgl. No elements are available for estimating the elevation of the bottom of the reservoir: by analogy with other geothermal fields and considering that no lithological variations are expected to occur downwards, the thickness is assumed to be in the order of 1,000-1,200 m. Within the zone of potential geothermal interest, a *first priority zone* (see Figure 5-15) can be singled out, delimited on two sides by NNW-SSE trending geoelectrical discontinuities between A and B and between B and C sectors and on the other two sides by two transversal discontinuities trending WSW-ENE. The zone thus delimited includes the main hydrothermal manifestations and covers a surface of about 8 km^2.

It should be reminded that the actual lateral extent of the first priority zone is associated with a very high degree of uncertainty. In fact, only the eastern boundary is well defined, while the other boundaries are based on somewhat flimsy evidences. At any rate, it is stressed that the identification of the first priority zone serves mainly the purpose of selecting drilling targets rather than of estimating the potential of the reservoir.

For this purpose, in view of the definition of the drilling program, a *second priority zone* (see Figure 5-15) was identified. Such zone is located over the shoulders of the Tendaho Graben to the west of the first priority zone, occupying an area of about 7 km^2 and extending within the positive gravimetric anomaly, but at the margin of the micro-seismic anomaly. From the geoelectrical point of view, the zone is characterized by the presence of a thick conductive unit, underlain by a resistive basement: the contact between the two units, assumed to reflect the top of the reservoir, occurs at an average elevation of -400 m asl, that is some 200 m higher than the elevation

registered in the first priority zone.

d. *Natural Fluids Flow Pattern.* The isotopic composition of the geothermal fluids (deriving from both literature and PhD data, see Table 5-5), as inferred from the chemical analysis of the Alalobeda hot springs compared with the isotopic values of the Ethiopian rainwaters, suggests that the reservoir hosts paleowaters, which infiltrated into it during one or more previous pluvial periods.

Table 5-5 Results of the isotopic analyses of fumarolic CO_2 and steam condensates collected during this study. All the gas samples come from the Alalobeda area, apart from sample G24 which proceeds from Ayrobera

Sample	Date	Northing	Easting	T	δ^2H-H_2O	$\delta^{18}O$-H_2O	$\delta^{13}C$-CO_2
Code		m	m	°C	‰ vs. V-SMOW		‰ vs. V-PDB
G5	26/09/2014	1287723	719661	97.8	-39	-5.7	-6.83
G6	26/09/2014	1287699	719599	97.9	-46	-6.2	-9.9
G10	26/09/2014	1288203	718849	97.9	-55	-8	-9.52
G18	26/09/2014	1290621	717324	97.8	-57	-7.8	-11.75
G19	27/09/2014	1285089	720297	97.9	-54	-7.1	-8.05
G20	27/09/2014	1284462	721439	98	-51	-6.8	-8.14
G21	27/09/2014	1284427	721444	98.2	-57	-7.3	-10.39
G22	28/09/2014	1287358	719155	97.3	-55	-7	-8.61
G23	28/09/2014	1287219	719217	96.7	-57	-7.6	-6.33
G24	28/09/2014	1315617	727913	97.2	-33	-5.2	-11.65

Such indication seems to be confirmed by the fact that tritium content in the water points to a residence time included between 500 and 3,000 years. It should be added that, during the possible future exploitation of the field, a hydraulic gradient could be created such as to recall fluids from peripheral regions, which are going to recharge the system. Independently from the age of the fluids, it may be assumed that meteoric water infiltrating deeply into the ground, upon getting in proximity of an active heat source represented by a magmatic intrusion, tends to heat up and to upflow in correspondence of sectors characterized by intense fracturing and hence by good permeability as well as by thinning or termination of the cap-rock. In the specific case of Alalobeda, it is deemed that the heat source occurs at an approximate depth of about 10 km and that the sector of enhanced permeability is found at the intersection of the major tectonic systems, namely the Red Sea and Main Ethiopian Rift ones. These fluids rise up to a depth of a few kilometres, where their temperature is presumably slightly in excess of 200 °C. They are of a sodium-chloride type: the Cl-B and Cl-Li relationships suggest that Cl is probably contributed almost entirely by magmatic HCl entering the roots of the geothermal system with other magmatic gases (i.e., CO_2 and He, as indicated by $\delta^{13}C$ values of CO_2 and $^3He/^4He$ ratios).

The uprising of the heated fluids is restricted by the presence of impervious formations (cap-rock), which formed in the past as a result of argillification processes at temperature lower than 200 °C. Fluids tend therefore to expand laterally through fractured basalt flows and to install convective cycles, typical of geothermal systems. Due to their temperature, different hydrothermal alteration processes develop in the convection zone with formation of minerals such as epidote, quartz, albite, adularia e chlorite, as well as of clay in the form of illite.

The outflow of the system is supposed to take place mostly along the main faults intersecting the geothermal system, as expressed by the distribution of the thermal manifestations, which consist with one exception of fumaroles and steaming ground. In fact, it is observed that these manifestations are located, in the surroundings of the inferred reservoir, along NNW-SSE trending faults, whereas, moving further away to the south, they tend to align along NNE-SSW structures.

Based on the gas composition, vapors of the fumaroles appear to have separated at T, P close to 100 °C, 1 bar. The only hot spring situated outside of the main manifestations, approximately 700 m to the NNW, consists on its side of natural steam condensate, possibly affected by mixing with local rainwaters.

The frequency of the manifestations suggests that outflow is more pronounced in the Graben plain, this situation not necessarily means that no outflow is taking place to the east, since it may be related to the presence of impervious sedimentary products on surface, hindering the emergence of geothermal fluids from depth.

e. *Thermodynamic and Chemical Conditions.* The reservoir is expected to be liquid-dominated with a temperature of 200-220 °C. Fluids have a Na-Cl composition with relatively high content of SO_4 are rather diluted (TDS around 1,400 ppm) and may exhibit some calcite scaling tendency. Nothing can be said at this stage on their possible content of NCG owing to the strong uncertainty on the CO_2 partial pressure of reservoir fluids.

5.4.2. The Menengai geothermal field

The Menengai geothermal field has been the object of geoscientific investigations since the '60s, while underground exploration started in 2011 through drilling of deep wells. Since that time until the end of December 2013, 20 wells have been drilled (out of which three were abandoned before reaching their final depth) and additional wells are being drilled (see Figure 5-19).

Considering the regional importance of the Menengai geothermal field, and the available huge quantity of direct data (deriving from the drilled wells), during the elaboration of the present study was decided to perform a 3D Natural State Model.

5.4.2.1. Geological setting

The huge volume of pyroclastic flows (see Figure 5-20) that brought about the formation of the Menengai caldera is likely related to the presence of a magmatic chamber, which may act as the main heat source of the geothermal system (Geotermica Italiana, 1987a,b). The occurrence of very recent volcanic products (lavas and tuffs) within the caldera indicates that such chamber is still active and its top is found at a very shallow depth, presumably in the 5 to 10 km range. Based on the temperatures registered in the wells (see Figures 5-23, 5-24 and 5-25), the most shallow portion of the magmatic chamber is situated in the western part of the caldera, in correspondence of wells MW-04 and MW-06.

The formations outcropping within the caldera and those intersected by the wells are of peralkaline trachytic composition, presumably derived from fractionation of basaltic magmas, and consist predominantly of lavas, with subordinate pyroclastic intercalations (Omondi, 2011) and with a progressive increase of intrusive products towards the wells bottom and in the central portion of the investigated sector (Lagat et al., 2010, 2011).

The structure at a regional level (see Figure 5-20) is controlled by the family of N-S faults of tensional type, which extend along the Rift and constitute the main Tectono-Volcanic Axes (TVA) recognized in the area, that is the Molo and Solai systems presumed to form a complex graben & horst system (Leat, 1984). However, within the Menengai caldera other fault systems become predominant, in particular the NNW-SSE structures, which are highlighted by the occurrence of well aligned eruption centres and fumarolic activity. Another important system corresponds to the E-W direction expressed by a long-liner extending between MW-01 and MW-03 and by other parallel faults, which seem to partly control the areal extent of the reservoir.

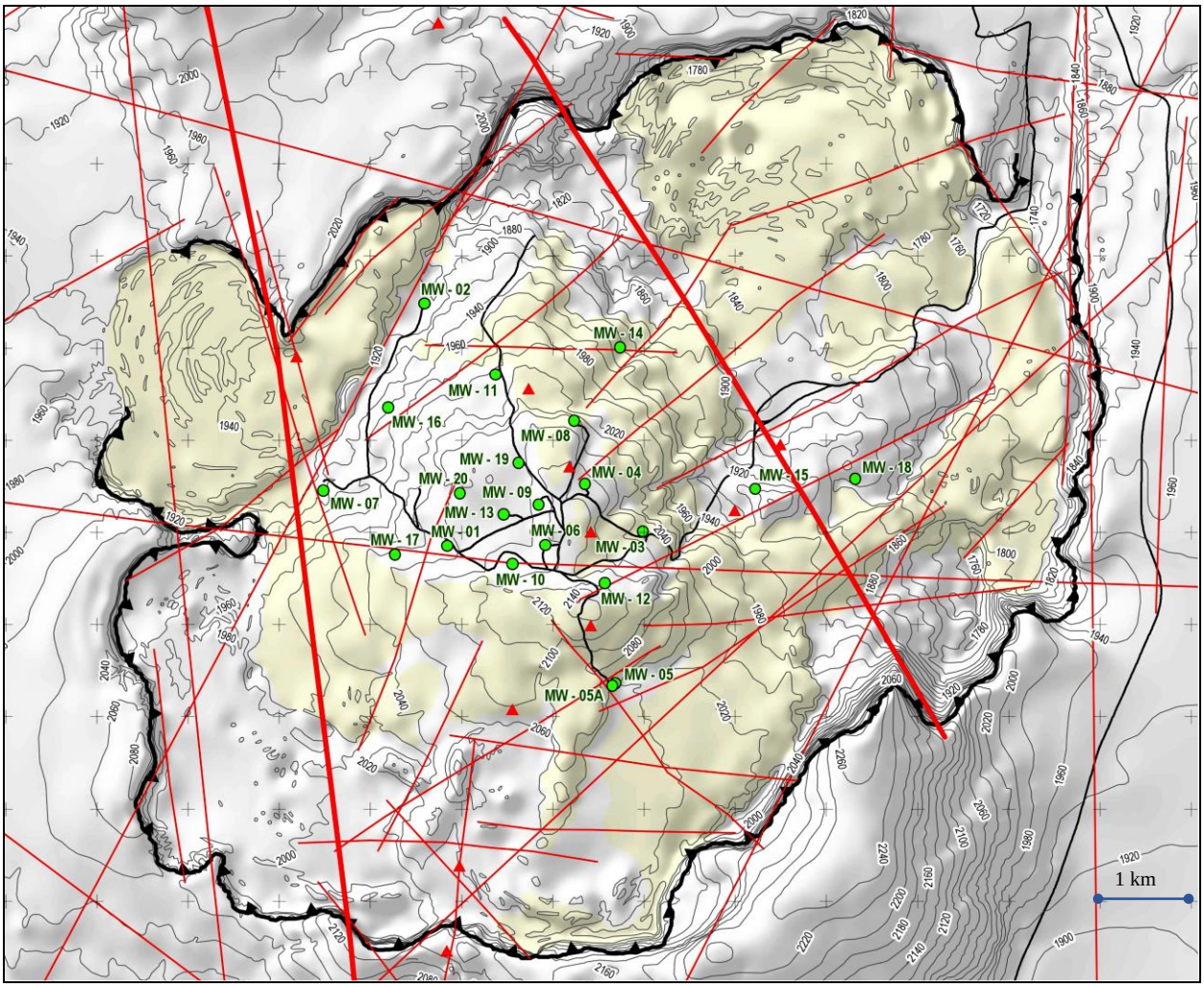

Figure 5-19 Structural Scheme of the Menengai Caldera and Wells Location (green dots). Yellow color: scoriaceous lava. Red line: faults. Red trianlges: volcanic vents

Two structures of the NNW-SSE system (trending N.7W and N.30W, see Figure 5-19) appear to be of major importance (Mibei et al., 2011), as indicated by their pronounced surface expression, their control over the volcanic emission centres and the association with high intensity of the linear features. These structures, also clearly expressed by the distribution of the micro-seismic events, define a block 4 to 6 km wide (see Figure 5-19), which extends throughout the caldera and where all the deep wells drilled to date are located, except MW-07, which falls at the western margin of this block.

As refers to secondary mineralogy (data deriving from drilled wells' the completion reports), it is observed that the minerals indicative of high formation temperature, that is quartz, pyrite and epidote, appear in general at an average depth of 600-800 m, corresponding to an approximate elevation of 1400 m asl. The only exceptions to this refer to wells MW-05A and partly MW-07, 08 and 12, where the high temperature minerals, which characterize the propylitic zone, are found below elevation 1000 m asl.

A pronounced dome-like shape of the top of the propylitic zone, as expressed by the first appearance of epidote, was recognized, being the upper portion in correspondence of a W-E oriented belt, which extends between MW-07 and MW-03. Such configuration might reflect the location of the main upflow sector of the geothermal system.

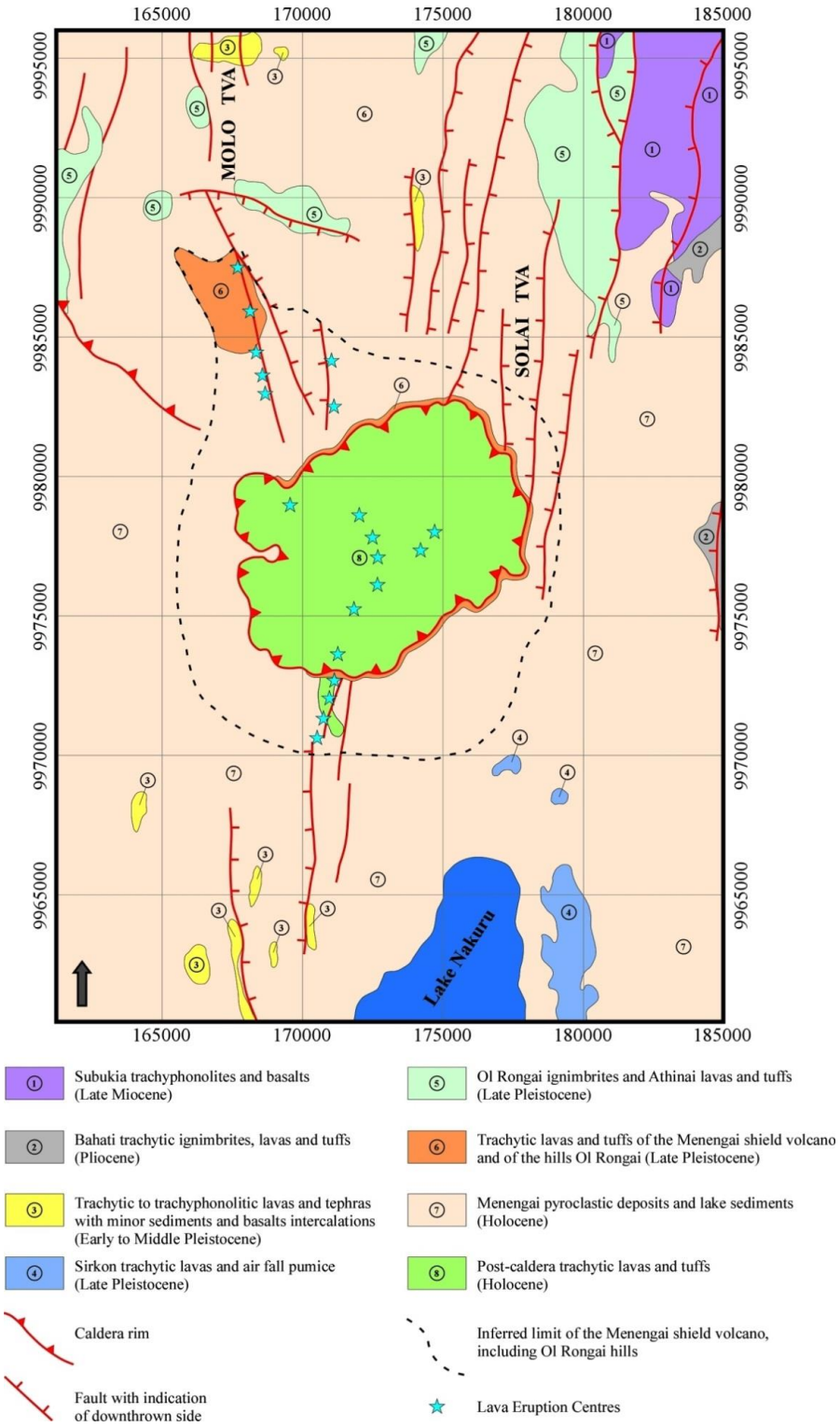

Figure 5-20 Simplified geological map of the Menengai caldera region

From the stratigraphic point of view, no specific geological units can be singled out as playing the role of cap-rock or reservoir. In fact, the whole stratigraphic sequence consists predominantly of trachytic lava, wherefore its permeability conditions depend essentially on the type and degree of hydrothermal alteration and on the extent and age of tectonic activity.

From the structural point of view (Figure 5-19), an intense neo-tectonic activity has taken place within the Menengai caldera, as expressed by the high density of the linear features. The above mentioned structural block delimited by the N.7W and N.30W faults is deemed to control the lateral

extent of the geothermal system and to host the most shallow and active portion of the magmatic chamber.

5.4.2.2. Geophysical data

The geophysical dataset available for the Menengai caldera and surrounding area includes gravity stations fairly regularly distributed throughout the Menengai caldera and in the northern region; ii) 80 time-domain electromagnetic (TDEM) stations and about 100 magnetotelluric (MT) stations distributed in an irregular way (see Figure 5-21) within the Menengai caldera (Saitet, 2012).

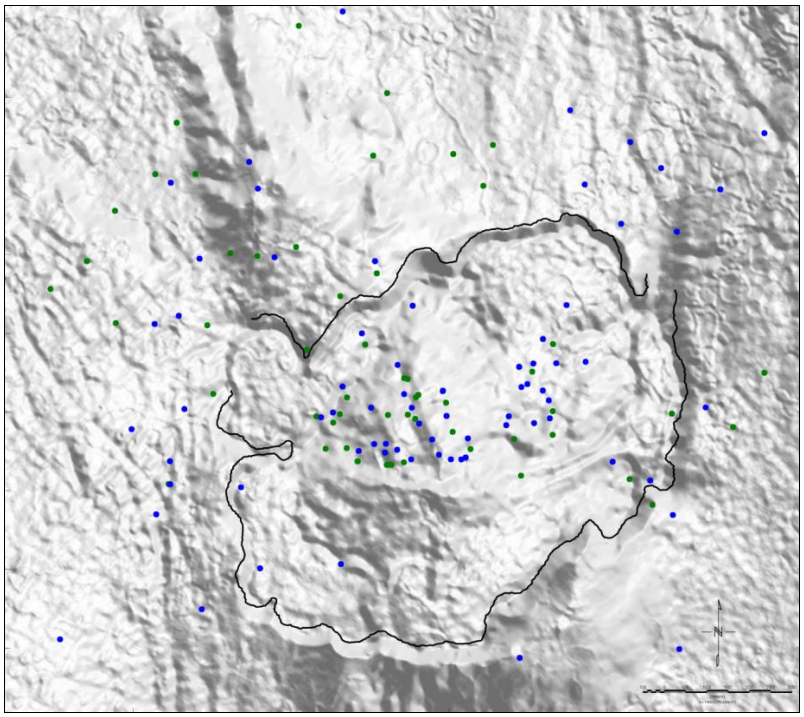

Figure 5-21 Location of TDEM (blue dots) and MT (green dots) station at the Menengai geothermal field

The analysis of gravity data puts into evidence a well-pronounced positive anomaly in correspondence of the Menengai caldera, which extends to the north, encompassing the Ol Rongai sector to the NNW. The anomaly can be modelled with a body, below the caldera, with a density of 2,900 kg m^{-3} enclosed in a surrounding medium of about 2,740 kg m^{-3}. The high-density body below the Menengai caldera could be interpreted as belonging to a magma chamber, although it is deemed that such interpretation should be further evaluated. In fact, recent literature suggests that the northward continuation of the gravity high in the Ol Rongai sector is due to a gabbroic intrusion associated with differentiation of a mafic (basaltic) magma (Simiyu, 2001). The presence of a less acid and therefore denser magma chamber beneath the caldera area and its surroundings, where generally a sequence of trachytic lavas crops out, is compatible with a possible path of magma differentiation. However, a density increase could also be related to secondary factors, such as the occurrence of high temperature hydrothermal alteration.

Inversion of MT data generally showed that four electrostratigraphic units can be recognized:

- An uppermost resistive unit, with a thickness of 100-300 m and a resistivity of 50-100 Ω m;
- An underlying upper conductive unit, with an average thickness of 600-800 m; and a resistivity usually ranging between 2 and 15 Ω m;
- A resistive basement with a resistivity is of the order of 100 Ω m, whose top may correspond to the top of the geothermal reservoir;

- A deep conductive unit, whose top is normally at a depth of some 10 km. Only in a few soundings, located around the major NNW-SSE fault in the eastern part of the caldera, the top of the conductive unit occurs at a depth in excess of 15 km. This unit has an average resistivity value of 5 Ω m and could be related to deeper magmatism (underplating).

The micro-seismic monitoring (Simiyu, 2009), conducted over a zone about 600 km^2 large centered around the Menengai caldera, identified the presence of three anomalies all characterized by a concentration of seismic events, shallow depth of the events themselves and low value of the V_p/V_s ratio, pointing to specific sectors with neo-tectonic activity and shallow depth of high temperature bodies. Two of the above anomalies occur in correspondence of the Molo and Solai TVA. The third and major one, under vapor dominated conditions, extends in the central portion of the Menengai caldera, encompassing a SW zone not yet tested by deep drilling.

5.4.2.3. Geochemical data

All the available geochemical data from deep geothermal wells (MW-01, 03, 04, 06, 09, 12 and 13; see Figure 5-22), surface manifestations, shallow aquifers and soil gases have been reviewed with the aim to reconstruct the geochemical model of the Menengai prospect (Clarke et al., 1990 and Leat et al., 1984). The main results of the review are summarized hereafter. On the basis of available geochemical data (GDC, 2012a,d), the Geothermal Reservoir present at depth inside the Menengai caldera comprises (see Figure 5-22):

(i) A shallow liquid dominated reservoir, at temperatures of 150-190 °C, as suggested by water geothermometers (solubility of the Quartz, Na-K e K-Mg), crossed by the wells MW-01, MW-03, MW-04, MW-12.

(ii) An intermediate reservoir, also crossed by a few wells, where temperatures inferred based on water geothermometers are 250-270 °C for wells MW-01, MW-04, and MW-12, but 230 °C only for well MW-03. It is possible that this intermediate reservoir is hydraulically connected with the deep one, at least in the sectors of wells MW-01, MW-04, and MW-12.

(iii) A comparatively deep reservoir, at temperatures from 280 to >340 °C, hosting fluids at different vapor/(vapor+liquid) mass ratios, y, as indicated by gas equilibria in the H_2O-CO_2-CH_4-H_2 system. In particular: (a) the central wells MW-06, MW-09, and MW-13, discharging superheated steam, as well as borehole MW-12 are connected with a deep vapor-dominated zone, where y is close to 1; (b) wells MW-04 and MW-01 (after the work over) intersect a deep two-phase zone where y is in the range 0.1 to 0.5; (c) wells MW-03 and well MW-01 (before the work over) seems to be in connection with a liquid-dominated deep zone, where y is close to 0. Well MW-01 has a very peculiar behavior since its deepest section has been connected with two deep feed zones with distinct vapor/(vapor+liquid) mass ratios. This fact is highlighted in the schematic cross-section of Figure 5-11 by the position of the well on the limit between the y~0 and the y~0.1-0.5 zones.

Irrespective of the provenance from the shallow or intermediate aquifers, all reservoir liquids belong to the Na-HCO_3 facies as Na (2441 to 3513 mg/kg) and total ionic carbonates (4786 to 8408 mg HCO_3/kg, with $HCO_3^- >> CO_3^{2-}$) largely prevail over other cationic constituents (K from 73.8 to 218 mg/kg, Ca from 0.11 to 0.89 mg/kg, and Mg from 0.05 to 2.37 mg/kg) and anionic ones. Average total dissolved solids range from 8659 to 13196 mg/kg (see Table 5-6).

Table 5-6 Chemical analyses of Lake Nakuru waters (data from Hecky and Kilham, 1973 and Melack and Kilham, 1974) and average composition of geothermal liquids (this report); contents in mg/kg

Well/Lake	T(° C)	pH	Na	K	Mg	Ca	Alk(HCO_3)	SO_4	Cl	F	SiO_2	TDS
MW-01 before w.o.	192	7.09	3513	218	0.05	0.80	8408	192	513	98.1	253	13196
MW-01 after w.o.	243	6.73	2965	136	0.18	0.16	6872	187	594	79.0	418	11251
MW-03	168	7.47	2441	73.8	2.37	0.11	5184	342	855	86.4	193	9177
MW-04	202	7.10	2740	122	0.05	0.89	6286	259	919	125	262	10714
MW-12	222	6.98	2486	87.4	1.62	0.20	4786	251	645	59.8	342	8659
Lake Nakuru	22	10.15	3305	236	0.88	<DL	7432	55	1024	130	208	12261

Regarding the pH determination, since the equations of Chiodini et al. (1991) cannot be applied to the Na-HCO_3 liquids of the Menengai geothermal field, the chemistry of the aqueous solution in equilibrium with paragonite, muscovite, clinochlore, calcite, K-feldspar, quartz, and fluorite at variable temperature (175, 200, 225, 250, 275 °C), variable P_{CO2} (1, 3, 10, 30, and 100 bar), and fixed Cl and SO_4 concentrations (700 and 200 mg/kg, respectively) was computed by means of the computer code EQ3, which is part of the software package EQ3/6, version 8 (Wolery and Jarek, 2003), using the most recent thermodynamic database (Wolery and Jove-Colon, 2007). Results were then processed through multiple regression analysis, obtaining the following relations (concentrations in mg/kg; temperature in K):

$$\mathrm{pH} = 5.9133(\pm 0.0511) + \frac{1998.9(\pm 37.6)}{\mathrm{T}} - 0.88024(\pm 0.01395)\cdot \log(\mathrm{Na}) \qquad (1)$$

$$\log \mathrm{P}_{\mathrm{CO}_2} = 2.6126(\pm 0.3405) - \frac{4381.1(\pm 250.8)}{\mathrm{T}} + 2.1641(\pm 0.09295)\cdot \log(\mathrm{Na})\,. \qquad (2)$$

The squared regression coefficients are 0.9958 for equation (1) and 0.9696 for equation (2). Equations (1) and (2) were then used to compute pH and P_{CO2} for all the available samples of reservoir liquids. Therefore, pH values, calculated through the above-mentioned mineral-solution equilibrium model, vary from 6.7 to 7.5.

With reference to gas geochemistry, it was observed that gas equilibrium temperatures of fluids from wells MW-01, MW-04, MW-09, MW-12, and MW-13 were generally > 340 °C, whereas lower equilibrium temperatures are indicated by fluids from wells MW-03 (280-300 °C) and MW-06 (from 280 to >340 °C). These equilibrium temperatures are similar to or somewhat higher than those measured in the deepest portions of Menengai wells, suggesting that gases are chiefly contributed by the deepest high-temperature zones of the geothermal reservoir.

The analysis of the gas equilibrium (CH_4/CO_2, H_2/H_2O and H_2/N_2, under redox conditions fixed by the $FeO\text{-}FeO_{1.5}$ redox buffer of Giggenbach, 1987 and CH_4, CO_2, H_2, and H_2O without any constraint on redox potential) suggests that there is an increase in y, that is in vapor/(vapor + liquid) mass ratio, moving not only towards the central zone (where the vapor-discharging wells MW-06, MW-09, and MW-13 are located), but also at greater depths.

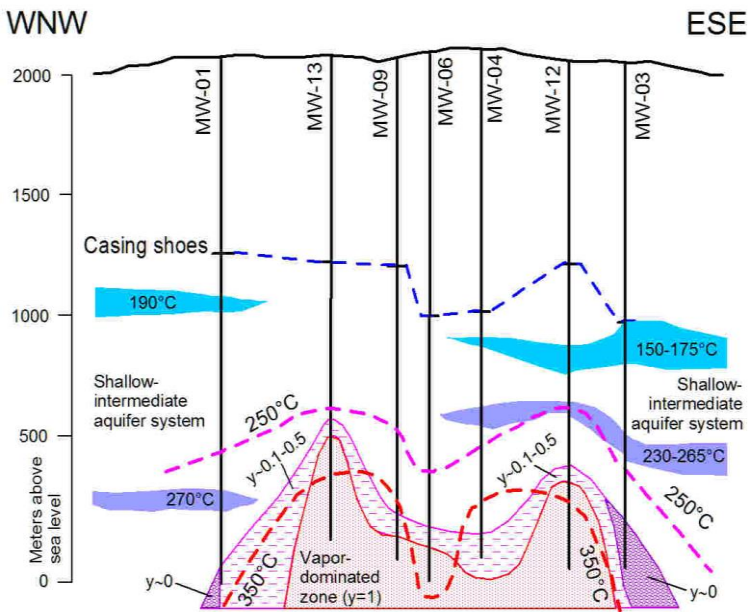

Figure 5-22 Schematic cross-section through the central area of the Menengai caldera showing the geothermal reservoirs encountered by the deep boreholes MW-01, MW-03, MW-04, MW-06, MW-09, MW-12, and MW-13

5.4.2.4. Borehole data

The reservoir engineering evaluation was performed by reviewing the data collected during drilling and testing of 16 wells completed at the date this study was finalized, while 4 additional wells were abandoned because of drilling problems (MW-05, 10, 14 and 18). Available data consisted in wells stratigraphy and completion, record of partial and total circulation losses (GDC, 2011-2013); completion tests on 3 wells (MW-01, 02 and 19: water loss, step rate injection and falloff); pressure and temperature (P&T) surveys collected at well completion, during warm-up and production testing; spinner surveys on 3 wells (MW-02, 16 and 17); production tests on 7 wells (MW-01, 03, 04, 06, 09, 12, 13); composition of discharged fluids. Measurements performance in Menengai wells and data interpretation were complicated due to the challenging conditions encountered: extremely high temperatures, often above 300 °C up to supercritical values (≈ 390 °C) at bottom hole; presence of multiple feed zones over extended wellbore sections at rather different thermodynamic conditions, which were promoting important interzonal flows affecting both the recording of stabilized wellbore conditions and the well performance under production; presence of downhole scaling phenomena (mainly calcite and silica sinter) during production of some wells discharging two-phase fluids; contemporaneous operation of 4 drilling rigs requiring strong efforts in terms of personnel and equipment availability to implement all the necessary measurement and testing activities.

5.4.2.5. Reservoir engineering

Few pressure and temperature (P&T) logs and temperature build-ups were ran during drilling to minimize the associated risks. P&T logs were recorded during warm-up on all wells, while water loss tests and step rate injectivity tests were performed in 3 wells only (MW-01, 02, 19). P&T logs under flowing conditions were recorded in 4 wells (MW-01, 04, 12 and 13). Downhole logs were mostly ran using conventional mechanical instruments with calibration curves available up to 300 °C. As in several wells the downhole temperature exceeds 300 °C, reaching a maximum of 392 °C recorded in well MW-

04, the correction of pressure deflections for temperature effects above 300 °C was not always reliable (GDC, 2011-2013 and Suwai, 2011 and 2012).

Most of the wells encountered a liquid dominated shallow reservoir with temperatures ranging from 130 to 210 °C depending on well location distance with respect to the central area in correspondence of wells MW-06, 09 and 13, where the shallow reservoir was of reduced thickness or almost absent. Thanks to the wellbore cooling during drilling operations and cold-water circulation losses encountered, most of the wells exhibited a column of liquid water during the initial warm-up. Wells drilled in the hottest area experienced a faster warm-up with the evolution of boiling conditions downhole (MW-06, 08, 09, 12, 13). Figure 5-23 shows the P&T logs recorded in well MW-08 after 3 months of warm-up: boiling conditions were present from about 1200 to 1900 m depth along a column of liquid water. Other wells, generally located at the boundary of the present well field and crossing both the shallow and deep reservoirs, developed strong interzonal flows from upper cold liquid dominated feeds towards the deep ones, preventing the warm-up of the latter (well MW-01, 02, 05A, 16, 17). A good example of interzonal flows was given by well MW-05A drilled to the S of developed area. Figure 5-24 shows the progressive warm-up with an almost vertical T profile between 1000 m and bottom hole at 2080 m. Liquid conditions prevail everywhere downhole with a pressure pivot point of 62 bara at a depth of 1200 m.

Useful indications about the pressure distribution with depth in the central developed area can be obtained looking at Figure 5-25 (left) showing the pressure profiles recorded in well MW-01 during drilling and warm-up. Log P1 was recorded in the 17 ½" open hole (OH); logs P4 and P5 in the 12 ¼" OH; logs P6 and P9 were recorded during the initial warm-up, while logs P24 and P25 were obtained after the work-over performed to remove the obstruction found at 1780 m depth. During drilling of 17 ½" OH the static level was at about 1965 m asl, while it fell down to 1675 m asl in the subsequent section, indicating a hydraulic barrier between 1700 and 1600 m asl, which separated ground water circulation from deeper thermal aquifers. During the initial well warm-up after the final depth was reached, the static level was approximately the same as in the section above with a pivot point at about 1100 m asl. This suggests that the pressure was controlled by upper liquid dominated feeds belonging to the shallow reservoir which are locally close to hydrostatic equilibrium with colder thermal aquifers above. Logs P24 and P25 were ran during the warm-up after the well work-over performed to remove an obstruction found at approximately 1780 m depth during a long-term production test conducted in 2011.

These two logs showed a completely different pressure distribution now dominated by deep feeds whose temperature exceeds 310 °C. Figure 5-25 (center) presents the analysis of pressure gradients and fluid composition when the P24 and T24 logs were ran. A column of two-phase fluids was present at elevations of 1330-330 m asl, between two sections with gas static pressure gradient. The two-phase section was likely supported by a boiling column of fluid with an interzonal flow from deep feeds at about 400 m asl to the upper shallow reservoir feeds at 1050 m asl. Boiling promoted the exsolution of NCG (non-condensable gases), which accumulated in the colder upper well section, as clearly shown in the PT plot of Figure 5-25 (right). NCG content in boiling fluids was supporting the two-phase conditions with high local partial pressures, which can be estimated as large as 20-40 bar. These NCG pressure did not reflect the actual NCG reservoir content, which was much smaller, but were due to the accumulation of NCG within the wellbore because of boiling. The lower gas section contained saturated steam (SS) and superheated steam (SH) at about 370 °C, close to the critical temperature of water. This lower section at bottom hole was likely controlled by the extremely high temperature present in an impervious basement where heat conduction.

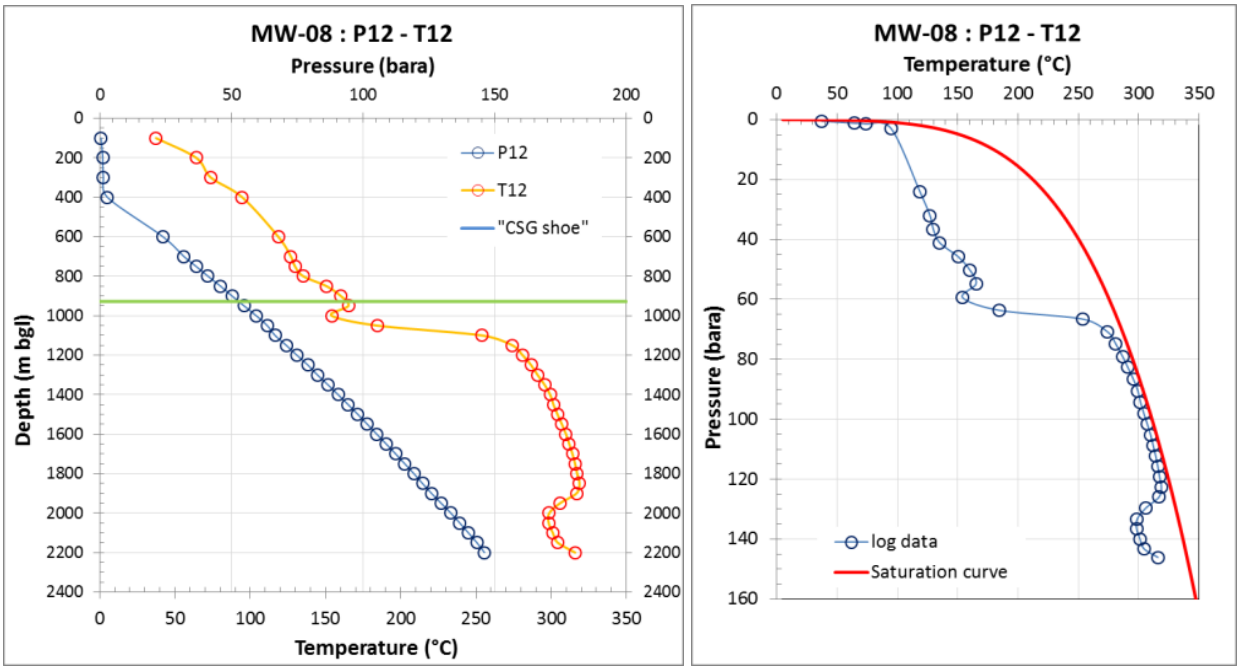

Figure 5-23 Temperature & pressure logs (left) and P&T measurements against the pure water saturation line (right) recorded in well MW-08 after 3 months warm up

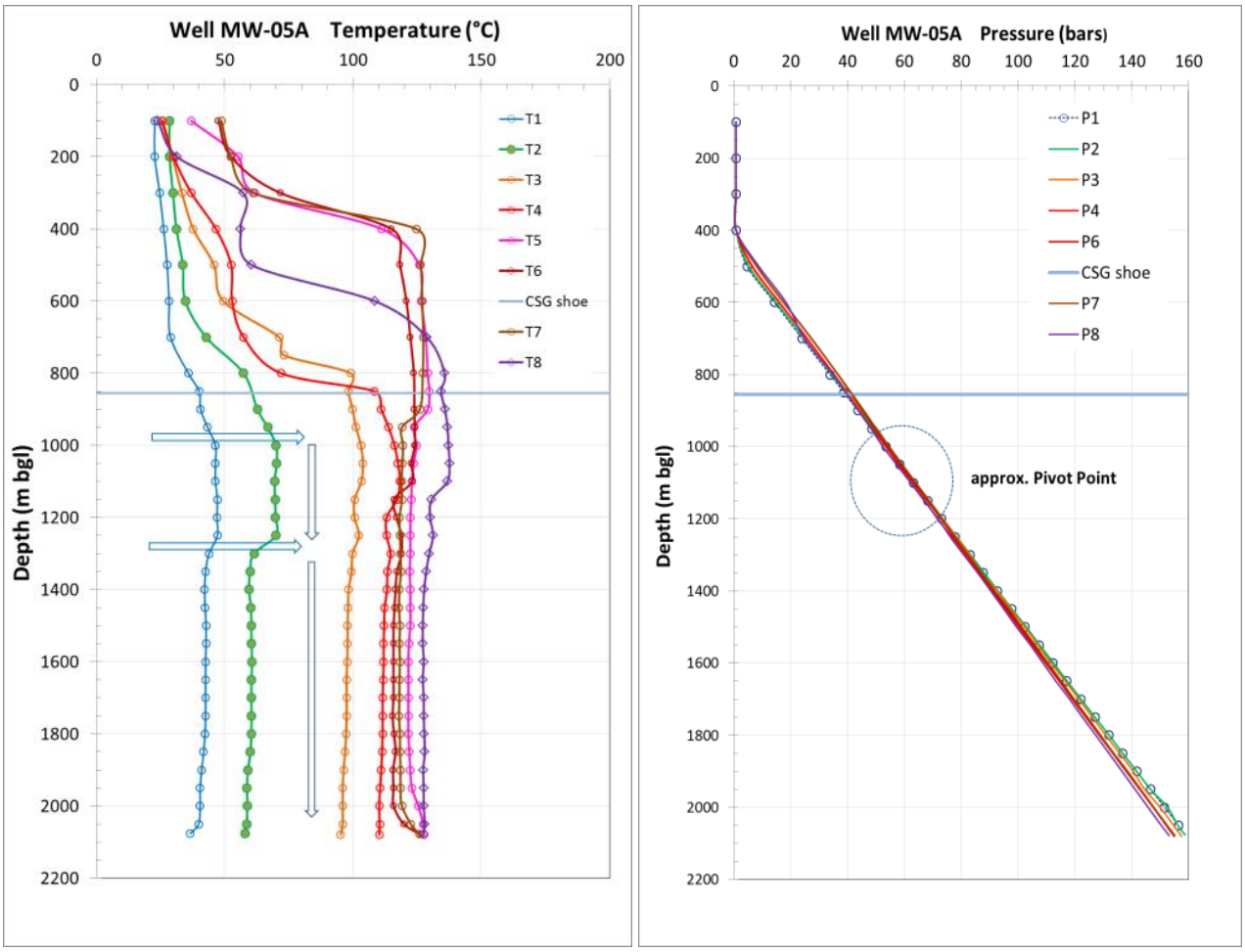

Figure 5-24 Temperature (left) and pressure (right) profiles recorded in well MW-05A during the warm up from March 26 to June 6, 2013

Logging and testing results proved that the shallow reservoir had a negative effect on both wellbore evolution during warm-up, with interzonal flows preventing the heating of deep well section due to the continuous down flow of cold brine, and on production capabilities. In fact, despite of a possible increment of total mass discharge, the mixture enthalpy was reduced and this also had an impact on the flowing well head pressure (WHP). Well MW-01 represented an exception to this general behaviour, with about 80 % of total mass coming from the shallow reservoir as estimated from geochemical data processing and heat and mass balance calculations, as specified here below.

During the first three horizontal discharge tests of well MW-01, that is until May 2012, silica temperature, 190 ± 11 (1s) °C, compares with Na-K temperature (197 ± 9 °C), whereas enthalpy temperature is significantly higher, with an average of 262 ± 19 °C. This spread of temperatures suggests the involvement of both: (i) shallow feed zones at temperatures of 190-200 °C, contributing a liquid phase with average enthalpy of 790 ± 124 kJ/kg, and (ii) deep feed zones at higher temperatures, probably contributing steam, as already recognized by GDC (2012a). Assuming that these deep feed zones are located at 1800-2000 m depth and have temperatures close to 320 °C, as hinted by the temperature log T25 recorded during the warm-up after the work over operation, the enthalpy of saturated steam from these zones is expected to be 2701 kJ/kg. A simple enthalpy balance indicates that the mass contribution of the shallow feed zones to total discharge corresponded to 81 % whereas that of the deep feed zones was of 19 %, with an uncertainty of 7 % on both terms.

But the steam supplied by shallow reservoir feeds amounts at separation pressure to less than 30 % of total steam production. The above considerations suggest to complete future wells by avoiding the negative effects of shallow reservoir feeds. Running of deeper production casing (CSG) shoes is deemed necessary and should be decided on a "well-by-well" basis as function of local encountered conditions, which need to be carefully evaluated during well drilling.

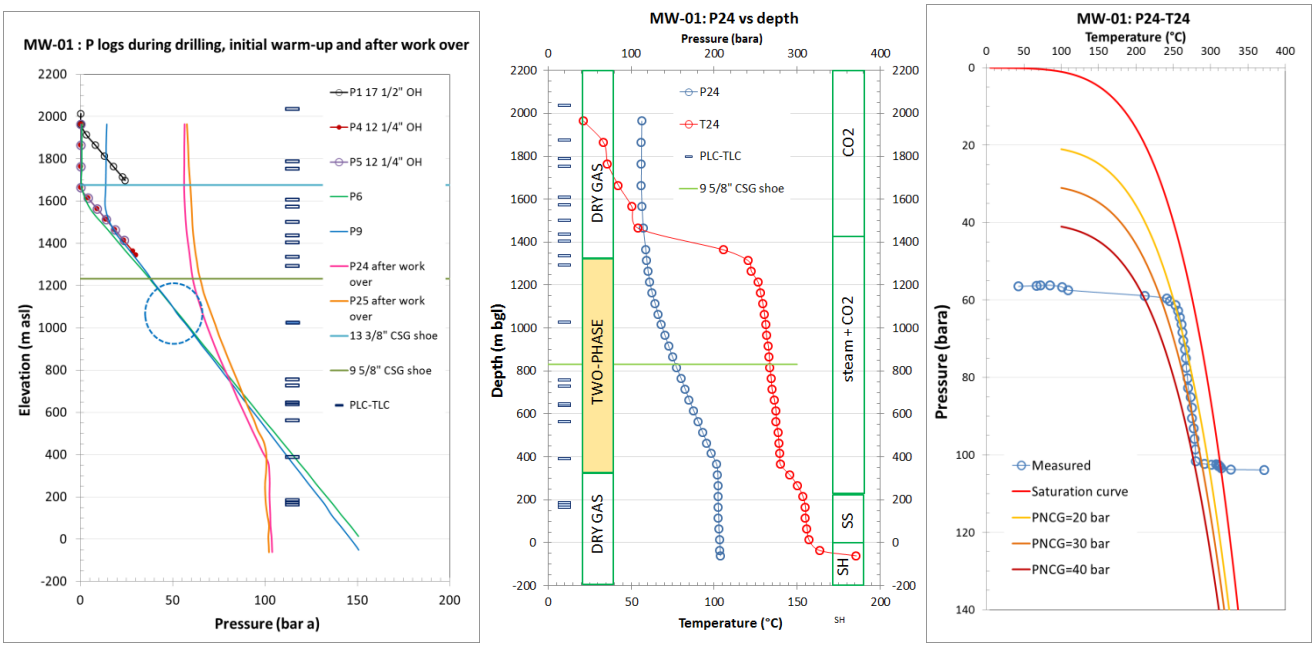

Figure 5-25 Pressure logs recorded during drilling and warm-up (left) P24-T24 logs recorded after the work-over (center), and P24-T24 logs plotted on the PT space against the water saturation curve and boiling curves of mixtures of water and CO_2 at fixed partial pressure(right)

The evaluation of hydraulic parameters of deep reservoir was attempted by using the pressure transients recorded during step-rate injection tests and subsequent fall-off. Figure 5-26 shows the step-rate injection test recorded at 1800 m in well MW-01 and the evaluation of the Injectivity Index (II).

Due to the presence of permeable zones below the instrument setting depth, cold water was also flowing beneath the P&T tools as clearly shown by the temperature reduction during injection from 180 °C down to 55 °C, with effects on recorded flowing pressure. Figure 5-27 shows the P&T recorded during the fall-off and the semi-log plot of pressure vs time for the evaluation of hydraulic transmissivity. After about 4 hours from injection shut-in, the temperature showed a sudden increment corresponding to a stabilization of pressure, suggesting that interzonal flows were likely to affect the pressure transient. The drawdown regression line was then evaluated using data recorded in the first 4 hours. The overall kh product was estimated in 12.3 Dm with a skin factor of -5. The II, kh product and skin factor estimated for wells MW-02 and MW-19 were 270 and 150 LPM/bar, 7.6 and 1.9 Dm, -4.4 and -5.5, respectively.

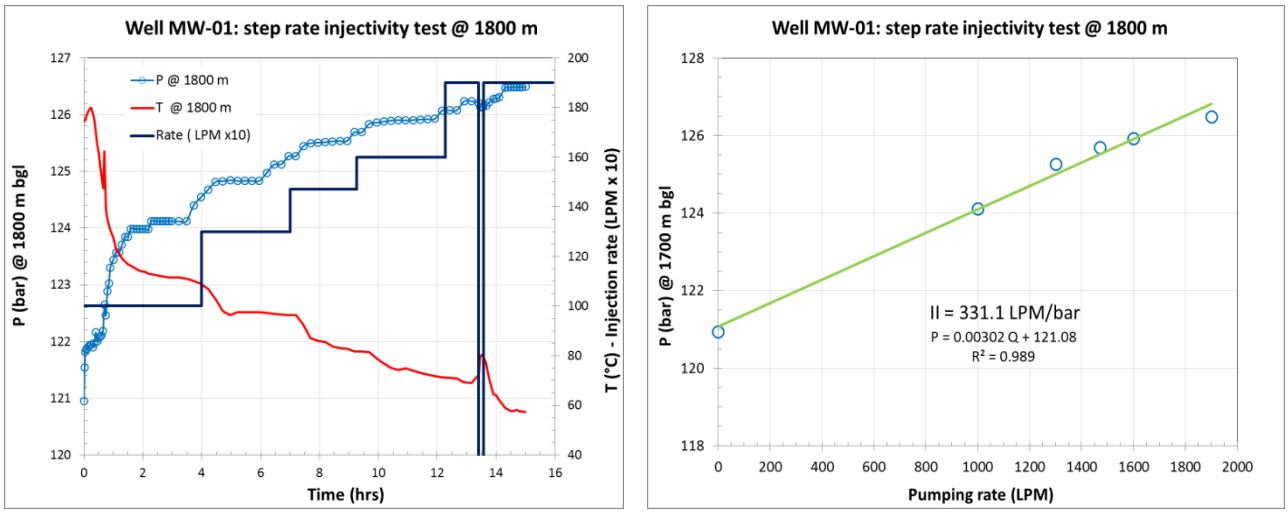

Figure 5-26 P&T at 1800 m depth and injection rate history during the step rate injection test performed in well MW-01 (left) and bottom hole P vs rate for the evaluation of II (right)

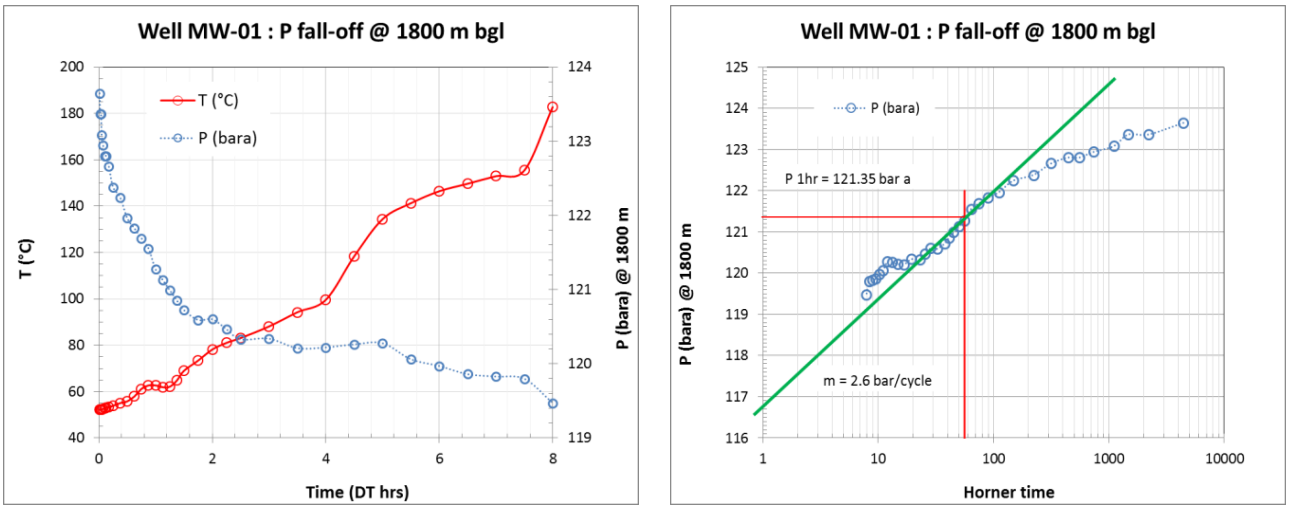

Figure 5-27 P&T at 1800 m depth recorded during the fall-off in well MW-01 (left) and the semilog plot of P vs Horner time for the evaluation of hydraulic transmissivity (right)

5.4.2.6. Production tests

Production tests were performed on 7 wells, out of which one, well MW-03, is a marginal two-phase producer discharging low enthalpy fluids from the shallow reservoir. Production tests were conducted using horizontal lines equipped with a lip pipe and discharging into one or two vertical twin-pipe atmospheric pressure separators (silencers). Brine rate was measured using sharp edged weir boxes. Total rate and enthalpy for two-phase discharge were computed using the R. James' approach by

combining the lip pressure and the weir box level readings (James, 1962 and 1970). Dry steam discharge rates were computed using lip pressure readings and the enthalpy estimated at local thermodynamic conditions.

Production enthalpy depends strongly on the contribution of low temperature shallow reservoir. When this contribution was remarkable, as in wells MW-01, 04 and 12 (Kipyego, 2012 and 2013), two-phase discharge was present with enthalpies ranging from 1200 up to 1600 kJ/kg. Wells MW-06, 09 and 13, all located in the middle of field developed area, were characterized by dry steam discharge after few days of initial two-phase production (Ofwona, 2002 and 2011 and Ofwona et al., 2011). Two-phase wells MW-01 and MW-04 were characterized by the decline of discharge potential linked to scaling phenomena downhole, clearly detected by obstructions found at depths of 1790 and 1560 m, respectively. Work over operations conducted in well MW-01 were able to restore well production at rates, enthalpies and WHP even higher than those recorded at well start-up. An obstruction was also detected after only two-weeks in well MW-12 at a depth of 1588 m, after an important initial rate decline. Well MW-06 was also showing a remarkable production decline, which was likely to be due to a combination of low reservoir permeability and scaling phenomena downhole. When production through 5" lip pipe started, a cycling discharge was recorded with sharp changes of WHP and total rate. Spot two-phase discharge was recorded during WHP surges, further indicating that cycling was probably linked to competing effects among multiple feeds with high enthalpy contrast. Cycling was followed by two-phase discharge. A few days after, a rather fast drop of WHP was recorded, partially recovered reducing the rate with 4" lip pipe. The relatively high CO_2 partial pressure and the processing of geochemical data with calculation of fluid chemical equilibrium suggested that the scaling was due to calcium carbonate precipitation.

The output curve in terms of mass rate and enthalpy vs WHP is shown for the two-phase wells MW-01 and MW-04 in Figure 5-28, and for the dry steam wells MW-09 and MW-13 in Figure 5-29. Both two-phase wells showed the decline of discharge rate in time, which can be interpreted as the result of scaling downhole. Both wells showed the dependency of enthalpy with WHP, with higher enthalpies recorded at high WHP (and low rates), in particular for well MW-04. This can be interpreted as the result of a lower contribution from the shallow reservoir when higher flowing pressures were present downhole.

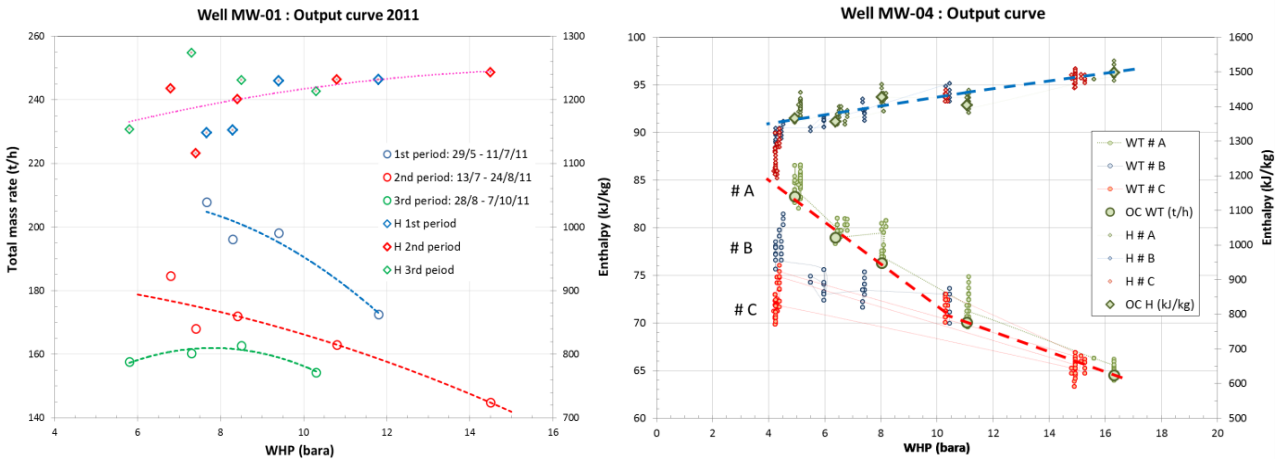

Figure 5-28 Output curves of wells MW-01 (production tests in 2011) andMW-04 (three subsequent steps #A, #B and #C). Both wells discharge a two-phase mixture

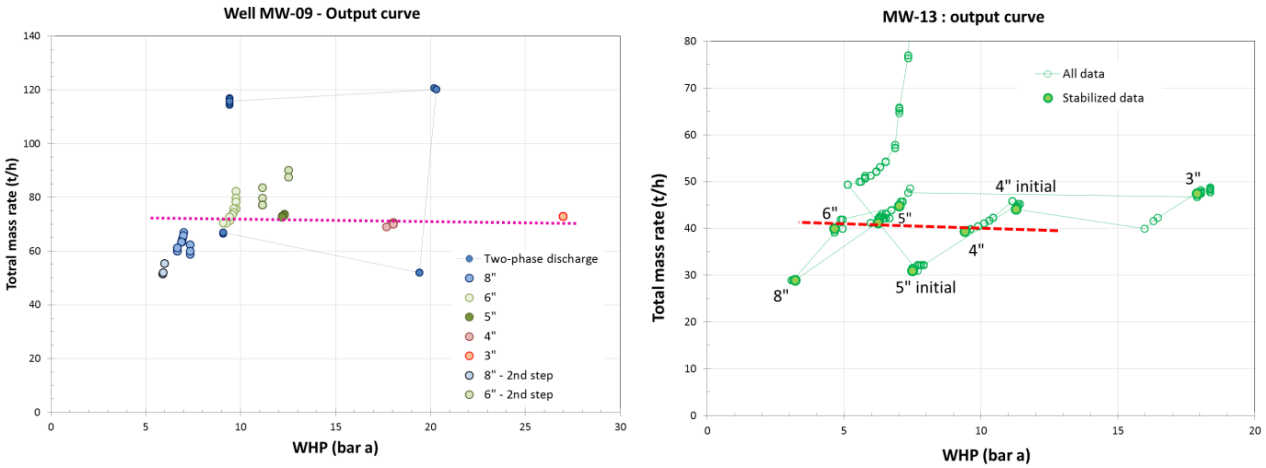

Figure 5-29 Output curves of wells MW-09 (left) and MW-13 (right), both discharging dry steam

The output curve of dry steam wells MW-09 and 13 was almost flat within the tested WHP range, with rates only gently increasing when WHP was reduced. Flat output curves suggest strong incremental pressure drops for limited rate increments, as occurring when flowing conditions were close to chocking. Combined wellbore and reservoir simulation at a well sector scale for MW-09, calibrated to reproduce the output curve, showed that the flat curve was due to two distinct factors: i) the down-hole drawdown, which is not linear as function of rate but characterized by additional losses proportional to the square of mass rate; ii) the discharge conditions approaching choking at wellhead for WHP lower than 20-30 bara. When choked flow conditions were approached (speed close to that of sound at local conditions) marginal increments of rate were obtained by further opening the well. The numerical simulations allowed also to estimate a possible increment of production rate for a well with reservoir conditions similar to that encountered by MW-09, but completed with a larger production CSG of 13 3/8 ", of about 30 %.

5.4.2.7. Conceptual model

The conceptual model of a geothermal field represents the synthesis of all the information obtained by the analysis and interpretation of the available data (see Figure 5-30a,b), both from surface studies and from deep exploratory wells, and is used as the basis for the resource assessment and the study of the reservoir behaviour under exploitation, as well as for the evaluation of the field potential and the definition of the optimum development strategy. As far as the Menengai reservoir is concenrned, the essential features can be summarized, as follows:

a. *Heat Source.* All available elements point to the extremely positive setting of the Menengai area in terms of heat source, in consideration of: (i) the post-calderic, very recent age of the eruptions, witnessing the active nature of the magmatic chamber/s, still in a molten stage with temperatures in excess of 700 °C (ELC-GDC, 2015); (ii) the acidic nature of the erupted products, reflecting phenomena of differentiation which are generally accompanied by an uprising of the magma to depth lower than about 8 km (Lagat et al., 2010); (iii) the widespread distribution of the recent eruptive centres, suggesting the large volume of the magmatic chamber/s (Lagat et al., 2010).

b. *Geological Setting.* The permeability distribution within the Menengai geothermal system is attributable to two specific elements, namely the type of hydrothermal alteration and the degree of tectonic stresses, which affect the geological formations. The propylitic zone, reflecting high temperatures and competent nature of the rocks, exhibits a dome-shaped configuration, with the top located in correspondence of a W-E oriented belt extending between MW-07 to the west and MW-03 to the east. With reference to the degree of tectonic stresses, it is observed that an intense neo-tectonic activity has taken place in the interior of the caldera. Within this general structural pattern, two major features were identified, corresponding to two faults running NNW-SSE and N.7W-S.7E, which delimit a 4 to 6 km wide block, which is likely to be associated with a higher than average fracture density.

c. *Reservoir Geometry.* Two distinct geothermal reservoirs, hereinafter called shallow and deep reservoir, were recognized.

The top of the shallow reservoir occurs at an elevation included between 900 and 1300 m asl (except in MW-02, where it was not recognizable), corresponding to a depth bgl of 700-1100 m and being expressed in the temperature profiles by a short stretch of iso-temperature indicative of a convective cycle. Such depth approximately coincides with the start of the important circulation losses registered in the wells of the central part of the field below the cap-rock and, in terms of alteration mineralogy, with the top of the secondary quartz zone. The bottom of the shallow reservoir is accordingly inferred to occur at an elevation included between 600 and 1000 m asl.

Evidences for the existence of a shallow reservoir were recognized in all the wells drilled to date except for MW-02. This reservoir is therefore deemed to extend throughout most of the sector investigated by drilling, being probably delimited to the west and east by the two major structures running N.7W-S.7E and NNW-SSE, to the north by a line between MW-02 and MW-11 and to the south by a line just south of MW-5A. These boundaries would indicate an areal extent of the shallow reservoir of approximately 20 km^2.

The top of the deep reservoir exhibits a pronounced dome-shaped configuration, with the upper sector, at elevation of 600-900 m asl, extending in a W-E direction between MW-01 and MW-04/MW-12 and in a N-S direction between MW-08 and MW-10/MW-12. Beyond these points, a sharp drop appears to take place in all directions (see wells MW-5A, MW-11, MW-14, MW-15 and MW-17). The above described configuration is similar to that of the top of the epidote, except for the larger W-E continuation of the latter parameter, which extends between MW-07 and MW-03. The bottom of the deep reservoir, expressed by the start of the conductive regime which may reflect impervious conditions of the rocks, is found at elevation in the range of 0 / -200 m asl with local uprising, indicating an average thickness of the deep reservoir of 600-1,000 m in the central sector, dropping to <500 m in the peripheral one. The Menengai geothermal field resources have been classified into three distinct categories (see Figure 5-30a):

- Developed Area: it corresponds to the sector where all the present producing wells are concentrated, extending over a length of about 3 km in a W-E direction and of about 2.5 km in a N-S one and covering a total surface of approximately 7 km^2.
- Development Area: it encompasses a sector, located to the SW of the former area, defined from the structural and micro-seismic monitoring data, covering a total surface of about 3 km^2. The reservoir thickness in this category is interpreted to be in the order of several hundred meters.

- Expansion Area: it exhibits an oval shape, forming a sort of a halo around the above-mentioned categories; it is on the whole characterized by wells where adequate temperature conditions have been encountered, not accompanied by favourable hydrogeological conditions (MW-11, MW-15 and MW-17). These potential resources cover accordingly a surface of about 10 km^2. The reservoir thickness within the expansion area is interpreted to be in the order of few hundred meters. The total surface of the geothermal resources, combining these three categories, can be accordingly estimated in about 20 km^2.

d. *Natural Fluid Flow Pattern.* Due to lack of determination of the isotopic content in the fluids of the deep wells, no direct information is available on the nature of the main recharge of the deep reservoir. Possibly such recharge takes place along the borders of the caldera, associated with the presence of major structures, which may favour the deep infiltration of meteoric water, with minor contribution from the magmatic system in the form of steam and gas transfer.

Upon getting in the proximity of the heat source corresponding to the active and rather shallow magmatic chamber, waters heat up and start to rise, following deep seated faults and crossing the whole sequence of geological formations (from Tertiary to recent times). In the course of their upraise the hot fluids tend to boil and to expand laterally along horizons associated with widespread fracturing.

The main upflow zone is situated in the central part of the Developed Area, in correspondence of the sector where the magmatic chamber forms a plume-like structure, getting closer to surface. The two major faults running NNW-SSE and N.7W-S.7E seem to constitute a hydrogeological barrier to the eastern and western expansion of these fluids. No important escapes from the deep reservoir to the surface were identified. Its areal configuration suggests that the main outflow takes place along this W-E axis, possibly reflected by the geoelectrical anomaly recognized west of the caldera rim.

The recharge of the shallow aquifer appears to take place from the SSW of the sector under development. The fluids, upon getting above the deep reservoir, tend to heat up mostly as a result of conductive heat transfer and to reach their maximum temperature in coincidence with the main upflow zone of the deep reservoir. The main outflow of the shallow aquifer is likely to take place in an E to NE direction, moving then along a preferential N-S trend upon reaching the Solai Graben.

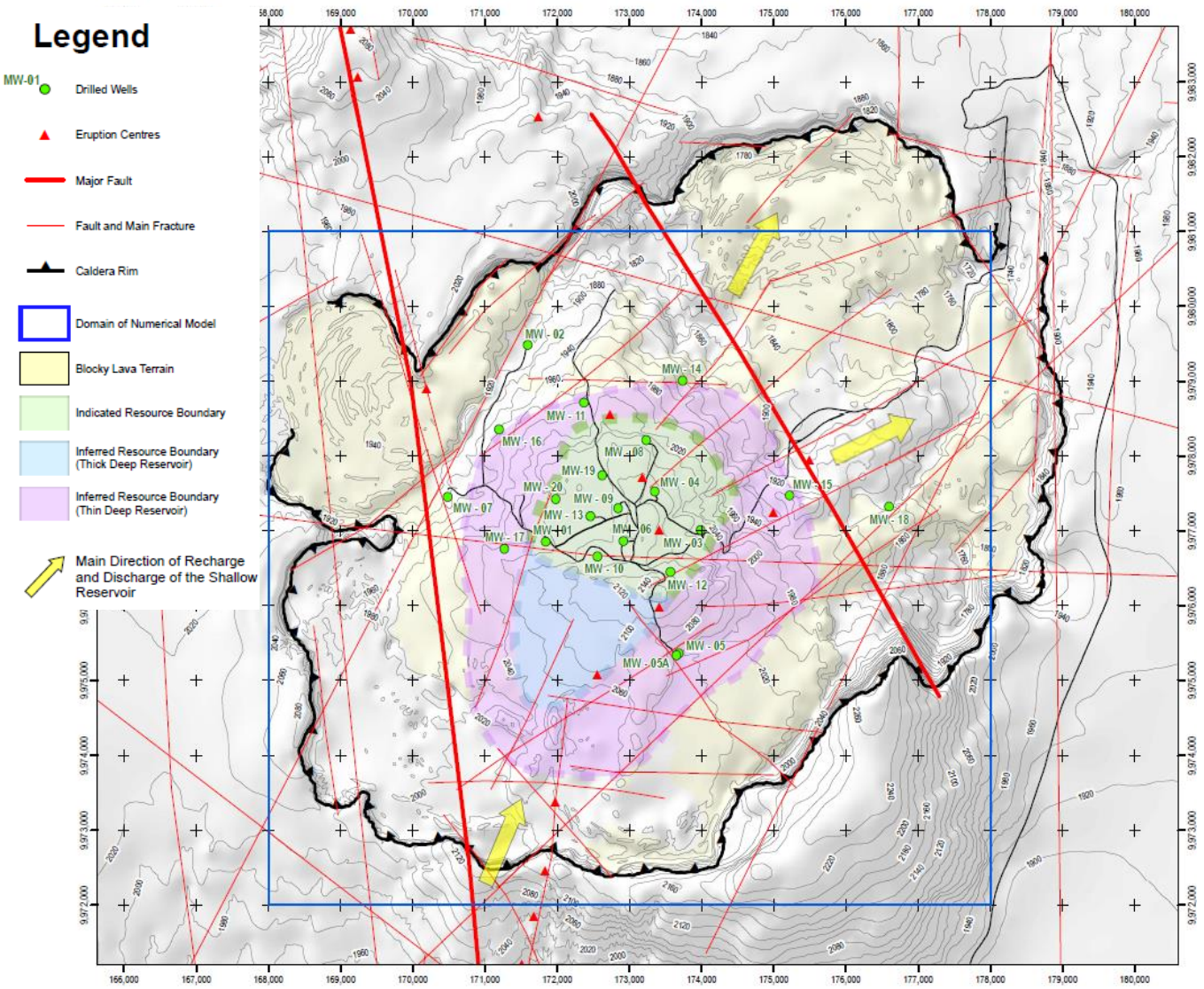

Figure 5-30a The figure shows the main structural features of the Menengai caldera with the presumed deep reservoir extension (colored area), the presumed shallow reservoir recharge direction and the numerical model extension

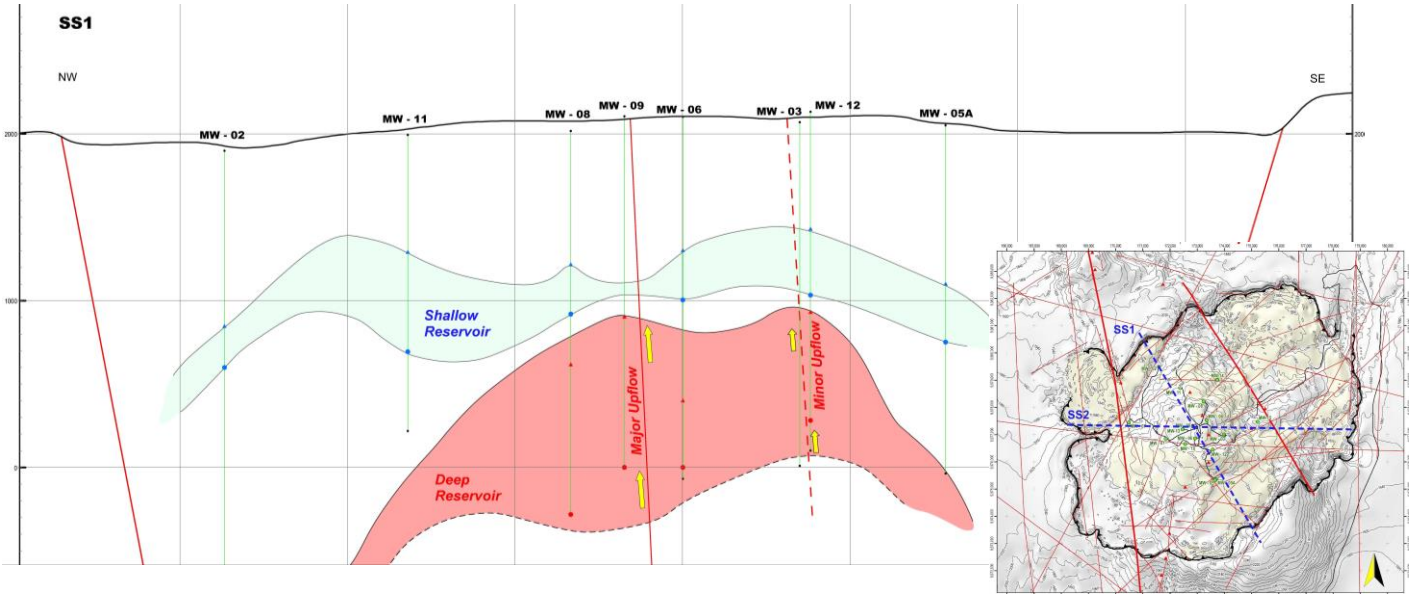

Figure 5-30b Conceptual model of the Menengai geothermal field, along SS1 cross section

5.4.2.8. 3D numerical thermal model

For the simulation of natural state and exploitation scenarios calculations were carried out with TOUGH2 V.2.0 (Pruess et al., 1999) numerical reservoir simulator, managed using Petrasim V.5.2 pre- and post-processing software package. Among the equation of state (EOS) modules available within TOUGH2 V.2.0, considering the non-negligible NCG content in Menengai field (represented mainly by CO_2), the EOS2 module for mixtures of water and CO_2 was employed.

Considering the 3D geometry of Menengai prospect and its relevant features, an unstructured Voronoi grid approach was chosen, with upper grid layers following the DTM (digital terrain model) elevations, and the reconstructed top and bottom of shallow and deep reservoirs. Petrasim allows as a first step to build a model at a conceptual level by defining the model geometry, layering, internal regions, boundary and initial conditions, sink and sources and petrophysical properties distribution, and in a second step to build the discretization grid. The numerical model was constructed on the basis of the conceptual model, including the two main faults, and the deep and shallow reservoirs structure. Rock types and properties were defined according to the results of well logging and testing data (see Tables 5-7). An unstructured grid is chosen according to the IFDM (Integral Finite Difference Model) spatial discretization approach on the horizontal plane with 1,398 elements per grid layer (Figure 5-31). For the construction of the Voronoi grid, the settings were: a maximum element area of 2E6 m^2; a maximum area of 1400 m^2 for refinement elements; a minimum refinement angle of 30.2°. On the vertical direction 24 layers were used, for a total of 33552 grid elements.

Initial and boundary conditions included the location of inflow and lateral outflow zones of the shallow reservoir, and the upflow in the deep reservoir. The reservoir is limited by the faults on the Eastern and Western sides, but the model domain extends outside these faults. The deep reservoir extends down to -300 m asl, with a profile obtained from wells log data. The hot intrusion located below is taken as the bottom thermal boundary, set at 330 °C, according to temperature measurements showing a conductive heat flow section at the reservoir bottom. The top boundary layer was at fixed conditions of 85 °C, according to borehole and steam vents temperatures.

The deep reservoir also has a 'rim' with the same porosity value, but lower permeability, that is not directly heated up by the bottom hot intrusion and which might represent the lower temperature section (at nearly 270 °C) of the reservoir evidenced by the geochemical findings, as well as the extension of the two-phase zone evidenced by the Vp/Vs distribution inferred by the seismic investigations (Simiyu, 2009). Major layers in the conceptual Petrasim model, to be distinguished from grid layers, were (from top to bottom):

Petrasim layers	**Description**
Top	A 300 m thick layer used to assign top thermal boundary conditions, followed by host rock down to the shallow reservoir
ShallRes	The shallow reservoir
Bulk	The host-rock
DeepRes	The deep reservoir, outcropping from the bottom, divided in two units.
Bottom	The bottom layer, used to set the thermal bottom conditions and containing the 'hot intrusion'.

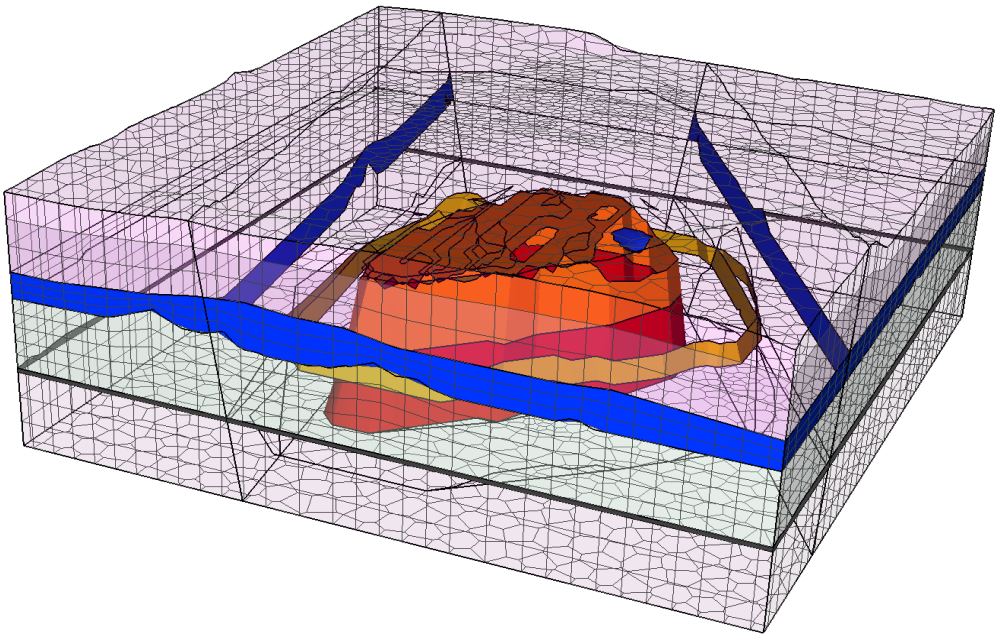

Figure 5-31 Menengai model structure, with the Shallow Reservoir in blue, the deep reservoir in orange, the hot intrusion in red and the external part of the deep reservoir in dark-yellow

According to the conceptual model, the deep reservoir is surrounded by very low permeability rocks, and is recharged by an up-flow of a 320 °C fluid with a CO_2 of 5% by weight. The shallow reservoir has a 12000 mg/kg salinity, with an inflow roughly corresponding to the rainfall inflow and an outflow to the W and N controlled by a constant pressure boundary set at 70 bar. While any possible effort was done to incorporate the major features of conceptual model (see Figure 5-30a,b) developed for the Menengai prospect, several assumptions were needed to develop the numerical natural state model. The calibration process allows reducing the uncertainties related to some of these assumptions. For others, the uncertainty remains high, in particular outside the area drilled so far. In Table 5-7 the properties of the main rock units assigned to the final 3D numerical model are reported.

Table 5-7 Main properties of rock domains used in the final 3D natural state model. The huge rock specific heat assigned to the bottom intrusion is used to maintain a constant temperature throughout the simulation. k_x,k_y: horizontal permeability; k_z: vertical permeability; φ: porosity; C_R: Heat Capacity of dry rock kJ/kg; λ_R: thermal conductivity; ρ_R: rock density kg/m^3

DOMAIN	DESCRIPTION	k_x, k_y (m^2)	k_z (m^2)	φ	c_R (kJ/kg)	λ_R (W/(m °C)	ρ_R (kg/m^3)
TOP	Top structure	1.E-22	1.E-22	0.02	1400	2.0	2600
SHALL	Shallow reservoir	2.E-14	2.E-15	0.06	1400	2.0	2600
BULK	Host Rock	1.E-22	1.E-22	0.02	1400	2.0	2600
RES	Deep Res. central part	2.E-14	1.2E-14	0.06	1400	2.0	2600
RESEX	Deep Res. external part	1.E-14	1.2E-15	0.06	1400	2.0	2600
BOTHH	Botton hot intrusion	1.E-22	1.E-22	0.02	1.E+50	2.0	2600

A series of simulations were performed trying to obtain a stable steady-state with pressure and temperature distributions reproducing those observed in drilled wells. During this iterative process, main changes applied were relative to the inflow of the shallow reservoir, the temperature at the model

bottom beneath the deep reservoir, the permeability of rock domains, and to the features of the upflow recharging the deep reservoir.

The results of the steady-state then were compared with the measured temperature profiles to check their reliability. Figure 5-32 reports the comparison between simulated and measured temperature in wells MW-01, MW-03, MW-06, MW-08, MW-09, and MW-12.

Simulated and measured temperature profiles are in reasonable agreement, considering that stable conditions were difficult to be observed in most of drilled wells because of inter-zonal flows and boiling process within the wellbore. The comparison suggests that the simulated natural state is able to reproduce both the deep and shallow reservoir temperature distributions, but is not accurate in the topmost part, mostly due to the thick layer used and to the shallow ground water aquifers crossed by the wells but not included in the model. Wells MW-06, MW-09, and MW-13 show a similar profile, being located in the main structure of the deep-reservoir not far from each other. MW-06 shows a clear feed at nearly 300 m asl that supplies dry steam and generate an upward heating of the borehole.

The simulated natural state is presented using the distribution of main thermodynamic parameters along vertical and horizontal sections. Liquid dominated and two-phase vapor dominated conditions are obtained for the shallow and deep reservoirs, respectively. Figure 5-33 shows (from a S view) the temperature distribution in a E-W section intermediate to Well MW-13, 9, and 3 with the major up-flow on the left (Western) side of the deep reservoir and a minor upflow in the other deep reservoir culmination. The N-S section of the deep reservoir with temperature distribution and total fluid flow, cut across well MW-09, is shown in Figure 5-34, where we can recognize the two up-flows. The figure shows the relationship between the inner, hotter volume of the reservoir and its morphology. The deep reservoir outflow, mainly represented by the fluids escaping upwards into the shallow reservoir and feeding the fumarolic field, is evidenced by the total flow vector. The pressure in the deep reservoir follows the same behaviour, as shown in Figure 5-37.

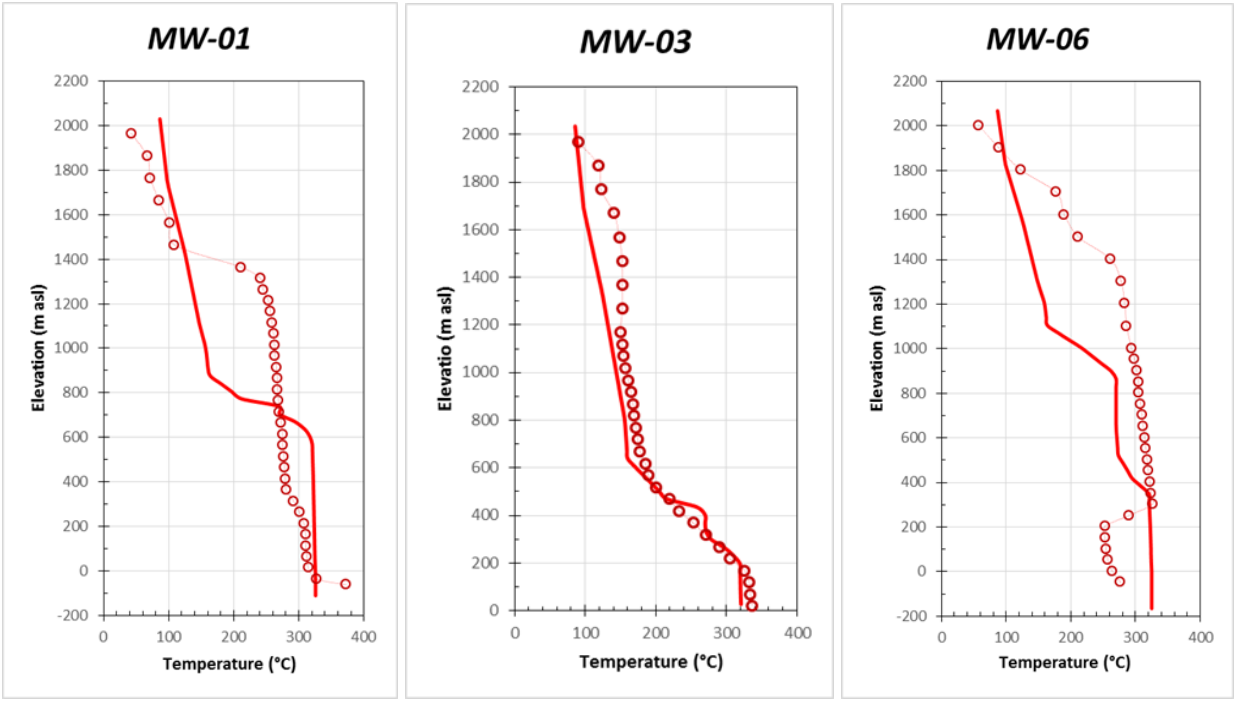

Figure 5-32 Simulated temperature profiles of selected wells (lines), compared to measured profiles (circles)

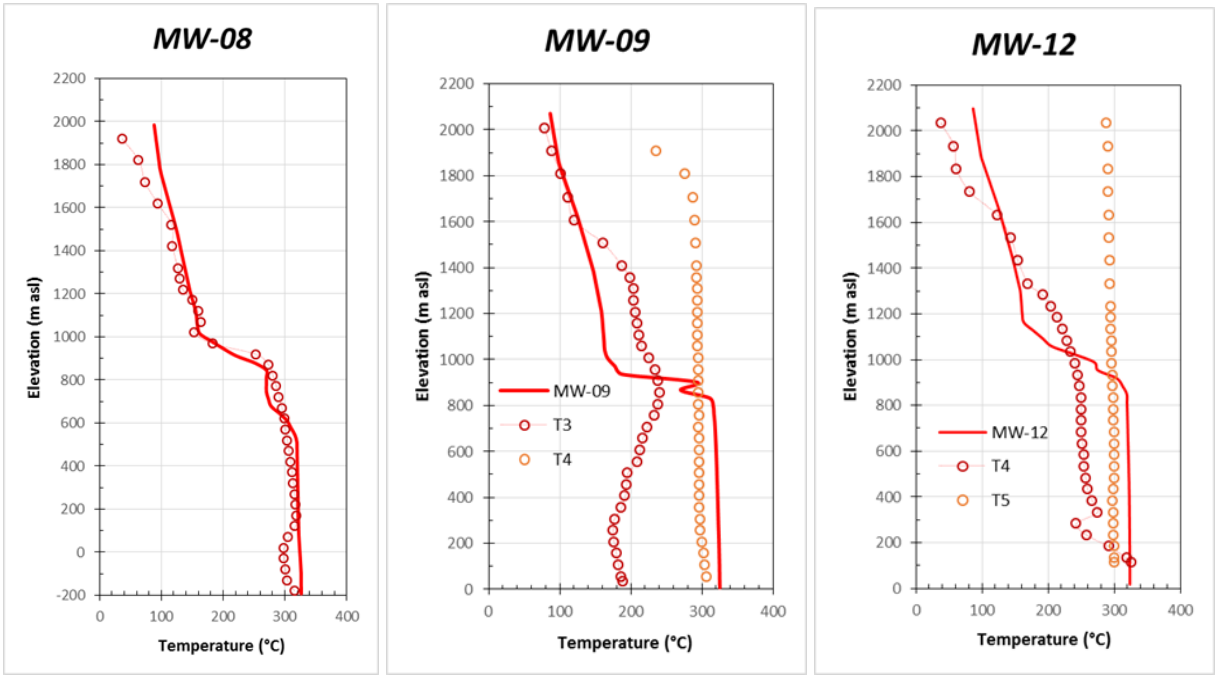

Figure 5-32 Continued

The simulated gas saturation distribution in Figure 5-35 shows that high values are present within the deep reservoir, whereas at its border the gas saturation is reduced to values as low as 0.2. Looking at the temperature distribution, the temperature rim at 270-300 °C could be observed. Such results are not unexpected, since pressure distribution in the deep reservoir is along a water-CO_2 mixture boiling curve, and CO_2 is concentrated mainly at the top of deep reservoir due to boiling and condensation linked to a heat pipe process.

For having a complete picture of the deep reservoir conditions, in Figure 5-36 the distribution of CO_2 in the deep reservoir is shown together with NCG flow vectors, evidencing the NCG accumulation at the top of the deep reservoir. The NCG flows to the upper culmination in the area within wells MW-06 and 09 where the highest top of the reservoir is found, and the impact of deep fluid on the shallow reservoir is more evident. Due to the consideration of fluids outflow from the deep reservoir towards the surface, an outlet for the deep reservoir is located in the structural top close to well MW-09, and controlled with a constant outlet pressure. It is evident the lack of a uniform pressure gradient in the whole structure. In particular, the deep reservoir shows a pressure lower than expected. Anyway, in particular in Figure 5-37, it is evident that the shallow and deep reservoirs are very close, and could have some hydraulic connection.

In summary, the modelled natural state is thus consistent with pressure and temperature distributions close to that provided by well logging, despite non well stabilized conditions were present down-hole in most of the drilled wells.

The steady-state modelling results were then used to simulate production and reinjection scenarios which are not discussed in the present work. These further modelling activities pointed out that some parameters are still poorly constrained, like the effective reservoir extension in the unexplored area.

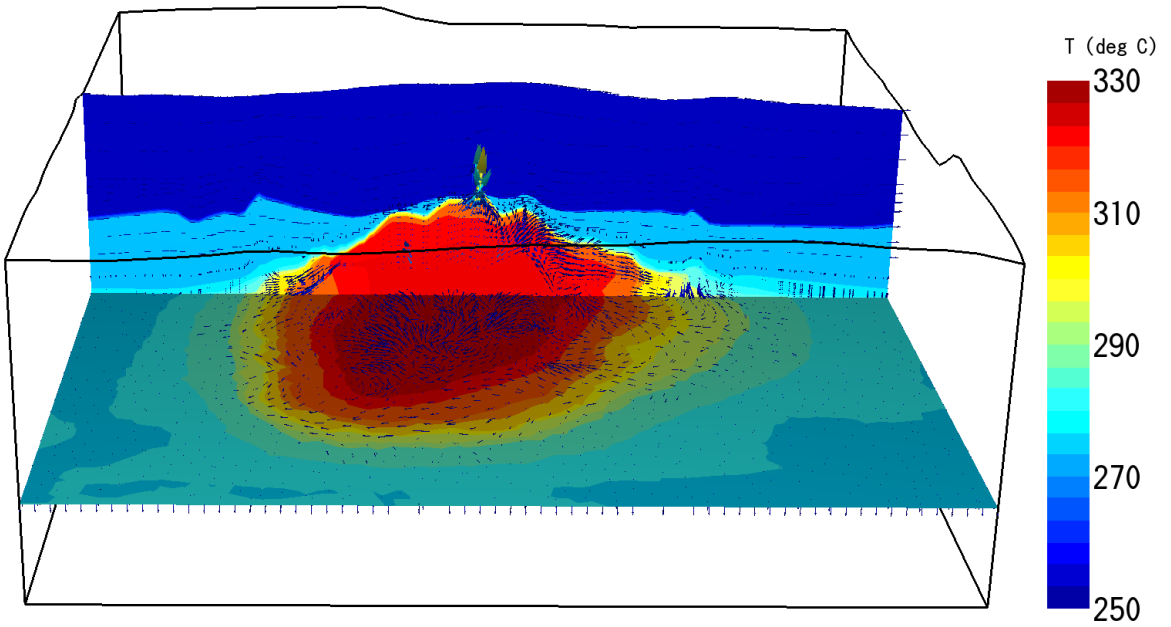

Figure 5-33 Reservoir temperature distribution with total fluid flow vectors along a E-W section at 9977400 m and a N horizontal section at -300 m asl

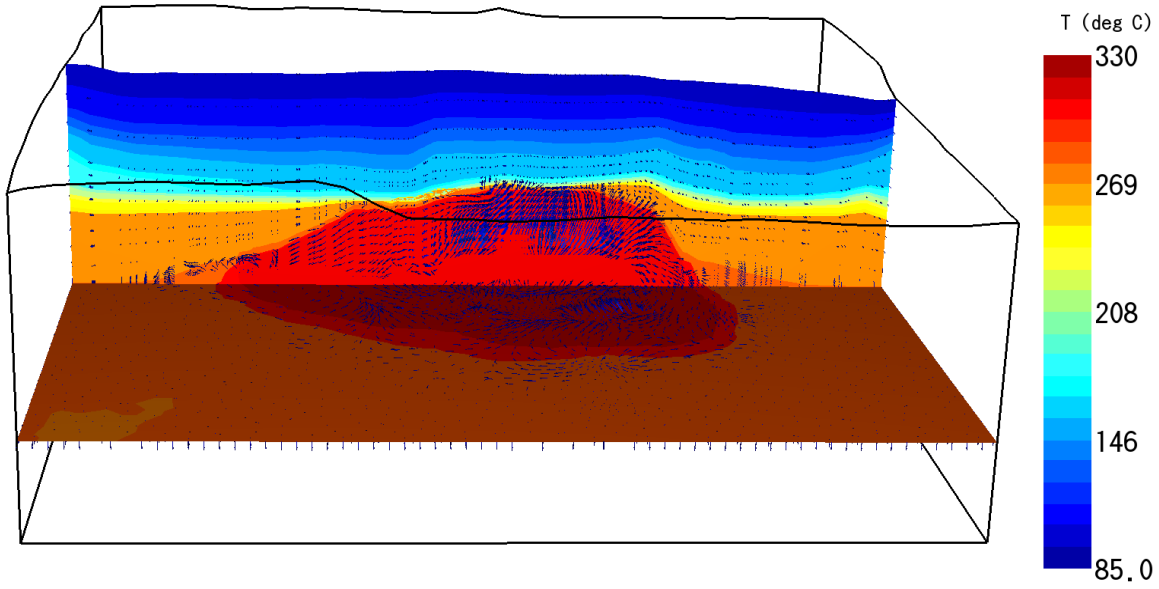

Figure 5-34 Reservoir temperature distribution with total fluid flow vectors along a N-S section at 172600 m E and horizontal section at -300 m asl

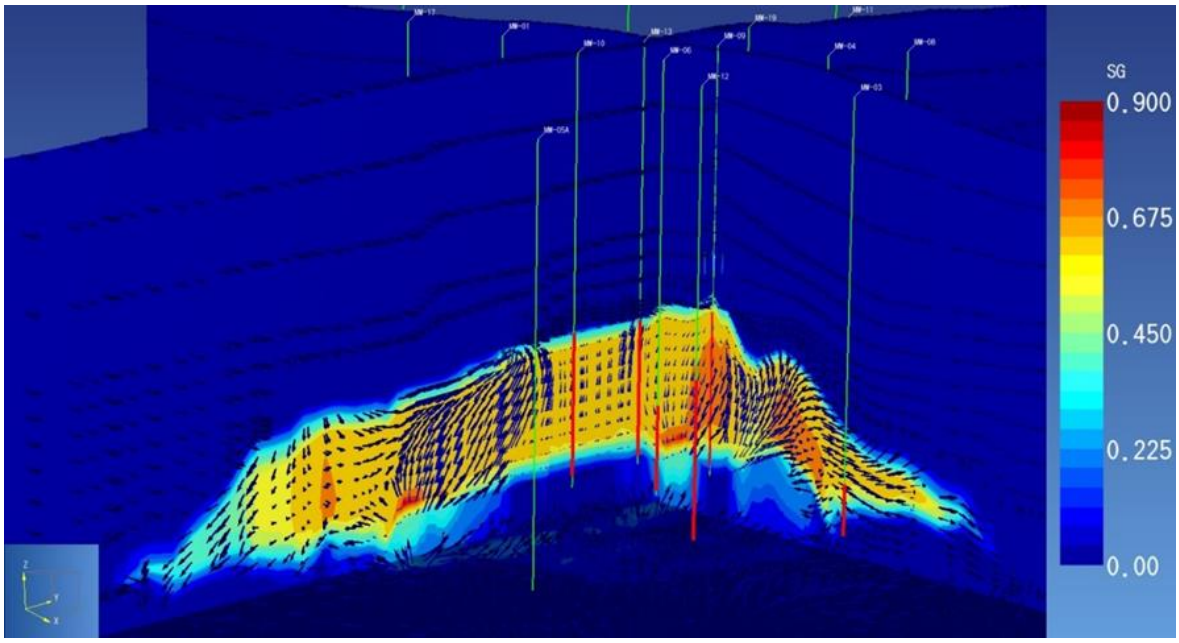

Figure 5-35 Gas phase saturation distribution within the deep reservoir with fluid flow vectors. Horizontal section at -200 m asl and vertical slices at 1.724E5 m E and 9.9773E6 m N, viewpoint from SE

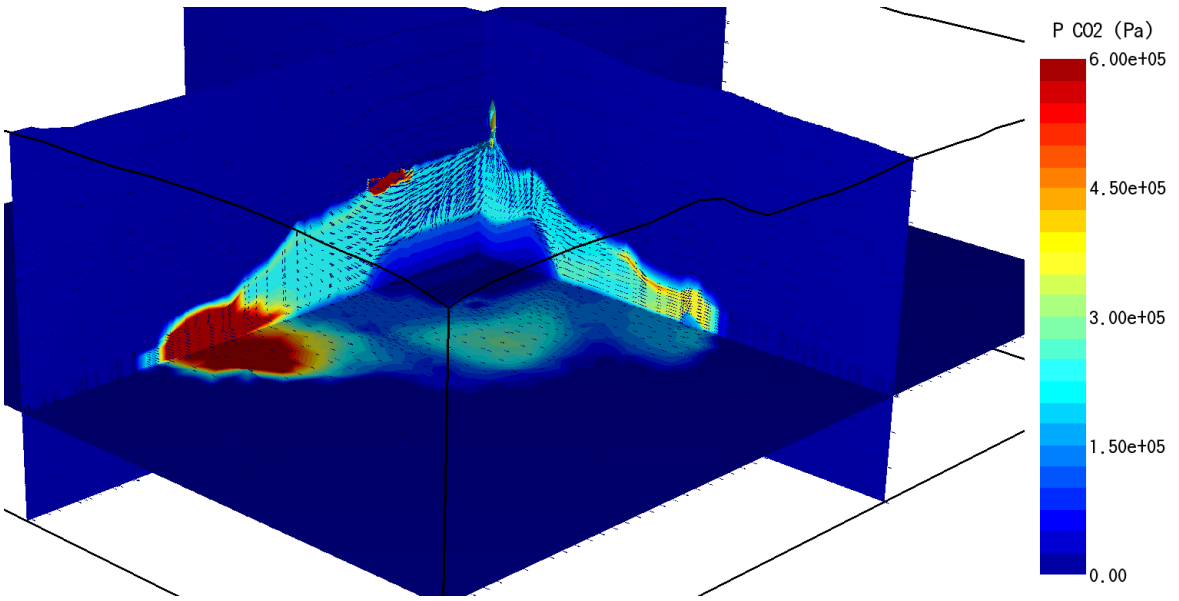

Figure 5-36 CO_2 partial pressure distribution with NCG mass flow vectors along a E-W section at 9977400 m N, a N-S section at 172700 m E, and a horizontal section at -300 m asl

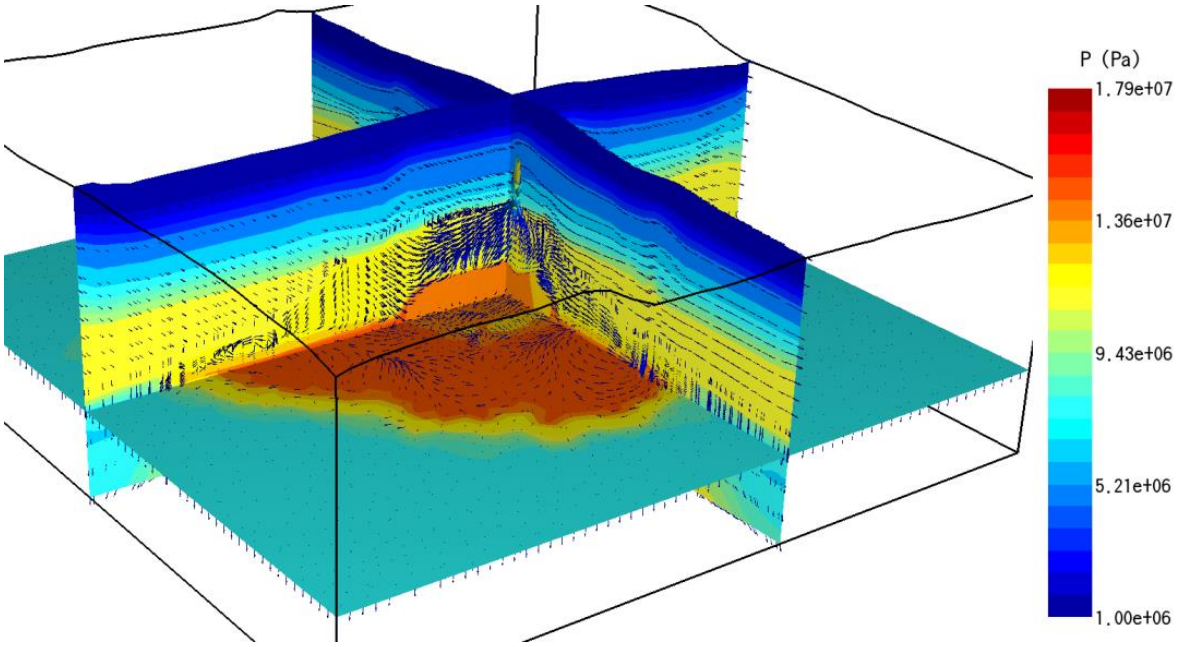

Figure 5-37 Reservoir pressure distribution with total fluid flow vectors along a E-W section at 9977400 m N, a N-S section at 172700 m E, and a horizontal section at -300 m asl

5.4.3. The Kiejo-Mbaka geothermal field

The Kiejo-Mbaka geothermal field falls within the Rungwe Volcanic Province (RVP), which is situated in the East Africa Rift System at the triple junction of the Rukwa, Usangu and Malawi rift basins (see Figure 4-3). Rifting started in the Cenozoic period and evolved until today (Delvaux et al., 1992, 1993, 2010 and Iranga, 1992).

5.4.3.1. Geological setting

The RVP formed during three separate stages: (1) Late Miocene: 9.2-5.4 Ma; (2) Late Pliocene-Early Pleistocene: 3.0-1.6 Ma; (3) Middle Pleistocene-Recent: since 0.6 Ma (Ebinger et al., 1989). Quaternary volcanism, of alkaline nature, is expressed by three still active major eruption centers, namely Ngozi, Rungwe and Kiejo, and by several small monogenic volcanic edifices. As result of the geological survey performed, the stratigraphic sequence and the geological evolution are summarized in Figure 5-38.

There is a very good agreement between the structural elements mapped in the field on the basis of stratigraphic and morphological evidence and the faults and fractures found from the remote sensing study. As a matter of fact, the structural trends emerging from the two approaches are (see Figure 5-39):

- *Livingstone rift-related NNW-SSE trend.* The main fault of this trend represents the eastern margin of the main rift and has a down-throw of as much as 1,000 m.
- *Mbaka fault-related NW-SE trend.* It constitutes the most evident structural element in the prospect area, being expressed by a series of faults with a SW dip (60-70°), out of which the Mbaka fault proper has a pronounced morphological relevance with an estimated down-throw of several hundreds of meters and appears to control the old Mbaka monogenic field.
- *Nyasa lake rift-related N-S trend.* This trend, responsible for the emission of the young Mbaka monogenic field, is interpreted as being of young age (about 1 Ma) and determined a progressive

lowering eastwards of the geological formations and the consequent outcropping of the metamorphic basement complex along the NE flank of the Mbaka fault.

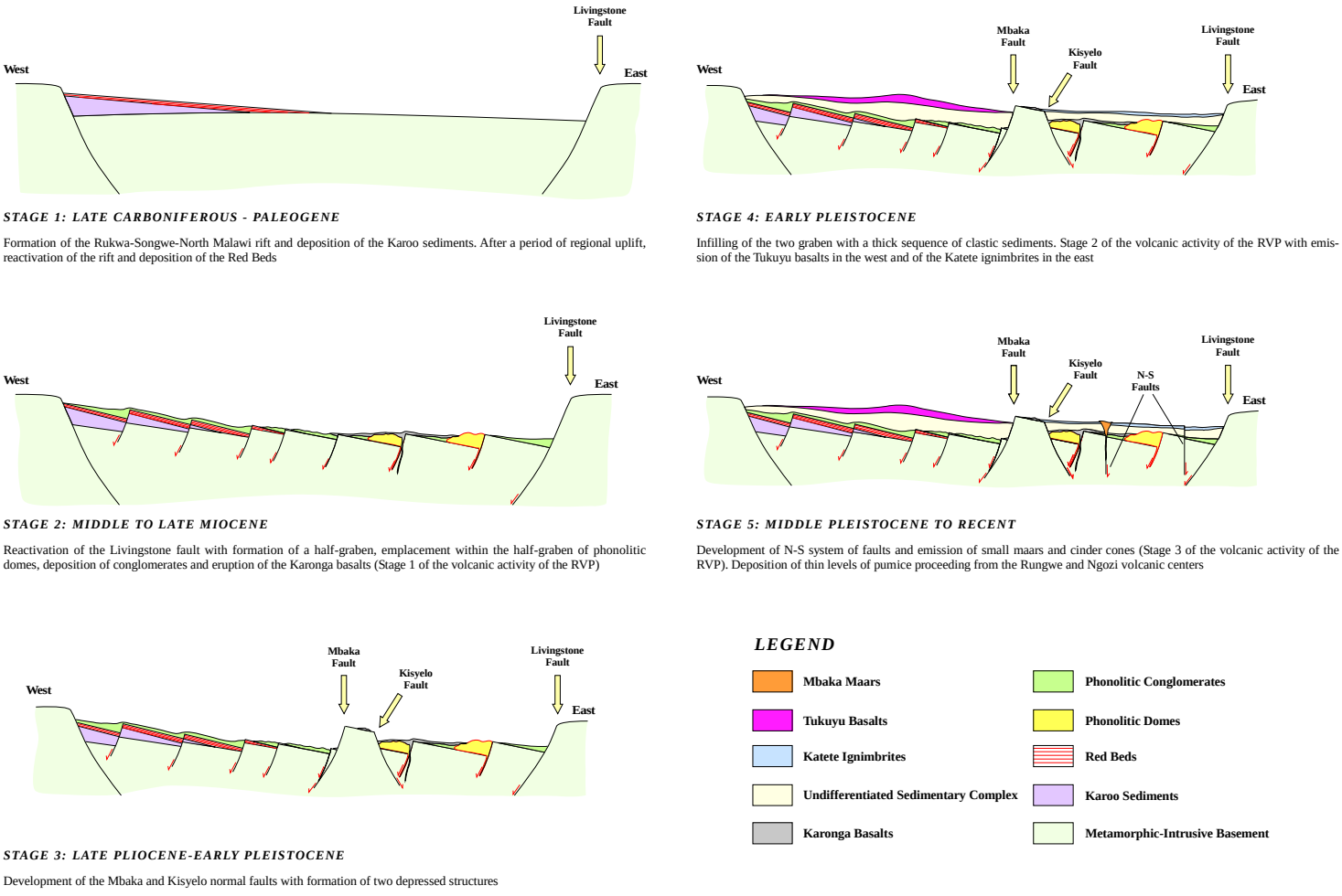

STAGE 1: LATE CARBONIFEROUS - PALEOGENE

Formation of the Rukwa-Songwe-North Malawi rift and deposition of the Karoo sediments. After a period of regional uplift, reactivation of the rift and deposition of the Red Beds

STAGE 2: MIDDLE TO LATE MIOCENE

Reactivation of the Livingstone fault with formation of a half-graben, emplacement within the half-graben of phonolitic domes, deposition of conglomerates and eruption of the Karonga basalts (Stage 1 of the volcanic activity of the RVP)

STAGE 3: LATE PLIOCENE-EARLY PLEISTOCENE

Development of the Mbaka and Kisyelo normal faults with formation of two depressed structures

STAGE 4: EARLY PLEISTOCENE

Infilling of the two graben with a thick sequence of clastic sediments. Stage 2 of the volcanic activity of the RVP with emission of the Tukuyu basalts in the west and of the Katete ignimbrites in the east

STAGE 5: MIDDLE PLEISTOCENE TO RECENT

Development of N-S system of faults and emission of small maars and cinder cones (Stage 3 of the volcanic activity of the RVP). Deposition of thin levels of pumice proceeding from the Rungwe and Ngozi volcanic centers

Figure 5-38 Kiejo-Mbaka geothermal field: geological history, resulting from the geological survey performed

The final combined analysis of the geological data suggests:

- Volcanism in the prospect is dominated by fault-related monogenic events, disproving the presence of magma chambers of significant volume and recent age at relatively shallow depth.
- The water recharge for the deep circuits is probably ensured by rainwater infiltrating in the rift faults related to the Livingstone system. Under this assumption, the deep groundwater circulation would largely be controlled by the Usangu rift-related trend striking ENE-WSW.
- The reservoir formations correspond to the products of the metamorphic basement complex, associated with poor primary permeability. The possibility of encountering adequate permeability for the formation of a commercial geothermal system must be therefore referred to the existence of neo-tectonic activity, which may determine the formation of a widespread network of fracturing.
- In this context, the N-S Nyasa lake rift-related trend is probably, in consideration of its young age and strong surface expression, the most effective tectonic system guaranteeing good secondary permeability.

- The absence of a clear potential heat source corresponding to a magmatic chamber suggests that any geothermal system possibly present in the Kiejo-Mbaka prospect is likely to be of an extensional type category.

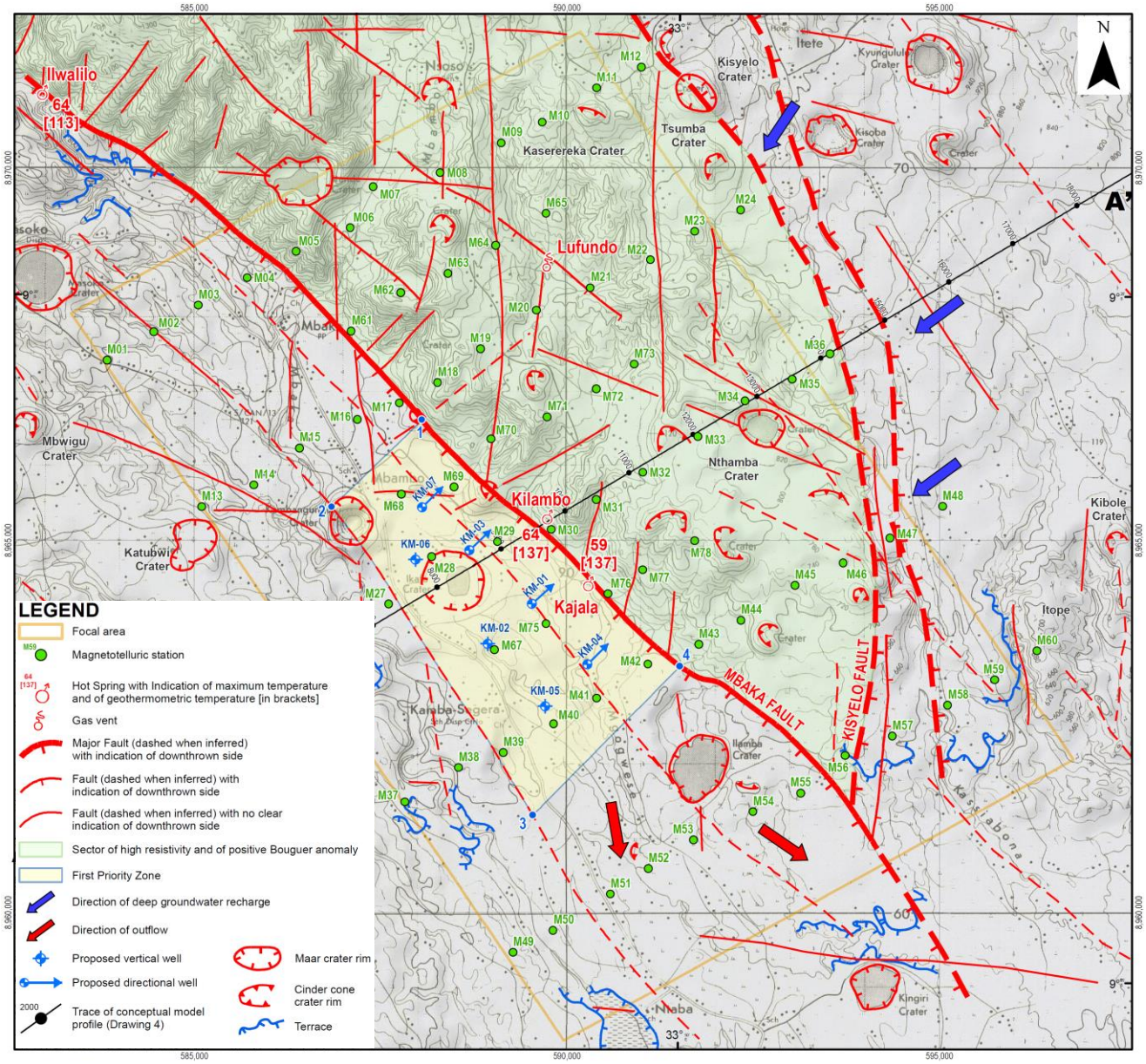

Figure 5-39 Kiejo-Mbaka geothermal field: synthesis map, resulting from the geological survey performed

5.4.3.2. Geophysical data

In the interpretation of the gravimetric data, standard processing techniques were applied to compute the Free Air and the complete Bouguer anomaly maps (Balmino et al., 2011; Brown et al. 1980; Nagy, 1966). As reference, the density of the amphibolitic schists of the metamorphic and intrusive complex (MIT) were adopted, estimated from both direct laboratory measurements and from the Parasnis approach. The adopted reference density resulted 3,000 kg/m^3. The final residual Bouguer anomaly map was derived by removing the regional field measured by the 25 additional points. The map shows an elongated gravimetric high trending NW-SE with values up to 24 mGal, surrounded by gravimetric lows as low as -6 mGal.

To reveal possible structural lineaments, the horizontal derivative of the residual Bouguer anomaly was computed. The highest values of the horizontal gradient were assumed to image areas where large horizontal density variations occur and hence to identify important structural lineaments (Parker, 1991). A good correlation was recognized between the gravimetric lineaments and structural lineaments, in particular with reference to the Mbaka faults and to the existence of important N-S trending fractures.

To enlighten the sources of the detected anomalies, a 2D and 3D modelling was performed. The results indicate that the positive residual Bouguer anomaly can be explained by a high-density basement of amphibolitic schists of the MIT (see Figure 5-40). In order to fit the gravimetric lows, the existence of a thick low-density layer was assumed, affecting the MIT basement below the shallow and thin low density layer of the Tukuyu lavas / Katete ignimbrites. This low density layer was modelled assuming a density of 2,500 kg/m^3 (i.e. -500 kg/m^3 of density contrast with respect to the unaltered amphibolitic schists), and interpreted as due to hydrothermal alteration of "low" temperature of the MIT.

The altered low-density region in the MIT basement well corresponds with the low resistivity regions imaged by the 3D model of the magnetotelluric data set both SW and NE of the Mbaka fault.

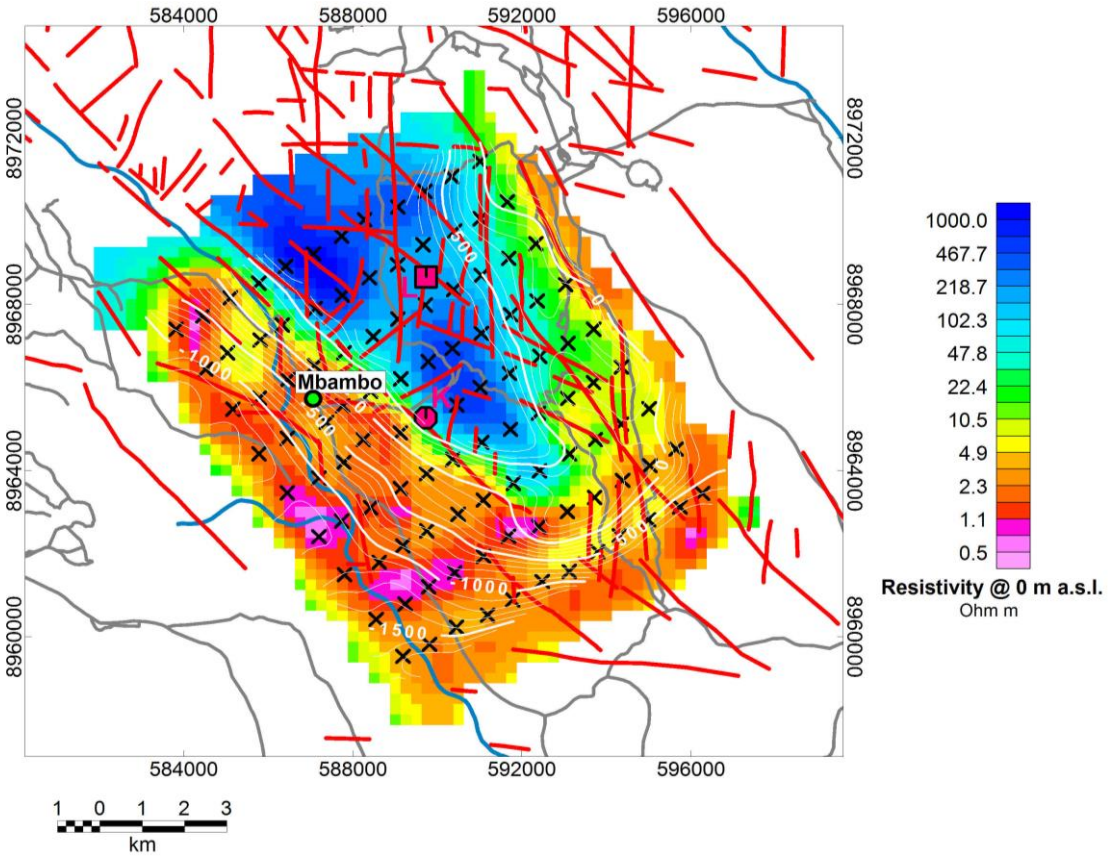

Figure 5-40 Bottom (white contour lines, 100 m) of the low density layer (-500 kg/m^3) derived from the 3D inversion superimposed on the resistivity slice at elevation 0 m extracted from the 3D resistivity model (ELC, 2017). Large magenta square and circle: Lufundo fossil and Kilambo manifestations respectively. Gray and light blue lines: main roads and rivers

The resistivity survey (Magnetotelluric -MT- and Time Domain Electromagnetic -TEM-) carried out in the Kiejo-Mbaka field comprises the current 76 MT/TEM stations, covering the RVP area. Impedances and tippers were estimated by means of the Remote Reference technique applied to both the standard LSQ and robust estimation methods (Sutarno, 2008). When necessary, a coherence rejection scheme was applied (Jones, 1984). The static shift effect was corrected by MT/TEM phase joint

inversion. From this procedure, three static shift correcting factors for each station were calculated and used to correct the average apparent resistivity (used in 1D modelling) and the xy and yx modes (used in 3D modelling).

From the geomorphological point of view, Kiejo-Mbaka area can be divided into three domains: (i) *Rift Basin*; (ii) *Rift Plateau*; iii) *Mbaka Fault Escarpment*. Such lithological differences were also found to be reflected in electromagnetic investigations results.

It is essential specify that for some stations, given the strong 3D effects over this part of the survey area, the xy-mode data instead of the average impedance was inverted. In fact, the average phase data were not possible to be satisfactorily fitted.

The model in Figure 5-41 is an example from the *Rift Basin*, west of the Mbaka fault, over the Neogene volcano-lacustrine sediments. From the top to the bottom, four layers can be pinpointed (see the blocky inversion, marked as a blue line):

i. A shallow resistive layer (~40 Ohm m, thickness ~60 m);
ii. A conductive layer (~8 Ohm m, thickness ~160 m), centred at a depth of about 120 m;
iii. A very conductive layer (~2 Ohm m, thickness ~610 m), centred at a depth of about 510 m and an extremely conductive layer (1 Ohm m, ~1500 m thick), centred at a depth of about 1400 m;
iv. A resistive layer (~55 Ohm m) at a depth of about 2300 m.

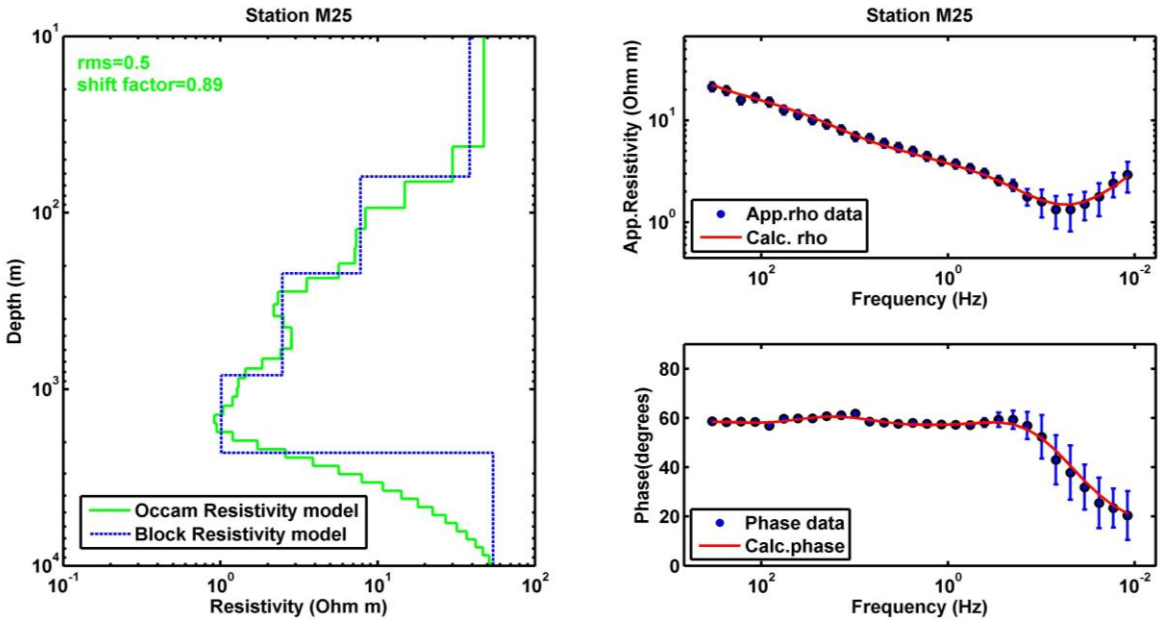

Figure 5-41 Example of MT 1D smooth inversion (left panel, green line) from the rift basin (station M25 in Fig. 5-39). The blocky model is shown as a blue line. Note the logarithmic scale for depth and resistivity

The resistivity value of the first layer was compatible with the soil and the underlying (likely altered) Tukuyu lavas (see Figure 5-38). The second layer could be interpreted as the older Neogene fluvio-lacustrine deposits; the subsequent two layers underneath, given their high conductivity (2 and 1 Ohm m, blocky inversion, blu line), were interpreted as a low-temperature alteration zone. The thickness of the 1 Ohm m layer seems more compatible with the presence of widespread alteration than thick clayey lacustrine deposits. The resistivity rising at depth suggests that the bedrock top could lie at about 2300 m; by comparison with the geological cross-section, it is likely that the bedrock is constituted by the Mesozoic Red Sandstones and Mudstones (Dinosaur Beds). Given the observed low resistivity, a certain degree of high-temperature alteration could affect these rocks.

The model in Figure 5-42 is an example from the *Rift Plateau*, at a site about 4 km far from the Mbaka fault escarpment (M36). This site is located over the Katete Ignimbrites. The following five electrostratigraphic units were identified:

i. A shallow moderately resistive layer (~25 Ohm m, thickness ~70 m);
ii. A conductive layer (~12 Ohm m, thickness ~210 m), centred at a depth of about 160 m and a very conductive layer (~2 Ohm m, thickness ~350 m), centred at a depth of about 450 m;
iii. A resistive layer (~85 Ohm m, thickness ~1,500 m), centred at a depth of about 1250 m;
iv. A very conductive layer (~6 Ohm m, thickness ~1410 m), centred at a depth of about 2800 m
v. A resistive layer (~450 Ohm m) at a depth of about 3500 m.

The moderately resistive surficial layer centred can be correlated with the Katete Ignimbrites, while the third conductive layer (2 Ohm m) can be interpreted as a low-temperature alteration horizon in the Precambrian Livingstone Gneiss (see Figure 5-38). The second layer (12 Ohm m) could be explained as a transition layer between the shallow unaltered rocks and the altered zone centered at 450 m. The fourth layer likely represents the relatively fresh Gneiss, while the underlying conductive layer (6 Ohm m) can represent another low-temperature and thick alteration zone. The unaltered Precambrian Gneiss plausibly constitutes the last layer.

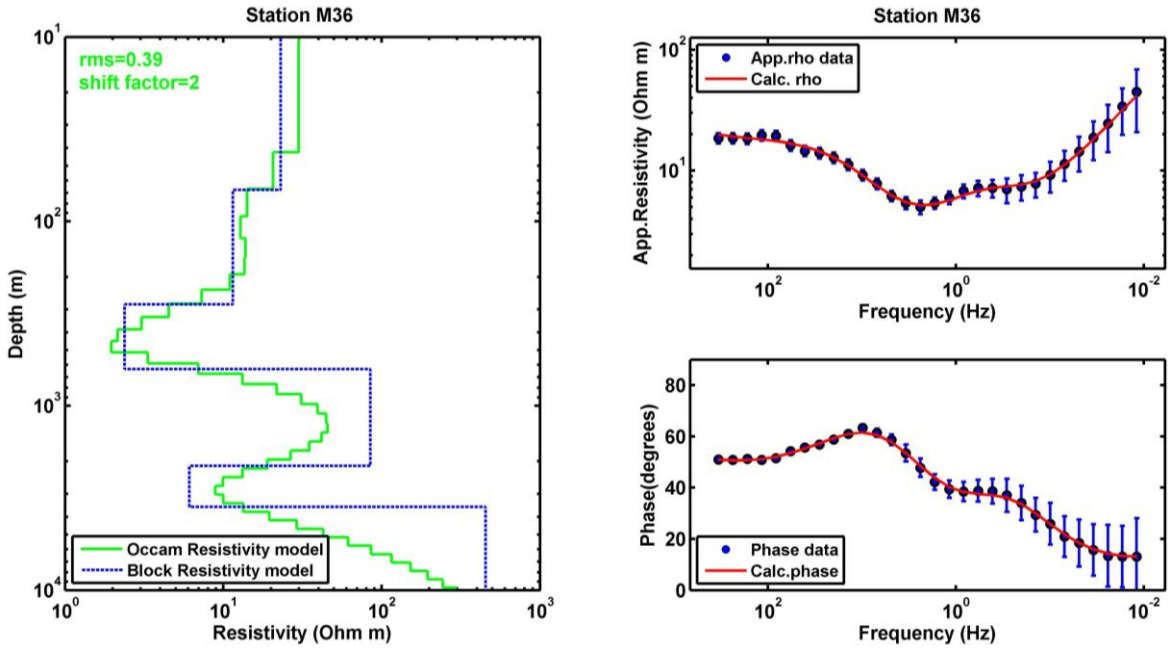

Figure 5-42 Example of MT 1D smooth inversion (green line) from the rift plateau (station M36 in Fig. 5-39). The blocky model is shown as a blue line. Note the logarithmic scale for depth

Figure 5-43 shows an example of the Mbaka Fault Escarpment. This site is located over the MIT. For this station (M19) the xy apparent resistivity and phase were inverted. The following three electrostratigraphic units were identified:

i. A resistive layer (~170 Ohm m, thickness ~500 m);
ii. A resistive layer (~230 Ohm m, thickness ~2000 m), centred at a depth of about 1200 m;
iii. A very resistive layer (~1170 Ohm m) at a depth of about 2500 m.

The resistivity values of the first two layers are compatible with the slightly altered metamorphic basement, while the third one can be interpreted as the unaltered bedrock.

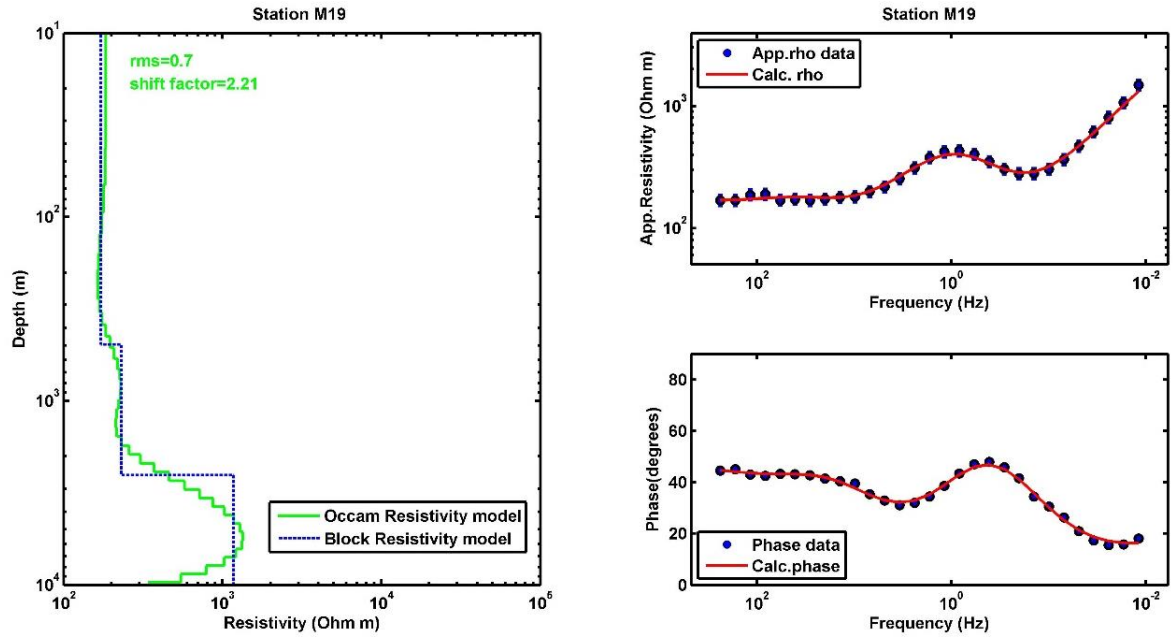

Figure 5-43 Example of MT 1D smooth inversion (left panel, green line) from the Mbaka fault escarpment (station M19 in Fig. 5-39). The blocky model is shown as a blue line. Note the logarithmic scale for depth and resistivity

The 3D inversion was carried out with several initial models and datasets, namely Tz and Z+Tz inversions, both with fine and coarse horizontal gridding (250 and 400 m); lowest misfits were reached using the coarse one. All the inversion runs produced models with the same general features, namely a resistive central body and conductive regions around it. The model here discussed was obtained from a Z+Tz inversion, started from a priori model obtained from the T inversion carried out using a 100 Ohm m half space as priori model.

From the 3D inversion, resistivity cross-sections (see Figure 5-44 for their location) were prepared; a selection of these profiles (PT03) is represented in Figures 5-45, while Figure 5-46 represents horizontal slice at elevations from 800 m asl to -600 m asl.

The 3D inversion allowed to much better understanding the geometry of the resistivity structures present in the Kiejo-Mbaka geothermal area. Though the lithology in the area is dominated by the MIT and Livingstone (LIV) metamorphic complexes, several anomalous resistivity zones can be identified. This leads to infer that resistivity is not directly related to lithologies. The resistive "core" (R) is well associated with the old metamorphic basement, as shown in the resistivity slice -200 m asl (see Figure 5-46). This resistivity body (R) deepens toward SE, as observed from the modelled 100 Ohm m isoresistive surface and from the resistivity cross-sections (Figure 5-45).

This resistivity body is delimited by two surfaces: one SW-dipping with a high-angle and one NE-dipping and less inclined. The first is associated with the Mbaka fault, while the second one has a direction compatible with the Livingstone fault system. Moreover, the weak inclination of this latter suggests that it could be interpreted as the top surface of a tilted block. This is apparently in accordance with the general tectonic setting of the Karonga graben described in Ebinger et al. (1993), who hypothesised the presence of NE-tilted blocks between the Mbaka fault and the Livingstone border fault. The resistive basement is apparently affected by a relatively conductive zone at shallow depths, in the immediate surroundings SW of Lufundo manifestations (see Figure 5-46). This feature could be interpreted as a high-T alteration zone.

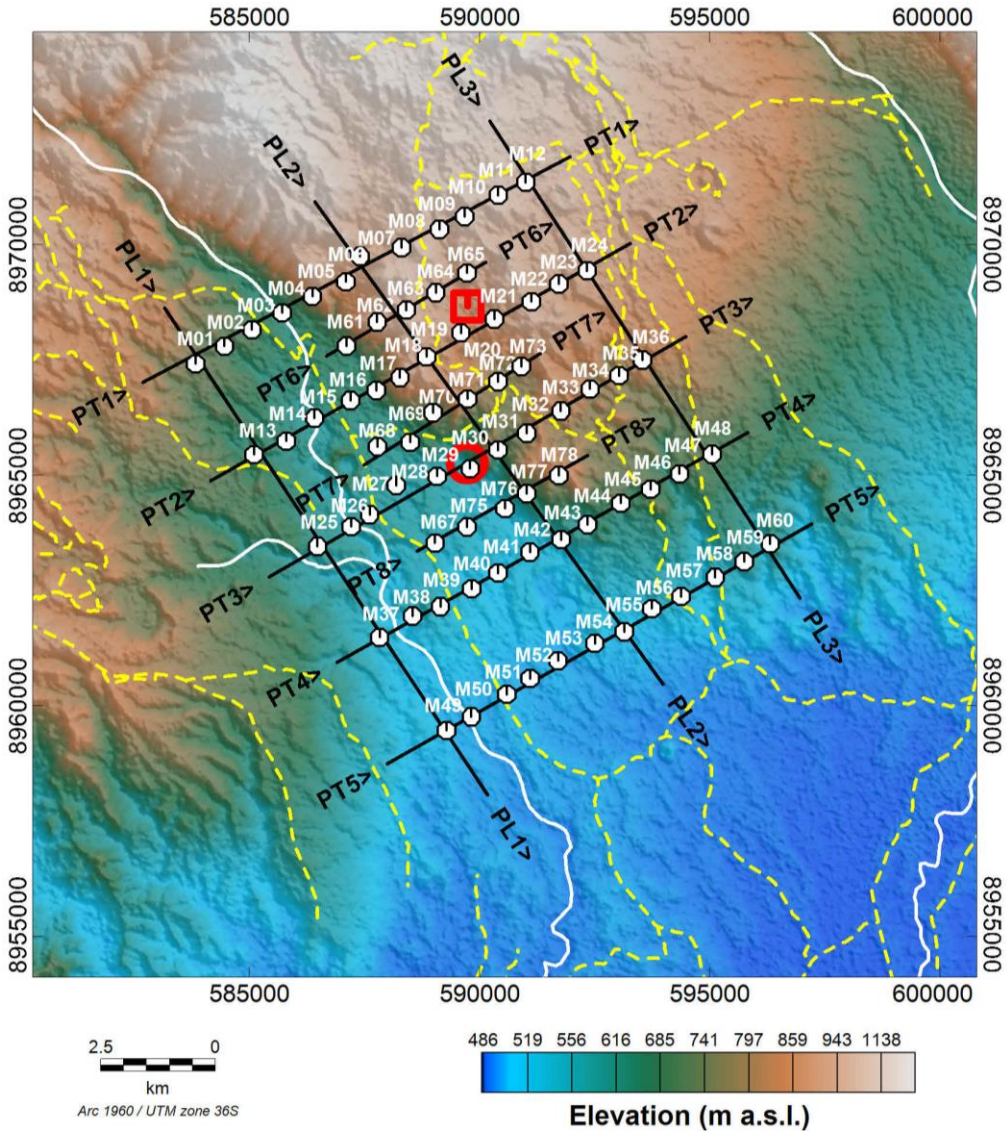

Figure 5-44 Location of the vertical slices of the 3D resistivity model (blue lines) shown in the following figure. The > symbol indicate the orientation of the corresponding pseudosections. White circles mark the MT sites. Red circle indicates the Kilambo hot springs, and the red square the Lufundo manifestations. Dashed yellow lines refer to main roads, while white lines to main rivers

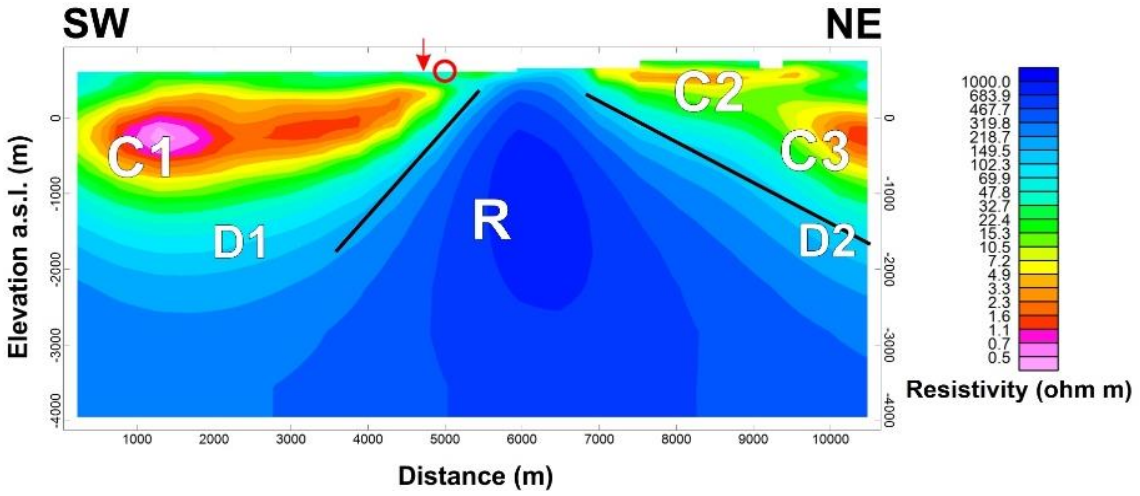

Figure 5-45 Section PT3 (see Fig. 5-44 for its location). The red circle indicates the location of the Kilambo manifestations. Red arrow marks the Mbaka fault trace

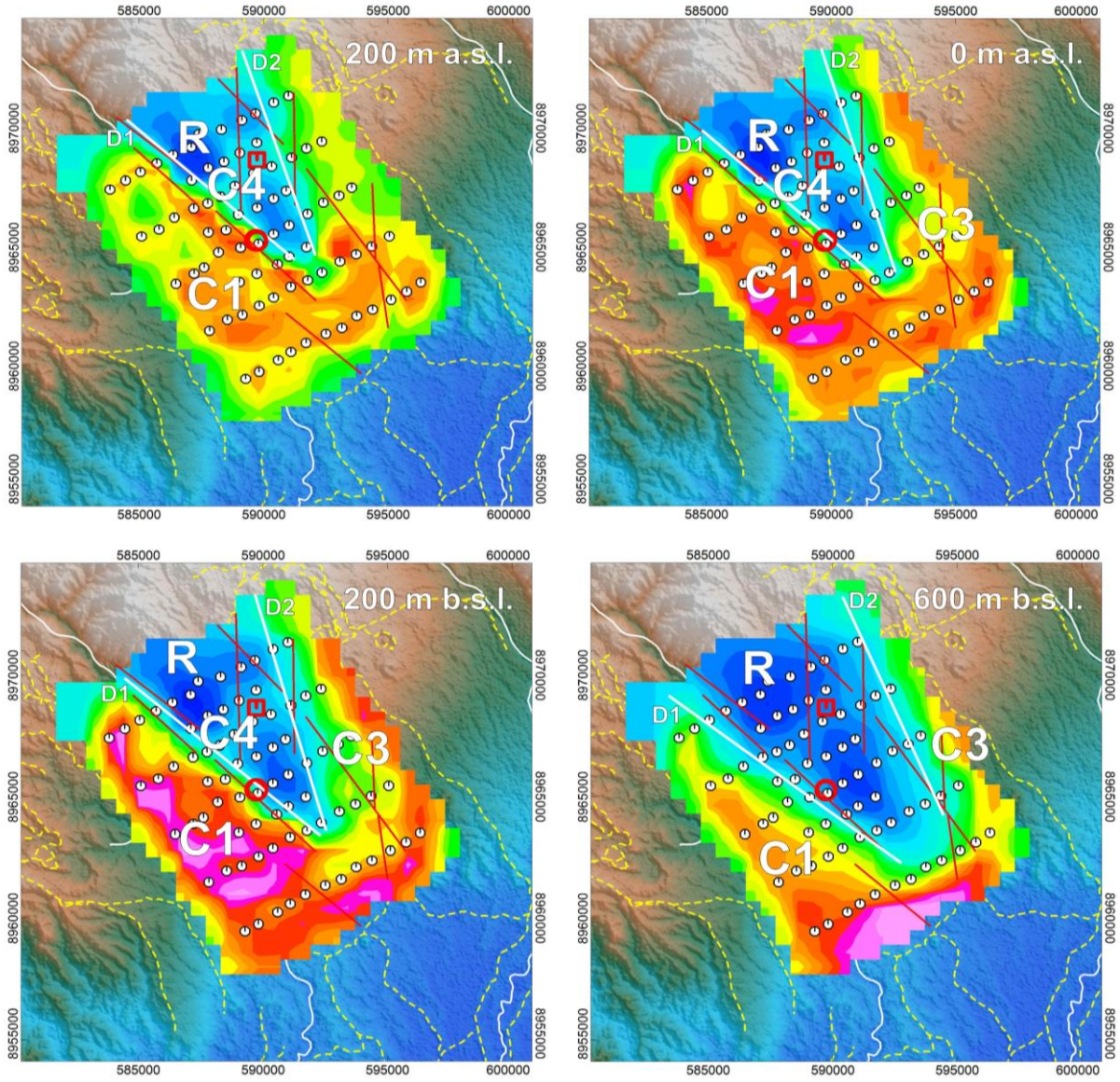

Figure 5-46 Horizontal slices of the 3D model from 800 m asl to -600 m a.s.l. White circles: MT stations. Red circle: Kilambo hot springs; red square: Lufundo manifestations. White straight lines: inferred lineaments. The main resistivity features are labelled by "R", C1", "C2", "C3" and "C4". White lines: main rivers, while yellow lines the main roads. Scale of resistivity is the same of Figure 5-45

Figure 5-47 shows the main resistivity survey findings superimposed on the geological map, together with the recognized faults. Notice that the showed features do not necessarily refer to the same depth.

The AZ1, AZ2, AZ3 alteration zones (Figure 5-47) were inferred by considering the 10 Ohm m isoresistive contour line. The AZ4 zone was identified by considering the 50 Ohm m contour line. Therefore, while the first three have to be referred as low-T alteration zones, the latter might be considered as a high-T one. Based on the geological results, all the alteration zones should affect the metamorphic basement.

Zone AZ1 was delineated from the -600 asl resistivity slice. It is limited toward SE in order to avoid possible inclusion of lacustrine sediments. Notice that this zone, being retrieved from a slice that lies 1200 m below the ground surface in the plain area, and given the SW-dipping of the Mbaka fault, could also affect the foot wall, not only the hanging wall. In fact, observing the trace of the Mbaka fault

at surface, it can be easily assessed that at that depth, it would lie within the AZ1 zone.

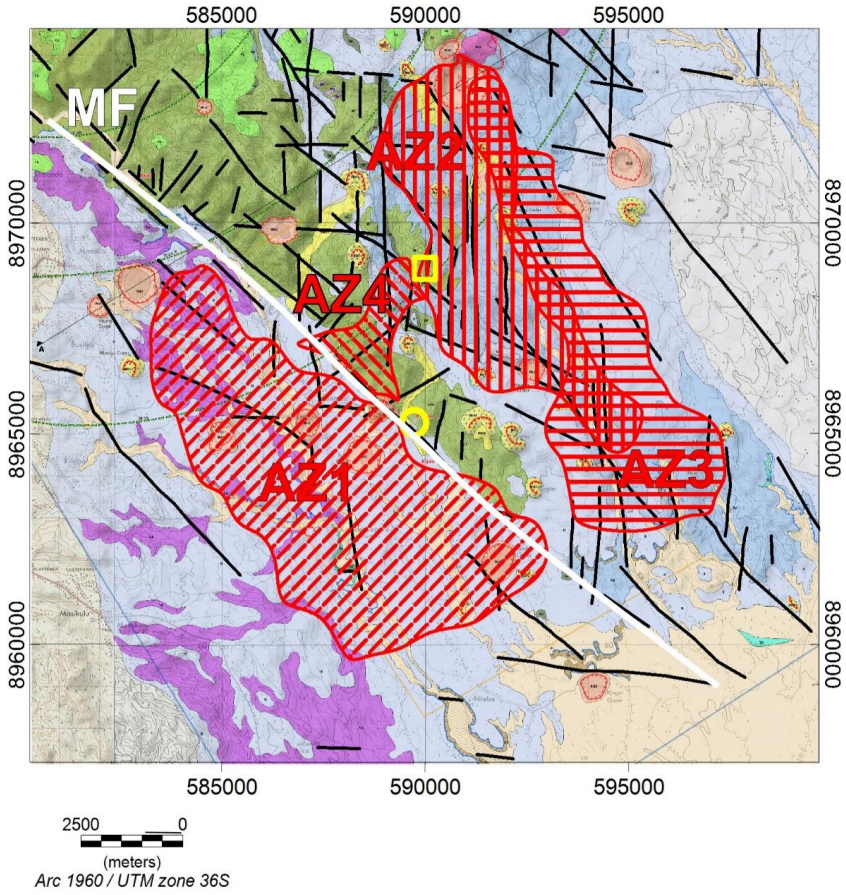

Figure 5-47 Synthesis map with the main findings superimposed on the geological map. Yellow circle: Kilambo hot springs; yellow square: Lufundo manifestations. AZ1, AZ2, AZ3, AZ4: alteration zones, marked by different hatches. MF: Mbaka fault trace. For the geological map legend, see Figure 5-38

The AZ2 zone included the C2 anomalies (see e.g. Figure 5-45), well visible from the 600 and 200 m asl slices. This zone could be interpreted as a low-T alteration zone related to the Lufundo manifestations.

The AZ3 zone was identified from the -200 asl slice; it is limited toward SE in order to avoid possible inclusion of lacustrine sediments. This zone was only partially investigated by MT, and its eastern limit is to be regarded as hypothetical.

Zone AZ4 was pinpointed by observing the 200 asl resistivity slice. It could be correlated with the N-S fault passing about 1 km W of Lufundo, and it could represent a high-T alteration zone possibly associated with the Lufundo manifestations.

5.4.3.3. Geochemical data

Kilambo-Kajala - The hot springs of Kilambo and Kajala (see Figure 5-39) represent the discharge of a unique fault-controlled geothermal circuit, but distinct from the Ilwalilo geothermal circuit, with outlet temperature up to 64 and 59 °C, respectively, total flowrate in the order of 10 and 5 L/s, respectively, and natural heat discharge of 2.5 and 1.3 MW thermal, respectively, for a total of 3.8 MW thermal.

Reservoir temperature is probably 137 ± 2 °C, as indicated by the silica geothermometer, in acceptable agreement with (i) the saturation indices vs. temperature plot (see Figure 5-48),

hypothesizing equilibrium with K-feldspar to compute Al concentration, and (ii) the most realistic solution of the iso-chemical geothermometric mixing model. Available $\delta^{13}C$ values of CO_2, in the range -5.5 to -6.0 ‰, suggest that CO_2 is chiefly supplied by deep sources and a continuous flux of CO_2 occurs through the geothermal system of interest.

The Kilambo-Kajala reservoir liquid has Na-HCO_3 chemical composition (see Figure 5-49 and Table 5-7), which is acquired through interaction of meteoric waters with basement rocks (mainly gneisses) sustained by conversion of CO_2 to HCO_3. The main anionic constituents are HCO_3, Cl, and SO_4. The major cations are Na and K, whereas Ca reservoir concentration is 2.1 mg/L, assuming calcite saturation, and Mg reservoir content is 2.3 mg/L, hypothesizing equality of silica and K-Mg temperatures. The δ^2H and $\delta^{18}O$ values of H_2O indicate that the Kilambo-Kajala hot spring waters are of meteoric origin, in spite of their negative oxygen shift, which is probably due to exchange of oxygen isotopes between water and CO_2. Based on the δ^2H - elevation relation reconstructed during this work, recharging meteoric waters infiltrate at average elevation of about 1,950 m asl, at a distance of ~14-17 km.

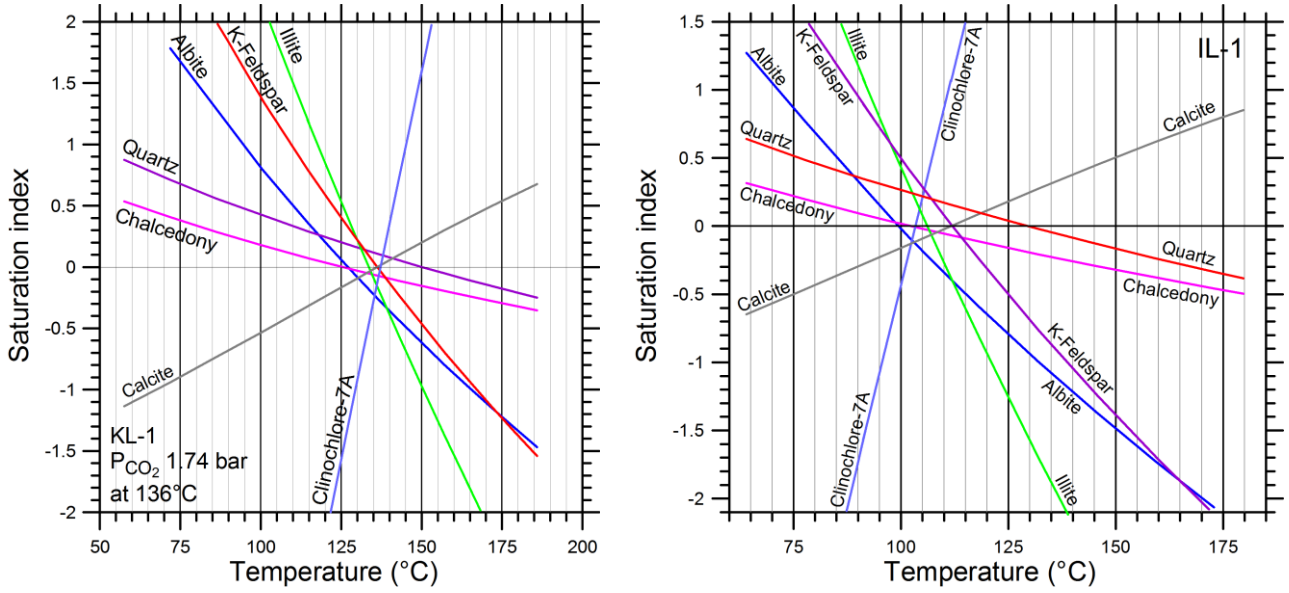

Figure 5-48 SI vs. temperature plot for sample KL-1 from Kilambo (Left) and IL-1 (Right) from Ilwalilo, obtained considering the initial Mg, Ca, and DIC concentrations in geochemical modelling

Based on the reservoir temperature of 137 ± 2 °C and the average surface temperature of 25 °C, the geothermal reservoir depth is estimated to be ~1.70 ± 0.03 km, assuming a local geothermal gradient of 66 °C km^{-1} that is double the normal one. Therefore, the geothermal reservoir is constituted at least by the volume of rocks present around the Mbaka fault below the Kilambo and Kajala hot springs at average depth of ~1.7 ± 0.03 km, although this figure is affected by a high uncertainty and have to be substantiated through further exploration. The geothermal reservoir might extends northwards underneath the Lufundo gas vent.

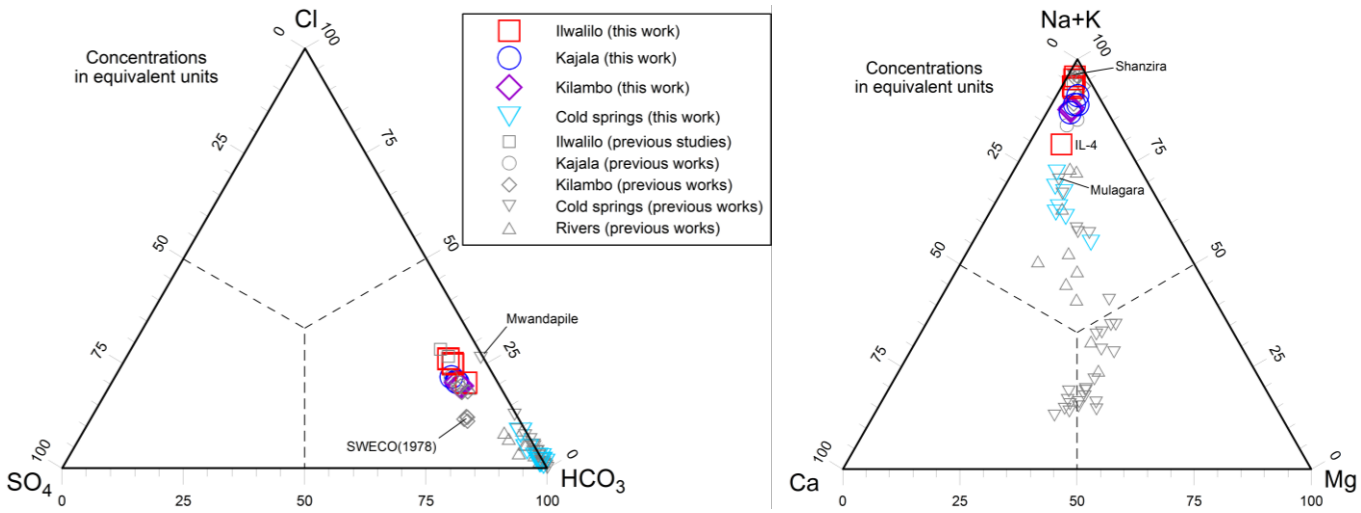

Figure 5-49 Triangular diagram of major anions (Left) and cations (Right) for the water samples collected in the Kiejo-Mbaka prospect area during this work and previous studies (SWECO, 1978; Makundi and Kifua 1985; Kraml et al., 2008; Ochmann and Garofalo, 2013; Delalande, 2009; Delalande et al. 2011)

Ilwalilo - The hot springs of Ilwalilo (see Figure 5-39 and Table 5-8) constitute the outflow of a fault-controlled geothermal circuit distinct from that of Kilambo-Kajala, with outlet temperature up to 64 °C, total flowrate of at least 5 L/s and minimum heat discharge of 1.3 MW thermal.

Reservoir temperature is probably 110-115 °C, as indicated by both silica and K-Mg geothermometers, in satisfactory agreement with (i) the saturation indices vs. temperature plot (see Figure 5-36), assuming equilibrium with K-feldspar to calculate Al concentration, and (ii) the most realistic solution of the iso-chemical geothermometric mixing model. Available $\delta^{13}C$ values of CO_2, in the interval -5.6 to -6.4 ‰, indicate that CO_2 is mainly contributed by deep sources and a continuous flux of CO_2 pass through the Ilwalilo geothermal system.

Similar to Kilambo-Kajala, also the Ilwalilo reservoir liquid has Na-HCO_3 chemical composition (see Figure 5-37), acquired through CO_2-driven interaction of meteoric waters with basement rocks (mainly gneisses).

The Ilwalilo hot spring waters are of meteoric origin, as they are positioned along the local meteoric water line in the correlation diagram of δ^2H vs. $\delta^{18}O$. The isotope-elevation relations calibrated during this thesis suggest that meteoric waters recharging the Ilwalilo thermal circuit infiltrate at an average elevation of about 2,180 m asl, either in the highlands to the NE of the Ilwalilo hot springs, at a distance of ~19-21 km, or in the southern flanks of Rungwe volcano, at similar distances from Ilwalilo. On the basis of reservoir temperature and average surface temperature, 25 °C, by assuming a local geothermal gradient of 65 °C km^{-1}. An estimate of the geothermal reservoir depth is ~1.5 km. although this depth is affected by considerable uncertainty and must be verified through further exploration. the geothermal reservoir is likely constituted by the volume of rocks present around the Mbaka fault below the Ilwalilo hot springs.

Table 5-8 Field data and results of the chemical and isotopic laboratory analyses of the water samples collected in the Kiejo-Mbaka area during this work. T is outlet temperature, Q is flow rate, EC is electrical conductivity, - = not determined. Type is as follows: HS = Hot Spring (T ≥ 30°C); CS = Cold Spring (T ≤ 25°C)

Code	Locality	Type	Sampling date	T	Q	pH	EC	Eh	Na	K	Ca
				°C	*L/s*		*µS/cm*	*mV*	*mg/L*	*mg/L*	*mg/L*
KL1	Kilambo	HS	09/10/2016	57.6	10	6.88	5207	-68.6	1203	62.5	87.2
KL2	Kilambo	HS	09/10/2016	63.3		6.81	5213	-55.1	1146	62	88.5
KL3	Kilambo	HS	09/10/2016	64	1	6.74	5157	-51	1172	63	91.5
KL4	Kilambo	HS	09/10/2016	50.1	0.05	6.92	5360	-62	1208	67.4	94.4
KL5	Kajala	HS	10/10/2016	58.9	0.5	6.66	5130	-64.2	1161	65.3	63.1
KL6	Kajala	HS	10/10/2016	42.3	0.5	6.36	4060	-92	928	51.9	76.9
KL8	Kajala	HS	10/10/2016	55.2	0.3	6.75	4916	-88	1088	62.8	46.2
KL9	Kajala	HS	10/10/2016	46.1	1.5	6.51	4625	-107	1045	60.2	64.2
IL1	Ilwalilo	HS	11/10/2016	64	0.5-1	6.82	7084	-91.6	1630	74.5	39
IL2	Ilwalilo	HS	11/10/2016	51.8	0.5-1	6.55	5139	-99.4	1186	55	49
IL3	Ilwalilo	HS	11/10/2016	52.7	0.1-0.15	6.47	6088	-127	1472	63.1	42.5
IL4	Ilwalilo	HS	11/10/2016	35.7	Oct-20	6.25	1615	-67.4	292	16	45.5
IL5	Ilwalilo	HS	11/10/2016	53.8	01-Mar	6.52	5027	-80	1155	62	47
KJ1	Kiejo	CS	07/10/2016	21.2	0.2	4.92	114.8	5.1	14.5	5.9	4.4
KJ2	Kiejo	CS	07/10/2016	18.3	1.5	6.26	103.2	-4	12.4	5.6	4.7
KJ3	Kiejo	CS	08/10/2016	-	-	-	-	-	-	-	-
KJ4	Kiejo	CS	08/10/2016	20.8	0.5	4.78	78.73	31.2	8.6	4.2	3.4
SM1	Suma	CS	12/10/2016	24	0.05-0.1	7.35	342.8	-49.5	39.3	11.7	14.2
IG1	Igoma	CS	13/10/2016	17.6	0.03	6.68	76	-62	8.2	3.3	2.6
IG2	Igoma	CS	13/10/2016	14.9	0.3	7.3	83.4	-37	8.5	6.5	2.7
IG3	Igoma	CS	13/10/2016	15.1	0.2	6.85	58.7	-73	6.35	3.35	2.7

Table 5-8 Continued

Code	Mg	Alk Tot	SO_4	Cl	F	NO_3	SiO_2	Li	B	Fe	As	TDS
	mg/L	*mg HCO_3/L*	*mg/L*	*mg/L*	*mg/L*	*mg/L*	*mg/L*	*mg/L*	*mg/L*	*mg/L*	*mg/L*	*mg/L*
KL1	34.7	2635	236	423	2.71	<0.05	128	0.7	0.89	0.481	0.176	4852
KL2	34.8	2684	234	422	2.77	<0.05	128	0.67	0.89	0.636	0.191	4802
KL3	35.6	2696	238	431	2.8	<0.05	126	0.7	0.92	0.399	0.202	4856
KL4	35	2666	248	444	2.78	<0.05	130	0.71	0.95	0.554	0.201	4895
KL5	40.9	2532	237	430	2.16	<0.05	137	0.7	0.94	0.782	0.211	4668
KL6	29.5	2037	188	342	1.86	<0.05	102	0.55	0.73	0.01	0.135	3758
KL8	30	2324	235	423	2.79	<0.05	117	0.65	0.89	0.042	0.194	4329
KL9	31.9	2342	215	391	2.53	<0.05	113	0.6	0.83	0.01	0.159	4265
IL1	15	3155	274	720	7.7	<0.05	89.2	0.95	1.37	0.047	0.296	6004
IL2	19	2428	197	512	5.54	<0.05	73	0.65	0.98	0.006	0.177	4524
IL3	15.2	2800	245	635	6.7	<0.05	85.3	0.85	1.23	0.02	0.272	5365
IL4	14.2	753	53	122	1.85	<0.05	41.6	0.15	0.28	0.006	0.032	1339
IL5	16	2358	191	506	5.56	<0.05	73.3	0.64	0.97	0.009	0.102	4414
KJ1	1.9	75	0.6	1.1	0.18	1.2	45.7	<0.05	<0.05	0.004	<0.005	150
KJ2	1.85	71	0.33	0.62	0.18	<0.05	53.8	<0.05	<0.05	0.016	<0.005	150
KJ3	-	-	-	-	-	-	-	-	-	-	-	-
KJ4	1.6	52	0.15	0.73	0.12	<0.05	47.6	<0.05	<0.05	0.004	<0.005	118
SM1	11.2	217	0.5	1.3	0.34	<0.05	61.8	<0.05	<0.05	0.322	<0.005	357
IG1	0.85	35	0.4	1.9	0.12	11.5	25.1	<0.05	<0.05	0.005	<0.005	89
IG2	0.86	43	0.7	1.2	0.13	11.6	27.5	<0.05	<0.05	0.147	0.005	103
IG3	1	42.7	0.3	0.35	0.15	0.3	26.5	<0.05	<0.05	0.006	<0.005	84

Table 5-8 Continued

Code	TIS	∑ Cations	∑ Anions	%dev	DIC	CO_2	P_{CO2}	SI calcite	$\delta^{18}O$-H_2O	$\delta^{2}H$-H_2O
	meq/L	*meq/L*	*meq/L*		*mg HCO_3/L*	*mg/L*	*bar*		*‰ vs. VSMOW*	
KL1	121	61.1	60.2	0.8	3130	356	0.496	0.9	-5.7	-27
KL2	119	58.7	60.9	-1.8	3280	432	0.656	0.92	-5.79	-27.2
KL3	121	60.1	61.4	-1.1	3400	511	0.783	0.87	-5.7	-27.4
KL4	123	61.9	61.5	0.3	3120	329	0.403	0.88	-5.76	-27.5
KL5	117	58.7	58.7	0	3330	572	0.816	0.55	-5.73	-27.7
KL6	94.9	48	47	1	3370	964	1.01	0.066	-5.35	-25.3
KL8	109	53.7	55.1	-1.2	2920	432	0.578	0.44	-5.62	-27.2
KL9	107	52.8	54	-1.1	3400	766	0.867	0.23	-5.5	-26.3
IL1	154	76	78.1	-1.4	3830	493	0.755	0.61	-5.58	-30.1
IL2	115	57	58.6	-1.4	3420	713	0.9	0.23	-5.28	-27.4
IL3	138	69	69.3	-0.2	4150	973	1.25	0.13	-5.42	-28.5
IL4	33.4	16.5	17	-1.3	1470	519	0.463	-0.62	-	-
IL5	112	55.5	57.2	-1.5	3390	744	0.972	0.21	-5.25	-27.2
KJ1	2.43	1.16	1.28	-5.1	2110	1470	0.874	-3.9	-4.79	-22.8
KJ2	2.26	1.07	1.2	-5.7	163	66	0.036	-2.6	-4.9	-24.1
KJ3	-	-	-	-	-	-	-	-	-4.47	-20.9
KJ4	1.66	0.783	0.882	-6	2050	1439	0.845	-4.3	-4.61	-21.7
SM1	7.23	3.64	3.61	0.3	237	14.4	9.35E-03	-0.6	-4.77	-22.8
IG1	1.28	0.641	0.642	-0.1	52.6	12.7	6.70E-03	-2.8	-5.82	-32.1
IG2	1.49	0.741	0.76	-1.2	48.4	3.93	1.88E-03	-2.1	-5.75	-32
IG3	1.29	0.579	0.724	-11.1	57.9	11	5.31E-03	-2.5	-6.35	-36.8

5.4.3.4. Soil gas data

The results of the soil gas survey (see Figures 5-50, 5-51, 5-52, 5-53, 5-54) performed in the five areas (see Figure 5-39), in which CO_2 anomalies are present, can be summarized, as follows:

- *Kilambo-Kajala area* (Figure 5-50): high CO_2 fluxes were mainly distributed close to the natural emissions of thermal waters and gases, explaining why each single maximum was, more or less, separated from the others. However, these separated highs defined a general trend elongated in NW-SE direction (Mbaka fault). Moreover, some NNE-SSW anomalies seemed to be recognizable as well, suggesting the presence of active tectonic structures with this orientation.

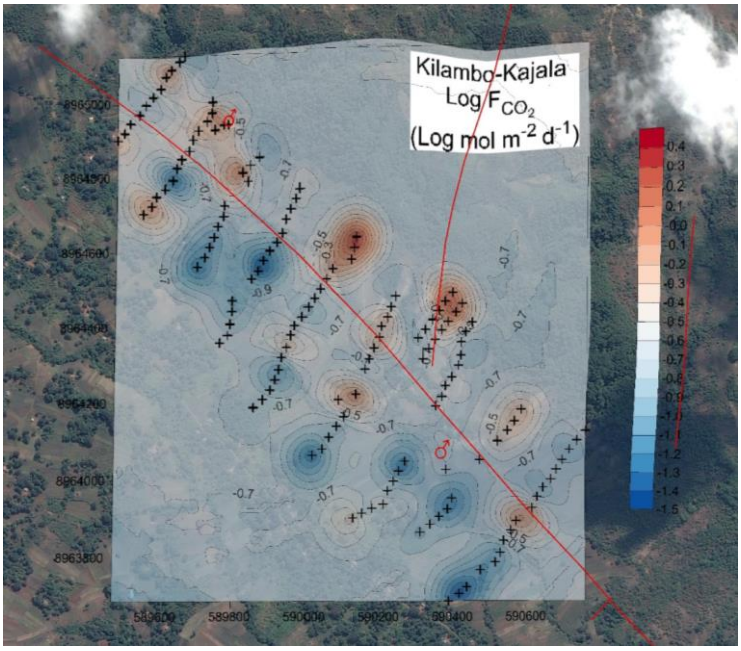

Figure 5-50CO_2 isoflux map of Kilambo-Kajala area. Red lines represent faults and fractures as showed in the structural map (Figure 5-39). Symbols as in Figure 5-39

- *Kiejo area* (see Figure 5-51): a discontinuous NW-SE trending alignment of high CO_2 flux values was shown by the isoflux map. This was in agreement with the occurrence of an active fault belonging to the Mbaka fault system.

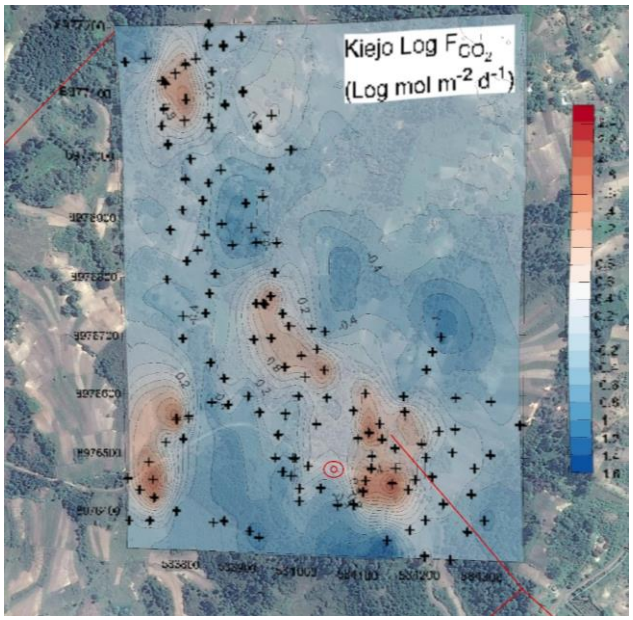

Figure 5-51CO_2 isoflux map of Kiejo area. Red lines represent fault and fractures as showed in the structural map (Figure 5-39). Symbols as in Figure 5-39

- *Lufundo area* (see Figure 5-52): the isoflux map clearly showed an alignment of CO_2 anomalies distributed along N-S and NNW-SSE directions, in agreement with evidences from Kilambo-Kajala and Kiejo areas. However, separated highs also suggested the correlation between CO_2 anomalies and NW-SE trending faults/fractures.

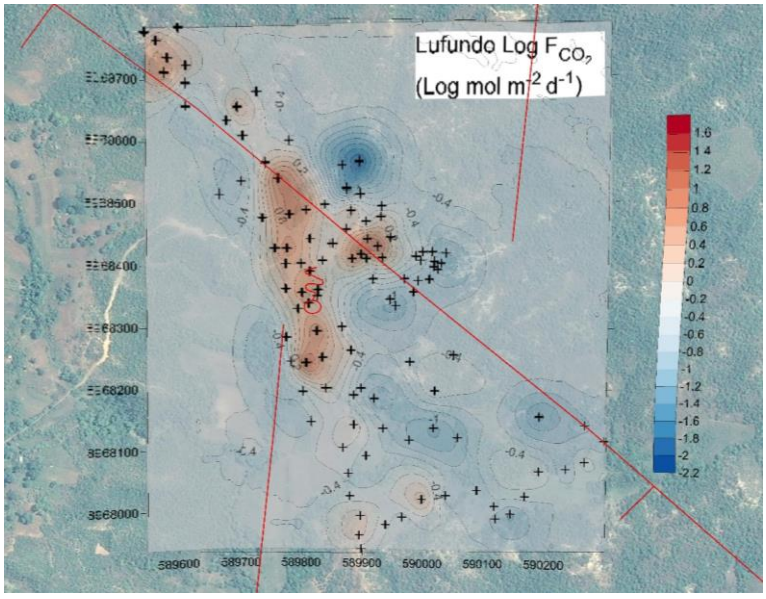

Figure 5-52CO_2 isoflux map of Lufundo area. Red lines represent faults and fractures as showed in the structural map (Figure 5-39). Symbols as in Figure 5-39

- *Ilwalilo area* (see Figure 5-53): the isoflux map showed a few local maxima located just close to the natural emissions of thermal waters and gases. The alignment of CO_2 fluxes, together with the distribution of thermal springs, are evidently controlled by the regional NW-SE trending Mbaka fault.

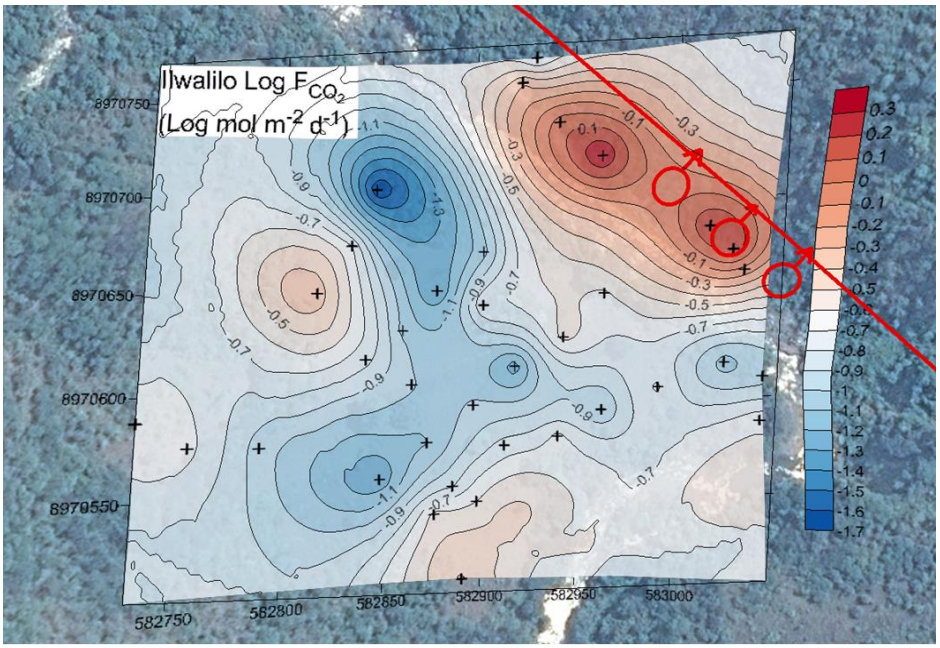

Figure 5-53CO_2 isoflux map of Ilwalilo area. Red lines represent faults and fractures as showed in the structural map (Figure 5-39). Symbols as in Figure 5-39

- *Itende area* (see Figure 5-54): despite the uncertainties in the elaboration of the isoflux map (as the pure nugget effect describes the spatial relation between CO_2 flux measurements), no significant CO_2 anomalies were identified and therefore no relation between the geographical distribution of the CO_2 diffuse flux and the local structural setting was observed. Only a cluster of significantly higher values was recorded in a small area located close to the NW corner of the investigated area. This high could be related to a local N-S tectonic structure.

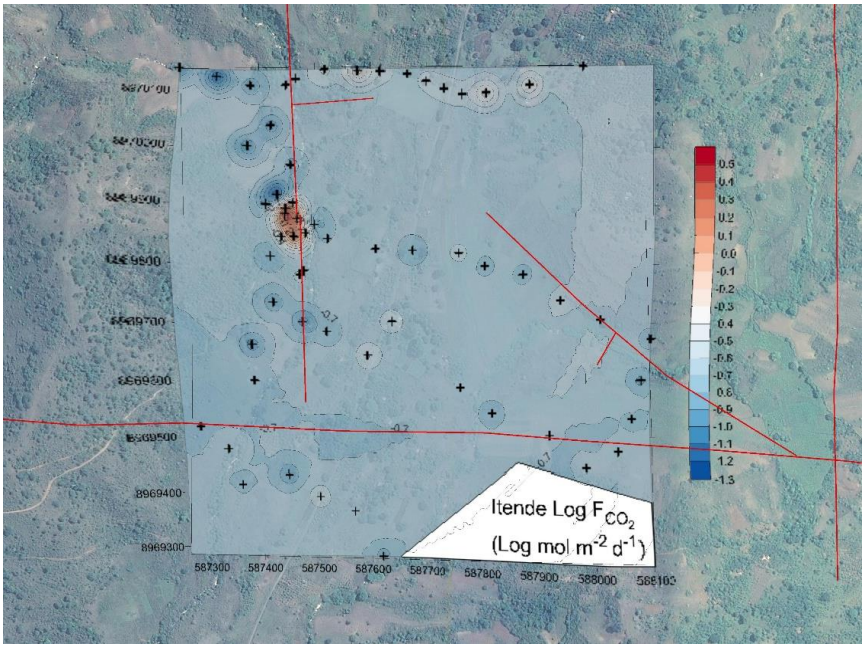

Figure –5-54 CO_2 isoflux map of Itende area. Red lines represent faults and fractures as showed in the structural map (Figure 5-39). Symbols as in Figure 5-39

Furthermore, the total output of deep CO_2 was computed for the investigated areas, obtaining the following values: 12.7 tons/day for *Kilambo-Kajala*, 0.22 tons/day for *Ilwalilo*, 43.0 tons/day for *Lufundo*, 41.6 tons/day for *Kiejo* and 8.4 tons/day for *Itende*.

Summing up the geographical distribution of the CO_2 flux anomalies is in very good agreement with the occurrence of NW-SE trending faults/fractures of the Mbaka system and N-S oriented tectonic structures. Moreover, it is important to note that:

- The thermal manifestations of the Kiejo-Mbaka prospect characterized by emission of hot waters and gases, that is the Kilambo-Kajala and Ilwalilo areas, showed relatively low soil CO_2 fluxes and weak highs.
- On the contrary, in Kiejo and Lufundo areas, where focused gas vents and zones with lack of vegetation are locally present, but hot springs are absent, CO_2 fluxes were higher and anomalies were significant, with maximum values of 295 and 221 $mol \cdot m^{-2} \cdot day^{-1}$, respectively. Also, it must be noted that the Lufundo area is characterized by outcrops of rock affected by hydrothermal alteration with occurrence of clay minerals, chlorite and silica minerals (based on field observation).

5.4.3.5. Conceptual model

There is no evidence of the existence of an adequate heat source in the Kiejo-Mbaka geothermal field, which might be related to either magmatic or plutonic activity, inasmuch as:

- ✓ Recent volcanic activity in the prospects is restricted to the maars and cinder cones dotting both the Mbaka plain and ridge and to the products of the Kiejo volcano, located some 15 km north of the Kilambo manifestations.
- ✓ In the former case, the volcanic products result from monogenic explosions or effusions of very small volume, presumably deriving from a very deep magmatic chamber, which can hardly have generated a wide and shallow thermal anomaly.
- ✓ A similar situation is recognized in the Kiejo volcano, responsible for the emission of basaltic products of very limited volumetric extent.
- ✓ The maar and Kiejo products do not comply with the favourable indications in terms of time persistency, volume and depth, wherefore they are deemed to exclude the existence of an adequate heat source in either a magmatic or plutonic form.

Under this situation, the Kiejo-Mbaka prospect can be classified as extensional domain play, wherein the principal source of heat is provided by the elevated mantle, and it can be either fault controlled or fault-leakage controlled.

a. *Geological Setting.* The undifferentiated sedimentary complex characterized by low permeability, due to either primary lithological features or because of low temperature hydrothermal alteration and/or weathering, corresponds to the cap-rock of the geothermal system. The reservoir formation corresponds to the lower part of the clastic sequence, presumably associated with relatively large grain size (e.g. micro-conglomerate), and possibly to the upper level of the metamorphic-intrusive basement.

In terms of geoelectrical features, the cap-rock and reservoir formations can be tentatively subdivided based on their resistivity values, classifying as cap-rock the portion of the sequence with resistivity <10 Ohm and as reservoir the portion with resistivity included between 10 and 50 Ohm m. These values have been assumed based on the conditions normally recognized in other geothermal fields in the world.

The NW-SE striking buried faults interpreted by the remote sensing study, which extend parallel to the Mbaka fault at a distance of 2 to 4 km, may constitute limits of structural blocks and hence restrain to the west the circulation of deep geothermal fluids brought up by the Mbaka fault itself. Moreover, they could have affected the surrounding rocks, enhancing their secondary permeability.

b. *Reservoir Geometry.* The main spatial features of the Kiejo-Mbaka geothermal reservoir can be described, as follows:

- ✓ Areal extent of the reservoir: The north-eastern limit of the reservoir clearly coincides with the Mbaka fault (see Figure 5-28), with some margins of uncertainty in relation with the actual dip angle of the fault and the thickness of the fractured zone around it. The south-western limit is tentatively set in correspondence of the fault running parallel to the Mbaka fault at a distance of 1.5 to 3 km, interpreted by the remote sensing study. Conventional limits are also established north-westwards and south-eastwards, since no indications in this context are provided by the MT data. It is only observed that, on the base of the geothermometric determinations conducted in the springs along the Mbaka fault, there is apparently an increase of temperature moving south-eastwards, although such inference derives from a quite limited number of determinations. In consideration of the above, the south-eastern and north-western limits of the reservoir are assumed to be somewhat eccentric with reference to the Kilambo manifestations, being set 3 km south-east and 2 km north-west of them, respectively.

  The above estimated areal extent is obviously related to the fault-leakage controlled hypothesis, assuming that the fluids ascending along the Mbaka fault spread laterally to the SW upon encountering a pervious horizon corresponding to the coarse grained sediments. By adopting the above mentioned geometric parameters, the *first priority zone*, represented in Figure 5-28, has an areal extent of 10 km^2.

- ✓ Top of the reservoir: The depth of the top of the fault-leakage controlled reservoir is interpreted based on the results of the MT 3D inversion as shown in profiles PT2, PT3, PT4 and PT5 (see Figure 5-44). Assuming the iso-resistive line of 10 Ohm m as the contact between cap-rock and reservoir, the top of the reservoir is deemed to occur at a depth of 1000-1200 m, with a tendency to dip to the SE, reaching a value of 1800 m in the southernmost profile PT5.

- ✓ Bottom of the reservoir: The bottom of the reservoir is assumed to correspond to the iso-resistive line of 50 Ohm m. The bottom of the reservoir is accordingly observed at an average depth of 1,500 m, corresponding to a thickness of the reservoir of 300-500 m. In profile PT5 the 50 Ohm m iso-resistive line drops to 2500 m, corresponding to a thickness of approximately 700 m.

d. *Natural Fluid Flow Pattern.* As the isotopic composition of the geothermal fluids suggests that the average infiltration elevation amounts to approximately 2,000 m asl (section 5.4.3.3), possible recharge zones might be located either (i) in the highlands NE of the Livingstone fault, at a distance of some 20 km (see hypothesis A, below, representing our preferred scheme of hydrothermal circulation) or (ii) in the northern portion of the Kiwira river watershed, at a distance of some 50 km (hypothesis B, the less probable).

Under hypothesis A, waters infiltrating in the Elton plateau penetrate deeply into the ground up to depths of several kilometres. The existence in the area of an anomalous thermal gradient related to the upwelling of the mantle determines a more pronounced heating of these waters

as compared with the "normal" situation. Assuming a gradient 1.5 times the Earth's average, that is 50 °C/km, temperatures of 140 °C would be reached at a depth of 2500 m. Deep groundwater flow takes place mostly to the southwest within products of the metamorphic-intrusive basement, moving preferentially along two systems of fractures, that is the Nyasa lake related trend (N-S) and the Usangu rift related trend (NE-SW). Upon reaching the Mbaka fault, the heated waters start to rise along it and, on encountering the basal horizon of the undifferentiated sedimentary complex characterized by fair permeability, spread laterally within this horizon, giving rise to a geothermal system (fault-leakage play). The upper portion of the sequence, presumed to consist mainly of fine grained products (e.g. claystone and siltstone) would restrict the upwards movement of the fluids, representing the cap-rock of the system with very low electrical resistivity values. A small portion of the fluids continues its upwards movement along the Mbaka fault, originating the Kilambo and Kajala manifestations.

Hypothesis B envisages a similar circulation scheme with groundwater flow towards the Nyasa lake, from NW to SE, but in this case the role of the Mbaka fault is somewhat different. The fault might represent the connection between the deep groundwater and the surface, but not necessarily constitutes the main pathway for allowing the uprise of the fluids to depths of about 1200 m from larger depths. Groundwater circulation would mostly occur in the bottom portion of the sedimentary sequence and a higher thermal gradient (100 °C/km) would have to be inferred. Under both hypotheses, the outflow of the system is supposed to take place mostly along the main SW-NE faults of the Mbaka system, with preferential movement towards the Nyasa lake.

e. *Thermodynamic and Chemical Conditions.* The thermodynamic and chemical characteristics of the Kiejo-Mbaka prospect have been inferred on the base of the nature and composition of the Kilambo and Kajala hot springs, extending along the Nugwisi river over lengths of 200 m at Kilambo and 500 m at Kajala (see Figure 5-28), whereas the distance between the two thermal sites is ~600 m. These hot springs occur along the Mbaka fault at the intersection with N-S trending faults and have a maximum temperature of 64 °C. Gas emission is abundant, especially at Kilambo.

The gas manifestations of Lufundo and Kiejo, on the other side, are probably unrelated with the fault-controlled or fault-leakage controlled geothermal system discharging at Kilambo and Kajala. The application of the geothermometric functions to these water samples indicates a deep temperature of about 140 °C, in substantial agreement with the temperatures derived from the H_2-Ar and H_2-N_2 gas geothermometers. The type of thermal manifestations, their chemical and isotopic characteristics and estimated temperatures concur in suggesting the water-dominated nature of the geothermal system.

Figure 5-55 depicts the 3D representation of the conceptual model of the Kiejo-Mbaka field. obtained by means of GIS and 3D graphic softwares.

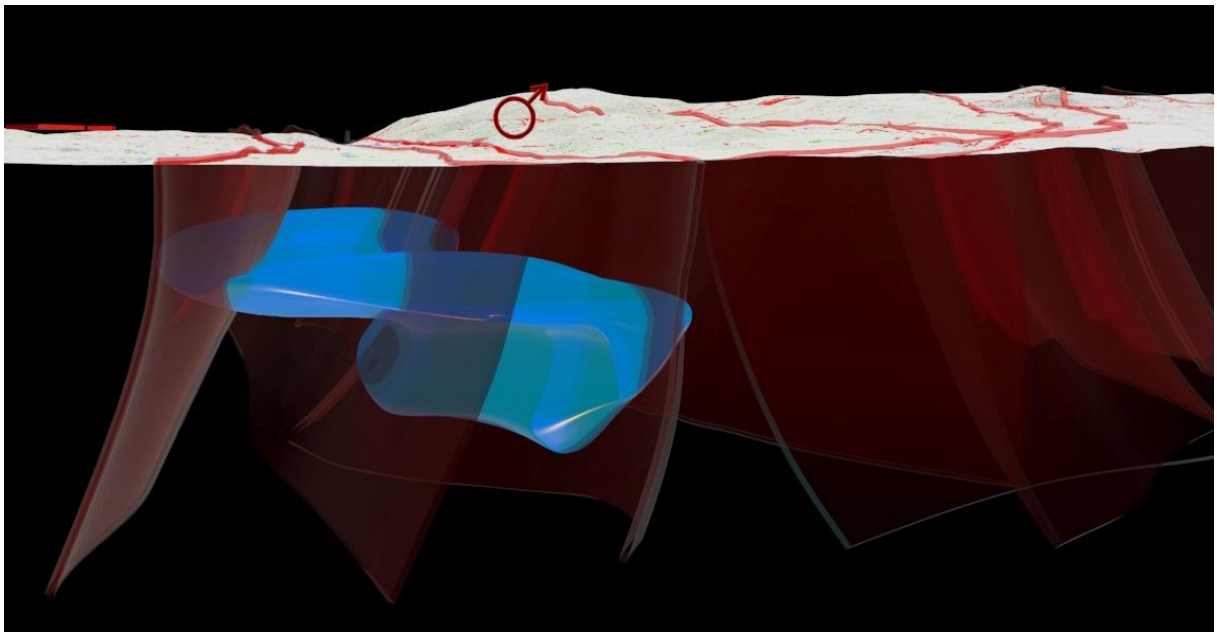

Figure 5-55a **Snapshot of the 3D model: circle with arrow represents Kiejo manifestations; red surface represents faults; light blue solid represents the reservoir**

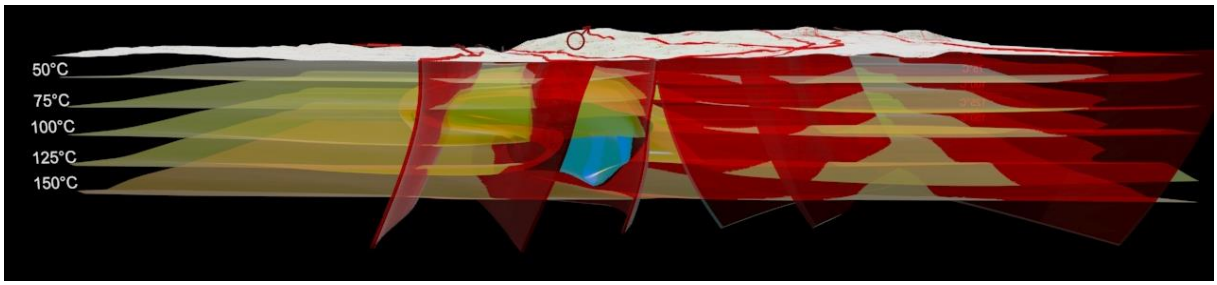

Figure 5-55b **Snapshot of the 3D model: circle with arrow represents Kiejo manifestations; red surface represents faults; light blue solid represents the reservoir; orange to yellow surfaces represent the isotherms**

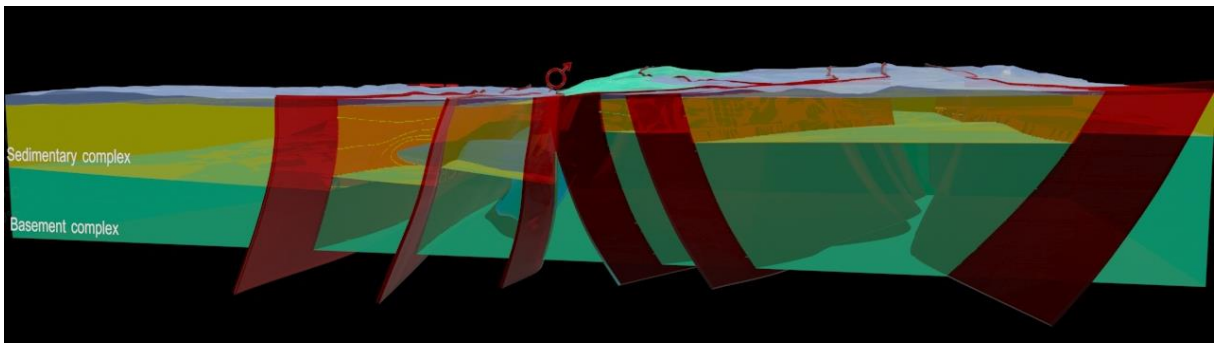

Figure 5-55c **Snapshot of the 3D model: circle with arrow represents Kiejo manifestations; red surface represents faults; light blue solid represents the reservoir; green volume represents the Basement Complex; yellow volume represents the Sedimentary Complex; violet volume represents the Recent Volcanics**

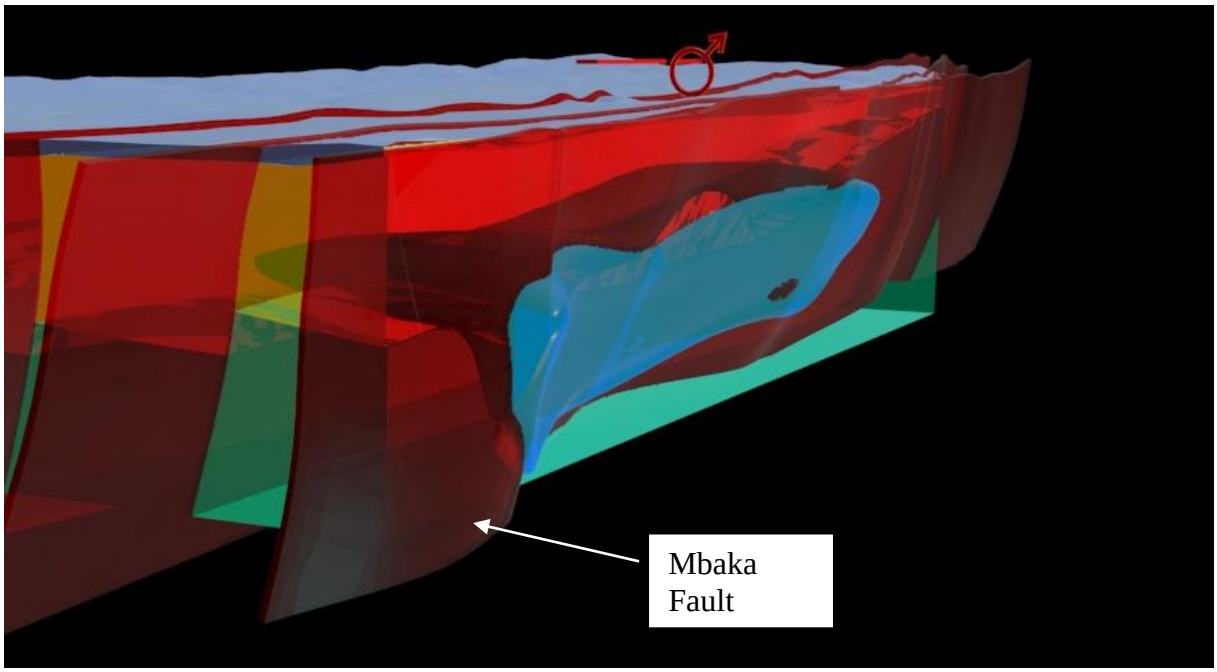

Figure 5-55d **Snapshot of the 3D model: circle with arrow represents Kiejo manifestations; red surface represents faults; light blue solid represents the reservoir; green volume represents the Basement Complex; yellow volume represents the Sedimentary Complex; violet volume represents the Recent Volcanics**

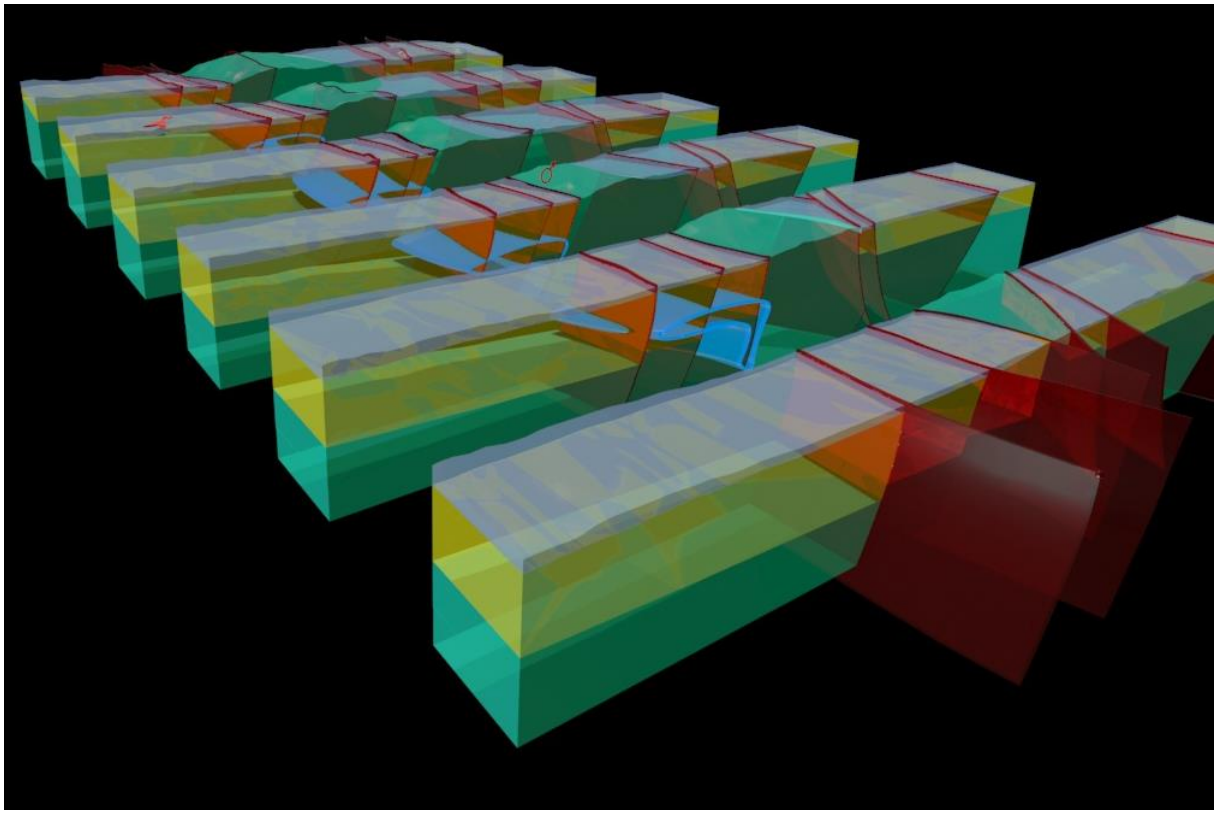

Figure 5-55e **Snapshot of the 3D model: circle with arrow represents Kiejo manifestations; red surface represents faults; light blue solid represents the reservoir; green volume represents the Basement Complex; yellow volume represents the Sedimentary Complex; violet volume represents the Recent Volcanics**

6. CONCLUSIONS

In this work, two major topics were basically addressed, namely an updated overview of the procedures for the exploration of geothermal resources was provided and how they contributed to characterise the different geothermal plays, in particular for the East African Rift System. Among the different prospects of the EARS investigated in this PhD study, three of them were studied in detail, being characterised by well-distinct, peculiar geological and geothermal features. Making specific reference to the geothermal resource, geothermal plays can be broadly separated into two types related to the mechanism by which heat is transported into the reservoir, inasmuch as the heat transport is dominated by *convection* (magmatic, plutonic and extensional domain -fault controlled-) or *conduction* (located predominantly at passive tectonic plate settings, where no significant recent tectonism or volcanism occurs). All the cases studied fall under the convection play type.

Alalobeda

This geothermal prospect is either a fault /fault-leakage controlled or magmatic geothermal system, occurring in a region of three superimposed rift zones: the Red Sea (NW-SE), the Main Ethiopian Rift (NNE-SSW) and, partly, the Gulf of Aden (ENE-WSW). Gravity anomalies highlighted the Tendaho graben configuration and the main fault systems, which in turn well corresponded to magnetic anomalies recorded by the basalts of the Afar Stratoid Series.

Geochemical analyses of water samples identified two water types: i) *Sodium-chloride* (Alalobeda hot springs and the reservoir liquids encountered in the Dubti prospect); ii) *Sodium-bicarbonate type (*natural steam condensate, possibly affected by mixing with local rainwaters). Hot springs indicate reservoir temperatures of 200-220 °C. Such temperatures are substantially consistent with those (185-225 °C) inferred from fumaroles gases. The western highlands of Ethiopia could act as the main groundwater recharge zone of the geothermal field. However, both the present-day precipitations regime and isotopic data argue that the Alalobeda geothermal reservoir hosts paleo-water seeped in early times. Groundwater is expected to flow mostly in the Afar Stratoid Series, reaching a depth of 1,500-2,500 m.

The Alalobeda geothermal field is characterized by a quite continuous seismic activity of low-energy (magnitude <4.0), consistently with the regional pattern. The seismicity cutoff-depth occurs at 3.5-5 km depth. The results of the MT survey showed extremely low resistivity values for the basaltic rocks of the Afar Stratoid Series registered outside of the Tendaho Graben. This is likely due to intense argillification phenomena, which accompany hydrothermal circulation. Along the SW shoulder of the Tendaho Graben, a very thick horizon of low-medium conductivity was detected, which can be at least partly interpreted as the cap-rock formation. South (of the Tendaho Graben?), an increase in resistivity (from 5 to 10 Ω m) of this horizon seems to indicate the end of the cap-rock and consequently could mark the limit of the geothermal system. Below the high-conductivity cap-rock, the more resistive basement (often in excess of 100 Ω m) can act as the reservoir formation, although its resistivity is somewhat higher than that commonly recorded in other geothermal fields.

Menengai

This field, occurring in a several km wide caldera, can be classified as convection-dominated magmatic play type. It was recognized as a promising geothermal prospect among the many existing along the Rift Valley in Kenya. After a series of geophysical investigations (micro-seismic monitoring, gravity and MT surveys), geological surveys, geochemical surveys (fumaroles sampling, soil gas

surveys) and a soil temperature survey, a first exploratory well MW-01 intercepted a deep reservoir with temperatures exceeding 300 °C. The deep reservoir extends beneath a shallower liquid-dominated reservoir at temperature of 190-200 °C. Irrespective of the provenance from the shallow aquifer, all reservoir liquids belong to the Na-HCO_3 facies. However, no presence of a clear cap-rock was identified; therefore, self-sealing processes were invoked in order to explain the existence of two distinct reservoirs.

Following the successful results of MW-01, an exploratory and development campaign started with the drilling of about twenty deep wells aimed at characterizing the deep reservoir properties, delineate the field extension and provide additional steam for power development. On the basis of available data, a conceptual model of the Menengai geothermal system was obtained. The system is characterized by a liquid dominated shallow reservoir at temperature ranging from 130 to 210 °C, which overlays a deeper high temperature, two-phase or vapour-dominated reservoir, with temperatures reaching 330 °C. A conceptual model of the entire system was developed incorporating surface exploration surveys and the findings derived from drilling, logging and testing of geothermal wells.

The conceptual model, integrated with production testing results, was used to build a 3D numerical model of the geothermal system in order to simulate its thermal structure, check the consistency of acquired data, and set up the tool for the subsequent modelling of exploitation scenarios. The modelling of the natural state was intended give a better picture of the reservoir thermodynamic conditions and simulate the mass and heat flows through the system. A steady-state condition modeling was at first carried out and calibrated against data obtained from geochemical investigations, well pressure and temperature profiles recorded under warm-up and flowing conditions, as well as available production test results. The 3D natural state reasonably reproduces the liquid dominated shallow reservoir just on top of the deeper, vapour-dominated high temperature reservoir which is feeding the dry steam wells drilled in the central area of the prospect. The deep reservoir is recharged by the up-flow of a high temperature mixture of steam and CO_2. The latter accumulates at the culminations of the deep reservoir due to the boiling and condensation processes associated to the heat pipe mechanism supported by the strong heat flow. The gas phase saturation declines, moving from the central vapour-dominated area towards the periphery of the deep reservoir, where the aqueous phase becomes strongly mobile. The thermodynamic conditions and rock properties of the lateral extension of the deep reservoir are poorly constrained by present drilled wells and need to be better characterized in the future, as they are fundamental for the reliable assessment of overall prospect potential.

Kiejo-Mbaka

This prospect can be classified as a fault-leakage controlled play (extensional domain play), in which convection takes place along the fault and the fluids can leak from the fault into permeable layers expanding laterally. It falls within the Rungwe Volcanic Province (RVP), which is situated in the East Africa Rift System at the triple junction of the Rukwa, Usangu and Karonga rift basins. Recent volcanism in the area is concentrated in the northern sector of the RVP, whereas in the southern sector, where the prospect is situated, it is expressed by eruptions of very limited volume and derived from deep sources, which can hardly contribute to the thermal anomaly.

Kiejo-Mbaka is underlain by Pre-Cambrian products of the metamorphic-intrusive complex, consisting mostly of biotitic gneisses and schists, amphibolites and metagabbroid bodies. The complex is sub-outcropping in the central portion of the focal area (Mbaka ridge) and is covered by a thick sequence of clastic sediments westwards and eastwards. Volcanic products (basalts and ignimbrites) derived from Pleistocene eruptions cover the area with a thickness never exceeding 200 m.

Several fault systems were recognized, among which the most important ones are NW-SE and N-S. The Mbaka fault, which controls the hot waters emergences and delimits to the west the Mbaka ridge, belongs to the NW-SE system and is associated with a series of vicariate parallel structures extending in the plain. The Kisyelo fault, which delimits to the east the Mbaka ridge, trends N-S to NNW-SSE.

Three groups of hot springs (Ilwalilo, Kilambo, and Kajala) are found along the Mbaka fault, with a maximum discharge temperature of 64 °C. Geothermometric determinations over these waters indicate a temperature of about 140 °C in Kilambo-Kajala and of about 115 °C in Ilwalilo. The reservoir fluid has a Na-HCO_3 chemical composition. The main zone of recharge of the system corresponds to the Elton plateau, which extend to the NE of the Livingstone fault, a major NNW-SSE structure delimiting eastwards the East Africa Rift.

The gravimetric and the electromagnetic surveys concurred to identify the existence of a block characterized by a pronounced positive Bouguer anomaly and high resistivity. Such a block corresponds to the Mbaka ridge, where the basement is either outcropping or sub-outcropping. In the plain which extends west of the Mbaka fault a conductive unit with an average thickness of 1,000 m, a resistivity as low as 0.5 Ohm m and a tendency to get thicker moving westward and southward was recognized. In the sector that extends east of the Kisyelo fault, two discontinuous conductive units were identified at shallow and intermediate depth. In both cases, these anomalies were referred to the sequence of clastic sediments and attributed to either primary (fine grained composition) or secondary (moderate temperature hydrothermal alteration) causes.

The reconstruction of the geometry of the reservoir was based on the hypothesis of a fault-leakage controlled play, assuming that the Mbaka fault represents a hydrogeological boundary to the eastern expansion of the heated fluids and taking into consideration the configuration of the conductive unit, interpreted as reflecting the cap-rock of the system. The SW limit of the reservoir is likely to correspond to a long-liner fault which runs about 2 km west of the Mbaka fault and the NW and SE limits have been conventionally set 2 km NW and 3 km SE of the Kilambo manifestations, respectively.

The comparison of the geothermal plays of EARS with other I had the opportunity to investigate in the frame of other international geothermal projects in South-East Asia and Central America, lead to some final remarks:

A. *the same geothermal play-types can be found in both compressive (subduction zone) and extensional (rifting) stress conditions, although their characteristics could be partially different.* The plutonic play-type is one typical example. In fore- or back-arc regions of fold-thrust belts along subduction zones (like e.g. the Mataloko geothermal field, Indonesia), a well-developed thick and continuous cap rock mainly formed by clay minerals (illite, smectite, clorite) is present. On the contrary, in a rifting region (EARS), the "classic" cap rock can be missing, like in the plutonic play of Menengai. From both geophysical results and direct information deriving from the drilled wells, the presence of any particular clay-rich layer was not revealed. The definition of cap rocks geometry (top/bottom) was inferred analysing the thermodynamic conditions (pressure and temperature distribution) recorded during the well testing activities.

B. *in a given geodynamic context a "zonation" of the play-types can be recognized*; this is well evident in the EARS. The Western Branch is dominated by the presence of fault/fault leakage controlled type. The presence of persistent volcanic activities is limited to two cases, namely: Virunga (DRC and Uganda) and Rungwe (Tanzania) Volcanic Provinces. On the other hand, in the Eastern Branch the volcanic activities are well represented by the presence of tens of volcanic

edifices (considering Eritrea, Djibouti, Ethiopia and Kenya). In these countries, magmatic and plutonic play-types are common, although also some cases of fault controlled geothermal systems are present, but to date they have not been studied in detail, due to their low temperature which renders these geothermal prospects of relatively low commercial interest.

C. *a different approach should be followed in order to characterize properly the geothermal fields present in the EARS;* we have to note that the common approach to investigate and study a geothermal prospect is to conduct geoscientific investigations, namely: geological, geochemical and geophysical (MT/TEM, gravity and seismic) surveys. In a subduction context the experts tend to believe primarily in the geophysical model derived from the resistivity survey, even because the values of ρ (ohm m), reported in literature, were calibrated in such environment. As mentioned in the Alalobeda (as well as in the Aluto-Langano) case study, unexpectedly low resistivity values were encountered in the basaltic rocks of the Afar Stratoid Series. Then, if the interpreted values of resistivity are simply associated with the standard values of cap rock and reservoir formations, the inferred geophysical conceptual model may be grossly incorrect. Therefore, it is essential to perform an accurate integrated interpretation of all the geoscientific results.

D. *a detailed structural survey is of primary importance especially in the fault-controlled plays, whereas its importance is often under-estimated*; it is important to stress that in the EARS, and especially in the case of fault-controlled play-types, more attention should be focused on the distribution and type of lineaments and faults systems. A high-resolution structural survey allows to define a detailed configuration of fractures and faults that may control the fluid upflow from the reservoir. This information collected at surface may then be linked to the information at depth derived from the geophysical models, strongly reducing the ambiguities of the geophysical interpretation.

E. *a more comprehensive approach to water classification is needed to distinguish mature waters from immature waters*. Some typical approaches and models developed in the subduction geothermal systems should be re-addressed. The geochemical framework of geothermal systems situated along Subduction Zones has been established long ago through extensive exploration, at the surface and at depth. Mature chloride waters hosted in geothermal reservoir migrate laterally and discharge at the surface at considerable distance from the geothermal field. Fumarole activity and steam-heated acid-sulfate waters mark the upflow zones. Peripheral bicarbonate waters occur at relatively shallow depths at some distance from the geothermal field. Acid chloride-sulfate volcanic waters are found in crater lakes. Consequently, the terms mature chloride waters, steam-heated acid-sulfate waters, peripheral bicarbonate waters, acid chloride-sulfate volcanic waters have been suggested by Giggenbach (1997). Only the Giggenbach's triangular diagram of major anions is often used for water classification in geochemical investigations performed in convergent-plate settings (although it is preferable a more comprehensive approach). On the contrary, the high-temperature geothermal reservoirs of the Eastern branch of the EARS (e.g., Olkaria and Menengai in Kenya, and Aluto-Langano in Ethiopia) host not only mature chloride waters but also mature bicarbonate-chloride and mature bicarbonate waters. Why?

In volcanic-magmatic regions, deep geothermal liquids are assumed to be produced through neutralization of initially acidic meteoric-magmatic aqueous solutions (e.g. Giggenbach, 1997). The few available data for volcanic gases indicate that subduction zones volcanic gases are enriched in Cl relative to hot-spot and divergent-plate volcanic gases (e.g. Symonds et al., 1994; Sawyer et al., 2008). Therefore, the comparatively small supply of Cl-bearing magmatic gas species (chiefly HCl) in the root of the Eastern EARS geothermal systems might be responsible of the

comparatively low Cl contents of related geothermal liquids (Marini and Pasqua, 2014). Irrespective of the reasons controlling the presence not only of mature chloride waters but also of mature bicarbonate-chloride and mature bicarbonate waters in the eastern EARS, it is evident that the terminology of subduction-zone geothermal systems cannot be used in other frameworks. The situation might be even more complicated in the western EARS. Therefore, a more comprehensive approach to water classification is needed to distinguish mature waters from immature waters.

In view of the foregoing final remarks (points A-E), the main aspects to be considered in the course of exploration and development of geothermal resources within the EARS, in comparison with the systems hosted in subduction zone environments, can be summarized, as follows:

- ✓ Hundreds of thermal manifestations occur within the EARS, which extends over a length of some 5000 km.
- ✓ In spite of such widespread and intense evidence of thermal anomaly, the present exploitation of geothermal resources for power generation is quite limited, if compared, for example, with the production registered along the Belt of Fire of Indonesia.
- ✓ Such somewhat disappointing situation can be related to two different causes: (1) Thermal manifestations are often not due to the presence of a hot magmatic source, but rather to the thinning of the earth crust, which determines a thermal anomaly of moderate intensity; (2) Numerous and extensive geoscientific investigations have been conducted, but only very few prospects have been directly tested so far through deep drilling.
- ✓ The planned program of drilling in several prospects of Ethiopia and Tanzania, to be carried out in the next few years, might on one side enhance the "geothermal performance" and on the other side provide basic information which can improve the overall understanding of the EARS characteristics.
- ✓ It is in particular very important to define the reasons why, in many instances, favorable thermal conditions are not accompanied by an adequate hydrogeological setting: it is in fact surprising that lithological units with brittle behavior (e.g. basalts) result to be almost impervious in an extensional environment characterized by neo-tectonic activity.
- ✓ Under this situation, it is essential, as mentioned above, to pay specific attention to the structural setting, in order to design the wells in such a way as to increase the chances of intersecting tectonic features. In fact, it is worth reminding that, while in most Indonesian fields permeability tends to be widespread throughout extensive structural blocks, in the EARS environment permeability itself appears in many cases to be limited to major faults.
- ✓ As refers to extensional plays, which represent the most common type especially in the western branch of the EARS, the corresponding systems tend to be partly overlooked due to their relatively low temperature (in principle in the order of 130-180 °C).
- ✓ Actually, as shown by the results of geothermal development in the Great Basin of Western USA and in Turkey, the exploitation of medium enthalpy resources tends to be more and more viable from the technical and economic viewpoints, thanks to the progress in the realm of combined cycle processing, and it now constitutes close to 10 % of the global geothermoelectric generation in the world.
- ✓ Similarly, direct use of geothermal resources is presently poorly applicable in the African socio-economic context, but it might become soon of paramount importance within the framework of enhanced exploitation of renewable energy sources.

- ✓ In conclusion, although the estimates of geothermoelectric potential reported in the country updates of paragraph 5.2 appear surely over-optimistic, it can be confidently stated that the geothermal resources hosted in the EARS are due to represent in the future, in one form or another, an invaluable asset for energy generation.

REFERENCES

Agarwal R., Al-Hussainy R., Ramey H.J. (1970). *An investigation of wellbore storage and skin effect in unsteady liquid flow*. I. Analytical treatment. Soc. Pet. Eng. J., 5, 279-290

AGEA AGEG 2010a "*The geothermal reporting code Second edition*"

AGEA AGEG 2010b "*Geothermal lexicon for resources and reserves definition and reporting*"

Aquater (1998). *Drilling of two geothermal wells in Tendaho - Wells TD-5 and TD-6 drilling report*. Report J3466, 32 pp.

Aquater (1996). *Tendaho Geothermal Project. Final Report*. Volume I

Aquater (1996). *Tendaho Geothermal Project. Final Repor*t. Volume II

Aquater (1995). *Well TD-4 - Drilling Report. Tendaho Geothermal Project*. Report H9385.

Aquater (1995). *Well TD-4 - Geological and Geoengineering Activities during Drilling and Well Testing*. Tendaho Geothermal Project. Report H9087.

Aquater (1995). *Well TD-3 - Drilling Report. Tendaho Geothermal Project*. Report H8900.

Aquater (1995). *Microseismic Survey - Final Report*. Tendaho Geothermal Project. Report H9565.

Aquater (1995). *Regional Isotopic Survey - Final Report*. Tendaho Geothermal Project. Report H9564.

Aquater (1995). *Surface Geochemical Monitoring - Final Report*. Tendaho Geothermal Project.

Aquater, (1994). *Well TD-3 - Geological and Geoengineering Activities during Drilling and Well Testing*. Tendaho Geothermal Project. Report H8418

Aquater (1994). *Well TD-2 - Drilling Report*. Tendaho Geothermal Project. Report H8463

Aquater (1994). *Well TD-2 - Geological and Geoengineering Activities during Drilling and Well Testing*. Tendaho Geothermal Project. Report H8016

Aquater (1994). *Well TD-1 - Drilling Report*. Tendaho Geothermal Project. Report H9548

Aquater (1990). *Well TD-1 - Geological and Geoengineering Activities during Drilling and Well Testing*. Tendaho Geothermal Project. Report H4207

Aquater (1991). *Geochemical Study of the Dubti and Alalobeda Geothermal Areas in the Tendaho Graben (Ethiopia)*. Tendaho Geothermal Project.

Aquater (1980). *Prefeasibility Study - Phase II - Final report*. Geothermal Resources Exploration Project - Tendaho Area. Report IDROGE A0635.

Aquater (1979). *Prefeasibility Study - Phase I*. Geothermal Resources Exploration Project - Tendaho Area. Report IDROGE A04221.

Arab N. (1972). *Seismic reflection and gravity investigations of the 'Widmerpool Gulf' in the East Midlands, with a study of linear seismic sources and data processing techniques involving computer graphics*. Ph.D. thesis, Univ. of Leicester, UK

Armstrong A.J. (2016). *Best Practices for Establishing Geothermal Legal Framework - Defining Geothermal Resources, International Precedent.* Proceedings, 6th African Rift Geothermal Conference: November 2-4, 2016 (Addis Ababa, Ethiopia), 6 pp

Atekwana E.A., Hogan J.P., Kampunzu A.B., and Modisi M.P. (2004). *Early structural evolution of the nascent Okavango rift zone, NW Botswana*. Proceedings of the East African Rift system: Geodynamics, Resources, and Environment Conference, Addis Ababa, 12-16.

Ballentine C.J., Burnard P.G. (2002). *Production, release and transport of noble gases in the continental crust*. Reviews in Mineralogy and Geochemistry, 47, 481-538

Balmino G., Vales N., Bonvalot S., and Briais A. (2011). *Spherical harmonic modeling to ultra-high degree of Bouguer and isostatic anomalies*. Journal of Geodesy. DOI 10.1007/s00190-011-0533-4

Baker B.H., and Wohlenberg J. (1971). *Structure and evolution of the Kenya Rift Valley*. Nature, 229, 538-542

Battaglini R., Raco B., Scozzari A. (2013). *Effective monitoring of landfills: flux measurements and thermography enhance efficiency and reduce environmental impact.* Journal of Geophysics and Engineering. 10(6): p. 064002

Battistelli A. et al. (2002). *Reservoir engineering assessment of Dubti geothermal field, northern Tendaho Rift, Ethiopia*. Geothermics, 31, 381-406

Battistelli A., Marcolini M., Pasqua C. (2012). *Recent Developments within the TOUGH2 Family of Reservoir Simulators with Application to the Modelling of Geothermal Reservoirs*. The 12th Annual Indonesian Geothermal Association Meeting & Conference (INAGA 2012) - Bandung, Indonesia, 6-8 November, 2012

Bennett, J.D. (2008). *Provisional Geological map of Malawi*, (1: 1,000,000 scale), Compiled by Geological Survey, Government of Malawi

Bertrami R., Cioni R., Corazza E., D'Amore F., Marini L. (1985). *Carbon monoxide in geothermal gases. Reservoir temperature calculations at Larderello (Italy)*. Geotherm. Res. Counc. Trans. 9, 299-303

Birt C.S., Maguire P.K.H., Khan M.A., Thybo H., Keller G.R., and Patel J. (1997). *The influence of pre-existing structures on the evolution of the southern Kenya Rift Valley - Evidence from seismic and gravity studies*. In: K. Fuchs, R. Altherr, B. Maller, and C. Prodehl, eds., Structure and dynamic processes in the lithosphere of the Afro-Arabian rift system. Tectonophysics, 278, 211-42

Birt C.S. (1996). *Geophysical investigation of active continental rifting in southern Kenya*. Ph.D. thesis, Univ. of Leicester, UK

Bourdarot, G. (1998). *Well Testing: Interpretation Methods*. Institut Français du Petrole, Paris, Editions Technip

Bourdet D., Whittle T., Douglas A., Pirard Y. (1983). *A new set of type curves simplifies well test analysis*. World Oil, 95-106

Bourdet D. (2002). *Well test analysis: the use of advanced interpretation models*. Handbook of Petroleum Exploration and Production. Elsevier, Amsterdam

Brabham P.J., and McDonald R.J. (1992). *Imaging a buried river channel in an intertidal area of South Wales using high-resolution seismic techniques*. Q. J. Engl. Geol., 25, 227-38

Broekstra J., Kampman A., van Harmelen F. (2002) *Sesame: A Generic Architecture for Storing and Querying RDF and RDF Schema*. In: Horrocks I., Hendler J. (eds) The Semantic Web - ISWC 2002. ISWC 2002. Lecture Notes in Computer Science, vol. 2342. Springer, Berlin, Heidelberg

Brown C., Girdler R.W. (1980). *Interpretation of African gravity and its implication for the breakup of the continents*. Journal of Geophysical Research: Solid Earth. Vol. 85, IssueB11, 10 November 1980, Pages 6443-6455

Calvin W.M., Coolbaugh M., Kratt C., and Vaughan R. (2005). *Application of remote sensing technology to geothermal exploration, in Rhoden, H.N., Steininger, R.C., and Vikre, P.G*. eds., Geological Society of Nevada Symposium: Window to the World, Reno, Nevada, May 2005, pp. 1083-1089

Chiodini G., Marini L. (1998). *Hydrothermal gas equilibria: The H_2O-H_2-CO_2-CO-CH_4 system*. Geochim. Cosmochim. Acta 62, 2673-2687

Chiodini G., Cioni R., Guidi M., Raco B., Marini L. (1998). *Soil CO_2 flux measurements in volcanic and geothermal areas*. Appl. Geochem., 13, 543-552

Chiodini G., Caliro S., Cardellini C., Avino R., Granieri D., Schmidt A. (2008). *Carbon isotopic composition of soil CO_2 efflux, a powerful method to discriminate different sources feeding soil CO_2 degassing in volcanic-hydrothermal areas*. Earth Planet. Sci. Lett., 274, 372-379

Chiozzi P., Verdoya M. (2018). *Heat-flow anomaly and residual topography in the Mascarene hotspot swell (Indian Ocean).* Int J Earth Sci (Geol Rundsch), DOI 10.1007/s00531-017-1459-8

Chorowicz J. (2005). *The East African rift system*. Journal of African Earth Sciences Volume 43, Issues 1-3, October 2005, Pages 379-410

Clarke M.C.G., Woodhall D.G., Allen D., Darling G. (1990). *Geological, volcanological and hydrogeological controls on the occurrence of geothermal activity in the area surrounding Lake Naivasha, Kenya*. British Geological Survey Report for the Ministry of Energy, Republic of Kenya.

Clark I. (1979). *Practical geostatistics*. Elsevier Science & Technology, 129 pp.

Craig H., Lupton J.E. (1977). *Isotopic geochemistry and hydrology of geothermal waters in the Ethiopian Rift Valley*. Scripps Inst. Oceanogr. Ref. Ser. 77-14, (Techn. Rep. UNDP and the Ethiopian Government), 140 pp.

Craig H. (1961). *Isotopic variations in meteoric waters*. Science, 133, 1702-1703

Darrah T.H., Tedesco D., Tassi F., Vaselli O., Cuoco E., Poreda R.J. (2013) Gas chemistry of the Dallol region of the Danakil Depression in the Afar region of the northern-most East African Rift. *Chemical Geology*, 339, 16-29

Deibert L., Hjartarson A., McDonald I., McIlveen J., Thompson A., Toohey B., Yang D. (2010). *The Canadian Geothermal Code for Public Reporting*. 2010 Edition. Calgary, Alberta: Canadian Geothermal Energy Association (CanGEA)

Delalande M., Bergonzini L., Gherardi F., Guidi M., Andre L., Abdallah I., Williamson D. (2011). *Fluid geochemistry of natural manifestations from the southern Poroto-Rungwe hydrothermal system (Tanzania): preliminary conceptual model*. Journal of Volcanology and Geothermal Research, 199, 127-141.

Delalande M. (2009). *Hydrologie et géochimie isotopique du lac Masoko et de lacs volcaniques de la province active du Rungwe (Sud-Ouest Tanzanie)*. PhD Thesis, University of Paris XI (Orsay), 284 pp.

Delvaux D, Kraml M, Sierralta M, Wittenberg A., Mayalla J.W., Kabaka K, Makene C (2010). *Surface Exploration of a Viable Geothermal Resource in Mbeya Area, Sw Tanzania. Part I: Geology of the Ngozi - Songwe Geothermal System*. Proceedings World Geothermal Congress 2010 Bali, Indonesia, 25-29 April 2010.

Delvaux D and Hanon M (1993). *Neotectonics of the Mbeya area, SW Tanzania*. Mus. roy. Afr. centr., Tervuren (Belg.), Dépt. Géol. Min., Rapp. ann. 1991-1992, (1993), 87-97.

Delvaux D, Levi K, Kajara R, and Sarota J (1992). *Cenozoic paleostress and kinematic evolution of the Rukwa -North Malawi rift valley (East African rift system).* Bulletin des Centres de Recherches Exploration-Production elf aquitaine 16, (1992), 383-406.

Dunkley P.N., Smith M., Allen D.J. and Darling W.G. (1993). *The geothermal activity and geology of the northern sector of the Kenya Rift Valley*. British Geological Survey Research Report SC/93/1

Dulanya Z. (2006). Geothermal Resources of Malawi - An overview. Proceedings, Thirty-First Workshop on Geothermal Reservoir Engineering. Stanford University, Stanford, California, January 30-February 1, 2006 SGP-TR-179

Earlougher R.C. (1977). *Advances in Well Test Analysis*. (Monograph 5), Society of Petroleum Engineer, Dallas, Texas, 264 pp

Ebinger C.J., Sleep N.H. (1998). *Cenozoic magmatism throughout east Africa resulting from the impact of a single plume*. Nature 395:788-791

Ebinger C.J., Deino A.L., Drake, R.E., Tesha A.L., Becker T., Ring U. (1993). *Tectonic Controls on Rift Basin Morphology: Evolution of the Northern Malawi (Nyasa) Rift*. Journal of Geophysical Research, vol. 98, no. B10, pages 17,821-17,836.

Ebinger, C.J., Deino A.L., Drake R.E., Tesha A.L. (1989). *Chronology of volcanism and rift basin propagation: Rungwe Volcanic Province, East Africa*. J. Geophys. Res. Solid Earth Planet, 94 (B11), 15785-15803.

Ebinger C.J., Bechtel T.D., Forsyth D.W., Bowin C.O. (1989). *Effective elastic plate thicknesses beneath the East African and Afar domes*. J. Geophys. Res. 94, 2883-2900

Economic Commission for Europe - ECE (2009). *United Nations Framework Classification for Fossil Energy and Mineral Reserves and Resources 2009*. United Nations Publication, ECE Energy Series No.39, ISBN ISSN 1014-7225

Egbert G.D. (1997). *Robust multiple station magnetotelluric data processing*. Geophys. J. Int., 130, 475-496, 1997

ELC-MoNREM (2018). *Prefeasibility Study Report Chiweta*. Prepared for MoNREM of Malawi. Assessment of Geothermal Resource in Malawi: A Reconnaissance and Prefeasibility Study. July 2018. Unpublished.

ELC-MoNREM (2018). *Prefeasibility Study Report Kasitu*. Prepared for MoNREM of Malawi. Assessment of Geothermal Resource in Malawi: A Reconnaissance and Prefeasibility Study. May 2018. Unpublished.

ELC-TGDC (2018). *Luhoi Final Report*. Prepared for TGDC under Surface Exploration and Training in Luhoi and Kiejo-Mbaka Geothermal Areas, project. February 2018. Unpublished.

ELC-TGDC (2017). *Kiejo-Mbaka Final Report*. Prepared for TGDC under Surface Exploration and Training in Luhoi and Kiejo-Mbaka Geothermal Areas, project. October 2017. Unpublished.

ELC-GSE (2016). *Conceptual Model Report*. Prepared for GSE under Consultancy Services for Geothermal Surface Exploration in Aluto Langano, Ethiopia. December 2016. Unpublished.

ELC-GSE (2016). *Conceptual Model Report*. Prepared for GSE under Consultancy Services for Geothermal Surface Exploration in Tendaho Alalobeda, Ethiopia. February 2016. Unpublished.

ELC-GDC (2015). *Updated Reservoir Capacity Report*. Under Consultancy Services for the Update of the Feasibility Study for 105 MW Menengai Geothermal Project. June 2015. Unpublished

ELC-GDC (2013). *Reservoir Capacity Report*. Under Provision of Consultancy Services for the Feasibility Study of Menengai Geothermal Power Project. November 2013. Unpublished.

Eppelbaum L.V. and Kutasov, I.M. (2008). *Designing an interference well test in a geothermal reservoir*. Proceedings, 33rd Workshop on Geothermal Reservoir Engineering, Stanford University, Stanford, SGP-TR-185

Faure G. (1986) *Principles of isotope geology*. Wiley, New York, 589 pp.

Foster A., Ebinger C., Mbede E. and Rex D. (1997). Tectonic development of the northern Tanzanian sector of the East African Rift System. Journal of the Geological Society, 154, 689-700, 1 July 1997

Foulger G.R. (1995). *The Hengill geothermal area, Iceland: Variation of temperature gradients deduced from the maximum depth of seismogenesis*. Journal of Volcanology and Geothermal Research 65 (1995) 119-133

Fournier R.O. (1979) *A revised equation for the Na/K geothermometer*. Geotherm. Res. Counc. Trans., 5, 1-16

Fournier R.O. and Truesdell A.H. (1973) An empirical Na-K-Ca geothermometer for natural waters. *Geochim. Cosmochim. Acta* **37**, 1255-1275

Franzson H. (1998). *Reservoir geology of the Nesjavellir hightemperature field in SW-Iceland*. Proceedings 19th Annual PNOC-EDC Geothermal Conference, Manila, p.13-2

Fritz H., Tenczer V., Hauzenberger C.A., Wallbrecher E., Hoinkes G., Muhongo S., Mogessie A. (2005). *Central Tanzanian tectonic map: A step forward to decipher Proterozoic structural events in the East African Orogen*. Tectonics 24(6), doi: 10.1029/2005TC001796. ISSN: 0278-7407

GDC (2013). *Menengai monthly drilling report for the month of December, 2013*

GDC (2013). *Borehole geological report. Well MW-16*

GDC (2013). *Preliminary borehole geological report. Well MW-17*

GDC (2013). *Borehole geological report. Well MW-18*

GDC (2013). *Borehole geology of Menengai well MW-19*

GDC (2013a). *Preliminary borehole geological report - Well MW-5A*

GDC (2013b). *Preliminary borehole geology of well MW-09*

GDC (2013c). *Preliminary borehole geology of well MW-10*

GDC (2013d). *Borehole geological report - Well MW-11*

GDC (2013e). *Borehole geology of well MW-12*

GDC (2013f). *Borehole geology of well MW-13*

GDC (2013g). *Stratigraphy MW-14*

GDC (2013h). *Borehole geological report - Well MW-15*

GDC (2012). *Well completion reports for Menengai well 1 to 8. Menengai Geothermal Project. GDC Report 2012*

GDC (2012a). *Well MW-01 Discharge Chemistry Report*

GDC (2012b). *Discharge Chemistry of Menengai Well 04*

GDC (2012c). *Discharge Chemistry of MW-06*

GDC (2012d). *Geohazard Monitoring Report - Creation of a geohazard monitoring baseline for the Menengai geothermal field. A Geochemistry Section Project*

GDC (2012a). *Menengai Geothermal Field. Geology of well MW-01*

GDC (2012b). *Menengai Geothermal Project. Geology report of well MW-02*

GDC (2012c). *Menengai Geothermal Project. Menengai well MW-03 geology report*

GDC (2012d). *Borehole geology of Menengai well MW-05*

GDC (2012e). *Menengai Geothermal Project. Borehole geology of Menengai well MW-06*

GDC (2012f). *Geology of well MW-07*

GDC (2012g). *MW-08: Geological well report*

GDC (2011). *Menengai Geothermal Project. Preliminary report of well MW-04*

Gebregziabher Z. (1998). *Geology and Hydrothermal Alteration in Wells TD-5 and TD-6, Tendaho Geothermal Field, Ethiopia*. UNU-GTP 1998, 4.

Gehringer, M., and Loksha, V. (2012). Geothermal handbook: *Planning and financing power generatio*n. The International Bank for Reconstruction and Development / The World Bank Group, Washington DC, United States, Energy Sector Management Assistance Program technical report 002/12, 164 pp. Web: http://www.esmap.org/Geothermal_Handbook

Geothermal Energy Association New Geothermal Terms and Definitions (2011). *A Guide to Reporting Resource Development Progress and Results to the Geothermal Energy Association*. 17 pp., http://geo-energy.org/pdf/NewGeothermalTermsandDefinitions_January2011.pdf

Geotermica Italiana s.r.l. (1987A). *Geothermal reconnaissance survey in the Menengai - Bogoria area of the Kenya Rift Valley.* TCD/CON 7/85-KEN 82/002, II - Geovolcanology.

Geotermica Italiana s.r.l. (1987B). *Geothermal reconnaissance survey in the Menengai - Bogoria area of the Kenya Rift Valley.* UN(DTCD)/GOK, I - Synthesis of results.

Gesto-Energia S.A. (2014). *Renewable Energy. Atlas of Mozambique: Resources and Projects for Power Generation*. ISBN 978-989-97416-3-8

Giggenbach W.F. (1997). *The origin and evolution of fluids in magmatic-hydrothermal systems*. In: Geochemistry of hydrothermal ore deposits, 3d Edition (H. L. Barnes, Ed.), Wiley, 737-796.

Giggenbach W.F., Sheppard D.S., Robinson B.W., Stewart M.K., Lyon G.L. (1994) Geochemical structure and position of the Waiotapu geothermal field, New Zealand. Geothermics 23, 599-644

Giggenbach W.F. (1991a). *Chemical techniques in geothermal exploration*. In Application of Geochemistry in Geothermal Reservoir Development. (F. D'Amore, co-ordinator), UNITAR, 119-144

Giggenbach W.F. (1991b). *Isotopic composition of geothermal water and steam discharges*. In Application of Geochemistry in Geothermal Reservoir Development. (F. D'Amore, co-ordinator), UNITAR, 253-273

Giggenbach W.F. (1988) Geothermal solute equilibria. Derivation of Na-K-Mg-Ca geoindicators. *Geochim. Cosmochim. Acta* **52**, 2749-2765

Giggenbach W.F. (1984). *Mass transfer in hydrothermal alterations systems*. Geochim. Cosmochim. Acta, 48, 2693-2711

Grant, M.A., & Bixley, P.F. (2011). *Geothermal reservoir engineering, II Edition*. Academic Press, New York

Gresta S., Patanè D., Ayana D., Zan L., Carletti A., Oluma B. (1997). *Seismological evidence of active faulting in the Tendaho Rift (Afar Triangle, Ethiopia)*. Pure and Applied Geophysics 149, 357-374.

GSE and BGR (2012). *Geoscientific Exploration for Development of the Tendaho Geothermal System*. Geothermal Resource Evaluation Core Process. BGR-GSE Geotherm Program I.

Gudmundsson A. (2005). *Geothermal Data Collection and Consultancy at Drill Site*. Proccedings World Geothermal Congress 2005, Antalya Turkey, 24-29 April 2005

Guidi M., Marini L., Scandiffio G., Cioni R. (1990). *Chemical geothermometry in hydrothermal aqueous solutions: the influence of ion complexing*. Geothermics, 19, 415-441

Horne, R.N. (1995). *Modern well test analysis, a computer aided approach*. 2nd edition, Petroway Inc., USA, pp. 257

IAEA/WMO (2013) Global Network of Isotopes in Precipitation. The GNIP Database. Accessible at: http://www-naweb.iaea.org/napc/ih/IHS_resources_isohis.html

Iranga M.D. (1992). *Seismicity of Tanzania: distribution in time space, magnitude and strain release*. Tectonophysics, 209 (1992), 313-320 pp. Elsevier Science Publisher B.V., Amsterdam.

James C.R. (1962). *Steam-water critical flow through pipes*. Proc. Institute of Mech. Eng., 176 (26), 741.

James C.R. (1970). *Factors controlling borehole performance*. U.N. symposium on the Dev, and Util. of Geoth. Resources, Pisa. Vol.2, Part. 2, 1502-1515.

Jones A.G., Jodicke H. (1984). *Magnetotelluric transfer function estimation improvement by a coherence-based rejection technique*. Paper presented at 54th Annual International Meeting, Soc. of Expl. Geophys., Atlanta, Ga., Dec. 2-6, 1984.

Kalberkamp U., Kebede S., Teklemariam M., Ali S., Amede Berhan Y., Gezaw T., Teclu A., Lemma Y., Dissasa M.N. (2012) Geoscientific Exploration for Development of the Tendaho Geothermal System. BGR-GSE report, 121 pp.

Kelly W.E. and Mareŝ S. (1993). Applied Geophysics in Hydrogeological and Engineering Practice. Elsevier Science. 289 pp.

Khan M.A., Mechie J., Birt C., Byrne G, Gaciri S., Jacob B., Keller G.R., Maguire P.K.H., Novak O., Nyambok I.O., Patel J.P., Prodehl C., Riaroh D., Simiyu S., and Thybo H. (1998). *The lithospheric structure of the Kenya Rift as revealed by wide-angle seismic measurements*. Geological Society of London Special Publication, 164, 257-69

Klein F.W. (2014). *User's guide to HYPOINVERSE-2000, a FORTRAN program to solve for earthquake locations and magnitudes*. USGS Open File Report 02-171

Kraml M., Schaumann G., Kalberkamp U., Stadtler C., Delvaux D., Ndonde P.B., Mnjokava T.T., Chiragwile S.A., Mayalla J.W., Kabaka K., Mwano J.M., Makene C. (2008). *Geothermal Energy as an Alternative Source of Energy for Tanzania, Final Technical Report of Phase I (2006-2009), Technical Cooperation with United Republic of Tanzania, GEOTHERM-Project 2002.2061.6,* Unpublished Report, 235 pp.

Kristmannsdóttir H. (1979). *Alteration of basaltic rocks by hydrothermal activity at 100-300°C*. In: Mortland, M.M., and Farmer, V.C. (editors), International Clay Conference 1978. Elsevier Scientific Publishing Co., Amsterdam, 359-367

Kipyego E.K. (2013). Assessment of Menengai Geothermal System for Future Production: A Preliminary Numerical Model. The university of Auckland. Master of energy. Project report

Kipyego E.K. (2012). MW-04 discharge test report. Menengai Geothermal Project. GDC Report April 2012

Lachenbruch A.H. (1970). *Crustal temperature and heat production: Implications of the linear heat-flow relation.* J. Geophys. Res., 75, 3291-300

Lagat J. (2011). *Geothermal surface exploration approach: case study of Menengai geothermal field, Kenya.* Proceedings, Kenya Geothermal Conference 2011

Lagat J. et al. (2010). *Menengai Geothermal Prospect: A geothermal resource assessment project report. Second edition.* GDC (Geothermal Development Company)

Laó-Dávila D.A., Al-Salmi H.S., Abdelsalam M.G., and Atekwana E.A. (2015). *Hierarchical segmentation of the Malawi Rift: The influence of inherited lithospheric heterogeneity and kinematics in the evolution of continental rifts*. Tectonics, 34, doi:10.1002/2015TC003953

Leat P.T. (1984). *Geological evolution of the trachytic caldera volcano Menengai, Kenya Rift Valley.* Journal of Geol. Society, 141, no. 6, 1057-1069

Leat P.T., Macdonald R. (1984). *Geochemical evolution of the Menengai caldera volcano, Kenya.* J. Geophys. Res., B89, 8571-8592

Lentsch D., and Schubert A. (2013). *Risk assessment for geothermal wells - a probabilistic approach to time and cost estimation*. GRC Transactions, 37, 971-977

Lentsch D., Savatis A., Schubert A., and Schoebel W. (2012). *Overcoming drilling challenges with rotary steerable technology in deep geotehrmal wells in the Molasse Basin of Southern Germany*. GRC Transactions, 36, pp. 165-169

Lomax A., Virieux J., Volant P., Berge C. (2000). *Probabilistic earthquake location in 3D and layered models: Introduction of a Metropolis-Gibbs method and comparison with linear locations*. In: Thurber CH, Rabinowitz N (eds) Advances in Seismic Event Location. Kluwer, Amsterdam

Makundi J.S., Kifua G.M. (1985). *Geothermal features of the Mbeya prospect in Tanzania*. Geothermal Resources Council Transactions, 9, 451-454.

Marini L. and Pasqua C. (2014). *Geochemical modeling of water-rock interaction processes in the geothermal systems of the continental rift zone of East Africa and related implications*. Proceedings, 5TH African Rift Geothermal Conference (ARGeo-C5) - Arusha International Convention Center (AICC) 27 - 31 October 2014

McNeill J.D. (1994). *Principles and applications of time domain electromagnetics techniques for resistivity sounding*. Geonics Technical notes, TN27

Mibei G., Lagat J. (2011). *Structural controls in Menengai geothermal field.* Proceedings, Kenya Geothermal Conference 2011.

Moeck I.S., Beardmore G., Harvey C.C. (2015). *Cataloging worldwide developed geothermal systems for geothermal play type*. Proceeding World Geothermal Congress 2015, Melbourne, Australia, 19-25 April, 9 pp

Moeck I.S. (2014). *Catalog of geothermal play types based on geologic controls*. Renewable and Sustainable Energy Reviews 37, 2014, pp. 867-882

Moeck I.S., Beardsmore G. (2014). *A new 'geothermal play type' catalog: Streamlining exploration decision taking*. Proceedings thirty-ninth Workshop on Geothermal Reservoir Engineering Stanford University, Stanford, California, February 24-26, 2014, 8 pp

Mohr P. (1992). *Nature of the crust beneath magmatically active continental rifts*. Tectonophysics, 213, 269-284

Mohr P. and Zanettin B. (1988). *The Ethiopian flood basalt province*. Macdougall, J.D. (Ed.), Continental Flood Basalts. Kluwer Acad. Dord., 63-110

Monroy Parada A.F. (2016). *Phases of geothermal development*. Proceedings "SDG Short Course-I on Sustainability and Environmental Management of Geothermal Resource Utilization and the Role of Geothermal in Combating Climate Change", organized by UNU-GTP and LaGeo, in Santa Tecla, El Salvador, September 4-10, 201

Mruma, A.H. (1995). *Stratigraphy and palaeodepositional environment of the Palaoproterozoic volcano-sedimentary Konse Group in Tanzania*. J. Afr. Earth Sci. 21(2), 281-290

Mussett A., Khan M., & Button S. (2000). *Looking into the Earth: An Introduction to Geological Geophysics*. Cambridge: Cambridge University Press. doi:10.1017/CBO9780511810305

Nagy D. (1966). *The Gravitational Attraction of a Right Rectangular Prism*. Geophysics, 31, 2, 362-371

Néstor, M.R. and Fernando S.V. (2001). Advances in the analysis of pressure interference test, Proceedings, 26th Workshop on Geothermal Reservoir Engineering Stanford University, Stanford, SGP-TR-162

New Mexico Statutes Annotated - NMSA - (1978). *New Mexico Geothermal Resources Conservation Act*: Section 71-5-1. NMSA, 1978)

Nielson D.L. (1996). *Natural analogs for enhanced heat recovery from geothermal systems*. Proceedings, Twenty-First Workshop on Geothermal Reservoir Engineering Stanford University, Stanford, California, January 22-24, 1996

Ochmann N., Garofalo K. (2013). *Geothermal Energy as an Alternative Source of Energy for Tanzania, Final Technical Report of Phase II (2010-2013), Technical Cooperation with United Republic of Tanzania, GEOTHERM-Project 2002.2061.6*, Unpublished Report, 156 pp.

Ofwona C.O., Kipyego E.K., Suwai J.J. (2011). *Preliminary well test data of Menengai exploration wells. Proceedings, Kenya Geothermal Conference 2011*. Kenyatta International Conference Center, Nairobi, Nov. 21-22, 2011

Ofwona C.O. (2011). *Discharge tests report for well MW-01. Menengai Geothermal Project. GDC Report August 2011*

Ofwona C.O. (2011). *Completion tests report for well MW-02. Menengai Geothermal Project. GDC Report July 2011*

Ofwona C.O. (2002). *A reservoir study of Olkaria East Geothermal System, Kenya*. UNU Geothermal Training Programme, Reports 2002 Number 1

Ólafur Flóvenz G., Spangenberg E., Kulenkampff J., Árnason K., Karlsdóttir R. and Huenges E. (2005). *The Role of Electrical Interface Conduction in Geothermal Exploration*. Proceedings World Geothermal Congress 2005 Antalya, Turkey, 24-29 April 2005

Ólafur Flóvenz G. (2012). *Phases of geothermal development*. Proceedings Renewable Energy Training Program, ESMAP (Energy Sector Management Assistance Program) - World Bank Group

Omenda P. (2010). *The geology and geothermal activity of the East African Rift*. Short Course V on Exploration for Geothermal Resources, organized by UNU-GTP, GDC and KenGen, at Lake Bogoria and Lake Naivasha, Kenya, Oct. 29 - Nov. 19, 2010

Omondi C. (2011). *Borehole geology and hydrothermal mineralization of wells MW-01 and MW-02, Menengai geothermal field, Central Kenya Rift Valley*, United Nation University, Geothermal Training Program, Iceland, Report 2011, Number 30

O'Sullivan M.J., Bodvarsson G.S., Pruess K., Blakeley M.R. (1985). *Fluid and Heat Flow in Gas-Rich Geothermal Reservoirs*. SPE Journal, 25 (2), 215-226

Parasnis D. (1986). *Principle of applied geophysics*. Springer Netherlands, 412 pp.

Parker M. and Marobhe I. (1991). *Review of Gravity Survey Data in Tanzania*. Eastern and Southern African Mineral Resources Development Centre (ESAMRDC)

Pasqua C., Verdoya M., Chiozzi P., Marini L. (2016). Evaluation of geothermal resources in a hotspot realm: Mauritius Island (Indian Ocean). Proceedings, 6th African Rift Geothermal Conference, Addis Ababa, Ethiopia, 2nd – 4th November 2016, 11 pp.

Pasquale V., Verdoya M., Chiozzi P. (2017). Geothermics, Heat Flow in the Lithosphere. Springer Briefs in Earth Sciences. Second Edition, DOI 10.1007/978-3-319-52084-1

Pasquale V., Chiozzi P., Verdoya M. (2010). *Tectonothermal processes and mechanical strength in a recent orogenic belt: Northern Apennines*. JOURNAL OF GEOPHYSICAL RESEARCH, VOL. 115, B03301, doi: 10.1029/2009JB006631

Pearson F.J., Truesdell A.H. (1978) Tritium in the waters of Yellowstone National Park. U.S. Geological Survey Open-file Report 78-701

Pinna P., Muhongo S., Mcharo A., Le Goff E., Deschamps Y., Ralay F., Milesi J.P., (2004). *1:2,000,000 Geology and mineral map of Tanzania*. BRGM: Orléans, France

Prodehla C., Ritter J.R.R., Mechie J., Keller G.R., Khand M.A., Jacobe B., Fuchsa K., Nyambok I.O., Obelg J. D., Riarohh D. (1997). *The KRISP 94 lithospheric investigation of southern Kenya - the experiments and their main results*. Tectonophysics, 278, 121-147

Pruess K., Oldenburg C.M., Moridis G.J. (1999). *TOUGH2 User's Guide, Version 2.0*. Report LBNL-43134

Ramey, H.J. Jr. (1970). *Short time well test data interpretation in the presence of skin effect and wellbore storage*. JPT 22(1):97-104

Revil A., Cathles L.M., Losh S., Nunn J.A. (1998). *Electrical conductivity in shaly sands with geophysical applications*. Journal of Geophysical Research 103: doi: 10.1029/98JB02125. issn: 0148-0227

Rutagarama U. (2012). *The role of well testing in geothermal resource assessment*. School of Engineering and Natural Sciences Faculty of Earth Sciences University of Iceland and UNU-GTP, Report 2012 n. 2

Sawyer G.M., Carn S.A., Tsanev V.I., Oppenheimer C., Burton M. (2008). *Investigation into magma degassing at Nyiragongo volcano, Democratic Republic of the Congo*. Geochem. Geophys. Geosyst., 9, Q02017, doi:10.1029/2007GC001829.

Scarsi P., Craig H. (1996) Helium isotope ratios in Ethiopian Rift basalts. *Earth Planet. Sci. Lett.*, 144, 505-516

Scholz C.A., Cohen A.S., Johnson T.C., King J.W., Moran K. (2006). *The 2005 Lake Malawi Scientific Drilling Project*. Scientific Drilling, 2, pp. 17-19

Searle R.C. (1970). *Evidence from gravity anomalies for thinning of the lithosphere beneath the rift valley in Kenya*. Geophys. J. R. Astr. Soc., 21, 13-31

Simiyu S.M. (2009). *Application of micro-seismic methods to geothermal exploration: examples from the Kenya Rift*. Short Course IV on Exploration for Geothermal Resources, UNU-GTP, KenGen and GDC, Lake Naivasha, Kenya, November 1-22

Simiyu S.M. and Keller G.R., (2001). *An Integrated Geophysical Analysis of the Upper Crust of the Southern Kenya Rift*. Geophys. J. Int. 147, 543-561

Sinclair A. (1991). *A fundamental approach to threshold estimation in exploration geochemistry: probability plots revisited.* Journal of Geochemical Exploration, 41(1): p. 1-22

Siripunvaraporn W. and Egbert G. (2000). *An efficient data-subspace inversion method for 2-D magnetotelluric data*. Geophysics, 65(3), 791-80

Slack P.D., and Davis P.M. (1994). *Attenuation and velocity of P-waves in the mantle beneath the East African Rift, Kenya*. In: C. Prodehl, G. R. Keller, and M. A. Khan, eds., Crustal and upper mantle structure of the Kenya Rift. Tectonophysics, 236, 331-58

Stefanson V. and Steingrímsson B. (1980). *Geothermal Logging. An introduction to techniques and interpretation.* Orkustofnun report OS-89917/JHD-09

Steingrimsson B. and Gudmundsson Á. (2006). *Geothermal Borehole Investigations during and after Drilling*. Presentation at Workshop for Decision Makers on Geothermal Projects in Central America, San Salvador, El Salvador

Sutarno D. (2008). *Constrained robust estimation of magnetotelluric impedance functions based on a bounded-influence regression M-estimator and the Hilbert transform*. Nonlin. Processes Geophys., 15, 287-293.

Suwai J. (2012). *Pumping test report for MW-01. Menengai geothermal Project, GDC Report*

September 2012

Suwai J. (2012). *Long term discharge test report for MW-01. Menengai geothermal Project, GDC Report February 2012*

Suwai J. (2011). *Preliminary reservoir analysis of Menengai geothermal field exploration wells. UNU Geothermal Training Programme, Reports 2011, n. 32*

SWECO (1978). *Reconnaissance of Geothermal Resources*. Report for the Ministry of Water, Energy and Minerals of Tanzania, SWECO, Stockholm, Sweden and VIRKIR, Reykjavik, Iceland, 51pp.

Symonds R.B., Rose W.I., Bluth G.J.S., Gerlach T.M. (1994). *Volcanic-gas studies: methods, results, and applications*. In: "Volatiles in Magmas", M.R. Carroll and J.R. Holloway (Eds.), Mineralogical Society of America, Reviews in Mineralogy, 30, 1-66

Telford W.M, Geldart L.P., Sheriff R.E. (1990). *Applied geophysics (2nd edition)*. Cambridge University Press, 760 pp.

TGDC (2018). *Geothermal systems in Tanzania: Occurrence; assessment; development and utilization*. Geothermal technical review meeting, Dar Es Salaam, Tanzania. UNEP - 7 November 2018

Thurber, C.H. (1992). *Hypocenter velocity structure coupling in local earthquake tomography*. Phys. Earth Planet. Int., 75, 55-62

Thurmond A.K., Abdelsalam M.G., Thurmond J.B. (2006). *Optical-radar-DEM remote sensing data integration for geological mapping in the Afar Depression, Ethiopia*. Journal of African Earth Sciences, Vol. 44, Issue 2, February 2006, Pages 119-134.

Tulinius H., Ádám L., Halldorsdottir H., Yu G., Strack K.M., Allegar N., He L.F., and He Z.X. (2008). *Exploring for geothermal reservoirs using broadband 2-D MT and gravity in Hungary*. SEG 2008 Las Vegas Annual Meeting

Tulinius H., Þorbergsdóttir I.M., Ádám L., Hu Z., and Yu G. (2010). *Geothermal evaluation in Hungary using integrated interpretation of well, seismic, and MT data*. Proceedings World Geothermal Congress 2010 Bali, Indonesia, 25-29 April

UNECE, IGA (2016). *Application of UNFC-2009 to Geothermal Energy Resources*. IGA Resources & Reserves Committee-UNECE Task Force. October 2016

Ussher G., Harvey C., Johnstone R., Anderson E. (2000). *Understanding the resistivities observed in geothermal systems*. Proceedings World Geothermal Congress 2000 Kyushu - Tohoku, Japan, May 28 - June 10, 2000

Van Straaten P. (1989). *Nature and structural relationships of carbonatites from Southwest and West Tanzania. Carbonatites: Genesis and Evolution*. Unwin Hyman, London, 177-199 pp.

Wheildon J., Morgan P., Williamson K.H., Evans T.R., and Swanberg C.A. (1994). Heat flow in the Kenya Rift Zone. In: C. Prodehl, G. R. Keller, and M. A. Khan, eds., Crustal and upper mantle structure of the Kenya Rift. Tectonophysics, 236, 131-49

Wolery T.W. and Jarek R.L. (2003). Software user's manual. EQ3/6, Version 8.0. Sandia National Laboratories -U.S. Department of Energy Report, 376 pp.

Wolery T.W. and Jove-Colon C. (2007). Qualification of thermodynamic data for geochemical modeling of mineral-water interactions in dilute systems. Sandia National Laboratories Report ANL-WIS-GS-000003 REV 01, 412 pp.

Yu G., He Z. X., Hu Z., Þorbergsdóttir I. M., Strack K.-M., Tulinius H. (2009). *Geothermal exploration using MT and gravity techniques at Szentlőrinc area in Hungary*. SEG Houston 2009 International Exposition and Annual Meeting

Zemedkun M.T. (2018). *Geothermal Outlook in East Africa*. Geothermal technical review meeting, Dar Es Salaam, Tanzania. UNEP - 7 November 2018